The Dissertation Committee for Boonam Shin
certifies that this is the approved version of the following dissertation:

Laboratory Investigation of the Stiffness and Damping Properties of Binary and Gap-Graded Mixtures of Granular Soils

Committee:

Kenneth H. Stokoe II, Supervisor

Brady R. Cox

Robert B. Gilbert

Chadi El Mohtar

Clark R. Wilson

Laboratory Investigation of the Stiffness and Damping Properties of Binary and Gap-Graded Mixtures of Granular Soils

by

Boonam Shin

DISSERTATION

Presented to the Faculty of the Graduate School of

The University of Texas at Austin

in Partial Fulfillment

of the Requirements

for the Degree of

DOCTOR OF PHILOSOPHY

THE UNIVERSITY OF TEXAS AT AUSTIN

December 2018

In the will of God,

he was always working for me, and

he is even now working for me.

Acknowledgments

First and foremost, I would like to thank specially Dr. Stokoe for his guidance, support, and his unlimited enthusiasm. Thank you for always treating me with kindness and sharing your insights on many aspects of soil dynamics, researching, and even life.

I am also grateful for the advice and kindness of Dr. Cox, Dr. Gilbert, Dr. El Mortar, and Dr. Wilson who served on my Ph.D. committee.

I would also like to acknowledge Dr. Rathge, Dr. Zornberg, Dr. Boyles, and Dr. Engelhardt for their excellent supports during my graduate courses and researches.

The efforts of many fellow graduate students whose assistance with many aspects of this study are sincerely appreciated. I would also like to extend my thanks to Bohyoung Lee, Sungmoon Hwang, Gunwoong Kim, Julia Robert, Andrew Keene, Yaning Wang, Benchen Zhang, Zhongze (Steve) Xu, and Reihaneh Hosseini for all of the effort and help.

I would like to thank Alicia Zapata for your administrative support and the kind advice for my life.

Lastly, with all my heart, I would like to thank my both parents, my sister and her family, my two children (Roy and Chloe) and my lovely wife for their constant prayer, love, and support.

Laboratory Investigation of the Stiffness and Damping Properties of Binary and Gap-Graded Mixtures of Granular Soils

Publication No. _____

Boonam Shin, Ph.D.
The University of Texas at Austin, 2018

Supervisor: Kenneth H. Stokoe II

Sandy and gravelly soils are encountered in many natural soil strata such as alluvial, fluvial, residual, and glacial deposits. These granular materials are used in the construction of many types of man-made geotechnical structures, fills, and ground improvements. A need exists to understand the dynamic behavior of these sandy and gravelly mixtures. A "binary packing model" has been proposed by some researchers to represent a simplified model for some sandy and gravelly soils that are composed of only a few, quite different, particle sizes (typically more than a factor of 20, and a factor of 34 used in this study) created during construction of geotechnical systems or in the natural environment. In other cases, gap-graded materials have been created. The packing condition and void distribution in the two types of gradations are complicated due to large variations in particle size and construction conditions. Up to now, no systematic studies have been conducted to evaluate key

factors in the soil matrix (i.e., the parent materials in these mixtures) affecting the dynamic properties (i.e., shear modulus, G, and material damping ratio, D) of the binary and gap-graded mixtures considering the packing state of the matrix particles.

In binary granular soils, estimating the critical packing condition, which represents the case when all void space between the large particles are completely filled with each group of small particles, is important. Additionally, the associated critical small-particle content (SPC*), which is the small-particle content (SPC) under the critical packing condition, can be calculated using the void ratios of the small-particle and large-particle materials.

In this research, systematic variations of the parent materials in binary and gap-graded mixtures (i.e., the small and large particles in binary mixtures) were created, and the dynamic torsional resonant column (RC) testing was performed on a wide range of particle packing conditions. Some findings are: 1) the binary and gap-graded specimens for SPC $\geq$ 76% behaved very similarly to their parent poorly graded sand in both the small-strain and nonlinear dynamic properties; 2) the binary specimens for 15% $\leq$ SPC $\leq$ 100% showed a clear trend in the relationship of small-strain shear modulus at one atmosphere (A_G) and void ratio (e); 3) the binary specimens for 23% $\leq$ SPC $\leq$ 36%, which were in the range of SPC*, showed the highest stiffnesses and most nonlinearity; and 4) overall, the void ratio was a better parameter than the uniformity coefficient to estimate the nonlinear behavior of the specimens for 0% $\leq$ SPC $\leq$ 39%.

Table of Contents

List of Tables

List of Figures

Chapter 1

Introduction

1.1 BACKGROUND

Stiffness and material damping are two important dynamic properties in the design and construction of many geotechnical systems. These properties are generally expressed by stiffness moduli, (i.e., constrained modulus, M, and shear modulus, G) and material damping ratio in shear, D_s or D. Rarely, if ever, is material damping in constrained compression, D_c, measured. The relationship between the dynamic stiffnesses and body wave velocities is:

$$M = \rho \times V_p{}^2 \tag{1.1}$$

$$G = \rho \times V_s{}^2 \tag{1.2}$$

where:

V_p = constrained compression wave velocity;

V_s = shear wave velocity; and

ρ = the total unit mass of the material.

Shear strain is one of the most important variables affecting dynamic soil properties (Richart. et al. 1970 [28]). Typical variations of the shear modulus (G) and material damping ratio in shear (D) with shear strain, γ, are shown in Figure 1.1. These curves are generally characterized into three parts: (1) linear range (or small-strain range); (2) "nonlinear elastic" range; and (3) nonlinear range. In the linear range, the values of G and D are constant and independent of strain. Because in the linear range the shear modulus (G) is constant with a maximum value and the material damping ratio (D) is constant with a minimum value, the dynamic properties in the small-strain range (i.e., the linear range) are called the small-strain shear modulus, G_{max}, and the small-strain material damping ratio in shear, D_{min}, respectively. The boundary between linear and "nonlinear elastic" ranges is called the elastic threshold strain, γ_t^e, and the boundary between the "nonlinear elastic" and nonlinear ranges is called the cyclic threshold strain, γ_t^c. In the nonlinear elastic range the values of G and D begin to decrease and increase, respectively, as γ increases. However, both shear modulus (G) and material damping ratio (D) are essentially unaffected by number of loading cycles until the cyclic threshold strain.

Sandy and gravelly soils are encountered in many natural soil strata such as alluvial, fluvial, residual, and glacial deposits. These granular materials are used in the construction of many types of man-made geotechnical structures, fills, and ground improvements. A need exists to understand the dynamic behavior of these sandy and gravelly mixtures. A "binary packing

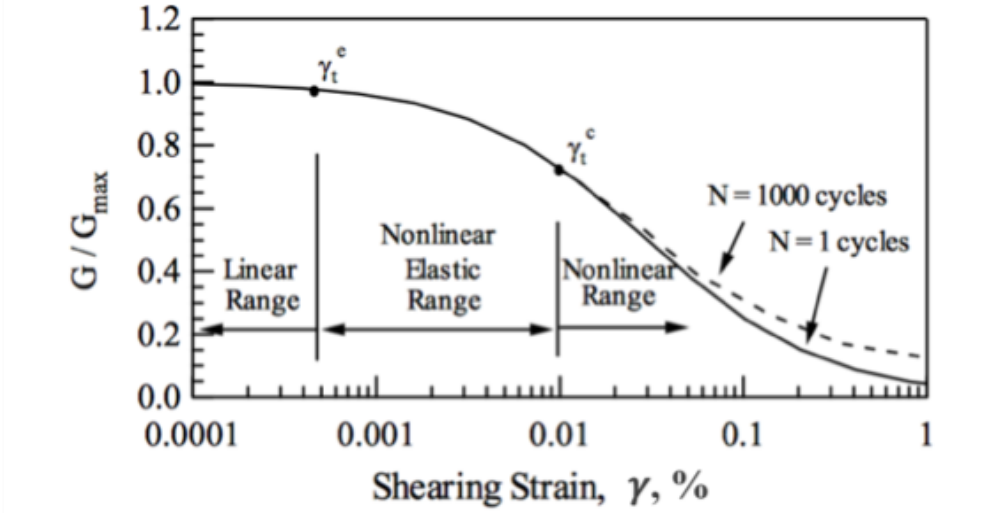

(a) Normalized Shear Modulus vs. Shear Strain (γ) Curve

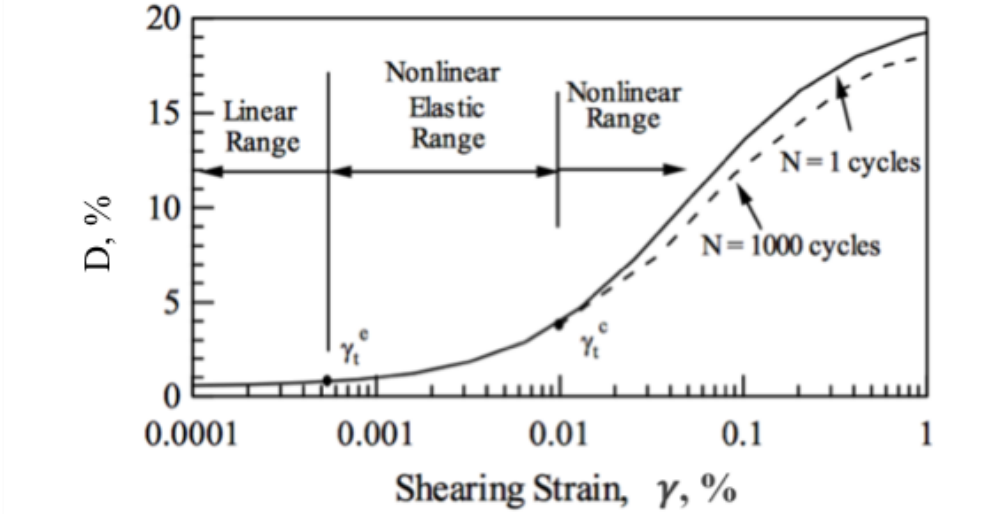

(b) Material Damping Ratio vs. Shear Strain (γ) Curve

Figure 1.1: Typical Linear and Nonlinear G/G_{max} - Log γ and D_s - Log γ Curves

model" has been proposed by various researchers to represent a simplified model for some sandy and gravelly soils created during construction of geotechnical systems or in the natural environment (Clarke, 1979; Marionet al., 1992; Koltermann and Gorelick, 1995; Kamann et al., 2007; and Choo, 2014). In other cases, gap-graded materials have been created. The packing condition and void distribution in the two types of materials (i.e., the binary and gap-graded materials) are complicated due to large variations in particle size and depositional and/or construction conditions. Up to now, no systematic studies have been conducted to evaluate the key factors affecting the dynamic properties (shear modulus, G, and material damping ratio in shear, D) of the binary and gap-graded mixtures in conjunction with the packing state of the matrix particles. Therefore, the research described herein was undertaken.

In binary granular soils, estimating the critical packing condition, which is the condition when all void spaces between large particles are completely filled with the groups of smaller particles, is important. Additionally, the associated critical small-particle content (SPC*), which is the small-particle content (SPC) under the critical packing condition, can be calculated using the void ratios of smaller and larger particle materials. In the ideal packing model, there are three major assumptions. These assumptions (Chang and Phantachang, 2016 [8]) are followings: (1) only two distinct particle sizes are considered, (2) the ratio of larger to smaller particle diameters is more than a factor of 20 (a factor of 34 was used in this study), and (3) the packing of the larger particles is not affected by the smaller particles, and vice versa.

In this research, systematic variations of the parent materials (i.e., the small and large particles in binary and gap-graded mixtures) were created, and the dynamic torsional resonant column (RC) testing was performed on a variety of particle packing conditions of binary and gap-graded mixtures.

1.2 OBJECTIVES OF THIS RESEARCH

The objectives of this research are: (1) to understand the theoretical background of the binary packing conditions and develop a platform to differentiate binary specimens, (2) to measure the dynamic properties of binary and gap-graded mixtures and to evaluate the applicability of the theoretical classifications on the basis of the behavioral characteristics (i.e., the dynamic properties), and (3) to develop relationships of the dynamic properties with the important factors for granular soils such as void ratio and gradation characteristics.

The first objective was accomplished by reviewing literature dealing with the "ideal packing models" in binary mixtures proposed and used by Clarke (1979) [10] and Koltermann and Gorelick (1995) [22]. The second objective involved the measurement and collection of the dynamic properties of binary and gap-graded specimens. The two dynamic properties such as shear modulus (G) and material damping ratio in shear (D) are the main players in this work. These dynamic properties are affected by isotropic confining pressure (σ_o), shear strain amplitude (γ) and mechanical properties such as void ratio (e) and gradation characteristics such as uniformity coefficient, C_u,

and median grain size, D_{50}. For the confining pressure, the parameter of total confining pressure (σ_o) has been used through the entire this study rather the parameter of effective confining pressure (σ'_o) due to the insignificant difference between the two parameters of the specimens tested in this study.

1.3 ORGANIZATION OF THE DISSERTATION

This dissertation is divided into eight chapters as follows. In Chapter Two, the general mechanics background required in this study such as stress and strain, the use of elasticity theory, seismic wave propagation and the relationship with dynamic properties of geotechnical materials are discussed.

In Chapter Three, the dynamic torsional resonant column (RC) testing method to determine dynamic soil properties is discussed. In the last section of this chapter, the analysis methods from the RC test results are outlined in detail.

In Chapter Four, a literature review of the effects of void ratio and gradation characteristics on the dynamic properties of sandy and gravelly soils is presented. Additionally, the "ideal binary packing models" in binary mixtures are introduced and the concept of the critical packing condition and the associated quantities (i.e., critical small-particle content, SPC*) are presented.

Based on the calculated critical small-particle content (SPC*), three classifications are suggested for binary mixtures in Chapter Five. These three classifications are applied to the reconstituted binary specimens that were

dynamically tested in this research. Information and a listing of binary and gap-graded mixtures which were tested in the RC device to obtain the representative dynamic properties are also presented.

In Chapter Six, test results of the linear dynamic properties of binary and gap-graded specimens measured using RC testing are presented. Relationships between the dynamic properties with void ratio and gradation characteristics are presented.

In Chapter Seven, the test results in the nonlinear range of binary and gap-graded specimens measured in the RC device are presented. The overall trends of nonlinear dynamic property variations are also discussed.

A summary of the study and conclusions are presented in Chapter Eight.

Chapter 2

Theory and Background of Dynamic Torsional Resonant Column (RC) Testing Methodology

2.1 INTRODUCTION

In geotechnical design and construction, understanding the engineering properties of geotechnical materials is critical. The main building blocks in understanding the material properties are the concepts of stress, strain and their relationship.

In Section 2.2, the general concepts in engineering (i.e., stress, strain and their relationship) are discussed. In Section 2.3, the dynamic properties such as shear modulus and material damping ratio are derived from stress wave (propagating stress waves) characteristics. The key variables used in this research are summarized in Section 2.4.

2.2 GENERAL MECHANICS BACKGROUND: FOR STATIC LOADING OF AN ISOTROPIC SOLID

2.2.1 Stress

Stress is defined as the force per unit area of a boundary, for all orientations of the boundary (Chen and Han, 2007). Quantitatively, stress is expressed by a stress tensor. With respect to any chosen coordinate system, the stress

tensor can be represented as a symmetric matrix of 3×3 real numbers. Figure 2.1 shows a schematic diagram of a second-order stress tensor.

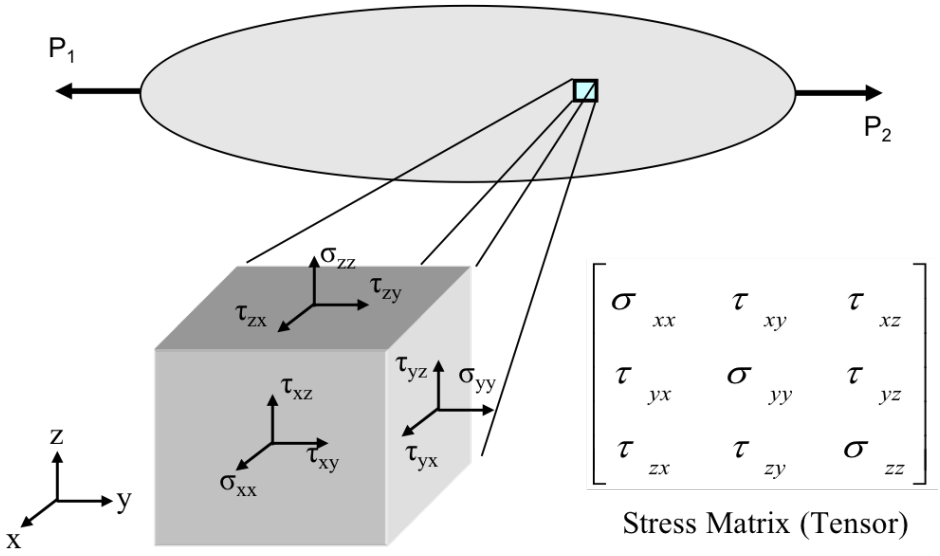

Figure 2.1: Stress Tensor (Gere and Timoshenko, 1990)

Stress state consists of normal and shear components, and each component has a unique physical significance. Generally, the normal stress and the shear stress are defined as:

$$\begin{bmatrix} \sigma_{xx} & \sigma_{yy} & \sigma_{zz} \\ \tau_{xy} & \tau_{xz} & \tau_{yx} \\ \tau_{yz} & \tau_{zx} & \tau_{zy} \end{bmatrix} = \begin{bmatrix} \frac{dF_x}{dA_x} & \frac{dF_y}{dA_y} & \frac{dF_z}{dA_z} \\ \frac{dS_y}{dA_x} & \frac{dS_z}{dA_x} & \frac{dS_x}{dA_y} \\ \frac{dS_z}{dA_y} & \frac{dS_x}{dA_z} & \frac{dS_y}{dA_z} \end{bmatrix} \tag{2.1}$$

where:

σ_{xx}, σ_{yy}, σ_{zz} = normal stresses in the directions of the x-, y-, and z-axes, respectively,

dA_x, dA_y, dA_z = surface areas for which the normal vector is in direction of the x-, y-, and z-axes, receptively,

dF_x, dF_y, dF_z = forces normal to surfaces dA_x , dA_y , dA_z, respectively,

τ_{ij} = shear stress generated on the surface dA_i due to the shear force for which the direction is j, and

dS_x, dS_y, dS_z = shear forces on surfaces dA_x, dA_y, and dA_z, respectively.

In a given loading condition, a body (or boundary) must be in moment equilibrium. Therefore, the stress matrix is diagonally symmetric and $\tau_{ij} = \tau_{ji}$. Accordingly, the stress matrix (the stress tensor, $[\sigma]$)is:

$$\left[\sigma\right] = \begin{bmatrix} \sigma_{xx} & \tau_{xy} & \tau_{xz} \\ \tau_{xy} & \sigma_{yy} & \tau_{yz} \\ \tau_{xz} & \tau_{yz} & \sigma_{zz} \end{bmatrix} \tag{2.2}$$

where:

$[\sigma]$ = the stress tensor,

$\sigma_{xx}, \sigma_{yy}, \sigma_{zz}$ = are normal stresses in directions of the x-, y-, and z-axes, respectively,

τ_{ij} = shear stress generated on the surface dA_i due to the shear force for which the direction is in the j-axis.

In the stress tensor, the shear stress component is denoted by τ (Greek: tau), and represents the component of stress coplanar with a material cross section. The shear stresses (τ) arise from the force vector components that are parallel to the material cross sections, while normal stresses (σ, Greek: sigma) arise from the force vector components that are perpendicular to the material cross sections on which they act as shown in Figure 2.1.

2.2.2 Strain

Deformation is defined as the change in shape of a structure due to the application of a force or forces. Strain is a description of this deformation in terms of relative displacement of particles in the body. Strain, like stress, has a directional property and is divided into normal strain, ϵ and shear strain, γ. The quantitative (or mathematical) expressions of the strains (Gere and Timoshenko, 1990) are:

$$\epsilon = \frac{\Delta L_n}{L_o} \tag{2.3}$$

$$\gamma = \frac{\Delta L_s}{H_o} \tag{2.4}$$

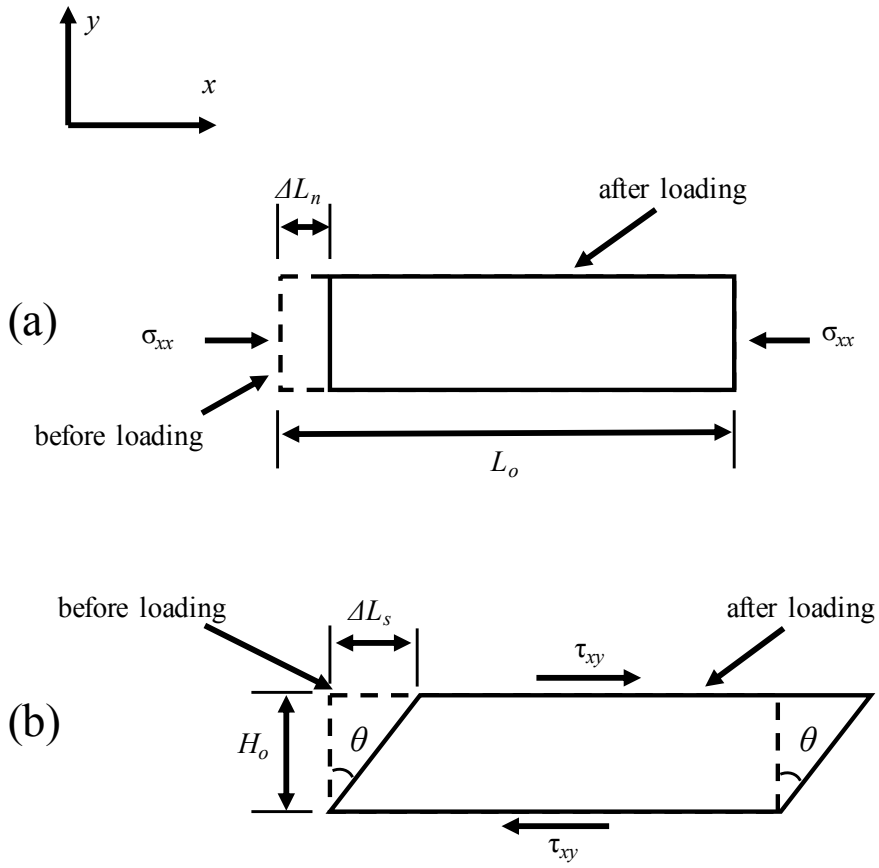

Figure 2.2: Illustrations of: (a) Normal Strain, ϵ and (b) Shear Strain, γ

The illustrations of the normal strain (ϵ) and shear strain (γ) are presented in Figure 2.2. In the Figure 2.2 (a), ΔL_n is the difference between the original length and the current length of an element, and L_o is the original length. In the Figure 2.2 (b), H_o is the original length of an element, ΔL_s is the deformation perpendicular to the original length, and θ is the angular

between the original length and the deformed line.

The three-dimensional strains of an infinitesimal element with an original length (L) that is approaching zero are redefined as (Gere and Timoshenko, 1990):

$$\epsilon_x = \frac{\partial u_x}{\partial x} \tag{2.5}$$

$$\epsilon_y = \frac{\partial u_y}{\partial y} \tag{2.6}$$

$$\epsilon_z = \frac{\partial u_z}{\partial z} \tag{2.7}$$

where:

ϵ_x = normal strain in the direction of the x-axis,

ϵ_y = normal strain in the direction of the y-axis,

ϵ_z = normal strain in the direction along the z-axis,

$\frac{\partial u_x}{\partial x}$ = differential displacement at any point in the direction along the x-axis,

$\frac{\partial u_y}{\partial y}$ = differential displacement at any point in the direction along the y-axis, and

$\frac{\partial u_z}{\partial z}$ = differential displacement at any point in the direction along the z-axis.

Similarly, the angular change of an infinitesimal element between two lines crossing this element in a body (θ) is defined as the general shear strain (γ). Shear strain is the limit ratio of the angular difference between any two lines in a body before and after deformation, assuming that the length of the lines approach zero. Given a displacement field (u_x, u_y, u_z), the shear strain can be expressed as (Gere and Timoshenko, 1990):

$$\gamma_{xy} = \frac{\partial u_x}{\partial y} + \frac{\partial u_y}{\partial x} \tag{2.8}$$

$$\gamma_{yz} = \frac{\partial u_y}{\partial z} + \frac{\partial u_z}{\partial y} \tag{2.9}$$

$$\gamma_{zx} = \frac{\partial u_z}{\partial_x} + \frac{\partial u_x}{\partial z} \tag{2.10}$$

where:

γ_{ij} = engineering shear strain in the directions along the i- and j-axes, and

$\frac{\partial u_i}{\partial_j}$ = differential displacement of the direction i at any point in the direction along the j-axis.

2.2.3 Stress-Strain Relationship

Characterizing the stress-strain relationship (constitutive law) of a material (e.g., for soils) is one of the key aspects needed to understand the

behavior of the material. There are three general classes of material models for solids: 1) elasticity, in which material behavior is perfectly reversible, 2) viscous-elasticity, in which a material displays irreversible and possibly time-dependent behavior, and 3) plasticity, in which the irreversible behavior is accounted for using sophisticated nonlinear relations.

In the elastic model with static loading, an ideal, homogeneous medium satisfies the following relationship between stress and strain (Gere and Timoshenko, 1990):

$$\sigma_x = E \times \epsilon_x \tag{2.11}$$

where:

E = the elastic modulus (equal to Young's modulus in the elastic range),

σ_x = normal stress in the x-direction, and

ϵ = normal strain in the x-direction.

Equation 2.11 is also called Hooke's law, which represents the linear proportionality between normal stress (σ) and normal strain (ϵ). The proportionality often is quantified by the elastic modulus (E, Young's Modulus).

Similarly, shear modulus, G, is defined as the ratio of the variation of the shear stress to the variation of the shear strain (Figure 2.2b). The

mathematical expression of the shear modulus is:

$$G = \frac{\Delta\tau_{xy}}{\Delta\gamma_{xy}} \tag{2.12}$$

where:

$\Delta\tau_{xy}$ = shear stress of the y-direction in the plane of the x-direction, and

$\Delta\gamma_{xy}$ = shear strain of the y-direction in the plane of the x-direction.

Shear modulus can be represented with Young's modulus (E) and Poisson's ratio (ν) in an elastic, homogeneous, and isotropic medium.

$$G = \frac{E}{2(1+\nu)} \tag{2.13}$$

where:

G = Shear Modulus,

E = Young Modulus, and

ν = Poisson's ratio.

2.2.4 Shear Stress and Shear Strain in Torsional Loading

The relationship between the shear stress (τ) and the shear strain (γ) can be represented by the variation in shear modulus (G). The shear modulus can be established by performing experiments. A torsional shear test is one of the experimental methods used to determine the shear modulus of a material (e.g., soils).

In the torsional test, it is assumed that a pure torque (T) is applied to the top of a specimen as shown in Figure 2.3. The torque (T) can be calculated from (Gere and Timoshenko, 1990):

$$T = \int_{r_i}^{r_o} dT = \int_{r_i}^{r_o} \tau(r) \times r \; dA = \int_{r_i}^{r_o} \tau(r) \times 2\pi r \; dr \tag{2.14}$$

where:

τ = shear stress at a distance r from the z-axis,

r_o = the outside radius of the specimen, and

r_i = the inside radius of the specimen (if the specimen is solid, r_i is zero).

In an ideal elastic model (an isotropic and homogeneous medium), the shear stress (τ) is calculated by (Gere and Timoshenko, 1990):

$$\tau = \tau_{max} \times \frac{r}{r_o} \tag{2.15}$$

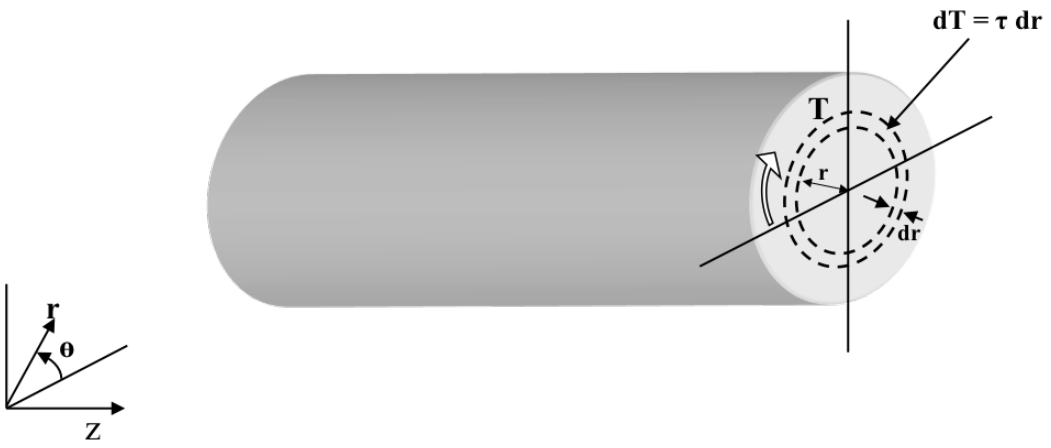

Figure 2.3: Torsional Load ,T, and the Resulting Shear Stress ,τ, Applied to a Cylindrical Specimen (from Gere and Timoshenko, 1990)

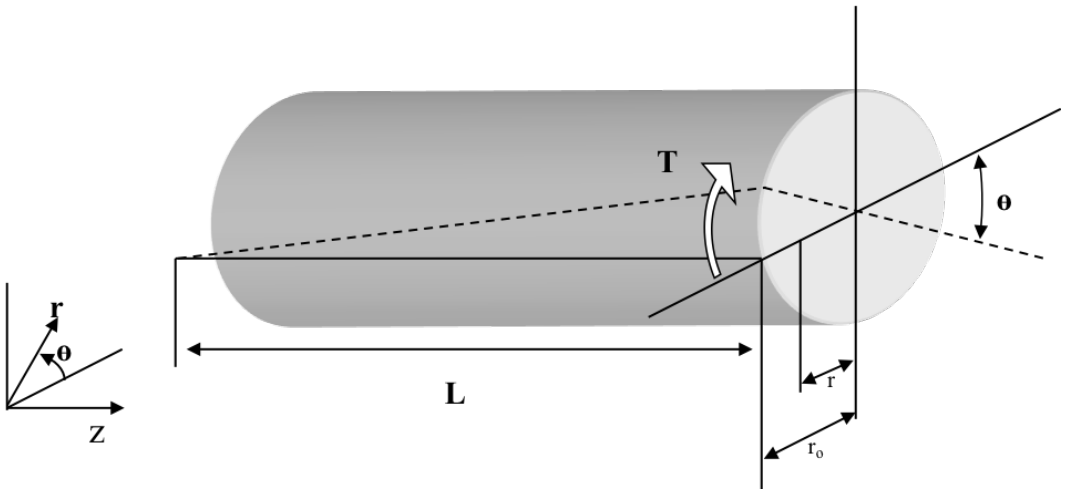

Figure 2.4: Torsional Shear Strain ,γ, due to Applied Torque (from Gere and Timoshenko, 1990)

where:

τ_{max} = maximum shear stress at $r = r_o$.

Therefore, the Equation 2.14 is:

$$T = \int_{r_i}^{r_o} (\tau_{max} \times \frac{r}{r_o}) \times 2\pi r \times r \; dr \tag{2.16}$$

$$= \frac{\tau_{max}}{r_o} \times \frac{\pi}{2} \times (r_o^4 - r_i^4) \tag{2.17}$$

$$= \frac{\tau_{max}}{r_o} \times J_p \tag{2.18}$$

where:

T = applied torque,

τ_{max} = maximum shear stress at $r = r_o$,

r_o = the outside radius of the specimen,

r_i = the inside radius of the specimen, and

J_p = the polar moment of inertia ($J_p = \pi \times (r_0^4 - r_i^4)/2$ for cylindrical specimens).

By definition, the torsional shear strain (γ) is calculated by (Gere and Timoshenko, 1990):

$$\gamma = \frac{u}{L} = \frac{r \times \theta}{L} \tag{2.19}$$

where:

u = angular displacement at any radius (r),

θ = angle of twist, and

L = original length of the specimen.

From the relationship between shear stress and shear strain, shear modulus (G) can be calculated as (Gere and Timoshenko, 1990):

$$\tau_{max} = G \times \gamma_{max} \tag{2.20}$$

where:

τ_{max} = maximum shear stress when $r = r_o$, and

γ_{max} = maximum shear strain when $r = r_o$.

This simple relationship should be used with caution beyond the elastic range (i.e., nonlinear deformation range). The nonlinear behavior of soil and

rock often do not lead to a closed-form expression, and must be evaluated through a complicated numerical process to closely approximate the shear stress and shear modulus value (Taylor, 1971).

To extend the elastic model to the nonlinear range, an equivalent radius (r_{eq}) and an effective secant shear modulus (G_{eff}) are defined. The definition of the effective secant modulus (G_{eff}) is (Taylor, 1971):

$$G_{eff} = \frac{T \times L}{J_p \times \theta} \tag{2.21}$$

where:

T = applied torque,

L = original length of the specimen,

J_p = area polar moment inertia, and

θ = angle of twist.

Additionally, the polar moment inertia (J_p) for the cylindrical shape is:

$$J_p = \int_A r^2 \, dA = \pi \ \times (r_o^4 - r_i^4)/2 \tag{2.22}$$

The equivalent radius (r_{eq}) is the radius for which G is equal to G_{eff}. The value of G_{eff} is the same as G over an entire specimen when the specimen is in the linear-elastic range.

Chen and Stokoe (1979) studied the radial distribution of shear strain to find a value of r_{eq} for soil specimens tested with the combined dynamic torsional resonant column and cyclic torsional shear (RCTS) device in order to evaluate an effective strain. They found that, for a solid soil specimen, the r_{eq} value varied from 82% of r_0 for a peak shear strain amplitude below 0.001% to 79% of r_0 for a peak shear strain of 0.1%. However, for simplicity, they decided to use a singe number of 0.82 for the r_{eq} value. The concept of r_{eq} with an effective number of $r_{eq} = 0.82$ is adopted in this study to calculate the shear strain and the shear stress in the dynamic torsional resonant column tests. This concept is described as:

$$\tau = \tau_{max} \times \frac{r}{r_0} \tag{2.23}$$

$$= \frac{r_{eq}}{r_0} \times \frac{r_o \times T}{J_p} \tag{2.24}$$

$$\gamma = r_{eq} \times \frac{\theta}{L} \tag{2.25}$$

where:

τ = shear stress,

γ = shearing strain, and

r_{eq} = 0.82 for a solid soil specimen.

2.3 DYNAMIC MATERIAL PROPERTIES

2.3.1 Stress Waves

The way that energy is generated by dynamic loadings such as earthquakes is in the form of fractures which create stress waves. An important characteristic of stress waves is how fast these waves propagate in soil and rock. Because their characteristics are directly correlated to other engineering properties, it is very important to understand theses stress waves.

Constrained compression waves (P waves) and shear waves (S waves) are the two types of body waves that travel through soil and rock, which are typically represented by a half space. Body waves travel through the mass of soil and rock, such as the earth as shown in Figures 2.5a and b. For a half space, other types of stress waves also exist. Rayleigh waves and Love waves are surface waves (Figures 2.5c and d). Surface waves travel along the soil surface due to the interaction between body waves and the surficial layers of the earth (Kramer, 1996). For example, Rayleigh waves are produced by interaction of P or SV waves (SV waves are S waves in which the particle motion is oriented in the vertical direction). Love waves result from the interaction of SH waves (S waves in which the particle motion is horizontal and perpendicular to the direction of S wave propagation). In the Figure 2.5, the direction of wave propagation (which is horizontal in this example) and the direction of particle

motion are illustrated for body waves and surface waves.

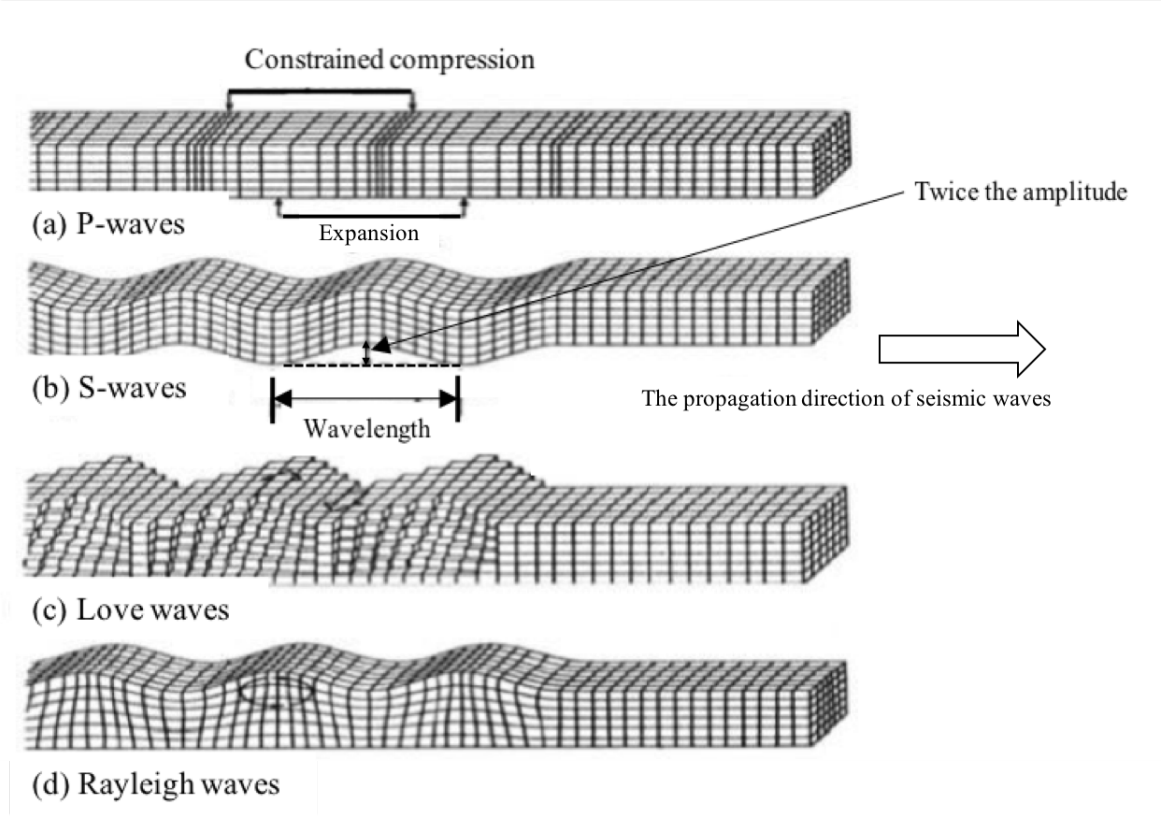

Figure 2.5: Propagation of Body Waves and Surface Waves in and along the Surface of a Uniform, Half Space: (a) Constrained Compression Waves, (b) Shear Waves, (c) Love Waves, and (d) Rayleigh Waves (after Bolt, 1993)

Generally, the properties of seismic wave propagation are related to the dynamic properties of a material such as elastic modulus, shear modulus and material damping ratio. The theory of the wave propagation through a finite solid rod is discussed in the following section.

There are three different types of the wave motion in a finite solid rod: (1) longitudinal compression, (2) torsional shear, and (3) flexural bending. In

Figure 2.6, these three different wave motions are shown in a finite rod. The longitudinal compression wave causes particles within the rod to move in a direction parallel to the direction of wave propagation, as shown in Figure 2.6a. The torsional shear wave causes the particles to move in a direction perpendicular to the direction of the wave propagation, as shown in Figure 2.6b. The flexural bending wave is generated due to the bending motion of the rod as shown in Figure 2.6c.

The longitudinal compression waves and torsional shear waves play important roles in understanding engineering properties of a material. In the next section, the relationship between wave motion and dynamic properties are discussed.

2.3.2 Longitudinal Compression Wave Propagation in a Solid Rod

The wave equation of one-dimensional longitudinal compression waves can be derived as (Richart et al, 1970):

$$\frac{\partial^2 u}{\partial t^2} = \frac{E}{\rho} \times \frac{\partial^2 u}{\partial x^2} \tag{2.26}$$

where:

u = particle displacement along the propagating direction,

t = time,

E = unconstrained elastic modulus (or Young's Modulus),

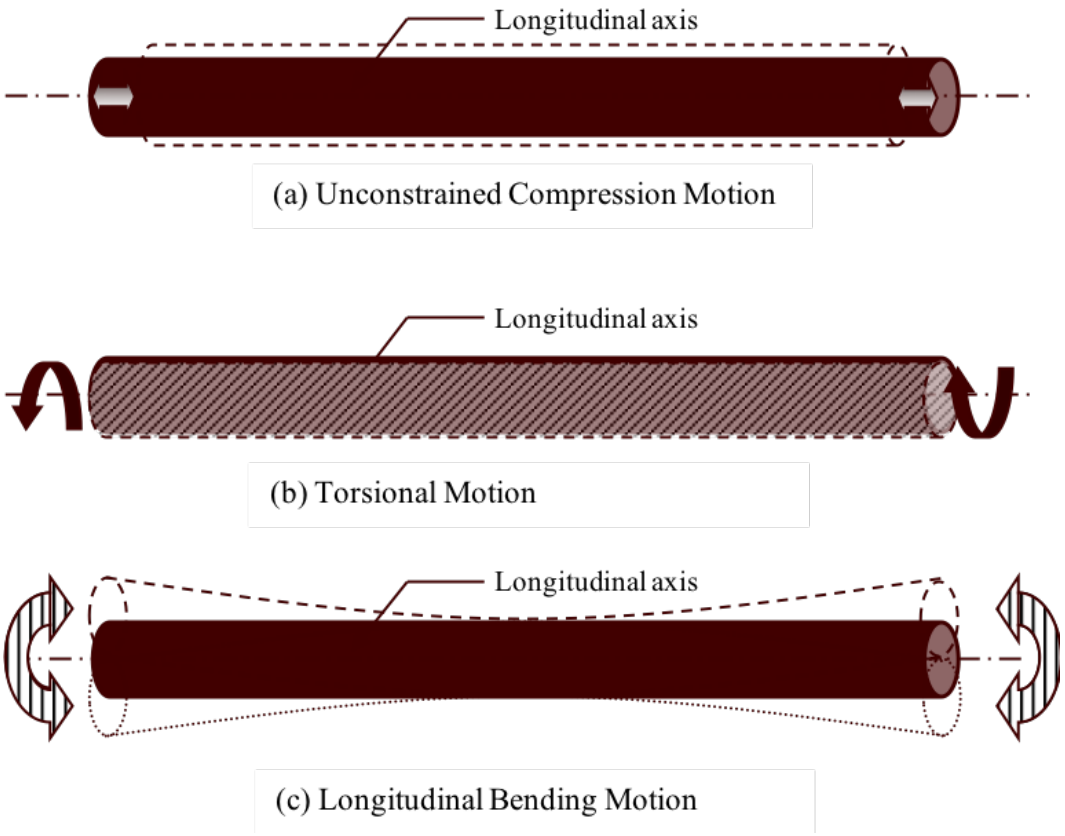

Figure 2.6: Three Different Types of Wave Motions in a Finite Solid Rod (Menq, 2003)

ρ = density of the rod material, and

x = coordinate of a particle along the x-axis.

In the case of lateral motion, which is perpendicular to the direction of wave propagation, the wave is unconstrained and its velocity is relatively slower than under the laterally constrained condition. When no lateral motion is allowed, the wave is constrained and the material is stiffer so that the velocity is faster.

Richart et al. (1970) provided the solution of the Equation 2.26:

$$\begin{aligned} u &= C_T \cdot [cos(\omega t) + i \cdot sin(\omega t)][cos(kx) + i \cdot sin(kx)] \\ &\quad + C_R \cdot [cos(\omega t) + i \cdot sin(\omega t)][cos(-kx) + i \cdot sin(-kx)] \end{aligned} \tag{2.27}$$

$$= C_T \cdot e^{i(\omega t + kx)} + C_R \cdot e^{i(\omega t - kx)} \tag{2.28}$$

where:

ω = angular frequency ($\omega = 2\pi/T = 2\pi f$),

T = period,

f = frequency,

k = wave number ($= 2\pi/\lambda$),

λ = wavelength,

$i = \sqrt{-1}$,

C_T = amplitude of the forward propagating wave which describes the transmitted longitudinal wave, and

C_R = amplitude of the backward propagating wave which describes the reflected wave.

In conclusion, they (Richart et al., 1970) derived the relationship between the wave property term (ω) and the material property (i.e., E) term:

$$\frac{\omega}{k} = f \cdot \lambda = V_c = \sqrt{\frac{E}{\rho}} \tag{2.29}$$

where:

V_c = unconstrained compression wave velocity.

Lastly, the typical shear moduli of various engineering materials are shown in Table 2.1.

Table 2.1: List of Young's Moduli of Various Materials (Matweb.com, 2007)

Material	**Young's Modulus (E) GPa**	**Young's Modulus (E) lb/in^2**
Rubber (small-strain)	0.01 - 0.1	1,500 - 15,000
Polypropylene	1.5 - 2	217,000 - 290,000
Oak Wood (along grain)	11	1,600,000
High-strength concrete (under compression)	34	5,000,000
Magnesium metal (Mg)	45	6,500,000
Sandstone	4.9 - 84.3	710,000 - 12,000,000
Granite	25.5 - 68.6	3,700,000 - 10,000,000
Aluminum alloy	69	10,000,000
Glass (all types)	72	3,900,000
Brass and bronze	103	5,570,000
Wrought iron and steel	190 - 210	30,000,000
Tungsten (W)	400 - 410	58,000,000
Diamond (C)	1,1,050 - 1,200	150,000,000 - 175,000,000

2.3.3 Torsional Shear Wave Propagation in a Solid Rod

The torsional shear wave has a similar governing equation as the longitudinal compression wave (Richart et al, 1970):

$$\frac{\partial^2 w}{\partial t^2} = \frac{G}{\rho} \times \frac{\partial^2 w}{\partial x^2} \tag{2.30}$$

where:

w = particle displacement normal to the propagating direction,

t = time,

G = shear modulus,

ρ = density of the rod material, and

x = coordinate of a particle along the x-axis.

The solution of the Equation 2.30 has the same complex form as the longitudinal compression wave (Richart et al, 1970):

$$w = C_T \cdot e^{\,i(\omega t + kx)} + C_R \cdot e^{\,i(\omega t - kx)} \tag{2.31}$$

where:

ω = angular frequency ($\omega = 2\pi/T = 2\pi f$),

T = period,

f = frequency,

k = wave number ($= 2\pi/\lambda$),

λ = wavelength,

$i = \sqrt{-1}$,

C_T = amplitude of the forward propagating wave which describes the transmitted longitudinal wave, and

C_R = amplitude of the backward propagating wave which describes the reflected wave.

They (Richart et al., 1970) also concluded the relationship between the wave property and the material property as:

$$V_s = f \cdot \lambda = \sqrt{\frac{G}{\rho}} \tag{2.32}$$

where:

V_s = shear wave velocity.

Because the shear wave is independent of lateral boundary constraints, which do not create expansion or contraction perpendicular to the direction of the wave propagation, the velocity in an unbounded medium is exactly the same as the velocity of torsional shear waves in rods.

The following equations show the two relationships between the shear modulus (G) and the unconstrained modulus (Young's Modulus, E) in a rod, and also the shear modulus (G) and the constrained modulus (M) in a half space:

$$E = G \cdot 2(1 + \nu) \tag{2.33}$$

$$M = G \cdot \frac{(2 - 2\nu)}{(1 - 2\nu)} \tag{2.34}$$

where:

ν = Poisson's ratio.

Lastly, the typical shear moduli of various engineering materials are shown in Table 2.2.

Table 2.2: List of Shear Moduli of Various Materials (Matweb.com, 2007)

Material	**Shear Modulus (G) GPa**	**Shear Modulus (G) lb/in^2**
Rubber (small-strain)	0.0003	44
Polypropylene	0.117	17000
High-strength concrete (under compression)	14	2,000,000
Magnesium metal (Mg)	16	2,360,000
Sandstone	2.0 - 35.1	290,000 - 5,000,000
Granite	10.6 - 28.6	1,500,000 - 4,148,000
Aluminium alloy	26	3,730,000
Glass (all types)	27	3,900,000
Brass and bronze	38	5,570,000
Wrought iron and steel	80	11,600,000
Tungsten (W)	156	22,600,000

2.3.4 Initial and Boundary Conditions

In the general solution of the wave equation (Equations 2.28 and 2.31), there are two undetermined coefficients: (1) C_T, the amplitude of the forward propagating wave which describes the transmitted longitudinal wave; and (2) C_R, the amplitude of the backward propagating wave which describes the reflected wave. These coefficients can be determined using the initial conditions and the boundary conditions. The initial conditions are generally given in the form of the initial displacement condition and the initial velocity condition (Richart et al, 1970):

$$u(x,t) = f(x) \tag{2.35}$$

$$\frac{\partial u(x,t)}{\partial t} = g(x) \tag{2.36}$$

where:

u = displacement at location x in time t,

x = the space coordinate,

t = the time coordinate,

$f(x)$ = the initial displacement function, and

$g(x)$ = the initial velocity function.

On the other hand, the general boundary conditions for a finite rod are generally classified into two types: "fixed" boundary condition, and "free" boundary condition. The fixed boundary condition indicates no displacement at the boundary, while the free boundary condition indicates that the first-order derivative of displacement (velocity) is zero. The following equations represent the boundary conditions as:

$$u(x,t) = 0 \qquad for\ fixed\ boundary\ condition \tag{2.37}$$

$$\frac{\partial u(x,t)}{\partial x} = 0 \qquad for\ free\ boundary\ condition \tag{2.38}$$

where x is the locations of the ends.

Accordingly, three combinations of the boundary conditions are possible: (1) fixed-fixed, (2) fixed-free, and (3) free-free. In general, only the two conditions of "fixed-free" and "free-free" are typically considered.

2.3.5 Energy Dissipation in a Single Degree of Freedom and Material Damping Ratio

The energy dissipation of a propagating wave can be represented in terms of a material damping ratio, D. In physics and engineering, material damping is often mathematically modeled as a force with a magnitude proportional to the velocity of an object but in the opposite direction. This type of damping is denoted as viscous damping. A one-dimensional damping force (F_D) due to mechanical viscous damping is represented (Richart et al, 1970) by:

$$F_D = -cv \tag{2.39}$$

where:

c = viscous damping coefficient, and

v = velocity of an object.

By considering the damping effect as a damping force, the differential equation of oscillation with damping is derived by (Richart et al, 1970) as:

$$\frac{d^2u}{dt^2} + 2D\omega_n \times \frac{du}{dt} + \omega_n^2 \, u = 0 \tag{2.40}$$

where:

u = displacement,

D = material damping ratio, which is defined as $D = c/(2\sqrt{km})$, and

ω_n = circular natural frequency in simple harmonic oscillation system, which is defined as $\omega_n = \sqrt{k/m}$.

The solution of the above equation is represented by:

$$u(t) = ce^{-\omega t} \tag{2.41}$$

where:

c = the integral constant,

ω_r = circular resonant frequency, which is defined as $\omega_r = \omega_n(D \pm \sqrt{(D^2 - 1)})$.

If the damping ratio is equal to 1.0 (which is 100%), the system is referred to critically damped. If the damping ratio is greater than 1.0, the system is referred to overdamped. Therefore, the amplitude of motion will decay exponentially (Richart et al, 1970).

2.4 SUMMARY

The general engineering concepts such as stress, strain and their relationship are important building blocks in understanding the geotechnical material properties. Stress is defined as the force per unit area of a boundary and the quantity is typically expressed by a stress tensor. Strain is a description of deformation in terms of relative displacement of particles in a body. The stress-strain relationship can be determined by measuring load and the calculating stress and by measuring deflection and the calculating strain of the body either in the laboratory or in the field.

Dynamic stiffness moduli are typically determined through the measurements of compression wave velocities (e.g., V_C and V_P) and shear wave velocity (V_S). Material damping ratio is defined as the energy dissipation ratio per one cycle of vibration motion.

Chapter 3

Methodology of the Dynamic Torsional Resonant Column (RC) Test

3.1 INTRODUCTION

In this chapter, an overview of the dynamic torsional resonant column (RC) is discussed. The methodology followed in determining dynamic soil properties from RC testing is also discussed. The RC test is a robust way to determine dynamic properties such as shear modulus, G, and material damping ratio, D, of sandy and gravelly soils, hence, the reason for using RC testing to evaluate the binary and gap-graded granular soils.

In Section 3.2, the general information about the RC equipment is presented. A methodology of analyzing the results from the RC test is outlined in Sections 3.3 and 3.4.

3.2 OVERVIEW OF DYNAMIC TORSIONAL RESONANT COLUMN EQUIPMENT

3.2.1 General Information

The dynamic torsional resonant column (RC) device was developed over several decades by Professor Stokoe and his graduate students (Isenhower, 1979; Lodde, 1982; Ni, 1987; and Kim, 1991) at the Soil and Rock Dynamics

Laboratory at the University of Texas at Austin. This dynamic testing device has evolved and been innovated for increased capabilities and accuracy (Menq; 2003 [26] and Keene; 2017 [19]).

The RC test is an efficient way of measuring dynamic material properties such as shear modulus (G) and material damping ratio in shear (D) of all types of soils and rocks. This device can perform a variety of testing with using a single specimen. This testing includes: (1) time-dependency testing (small-strain testing), (2) stress-dependency testing (changing of confining pressure testing), and (3) strain-dependency testing (nonlinear strain testing). The RC equipment is composed of four systems: (1) a confining system (isotropic and anisotropic confinement conditions), (2) a driving system (torsional excitation), (3) a height-change monitoring system, and (4) a response monitoring system. The overall device is controlled by a microcomputer system with automated data acquisition and processing (Keene, 2017 [19]).

3.2.2 RC Confining System

The confining system consists of an outer cylinder (diameter-8.5 in. and height-18.0 in.), two end plates (a top and a base), and either four or six vertical rods that connect and secure the cylinder and end plates (Figure 3.1). All components of this confining system were manufactured using stainless steel. The stainless steel prevents the possibility of magnetic interactions between the confining system and the magnets attached to the drive plate in the drive system. This confining system is capable of handling pressures up to 450 psi

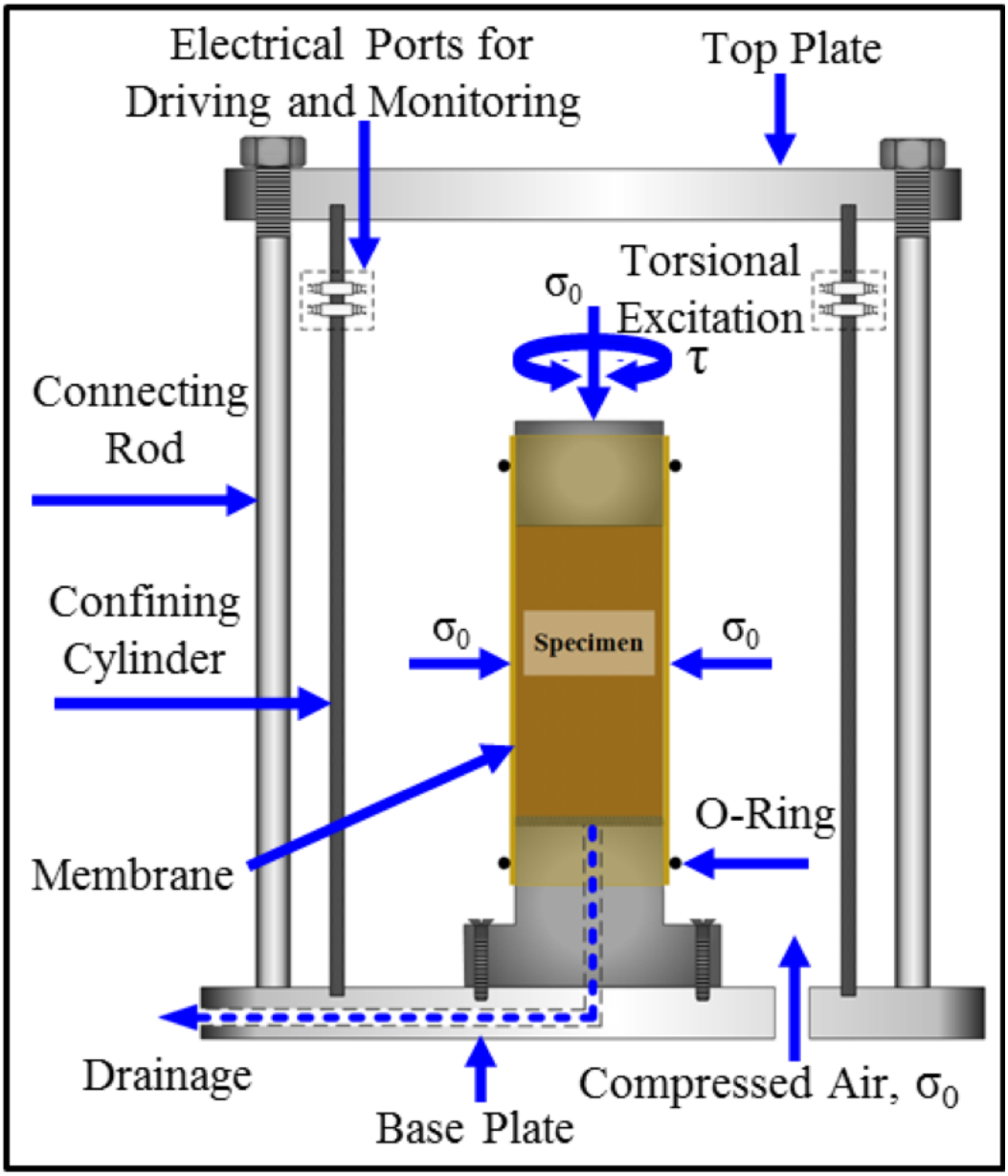

Figure 3.1: Simplified Configuration of RC Confining System (Keene, 2017)

(30.6 atm). The pressure inside of the cell is regulated using either a Fairchild model 30 regulator from 2 to 90 psi or a Tescom 44-2200 model regulator from 80 to 450 psi. For pressures between 2 to 90 psi (relatively low pressures), the building air supply is used as the confining pressure. At higher pressures ranging from 80 up to 450 psi, nitrogen gas from a high-pressure "bottle tank" is used. It is always important that great care is to be taken in managing these pressures.

Before placing the outer confining cylinder on the base plate, a metal base pedestal is fixed with 4 to 6 screws onto the bottom plate. Once the reconstitution of a specimen is done, a top cap with the same diameter as the specimen is placed. For isotropic confinement, a membrane is placed around the outside of the specimen. The membrane extends over portions of the top cap and base pedestal. Vacuum grease and O-rings are used on the top cap and base pedestal to seal the specimen inside the membrane and from the confining air pressure. It is important to note that the vertical stress on the specimen is slightly larger (less than about 0.15 psi for a 2.8-in. diameter solid specimen) than the horizontal stress due to the combined weight of the top cap and the driving system

During testing in this research effort, the pore water or pore air pressure inside the specimen was vented to room pressure through a drainage line so that no positive pore water pressure was generated.

3.2.3 RC Driving System

The main components of the driving system are: (1) a four-armed aluminum drive plate, (2) four permanent rectangular magnets, and (3) eight drive coils arranged in sets of two drive coils associated with each magnet. As shown in Figure 3.2, the drive plate is carefully attached to the top cap with four bolts so that there is no slippage between the top cap and the drive plate. Each set of drive coils consists of two elliptical drive coils, one coil that surrounds each end of the permanent magnet. The four permanent magnets are securely attached to the four arms of the drive plate.

The system is driven by a electrical, sinusoidal voltage signal that passes through the drive coils to generate torsional motion. Three different drive systems (drive systems Nos. 4, 5, and 9) were used in this research. The maximum torque of each system was about 0.60 lb-ft (82 N-cm). Typically, the level of torque depends on the strength of magnets, the dimensions of drive coils, the electromagnetic characteristic of drive coils, the width of gap between the magnet and drive coils, and the characteristics of the powering equipment. The operator manually assigns input voltages depending on the targeted level of strain.

In this study, a PXI 6251 DAQ module was used to perform frequency sweeps with a constant force amplitude. For high-amplitude dynamic torsional resonant column (HARC) tests, the sinusoidal input current is switched to and amplified by a power amplifier (HP 6824A) before passing to the drive coils.

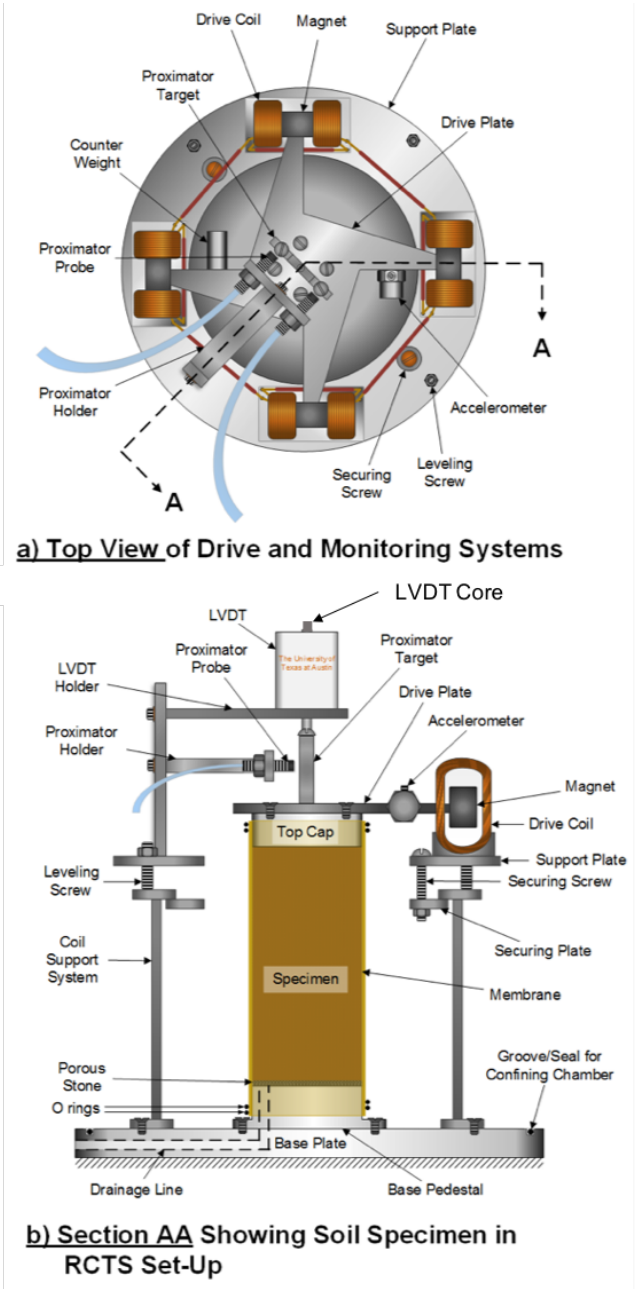

Figure 3.2: General Configuration of RCTS Equipment (Keene, 2017) (*Only the RC portion of the dynamic torsional resonant column (RC) and cyclic torsional shear (TS) device was employed in this study.)

3.2.4 Specimen Height-Change Measurement System

To monitor the height-change of the specimen due to consolidation during confinement, a linear variable differential transducer (LVDT) is used. The change in height of the specimen during testing is important because it allows an estimate of the change in void ratio and total unit weight to be made based on the assumption of isotropic strain under isotropic confinement. These values are needed in the data reduction. The height-change measurement system consists of an LVDT (Columbia Model SH-200-53R), and the PXI 4462 and PXI 6251 DAQ modules. The LVDT core is not in contact with the LVDT coil housing so that no friction occurs during RC testing.

As seen in Figure 3.2, the LVDT core rod is attached to the center of the drive plate so that the LVDT coil housing, which surrounds the core, does not physically touch the LVDT core. In this system, the PXI 4462 generates the input signal for the LVDT coil at a frequency of 500 Hz and a voltage level of 4.77 RMS volts. The output signal from the LVDT is read simultaneously with the PXI 6251 DAQ module. The height-change is calculated from the output voltage combined with the calibration factor.

3.2.5 Motion Monitoring System

In the RC test, measurements are dynamic and generally performed in the frequency range of 20 to 200 Hz. Because of these relatively high-frequency motions, an accelerometer is normally used to monitor the motions. In this case, inertia of the top cap, drive plate, and soil sample do enter the calculation

of the response. The motion signals of the torsional loading of the specimen are monitored by an accelerometer attached to the drive plate (Figure 3.2). The accelerometer signal is conditioned with a signal conditioner (i.e., a charge amplifier), as illustrated in Figure 3.3. The conditioned signal is monitored with a voltmeter and an oscilloscope in the PXI 6251 DAQ module. Finally, the microcomputer generates a dynamic response of motion vs. frequency and the strain amplitude is calculated. Based on the dynamic response curve, the resonant frequency and peak acceleration amplitude are determined, as shown in Figure 3.4. Additionally, the half-power bandwidth method is used to calculate material damping ratio at small strains while the free-vibration decay method is used at larger strains. More details about the data analysis are presented in the Section 3.3.

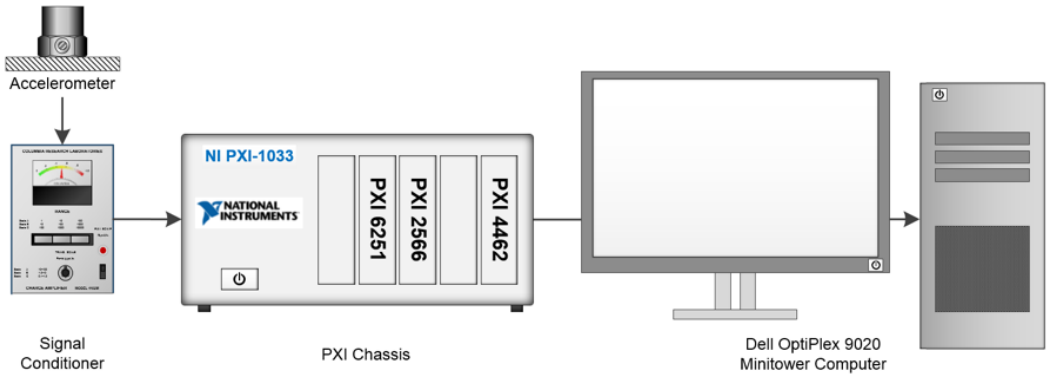

Figure 3.3: General Configuration of RC Motion-Monitoring Equipment (Keene, 2017)

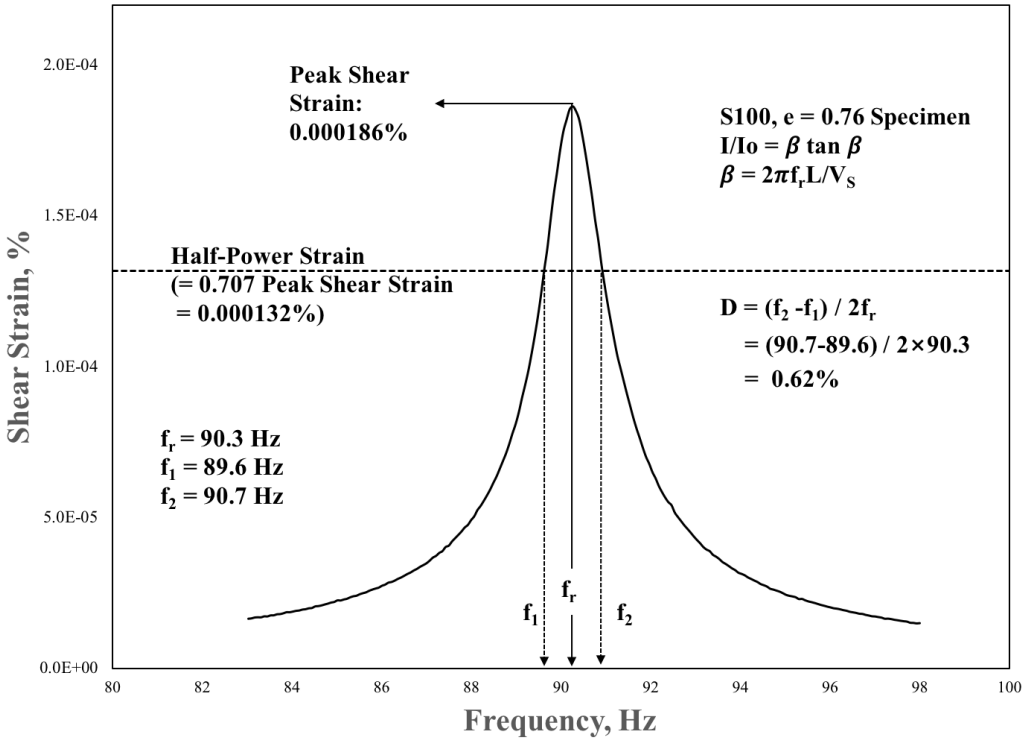

Figure 3.4: The Dynamic Response Curve Obtained in a Small-Stain Dynamic Torsional Resonant Column Test for the S100 with $e = 0.76$ Specimen Tested in this Study

3.3 OVERVIEW OF DYNAMIC TORSIONAL RESONANT COLUMN DATA ANALYSIS

3.3.1 Shear Modulus, G, Determined from RC Testing

As mentioned previously, the response of the soil specimen due to the drive plate excitation is recorded by the dynamic monitoring system (Section 3.2.5). As a result, a dynamic response curve in the frequency domain is obtained, as shown in the Figure 3.4. This response curve is one of the key measurements performed in RC testing which results in determination of

the resonant frequency of the specimen and the peak shear-strain amplitude. Normally, the shape of the dynamic response curve under small-strain loading is a symmetrical bell-shaped curve as shown in the Figure 3.4. The resonant frequency (f_r) is used to calculate a shear wave velocity with the following equation:

$$\frac{I}{I_o} = \frac{\omega_r \, l}{V_s} \, tan \, \frac{\omega_r \, l}{V_s} \tag{3.1}$$

where:

I = mass polar moment of inertia of the soil specimen,

I_o = mass polar moment of inertia of the top cap and drive system,

ω_r = circular resonant frequency ($\omega_r = 2\pi f_r$),

l = length of the soil specimen, and

V_s = shear wave velocity of the soil specimen.

The measured shear wave property (V_s) is easily transformed to the stiffness property (shear modulus, G) using the total unit weight (γ_t) of the material and gravitational acceleration (g) (as discussed in Section 2.3.3):

$$G = \rho \, (= \frac{\gamma_t}{g}) \times V_s^2 \tag{3.2}$$

where:

G = shear modulus,

ρ = mass density, and

V_s = shear wave velocity of the soil specimen.

Once the resonant frequency (f_r) and the corresponding amplitude (the output voltage of the accelerometer, A_c) are determined from the response curve, the shearing strain can be calculated using by the following two equations:

$$\gamma = r_{eq} \times \frac{\theta_{max}}{L} \tag{3.3}$$

where:

γ = shearing strain,

r_{eq} = equivalent radius, and

θ_{max} = angle of twist at the top of the specimen (degrees)

$$\theta_{max} = \frac{A_c \; T_r^2}{4\pi^2 \; CF} \times \frac{1}{D_{ac}} \tag{3.4}$$

where:

A_c = output voltage of accelerometer (volts),

T_r = resonant period (seconds),

CF = accelerometer calibration factor (volts/in./sec^2), and

D_{ac} = accelerometer displacement (inches).

Chen and Stokoe (1979) [9] studied the radial distribution of shearing strain. They found that approximately 82% of the outer specimen diameter (r_o) value was appropriate for an effective radius (r_{eq}) for peak shearing strain (γ_{max}) $< 0.001\%$. They also recommended 79% of the r_o value for $\gamma_{max} > 0.1\%$. However, for simplicity, the recommendation of 82% of the r_o value was used for all strain levels in this research.

3.3.2 Equivalent-Viscous Material Damping Ratio, D: Measurements in the Linear Strain Range

The material damping ratio of the specimen is also determined from the response curve using the half-power bandwidth method, but only for testing conducted in the linear range as shown in Figure 3.4. The theoretical relationship is (Van Hoff, 1993):

$$D = \frac{f_1 - f_2}{2f_2} \tag{3.5}$$

where:

$f_{1,2}$ = the lower and upper frequencies at which the shear strain amplitude is equal to the half-power peak amplitude ($0.707A_{max}$),

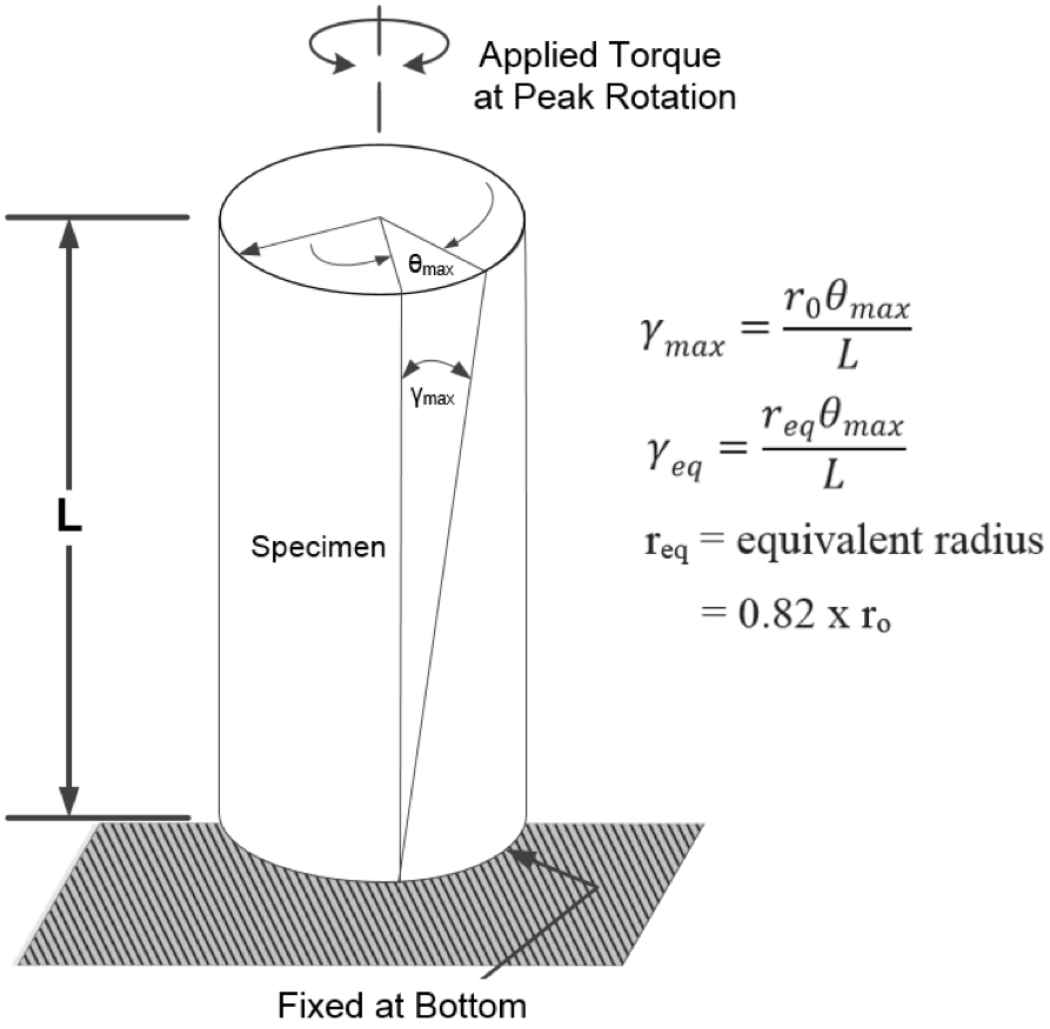

Figure 3.5: Shearing Strain of a Specimen in RC Testing

f_r = the resonant frequency of the specimen, and

A_{max} = the peak amplitude at f_r.

Furthermore, the material damping ratio at the small strain can also be obtained from the free-vibration-decay curve as illustrated in Figure 3.6. The measurement is performed separately from the frequency sweeping tests (response curve analysis in Figure 3.4). After finishing the frequency sweeping tests, the drive plate is excited at the resonant frequency determined from the response curve with the output voltage at which the peak shear strain was measured. The excitation level is continued until steady-state motion is achieved, and then the system power is suddenly shut off as can be seen in Figure 3.6a. The specimen then vibrates freely, and the free-vibration decay is recorded. The decay of shearing strain amplitude during this free-vibration occurs naturally. The decay from three (or more) successive strain amplitudes of motion is used to calculate the logarithmic decrement (δ):

$$\delta = \frac{1}{n} ln \frac{z_1}{z_{n+1}} \tag{3.6}$$

where:

z_1 and z_{n+1} = the successive strain amplitudes of free-vibration motion.

In Figure 3.6b, the log shear strain amplitude is shown versus the number of cycles of the free-vibration motion in the small-strain range. From the

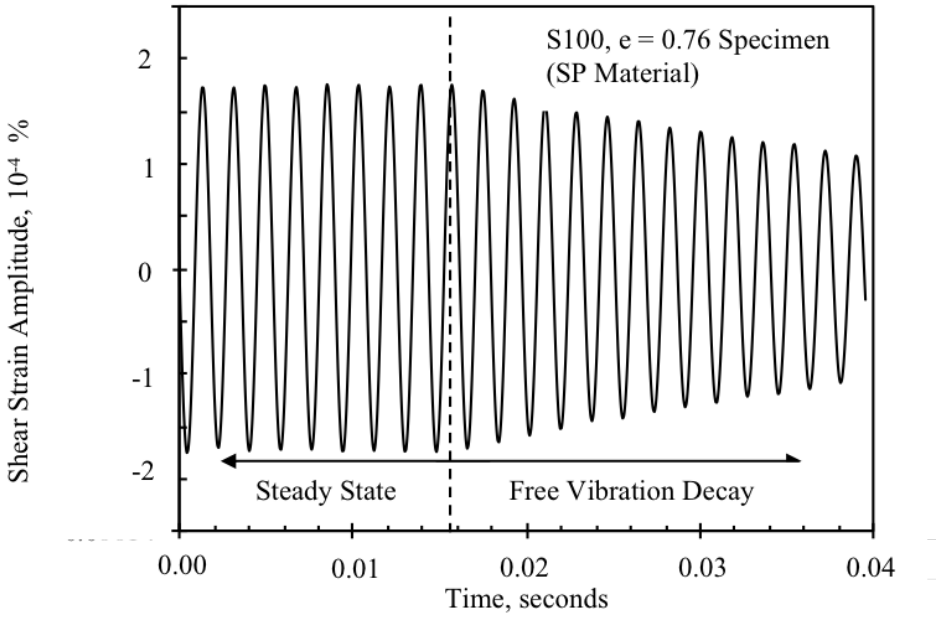

(a) The Steady State and Free Vibration Decay

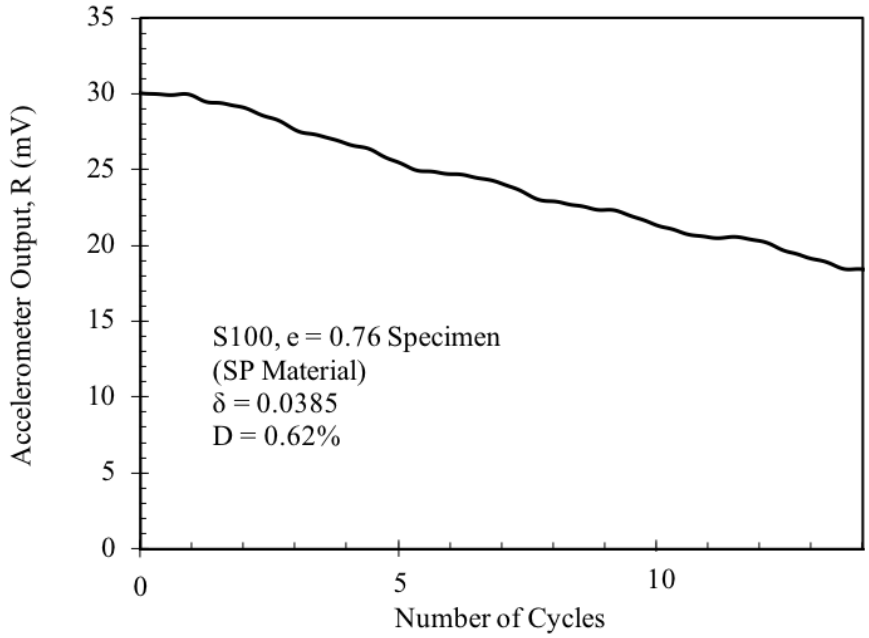

(b) The Log Decrement Evaluation

Figure 3.6: Material Damping Ratio Measurement in RC testing using the Free-Vibration Decay Method for a Poorly-Graded Specimen Tested in this Study (the S100 with $e = 0.76$ Specimen)

log decrement, the material damping ratio (D) is calculated as follows:

$$D = \sqrt{\frac{\delta^2}{4\pi^2 + \delta^2}} \tag{3.7}$$

Background noise during testing can be an issue in measuring material damping ratios using the free-vibration decay method at very small strains. (Small strains are generally less than 0.0003% (Keene, 2017) [19].) On the other hand, the background noise for the strain level less than 0.0003% typically has a minor effect on measuring the frequency response curve. Therefore, the half-power bandwidth method is strongly preferred for measuring small-strain material damping ratios.

3.3.3 Equivalent-Viscous Material Damping Ratio, D: Measurements in the Nonlinear Strain Range

In the nonlinear strain range, symmetry in the frequency response curve is no longer maintained, and a serious error can be introduced by the half-power bandwidth method (Ni, 1987 [27]). Therefore, it is more reliable to use the free-vibration decay method discussed in the previous section for determining the material damping ratio of soils and rocks in the nonlinear range.

In Figures 3.7a and 3.7b, the frequency response curve and free-vibration decay curve in the nonlinear range for a poorly-graded sand specimen tested in study (the Specimen of S100 with $e = 0.76$) are presented, respectively. As can be seen in the Figure 3.7a, the frequency response curve is highly asymmetric

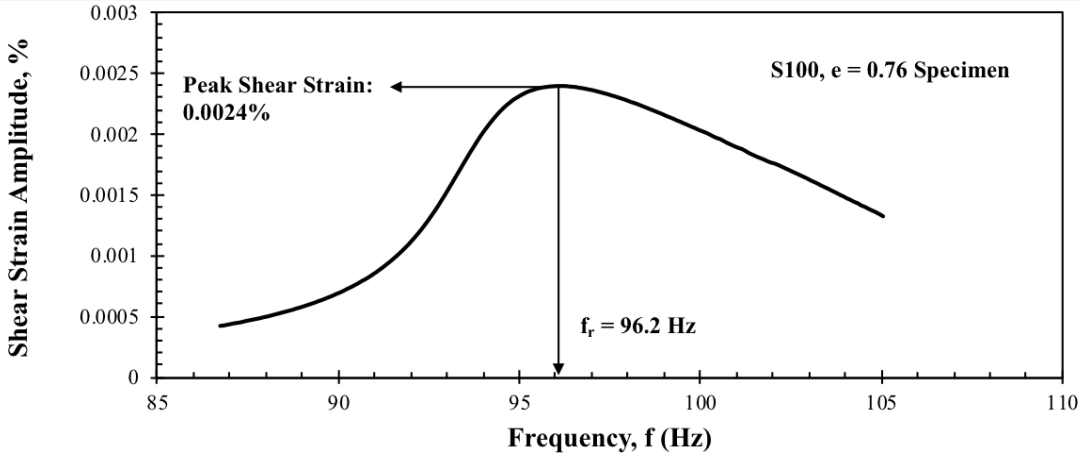

(a) Frequency Response Curve in the Nonlinear Range

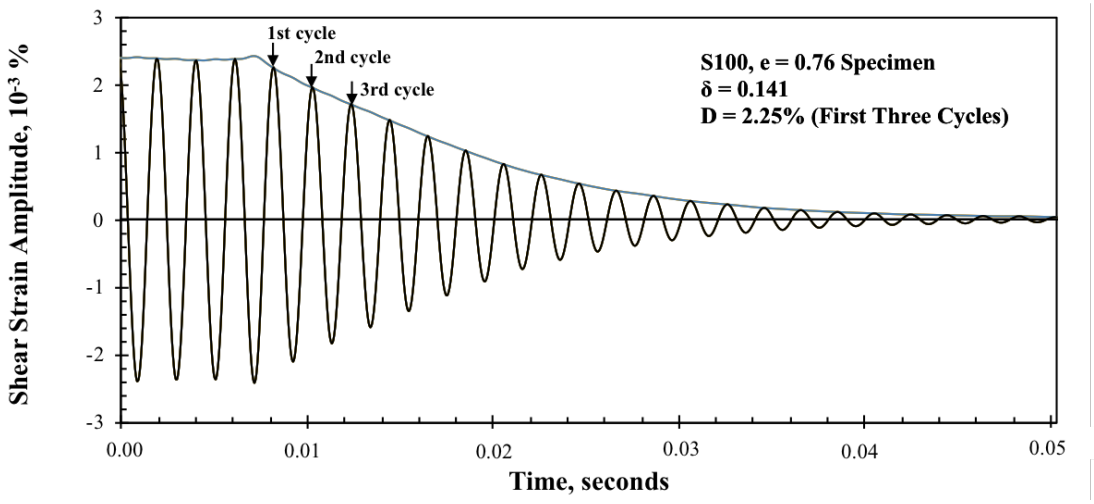

(b) Free Vibration Decay Method in the Nonlinear Range

Figure 3.7: Material Damping Ratio Measurement in RC testing using the Free-Vibration Decay Method for a Poorly-Graded Specimen Tested in this Study (S100 with $e = 0.76$)

so that the half-power bandwidth method is no longer reliable for the material damping ratio measurements. Therefore, the free-vibration decay method is used to measure material damping ratio in the nonlinear range with the same methodology for the small-strain analysis described in Section 3.3.3. For the calculation of material damping ratio in the nonlinear range using the free-vibration decay method, the shear strain amplitudes of the first three cycles are used to determine the logarithmic decrements (Figure 3.7b).

3.4 SUMMARY

The dynamic torsional resonant column (RC) device are used to measure both shear modulus and material damping ratio in both linear and nonlinear ranges in this research. An overview of the equipment and data analysis procedures is presented in this chapter before discussing the material tested and the test results. The RC test is based on the one-dimensional wave equation derived from the theory of elasticity. The shear modulus is obtained by measuring the first-mode resonant frequency while material damping is evaluated from either the free-vibration decay curve or from the width of the frequency response curve assuming viscous damping. Material damping ratio in the nonlinear range is only measured from the free-vibration decay method due to the background noise.

Chapter 4

Review of Literature Related to Sandy and Gravelly Soils and Binary Mixtures

4.1 INTRODUCTION

In this chapter, literature associated with three aspects of this research are reviewed. In Section 4.2, factors that affect the dynamic properties (i.e., shear modulus, G, and material damping ratio in shear, D) of sandy and gravelly soils in the small-strain range are first discussed. Small-strain range is defined as the strain amplitude that is lower than $10^{-4}\%$ in this chapter that is well accepted in the published literature (Menq, 2003 [26]). Factors that affect the dynamic properties of sandy and gravelly soils in the nonlinear range are then discussed in the Section 4.3. Recommended curves suggested by Darendeli (2001) [11], and numerical models of nonlinear dynamic properties proposed by other researchers are also presented in Section 4.3 In Section 4.4, maximum and minimum void ratios of mono-spherical particles and "ideal binary packing models" are introduced and briefly derived. The two ideal packing conditions, "fine packing", which is also called Small-Particle-Packing Dominated (SPPD) condition in this research, and "coarse packing", which is also called Large-Particle-Packing Dominated (LPPD) condition in this research, induce the important theoretical concept of the critical packing condition to understand

and classify binary mixtures based on the packing conditions. The concept of critical packing condition and the associated quantities are discussed in the Section 4.4.

4.2 SMALL-STRAIN DYNAMIC PROPERTIES OF SANDY AND GRAVELLY SOILS

4.2.1 Effects of Void Ratio and Isotropic Confining Pressure on G_{max} and D_{min} of Sandy and Gravelly Soils

In the geotechnical and earthquake engineering fields, the small-strain range is the range of shear strain amplitudes over which the dynamic properties of soils are constant. The general dynamic properties of soils and rocks most often considered are shear modulus, G, and material damping ratio in shear, D. In the small-strain range, the shear modulus (G) is constant with the maximum value and the material damping ratio in shear (D) is constant with the minimum value. The dynamic properties (G and D) in the small-strain range are called G_{max} (or G_o) and D_{min}, respectively.

As strain increases beyond the small-strain range, the value of G begins to decrease and the value of D begins to increase. The variations of these dynamic soil properties with shear strain amplitude is termed the nonlinear behavior or nonlinearity. And the shear strain boundary between linear (i.e. small-strain range) and nonlinear strain range is referred to elastic threshold shear strain, γ_t^e. The value of the elastic threshold shear strain (γ_t^e) varies depending on the characteristics of the materials. Generally, the γ_t^e values of soils are determined by dynamic testing such as dynamic torsional resonant

column (RC) and cyclic torsional shear (TS) tests in the case of the combined RCTS system at UT.

Hardin and Richart (1963) [16] performed dynamic RC tests to investigate the shear modulus of reconstituted sandy soils in the small-strain range. From their investigation, they suggested a generalized equation for G_{max} as:

$$G_{max} = C_G \; F(e) \; (\sigma'_o)^{n_G} \tag{4.1}$$

where:

C_G and n_G = constants depending on materials,

$F(e)$ = an empirical function of void ratio, e, and

σ'_o = effective isotropic confining pressure.

As seen in Equation 4.1, Hardin and Richart (1963) [16] found that the small-strain shear modulus (G_{max}) of sandy soils is mainly a function of void ratio, $F(e)$, and effective isotropic confining pressure, σ'_o.

Traditionally, the following F(e) forms have been frequently used:

$$F(e) = \frac{(2.973 - e)^2}{1 + e} \quad \textit{Hardin and Black} \; (1968) \tag{4.2}$$

$$F(e) = 1/(0.3 + 0.7e^2) \quad \textit{Hardin} \; (1978) \tag{4.3}$$

Hardin and Black (1968) also proposed that the small-strain shear modulus is proportional to the half-power of effective isotropic confining pressure for most clean sands; hence, the n_G value of 0.5 has been frequently used for the stress exponent term (n_G) for granular sand materials in Equation 4.1.

In Table 4.1, various void ratio functions ($F(e)$) and associated stress exponent values (n_G) proposed for different types of soils are presented. As seen in the table, the empirical void ratio functions can be classified into two groups: (1) hyperbolic functions, and (2) exponential functions. On the basis of the information in the Table 4.1, no universal void ratio function was observed that can be utilized over a wide range of materials.

Table 4.1: Various Void Ratio Functions ($F(e)$) and Stress Exponent Values (n_G) for Use with Equation 4.1 (Modified from Menq, 2003 and Mitchell and Soga, 2005)

Reference	**Soils**	**Void ratio**	**F(e)**	n_G
Hardin & Richart (1963),	Ottawa sand	0.37-0.78	$(2.174\text{-e})^2(1+e)^{-1}$	0.50
Hardin & Black (1966)	Crushed quartz	0.63-1.26	$(2.973\text{-e})^2(1+e)^{-1}$	0.50
Hardin & Black (1968)	NC Kaolinite	0.76-0.90	$(2.973\text{-e})^2(1+e)^{-1}$	0.50
Hardin & Black (1969)	A few soils	0.59-1.98	$(2.973\text{-e})^2(1+e)^{-1}$	0.50
Hardin & Drnevich (1972)	A few soils	0.57-0.98	$(2.973\text{-e})^2(1+e)^{-1}$	0.50
Marcuson & Wahls (1972)	Kaolinite	1.1-1.31	$(2.973\text{-e})^2(1+e)^{-1}$	0.50
	Bentonite	1.61-2.48	$(4.4\text{-e})^2(1+e)^{-1}$	0.50
Hardin (1978)	-	-	$(0.3+0.7e^2)^{-1}$	0.50
Iwasaki et al. (1978)	clean sands		$(2.17\text{-e})^2(1+e)^{-1}$	0.38
Kokusho (1980)	Toyoura		$(2.17\text{-e})^2(1+e)^{-1}$	0.50
Yu and Richart (1980)	clean sands		$(2.17\text{-e})^2(1+e)^{-1}$	0.50
Prange (1981)	Ballast		$(2.97\text{-e})^2(1+e)^{-1}$	0.38
Kokusho and Esashi (1981)	Crushed rock		$(2.17\text{-e})^2(1+e)^{-1}$	0.55
	Round gravel		$(2.17\text{-e})^2(1+e)^{-1}$	0.60
Kokusho et al. (1982)	NC clay	1.73-3.86	$(7.32\text{-e})^2(1+e)^{-1}$	0.60
Athanasopoulos & Richart (1983)	Powdered Kaolinite	0.9-1.2	$(0.3+0.7e^2)^{-1.361}$	0.49
Tanaka et al. (1987)	NC clay	1.73-3.86	$(2.17\text{-e})^2(1+e)^{-1}$	0.60
Goto et al. (1987)	NC clay	1.73-3.86	$(2.17\text{-e})^2(1+e)^{-1}$	0.85
Lo Presti et al. (1993)	Ticino sand	0.61-0.8	$(2.27\text{-e})^2(1+e)^{-1}$	0.43
	Pisa clay	0.8-1.8	$e^{-1.43}$	0.44
	Garigliano clay	0.9-1.2	$e^{-1.11}$	0.58
	Fucino clay	1.6-3.0	$e^{-1.52}$	0.40
	Montalvo di Castro clay	0.6-0.8	$e^{-1.33}$	0.40
	Avezzano clay	1.0-1.8	$e^{-1.27}$	0.46
Shibuya & Tanaka (1996)	In-situ slight OC clay	1.3-4.5	$e^{-1.5}$	0.50
Shibuya et al. (1997)	Natural sediment	1.0-6.0	$(1+e)^{-2.4}$	0.50
Lo Presti et al. (1997)	Toyoura sand	0.81-0.98	$e^{-1.3}$	0.45
	Quiou sand	0.84-1.18	$e^{-1.3}$	0.62
Wichtmann & Triantafyllidis (2004)	Fine, medium sands	0.57-0.76	$(1.46\text{-e})^2(1+e)^{-1}$	0.42

*Note: Equation 4.1 - $G_{max} = C_G\ F(e)\ (\sigma'_o)^{n_G}$

Some researchers such as Digby (1981), Walton (1987), and Chang et al. (1991), etc. have used 'stress-strain' (or 'force-displacement') approach combined with Hertz-Mindlin contact theory to calculate G_{max} as a function of void ratio for a random packing of spheres. They assumed that displacement of every particle in a packing follows a uniform displacement field. This approach is referred to as the effective medium theory (Makse, 2004) [25]. For example, Chang et al. (1991) [6] applied this model to the small-strain case, where tangential forces do not exceed the frictional strength at contacts, and proposed the following equation:

$$G_{max} = \frac{5-4\nu}{10-5\nu}\left[\sqrt{\frac{2}{3}}\frac{N_c}{\pi(1-\nu)}\right]^{2/3}\left[\frac{1}{(1+e)}\right]G_{grain}{}^{2/3}\ \sigma_o'{}^{2/3} \tag{4.4}$$

where:

G_{grain} = shear modulus of particles,

ν = Poisson's ration of particles,

σ_o' = effective isotropic confining pressure,

N_c = coordination number (average number of contacts per spherical particle), and

$N_c = 13.28 - 8e$.

If the effect of void ratio on coordination number (e.g., Equation 4.4) is taken into account, a different void ratio function may be taken as:

$$F(e) = \left(\frac{13.28 - 8e^{2/3}}{1+e} \right) \tag{4.5}$$

It is easy to see that Equation 4.5 is quite different from the empirical void ratio functions presented in Table 4.1, and therefore may not represent the effect of void ratio on G_{max} of soils in practice (Bui et al., 2010 [5]).

The small-strain material damping ratio in shear, D_{min}, has been difficult to measure accurately due to background noise and equipment-generated damping which has often not been taken into account. In spite of those difficulties, Laird (1994) [24] suggested that the value of D_{min} could be determined by:

$$D_{min} = C_D F(e)(\sigma'_o)^{n_D} \tag{4.6}$$

where:

D_{min} = small-strain material damping ratio in shear,

C_D = dimensionless material damping ratio coefficient,

n_D = effective isotropic stress exponent, and

$F(e) = 1/(0.3+0.7\mathrm{e}^2)$ for granular materials.

Equation 4.6 indicates that the effective isotropic confining pressure and void ratio function play significant roles in determining the values of material damping ratios in shear as well as in determining the values of shear modulus in the small-strain range.

4.2.2 Effect of Grain Size Distribution on G_{max} and D_{min} of Sandy and Gravelly Soils

Grain size distribution is historically well known as one of key factors on the small-strain dynamic behavior of sandy and gravelly soils (Ishihara 1996 [17]). Often the gradation curve (i.e., as a result of sieve analysis) of a soil is characterized by median grain size, D_{50}, uniformity coefficient, C_u, and curvature coefficient, C_c. These gradation characteristics of D_{50}, C_u, and C_c. are determined by the USCS definitions: (1) D_{50} is the grain diameter at 50 percent passing, (2) $C_u = D_{60}/D_{10}$, where D_{60} is the grain diameter at 60 percent passing and D_{10} is the grain diameter at 10 percent passing, and (3) $C_c = D_{30}^2/(D_{10} \times D_{60})$, where D_{30} is the grain diameter at 30 percent passing. It should be noted that, as shown in this study, the curvature coefficient (C_c) can also be an important factor, but this factor has received little attention in soil dynamics.

Hardin and Richart (1963) [16] concluded that the effects of D_{50} and C_u for sandy soils were included in the effect of void ratio on the dynamic properties. The relationships of the grain size distribution characteristics (D_{50} and C_u) with the dynamic properties were extensively studied by Menq (2003)

[26].

Menq (2003) [26] tested 59 reconstituted gravelly and sandy soils using combined dynamic torsional resonant column and cyclic torsional shear test (RCTS) devices as well as large, free-free, large-scale RC device in the Soil and Rock Dynamics Laboratory at the University of Texas at Austin. He modified the equation of Hardin and Richart (1963) (Equation 4.1) and suggested that the modified equation, which can be expressed as:

$$G_{max} = C_{G3}\ {C_u}^{\ b1}\ e^x\ (\frac{\sigma_o}{Pa})^{\ n_G} \tag{4.7}$$

where:

C_{G3} is the G_{max} at 1 atm, C_u = 1.0, and e=1.0,

b1 = -0.20,

$x = -1 - (D_{50}/20)^{0.75}$,

$n_G = 0.48 \times {C_u}^{\ 0.09}$, and

P_a = atmosphere pressure (1 atm).

In Equation 4.7, the effect of D_{50} is taken into account in the exponent component of void ratio, x. Additionally, C_u affects both the value of G_{max} at one atmosphere (A_G) and the sensitivity of confining pressure change on the G_{max} (n_G).

Menq (2003) [26] also found that the G_{max} of a well-graded gravel is generally about 1.5 times higher than that of a poorly-graded sand. This finding indicates that the decrease in uniformity and increase in the median grain size mainly cause the increase in G_{max}. Moreover, he noted that G_{max} of a well-graded gravel increases more rapidly than that of a poorly-graded sand as confining pressure increases. For material damping ratio in his model, the D_{min} value of a well-graded gravel is lower than that of a poorly-grade find sand due to the effect of particle size, likely due to the increase in number of particle contacts. Comparisons of the relationships on the dynamic properties and the factors affecting the dynamic properties such as D_{50}, C_u and e between a poorly-graded fine sand (SP) and a well-graded gravel (GW) as well as gradation curves of both soils are presented in Figure 4.1.

4.3 NONLINEAR DYNAMIC BEHAVIOR OF SANDY AND GRAVELLY SOILS

4.3.1 General Background of Nonlinear Behavior of Granular Soils

The generalized variations of normalized shear modulus and material damping in shear are presented in semi-logarithmic scales as shown in Figure 4.2. In the figure, the y axis, which represents either G/G_{max} or D, is an arithmetic scale, and the x axis, which represents the shear strain, γ, is a logarithmic scale. In Figure 4.2 (a), a typical G/G_{max} - log γ curve is presented. In Figure 4.2 (b), a typical D - log γ curve is presented. As can be seen, the normalized shear modulus with shearing strain, G/G_{max} - log γ relationship (or

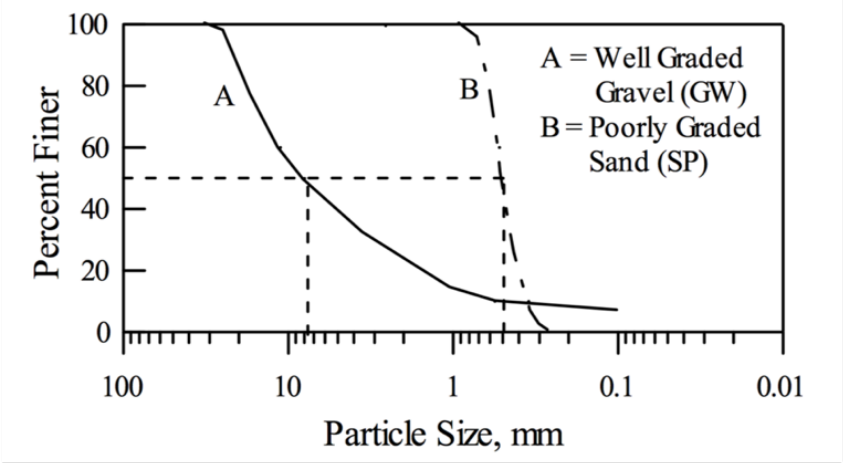

(a) Gradation Curves of GW and SP Soils

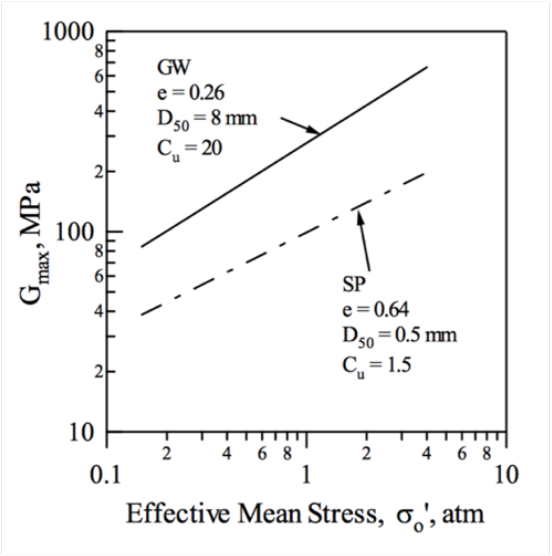

(b) Log G_{max} – log σ_o' Relationships of GW and SP Soils

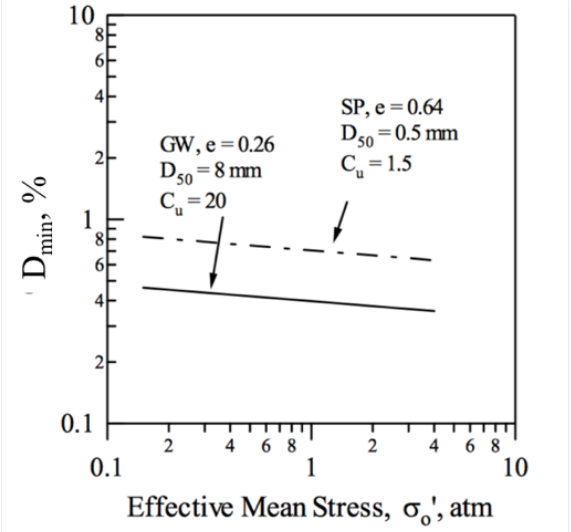

(c) Log D_{min} – log σ_o' Relationships of GW and SP Soils

Figure 4.1: Comparisons of Gradation Curves and Dynamic Properties for Dense Specimens of a Poorly-Graded Sand (SP) and a Well-Graded Gravel (GW), (from Menq, 2003)

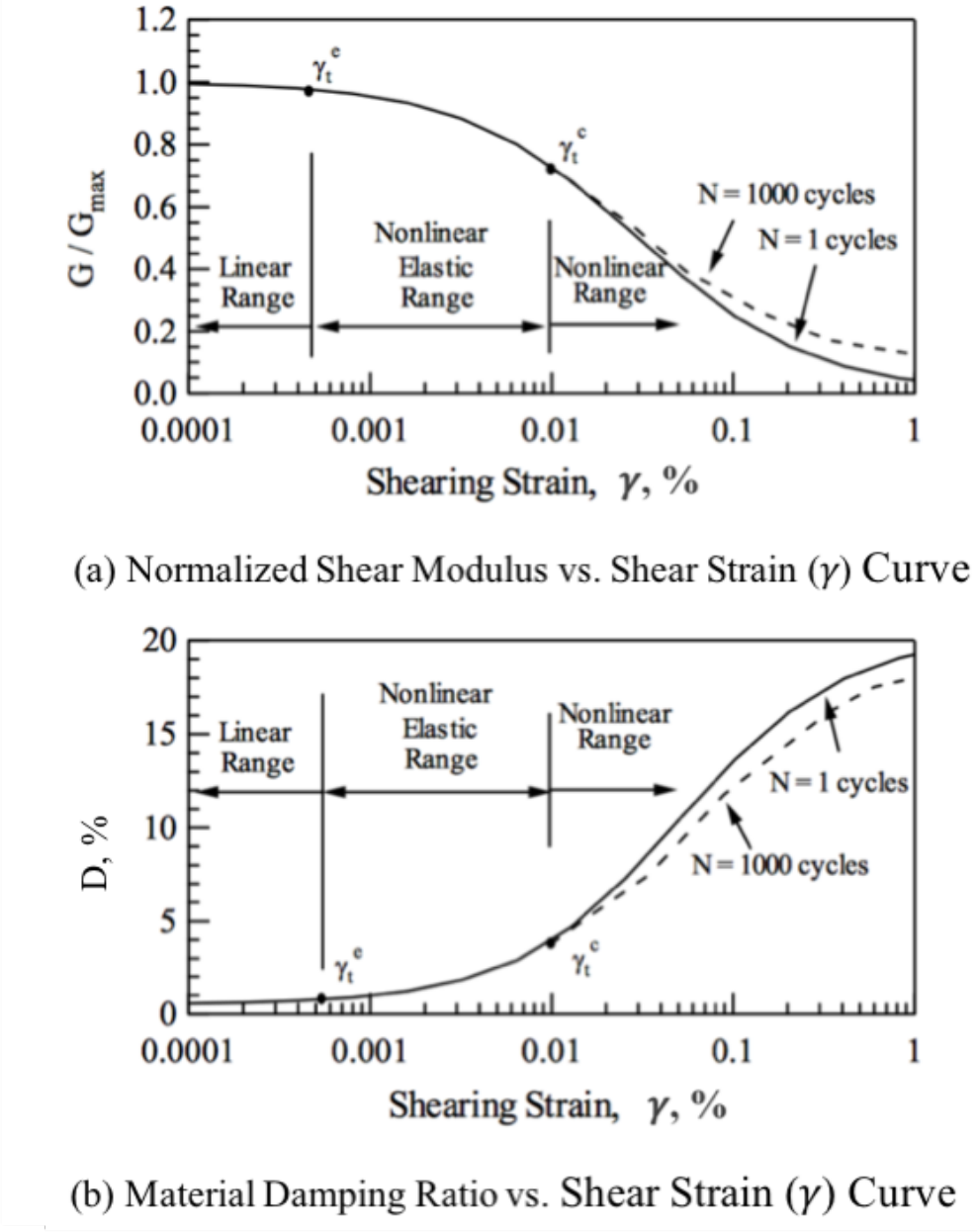

Figure 4.2: Typical Nonlinear G/G_{max} - log γ and D - log γ Relationships

the material damping ratio in shear with shearing strain, D - $\log \gamma$ relationship) is divided into three ranges as: (1) the linear range; (2) the "nonlinear elastic" range, and (3) the nonlinear range. The boundary between the linear and "nonlinear elastic" ranges is the elastic threshold strain, γ_t^e, and the boundary between "nonlinear elastic" and nonlinear ranges is the cyclic threshold strain, γ_t^c.

As seen in the Figure 4.2 (a), at $\gamma \leq \gamma_t^e$ the shear modulus is at a maximum value, denoted as the small-strain shear modulus, G_{max}, so that the normalized shear modulus (G/G_{max}) equals to 1.0 in the linear range. The material damping ratio in shear is at a minimum value, denoted as the small-strain material damping ratio in shear (D_{min}) at strain amplitudes lower than the elastic threshold strain (γ_t^e). In the "nonlinear" strain range, $\gamma_t^e < \gamma < \gamma_t^c$, the normalized shear modulus decreases and material damping ratio increases with increasing shearing strain. However, both shear modulus and material damping ratio in shear are essentially unaffected by number of loading cycles in the nonlinear elastic range. (On the other hand, both G and D are affected by loading frequency which is ignored in this discussion.)

As strain amplitude exceeds the cyclic threshold, γ_t^c, both shear modulus and material damping ratio in shear are strongly affected by strain amplitude and are functions of number of loading cycles. This strain range is called the nonlinear range. For dry granular soils of moderate densities, shear modulus increases (harden) and material damping ratio in shear decreases with an increasing number of loading cycles as the shearing strain exceeds γ_t^c. It

should be noted that soils behave nonlinearly in both the "nonlinear elastic" and nonlinear ranges. These two ranges are often referred to as the "nonlinear range" in the literature.

4.3.2 Effects of Effective Confining Pressure and Gravel Content on G and D

Tanaka et al. (1987) [32] tested a reconstituted gravelly soil to investigate the nonlinear behavior of gravelly soils. They found that the effective isotropic confining pressure and gravel content both affected the G/G_{max} - log γ and D - log γ relationships as shown in Figure 4.3. As the confining pressure increases, gravelly soils behave more linearly for both normalized shear modulus and material damping ratio, just as sandy soils do. The nonlinearity in these soils increases as the gravel content increases as seen by comparing Figure 4.3a and Figure 4.3b.

When it comes to comparison of nonlinearity, the concept of reference strain, γ_r, is very useful. Reference strain, γ_r, is the strain at which the G/G_{max} is 0.5. Reference strain (γ_r) was first clearly shown by Darendeli (2001) [11] for sands, silts, and clays and by Menq (2003) [26] for gravelly soils. Seed et al. (1986) [29] suggested that the nonlinear dynamic behavior of sandy soils is less than that of gravelly soils as shown in Figure 4.4. In the figure, the reference strain values of the mean G/G_{max} – log γ curves for sandy and gravelly soils are 0.036 % and 0.012 %, respectively. This trend agrees well with the overall trend by Tanaka et al. (1987) [32]; that is, the soils with less gravel content

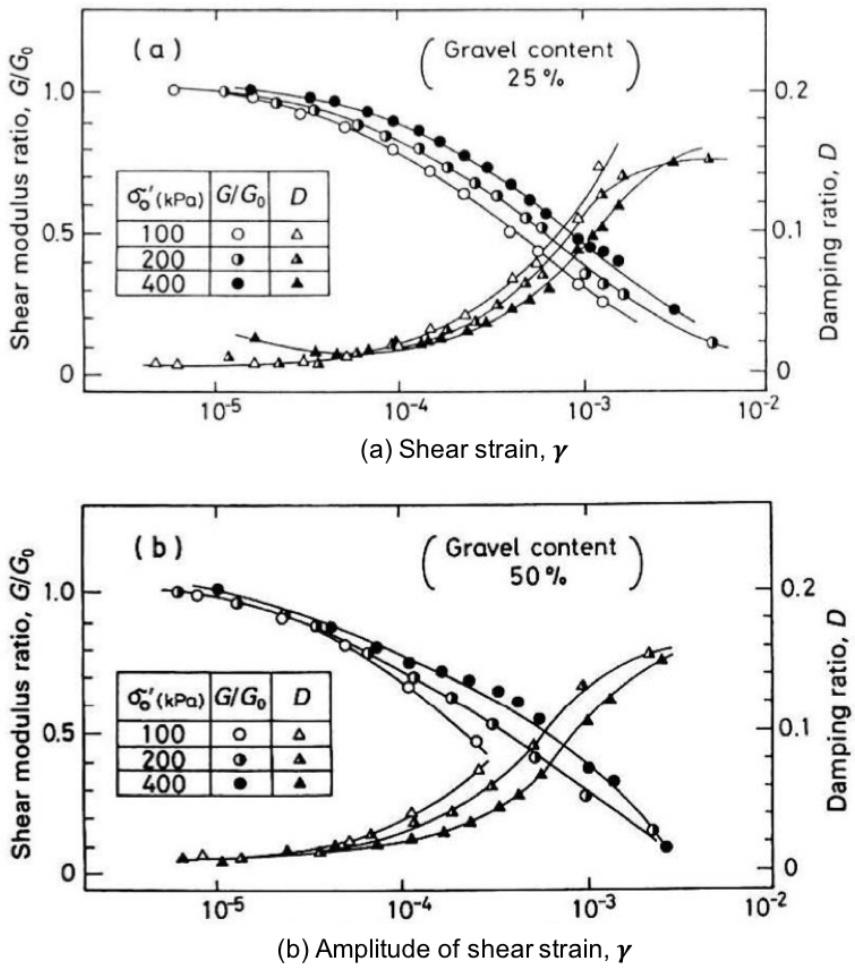

Figure 4.3: Comparisons of the Effects of Effective Isotropic Confining Pressure and Gravel Content on G/G_{max} – $\log \gamma$ and D – $\log \gamma$ Curves of Reconstituted Gravelly Materials (Tanaka et al., 1987)

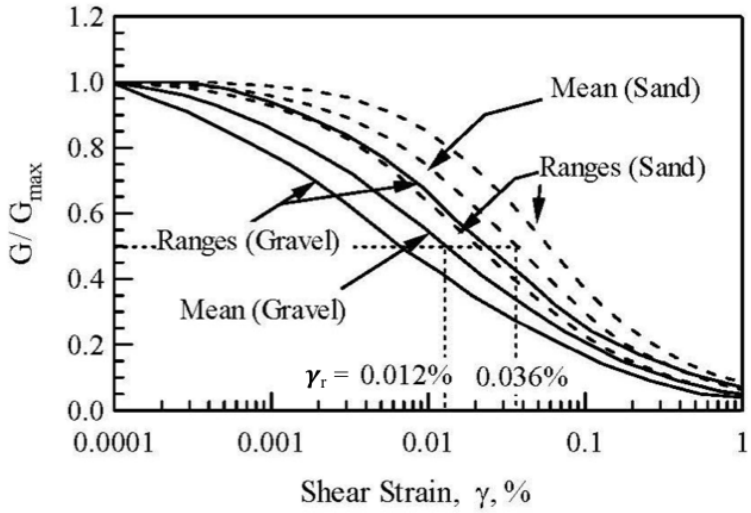

(a) Normalized Shear Modulus in the Nonlinear Range

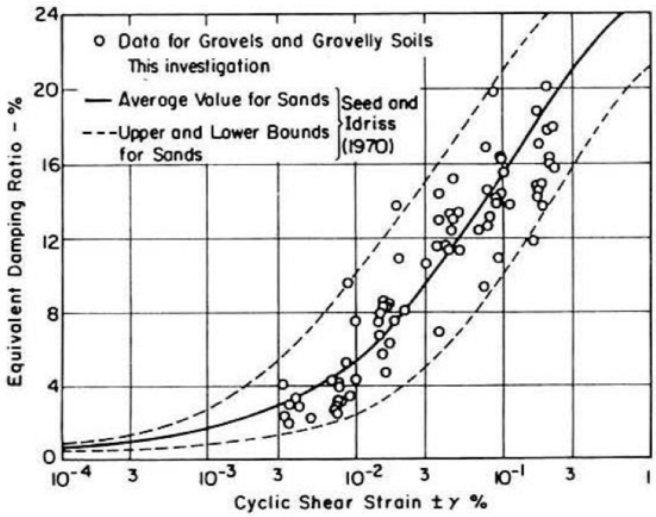

(b) Material Damping Ratio in the Nonlinear Range

Figure 4.4: G/G_{max} – log γ and D – log γ Curves of Gravelly and Sandy Soils Presented by Seed et al. (1986) with Values of γ_r Added by the Writer

behave more linearly in Figure 4.3, and this trend is more easily shown by using the reference strains of these two materials at the same effective stress.

Seed et al. (1986) [29] also determined a wide range in values of material damping ratio in shear (D) of sandy soils in terms of nonlinear behavior as presented in the Figure 4.4b. They also showed that the D values of most gravelly soils are included in the ranges presented for sands as seen in Figure 4.4b.

Comparisons of nonlinearity by Menq (2003) [26] between a well-graded gravel (GW) and a poorly-graded sand (SP) are shown in Figure 4.5. He found that the shear modulus (G) of a typical well-graded gravel in the nonlinear range is larger than that of a typical poorly-graded sand due to the effect of the higher uniformity coefficient (C_u) and median grain size (D_{50}) values. In other words, the reference strain of the GW soil ("A" soil in the figure) is smaller than that of the SP soil ("B" soil in the figure) due to the increase of C_u and D_{50}. This finding indicates the grain distribution characteristics have an impact on the nonlinear soil behaviors of sandy and gravelly soils. With respect to material damping ratio in shear in the Figure 4.5(b), the values of material damping ratio in shear of the SP soil in the small-strain range are slightly larger than those of the GW soil due to increases in D_{50}. However, in the nonlinear range, above the elastic threshold shear strain, γ_t^e, the nonlinear values of D of gravels are much larger than sand due to C_u.

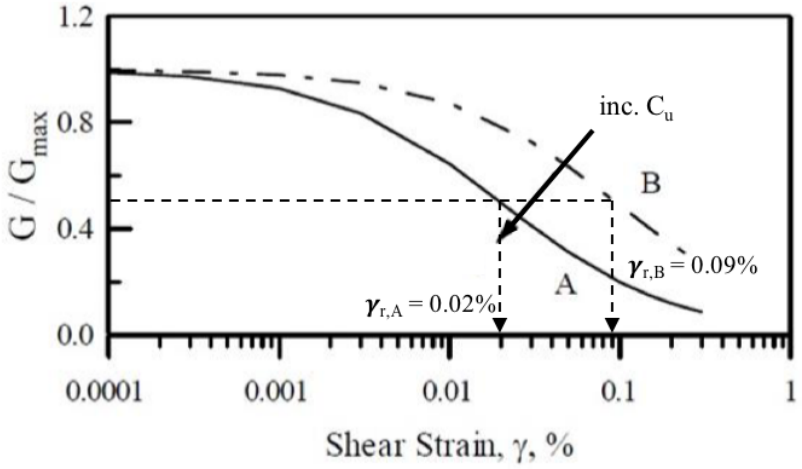

(a) G/G_{max} – log γ Relationship

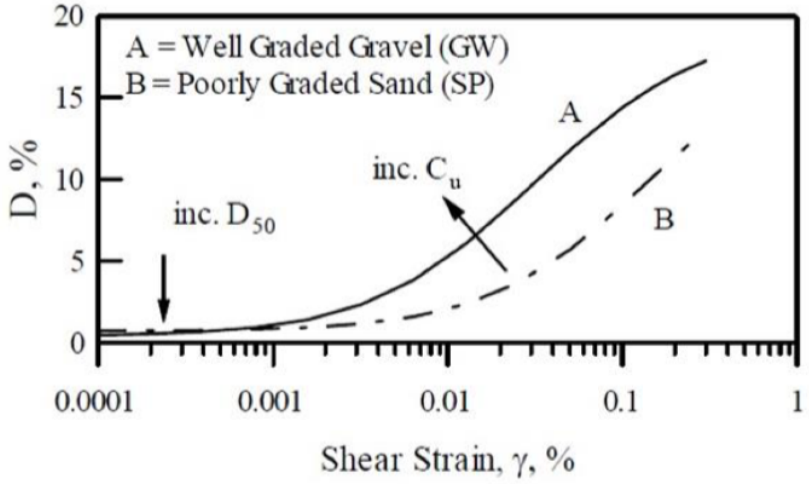

(b) D – log γ Relationship

Figure 4.5: Comparisons of the G/G_{max} – log γ and D – log γ Relationships for Dense Specimens of a Poorly-graded Sand (SP) and a Well-graded Gravel GW) (from Menq, 2003) with Values of γ_r Added by the Author

4.3.3 Effects of Reference Strain, γ_r, and Curvature Coefficient, a

Darendeli (2001) [11] proposed a modified hyperbolic model to evaluate and model dynamic soil properties in terms of normalized shear modulus. The hyperbolic model equation is as follows:

$$\frac{G}{G_{max}} = \frac{1}{1 + (\frac{\gamma}{\gamma_r})^a} \tag{4.8}$$

where:

γ = any given shearing strain,

γ_r = the reference shearing strain (with respect to G), and

a = the curvature coefficient in shear modulus reduction curve.

The effects of the reference strain, γ_r, and the curvature coefficient, a, on the G/G_{max} – log γ curve are presented in Figures 4.6 and 4.7, respectively. As illustrated in Figure 4.6 (a), the linearity of the G/G_{max} – log γ curve increases with increasing the reference strain. As a result, the corresponding shear stress-shear strain relationships ($\tau - \gamma$ curves) can be illustrated as shown in Figure 4.6 (b).

On the other hand, the overall slope of the G/G_{max} – log γ curve increases with increasing the value of a as presented in Figure 4.7. The impact of the curvature coefficient on the $\tau - \gamma$ curves is also presented in Figure 4.8. It is noteworthy that the curvature coefficient has an opposite impact on the

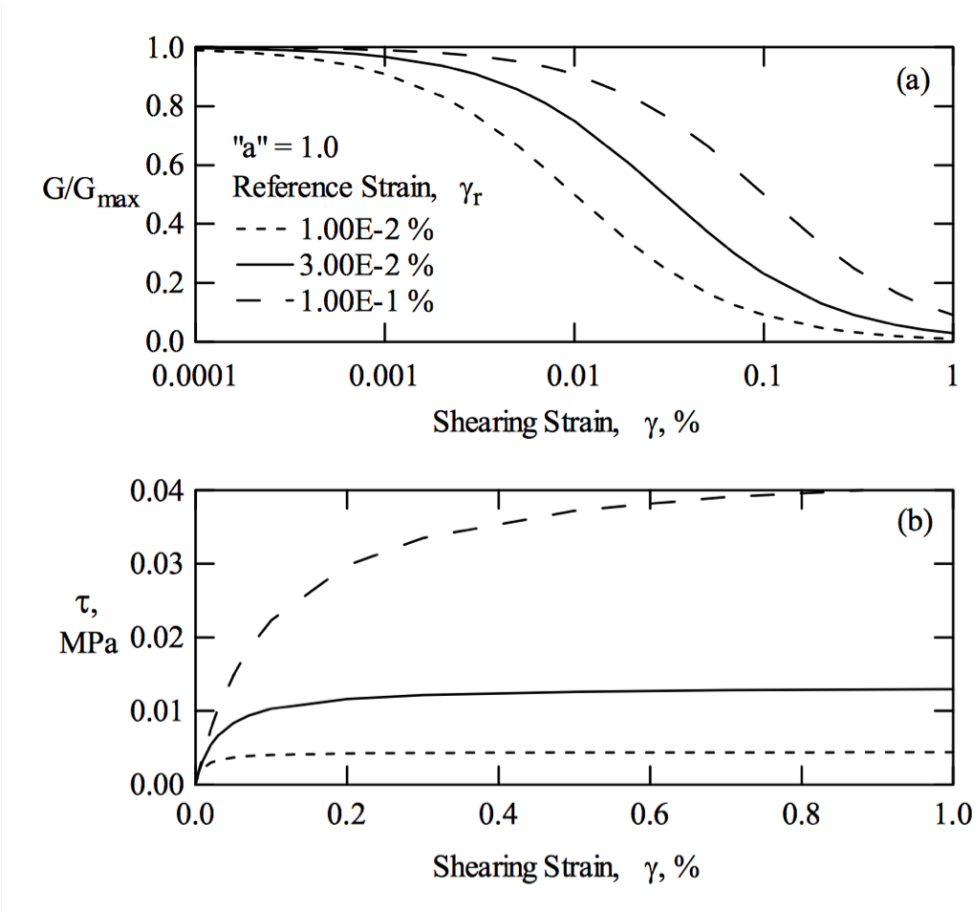

Figure 4.6: Effect of Reference Strain on (a) Normalized Modulus Reduction Curve and (b) Stress-Strain Curve (Darendeli, 2001)

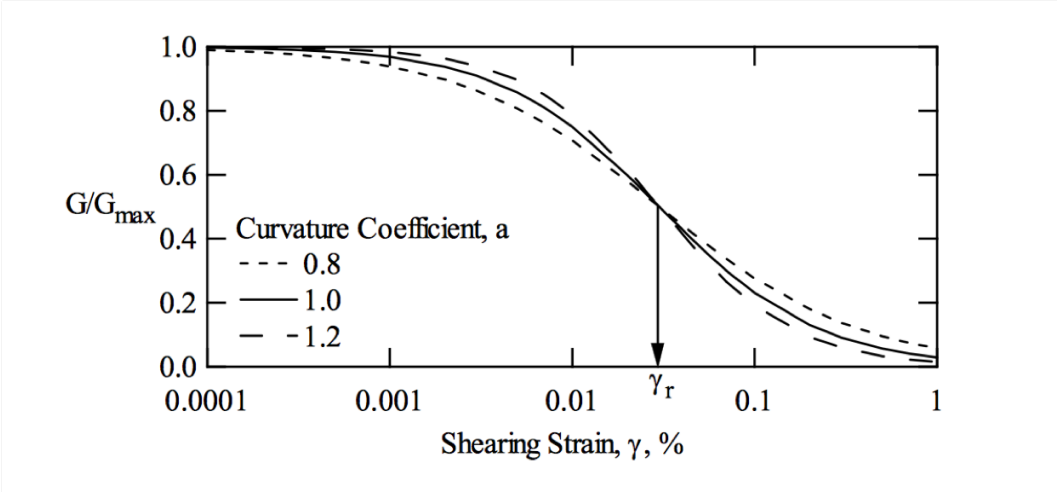

Figure 4.7: Effect of Curvature Coefficient, a, on the Normalized Modulus Reduction Curve (Darendeli, 2001)

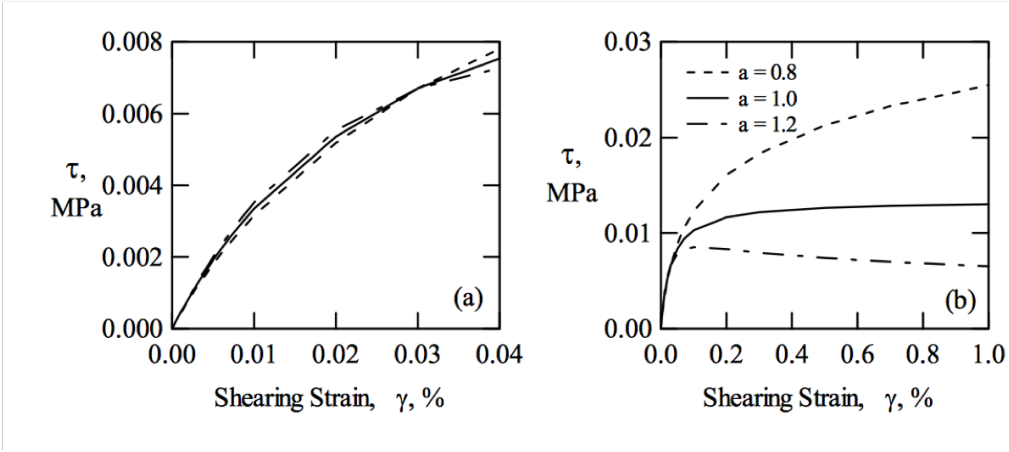

Figure 4.8: Effect of Curvature Coefficient on the Stress-Strain Curve (a) at Small and Intermediate Strains, and (b) at High Strains (Darendeli, 2001)

shear stress for shearing strains above and below the reference strain, γ_r. Shear stress increases with an increasing value of the curvature coefficient a at $\gamma < \gamma_r$, and decreases with an increasing value of the curvature coefficient at $\gamma > \gamma_r$.

4.4 LITERATURE REVIEW OF BINARY MIXTURES

In this section, the derivations of theoretically possible minimum and maximum void ratios of mono-spherical particles are first introduced (Section 4.4.1). In Section 4.4.2, the two ideal packing models and the boundary of the two ideal packing models, which is the call "critical packing condition", and the associated quantities are discussed.

4.4.1 Maximum and Minimum Void Ratios of Mono-Spherical Particles

Theoretically, five idealized packing conditions in mono-size spherical particles can possibly exist (See Figure 4.9.):

(1) The loosest possible packing in which the particles are touching each other is referred to as cubical or simple cubic (Figure 4.9 (a)). In this arrangement the particles are stacked on top of each other (entroid over centroid) to produce a structure that is unstable. It would not naturally occur in experiments;

$$e = \frac{6 - \pi}{\pi} = 0.90986 \tag{4.9}$$

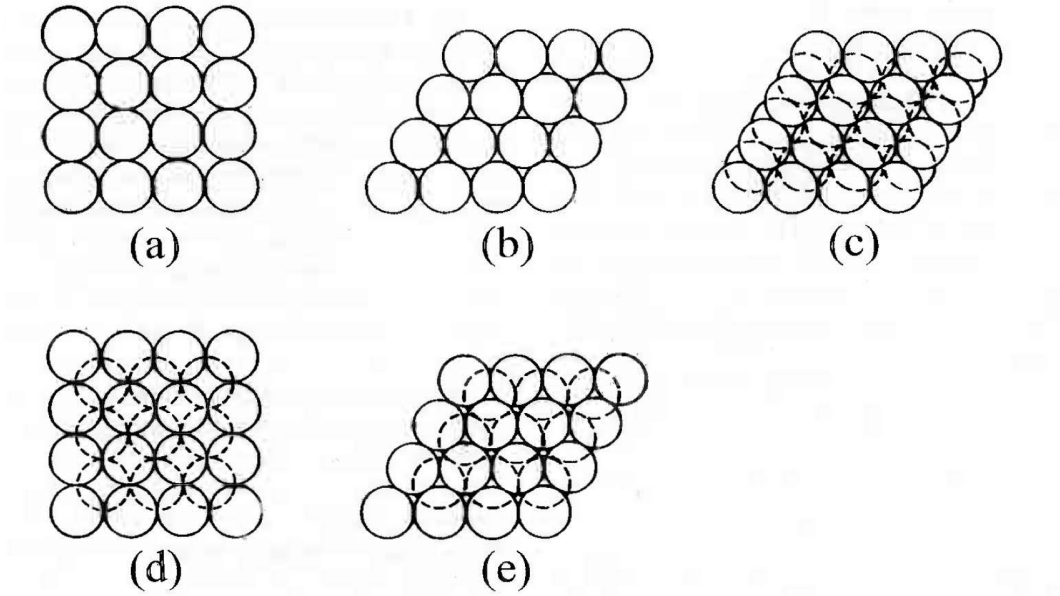

Figure 4.9: Theoretical packing conditions with mono-sized spheres: (a) simple cubic, (b) single stagger, (c) double stagger, (d) pyramidal, and (e) tetrahedral.

(2) Single stagger / cubical tetrahedral (Figure 4.9 (b)). In this pattern, each sphere touches six neighboring spheres in its own layer, and the spheres in different layers are stacked directly on top of each other;

$$e = \frac{3\sqrt{3} - \pi}{\pi} = 0.65399 \tag{4.10}$$

(3) Double stagger / double nested (Figure 4.9 (c)). This is similar with the single stagger, except each sphere in one layer had slid over and down to contact two spheres in the second layer; and

$$e = \frac{9 - 2\pi}{2\pi} = 0.43239 \tag{4.11}$$

(4) & (5) Two different densest packing conditions. (4) Face-centered cubical / pyramidal (Figure 4.9 (d)) and (5) close-packed hexagonal / tetrahedral packing conditions (Figure 4.9 (e)). Both packing conditions have the same void ratio of:

$$e = \frac{3\sqrt{2} - \pi}{\pi} = 0.35047 \tag{4.12}$$

From this information, it is assumed that the possible minimum void ratio is 0.35 and the maximum void ratio is 0.91 in a uniform spherical particles.

4.4.2 Binary Packing Model

Research about binary mixtures have been performed by many petrophysicists to predict the porosity of mixtures. Clarke (1979) [10] identified two types of ideal packing in binary mixtures: (1) "coarse packing", and (2) "fine packing." (See Figure 4.10.)

In the "fine packing", larger particles disperse in a fine-grained matrix. In other words, small particles are self-supported and large particles are suspended throughout the small particles matrix. In the "coarse packing", smaller particles are contained in the void spaces between load-bearing coarse-grained particles. In other words, the volumetric percentage of small particles is less than the volumetric percentage of void spaces between large particles taken alone and groups of small particles reside within the void spaces among self-supported, large particles.

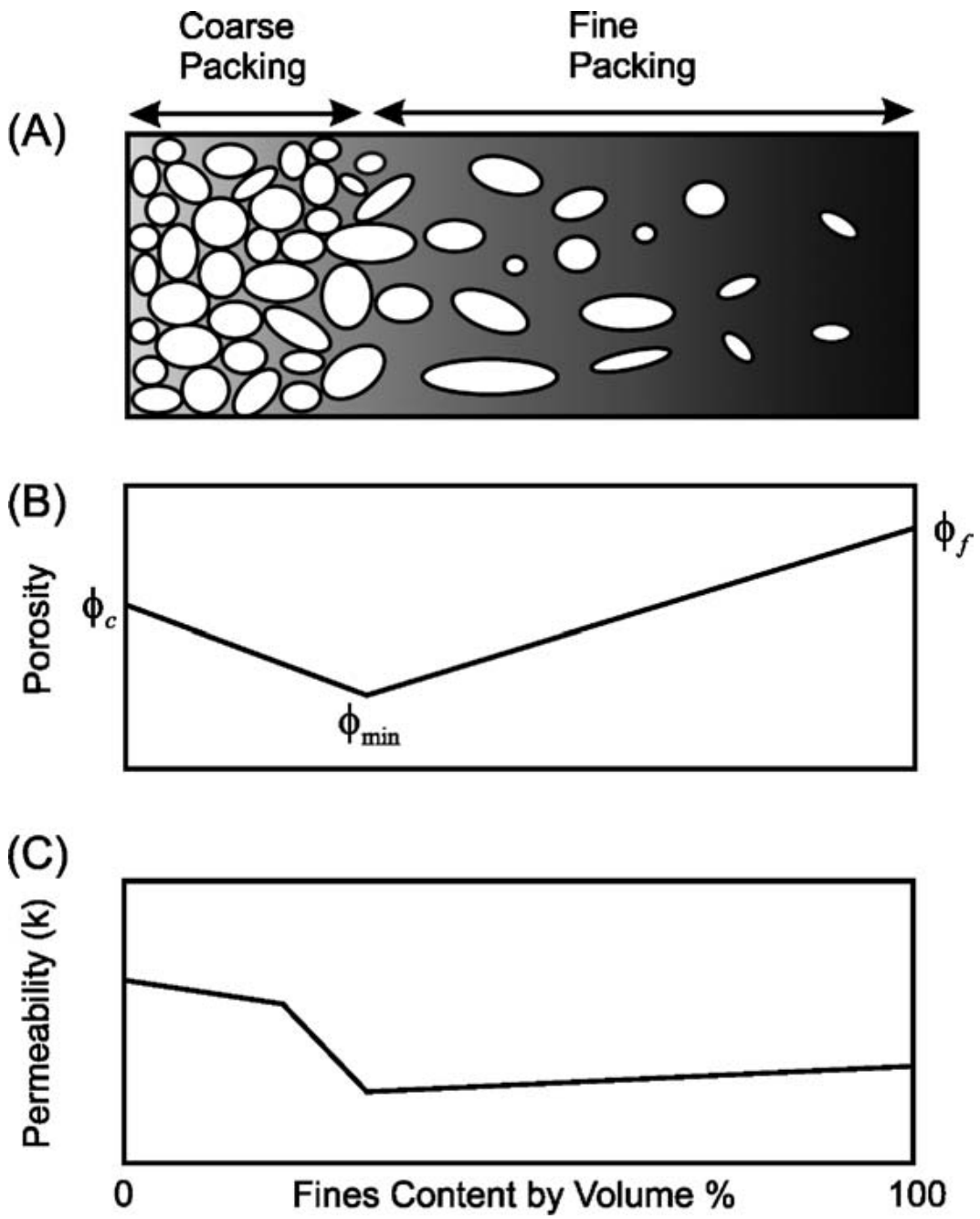

Figure 4.10: (A) Conceptual illustration of ideal packing, (B) Variation in porosity as a function of the finergrained content, and (C) Variation in permeability as a function of the finer-grained content (modified from Koltermann and Gorelick 1995)

In this dissertation research, the "fine packing" is called small-particle packing (SPP) and the "coarse packing" is called large-particle packing (LPP). In Figure 4.11, two specimens representing the two ideal packing conditions (SPP and LPP, respectively) are exemplified. For both specimens in the figure, all particles are same shape of sphere, i.e., mono-spherical particles. The large and small-particle diameters are 11.0 mm and 0.3 mm, respectively, resulting in the diameter ratio of 36.7 between small and large particles. Additionally, it is assumed that the two specimens are as densely packed as either the face-centered cubical / pyramidal or close-packed hexagonal / tetrahedral packing conditions (Figure 4.9) resulting in the void ratio of 0.35.

As shown in the Figure 4.10 (A), there exists a boundary between the two packing conditions (i.e., between SPP and LPP) in the ideal binary packing model. This boundary is denoted as the critical packing condition, which is all void spaces between large particles in the large-particle packing (LPP) are completely filled with the groups of small particles. In the critical packing condition, it is assumed that each group of small particles retains the porosity of the premixed, small-particle state. Additionally, the critical small-particle content, SPC*, which is the small-particle content associated with the critical packing condition, is often expressed with SPC_V*. (The subscription V indicates that this quantity is calculated in volume.) To derive the critical small-particle content (SPC_V*), it is convenient to state the phase relationships for each packing condition. In Figures 4.12a and 4.12b, the phase relationships for the two ideal packing conditions are presented, respectively. As mentioned

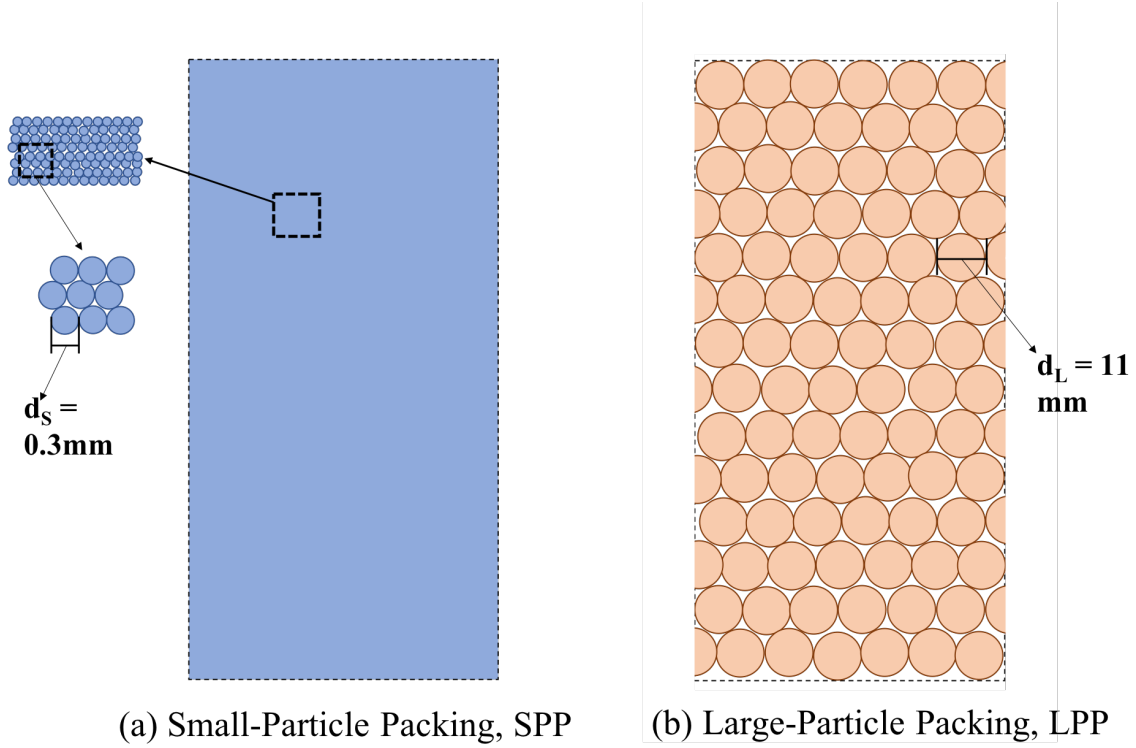

Figure 4.11: Ideal Packing Conditions: (a) Small-Particle Packing (SPP), and (b) Large Particle-Packing (LPP)

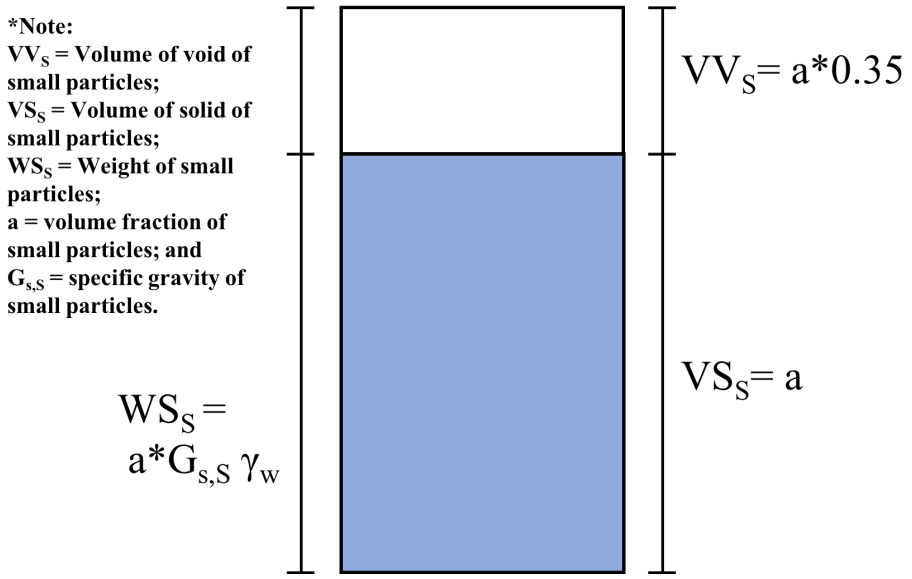

(a) Phase Relationship of Small-Particle Packing (SPP) Condition

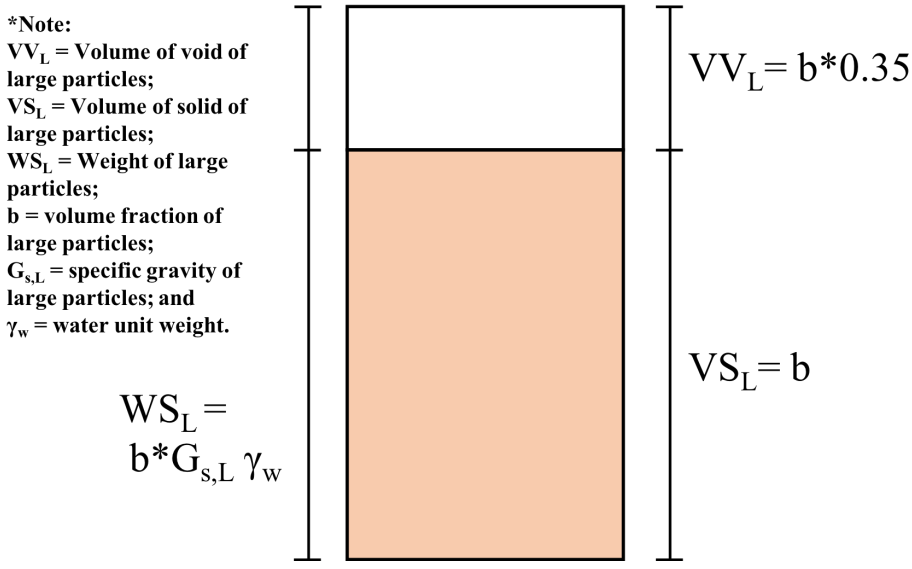

(b) Phase Relationship of Large-Particle Packing (LPP) Condition

Figure 4.12: Phase of Relationships of the Ideal Packing Conditions (SPP and LPP)

above, the void ratios for both ideal packing conditions are 0.35. In each phase relationship, the left side represents the weights for each phase and the right side represents the volumes of each phase. As can bee seen in the Figure 4.12a, the weight of small particles in the SPP can be calculated by the specific gravity of small particles ($G_{s,S}$) times water unit weight. The weight of large particles in the LPP (Figure 4.12b) is also calculated by the the specific gravity of large particles ($G_{s,L}$) times water unit weight.

In Figure 4.13, the critical packing condition and the associated phrase relationship is provided. As can be seen, the volume of solids of small particles and the volume of void can be calculated as 0.26 and 0.09, respectively, resulting in the volume of small particles filling in the void spaces between the large particles of 0.35. This result satisfies the definition of the critical packing condition that all void spaces between the large particles are completely filled with the matrix of small particles (i.e., each group of small particles). Accordingly, the critical small-particle content, which is the small-particle content associated with the critical packing condition, is identical to the porosity of the large-particle packing (LPP).

$$SPC_V^* = \frac{a + ae_S}{b + be_L} = \frac{be_L}{b + be_L} = \frac{e_L}{1 + e_L} = n_L \tag{4.13}$$

where:

SPC_V^* = volumetric critical small-particle content, %, and

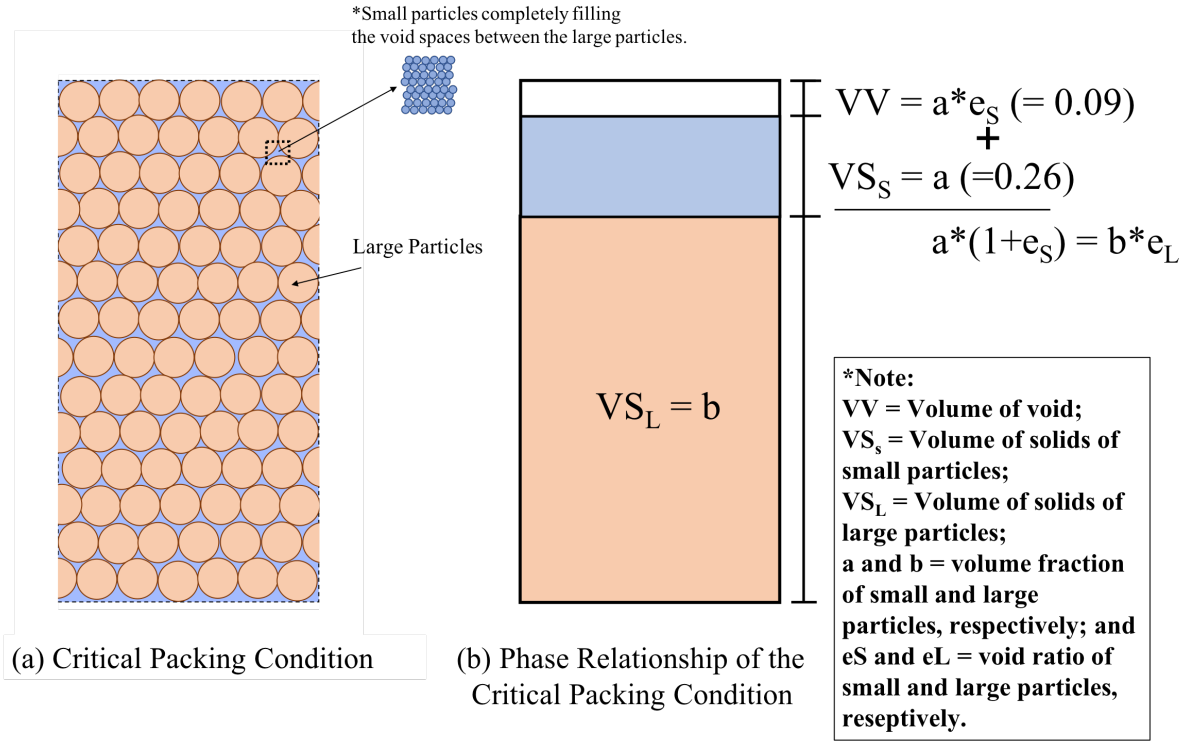

Figure 4.13: Phase Relationship of the Critical Packing Condition in the Ideal Packing Models

n_L = porosity of large-particle packing (LPP) condition.

The definition of volumetric critical small-particle content (SPC^*_V) is generally converted to a weight-based critical particle content, SPC^* to facilitate more convenient comparison between void ratios calculated from the ideal models and the data. (Marionet al., 1992; Clarke, 1979; Koltermann and Gorelick, 1995; Kamann et al., 2007; Choo, 2014).

$$SPC^* = \frac{aG_{s,S}\gamma_w}{bG_{s,L}\gamma_w + aG_{s,S}\gamma_w} \tag{4.14}$$

where:

SPC^* = weight-based critical small-particle content, %,

a *and* b = volume fractions of small and large particles, respectively,

$G_{s,S}$ *and* $G_{s,L}$ = specific gravities of small and large particles, respectively, and

γ_w = unit weight of water.

If $G_{s,S}$ and $G_{s,L}$ are reasonably similar one another, the Equation 4.14 can be re-written as:

$$SPC^* = \frac{a}{a+b} = \frac{e_L}{1+e_S+e_L} \tag{4.15}$$

where:

e_S and e_L = void ratios of small and large particles, respectively.

The state when SPC is greater than SPC^* (i.e., $SPC > SPC^*$) is denoted as the small-particle-packing dominated, SPPD, condition in this dissertation study. On the other hand, the state when SPC is less than SPC^* (i.e., $SPC < SPC^*$) is denoted as the small-particle-packing dominated, LPPD, condition in this dissertation study.

Figure 4.14 compares the three different states in terms of the packing conditions: (1) small-particle-packing dominated (SPPD), (2) critical packing condition with the critical small-particle content (SPC*), and (3) small-particle-packing dominated (LPPD).

Thevanayagam and Martin (2002) [33] emphasized that the SPC* for a specific composition is a range rather than a single value, with more wide range than the theory-based values, and this range is often called "transition zone" or TZ in the literature. Soils in the transition zone (TZ) are in a metastable condition where the engineering characteristics are quite different from those of either SPPD or LPPD.

Comparing data to predictions made with the ideal-mixing models shows consistent underpredictions of porosity for sediment mixtures because of nonideal mixing (e.g., Yu et al., 1997; Koltermann and Gorelick, 1995; Kamann et al., 2007). Predicted porosities for angular coarse particles deviate

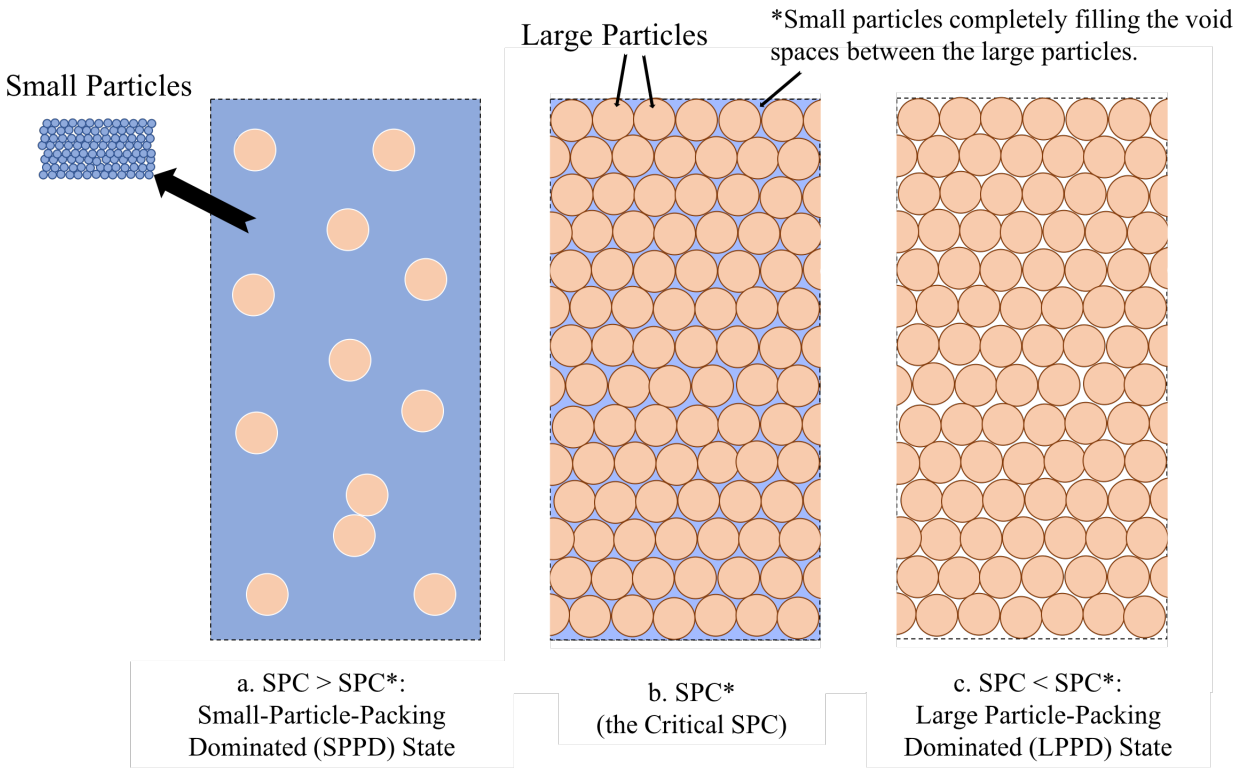

Figure 4.14: Schematic of Three Possible Binary Conditions

even further from the ideal-mixing models (Shakoor and Cook, 1990). The underpredictions of the ideal packing models is well shown in Figure 4.15 (Koltermann and Gorelick 1995) [22]. The greatest underprediction occurs at the minimum porosity. This is shown in results presented in the Figure 4.15 and also in results from other experiments on sediments made of uniform spheres and of angular grains (Furnas 1929; McGeary 1961; Shakoor and Cook 1990).

Koltermann and Gorelick (1995) [22] modified the ideal mixing models by introducing a weighting coefficient, ψ, that reflects the relative proportions of coarse and fine packing and varies between one and a minimum value, ψ_{min}. Their results indicates that the modified model, which they called the fractional-packing model, predicted the porosities of mixtures better than the ideal model; however, the physical meaning of the ψ coefficient in the fractional packing is not very clear. Furthermore, when ψ_{min} is very small, the minimum porosity does not occur at ψ_{min} as it should (Kamann et al., 2007 [18]).

4.5 SUMMARY

Literature review discussing variables that affect the dynamic properties of sandy and gravelly soils in the linear and nonlinear ranges are presented in this chapter. The effects of isotropic confining stress, void ratio, and gradation characteristics on small-strain shear modulus (G_{max}) and small-strain material damping ratio in shear (D_{min}) are discussed. Factors that affect the dynamic properties of granular soils in the nonlinear range are then discussed.

Theoretical possible packing conditions in mono-size spherical particles

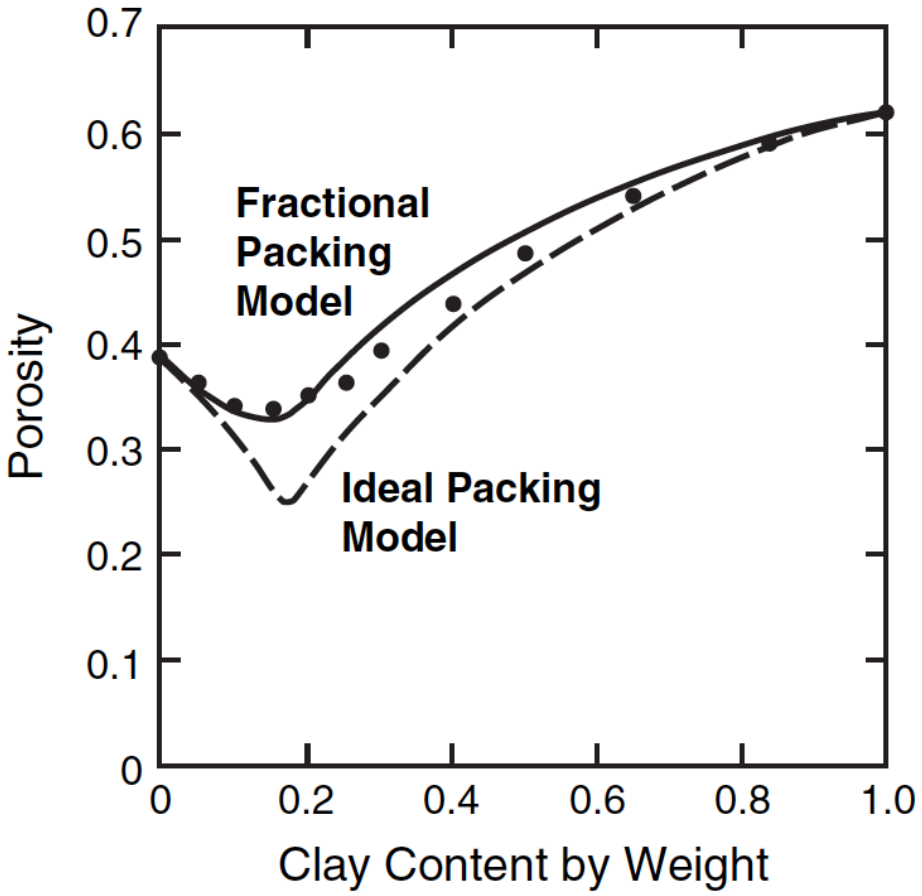

Figure 4.15: Comparison of porosities computed and the ideal packing models to experimental data (from Koltermann and Gorelick, 1995).

are introduced. Based on the introduction, it is assumed that the possible minimum void ratio is 0.35 and the maximum void ratio is 0.91 in a uniform spherical particles. Two different ideal packing models such as small-particle packing (SPP) and large-particle packing (LPP) are discussed. As the boundary between theses two packing conditions, the concept of the critical packing condition and the associated critical small-particle content (SPC*) are theoretically derived in this chapter.

Chapter 5

Test Materials, Specimen Preparation, and Test Procedure

5.1 INTRODUCTION

The purpose of this dissertation study is to determine the variables that affect the dynamic properties of binary and gap-graded materials and to assess the impacts of these variables. As discussed in Chapter 4, the predominant packing condition (either small-particle packing or large-particle packing) in a binary mixture depends on the ratio of the material's two distinct types of particles. Additionally, estimating the critical packing condition of a binary mixture (i.e., the boundary between the two different packing conditions where all void spaces of large particles are filled in with each group of small particles) is critical not only to predicting the predominant packing conditions, but also to understanding the dynamic behavior of the different conditions.

In the study of the binary mixtures, six poorly-graded (SP and GP) specimens, and 28 binary specimens were tested. The six poorly-graded specimens are composed of three poorly-graded sand (SP) specimens and three poorly-graded gravel (GP) specimens. The SP specimens were constructed with washed mortar sand (WMS). This WMS is a standard poorly-graded

sand used in the soil dynamic laboratory at the University of Texas at Austin. The poorly-graded gravel (GP) specimens were constructed with a river gravel (RG). The 28 binary specimens were created using different combinations of the SP material and the GP material.

In the study of the gap-graded specimens, one well-graded sand (SW) specimen, and seven gap-graded specimens were tested. The SW specimen was manufactured by seven different particle sizes from the WMS used for the SP material. The seven gap-graded specimens were manufactured by combining various amount of the well-graded sand and the GP material.

Sections 5.2 and 5.3 below present the physical properties of the poorly-graded and binary specimens. In Section 5.4, the binary specimens are grouped on the basis of critical packing condition. The physical properties of the gap-graded specimens are discussed in Section 5.5. In Sections 5.6 and 5.7, the details of specimen preparation and test procedure are discussed, respectively. The symbols used in discussing the binary and gap-graded granular soils are listed in Table 5.1.

Table 5.1: List of Symbols Used in Discussing Binary and Gap-Graded Granular Soils

Begin of Table 5.1		
Symbol	**Units**	**Definition**
C_c	-	Coefficient of curvature
C_u	-	Uniformity Coefficient
D_{10}	(mm)	Diameter for 10% finer by weight
D_{30}	(mm)	Diameter for 30% finer by weight
D_{60}	(mm)	Diameter for 60% finer by weight
e $(= e_g)$	(decimal)	Void ratio (= Global Void Ratio)
e_{min}	(decimal)	Minimum void ratio
e_{max}	(decimal)	Maximum void ratio
D_r	(percent, %)	Relative density
G_s	(decimal)	Specific gravity
γ_d	(pcf)	Dry unit weight
γ	(percent, %)	Shear strain
γ_r	(percent, %)	Reference strain
w	(percent, %)	Moisture content
$USCS$	-	Unified Soil Classification System
SP	-	Poorly-graded sand (USCS)
GP	-	Poorly-graded gravel (USCS)
SW	-	Well-graded sand (USCS)
WMS	-	Washed mortar sand
RG	-	River gravel
SPC	(percent, %)	Small-particle content
SPC^*	(percent, %)	Critical small-particle content

Continuation of Table 5.1		
Symbol	**Units**	**Definition**
LPC	(percent, %)	Large-particle content
SPP	-	Small-particle packing
LPP	-	Large-particle packing
LTN	-	Load transfer network
$SPPD$	-	Small-particle-packing dominated
$LPPD$	-	Large-particle-packing dominated
TZ	-	Transition zone
RC	-	Dynamic torsional resonant column
$S100$	-	Specimens of 100% small particles
$L100$	-	Specimens of 100% large particles
$S85L15$[1]	-	Binary specimens of 85% small particles and 15% large particles
S_w85L15[2]	-	Gap-graded specimens of 85% small particles and 15% large particles
$L85S15$[3]	-	Binary specimens of 85 % large particles and 15 % small particles
$L85S_w15$[4]	-	Gap-graded specimens of 85 % large particles and 15 % small particles
G_{max}	(ksf)	Small-strain shear modulus
D_{min}	(percent, %)	Small-strain material damping ratio in shear
G	(ksf)	Shear modulus
G/G_{max}	-	Normalized Shear modulus
D or D_s	(percent, %)	Material damping ratio in shear
P_a	(1 atm = 14.7 psi)	One Atmosphere

[1] A example of binary specimen descriptions for SPC $\geq$ LPC.
[2] A example of gap-graded specimen descriptions for SPC $\geq$ LPC.
[3] A example of binary specimen descriptions for SPC $<$ LPC.
[4] A example of gap-graded specimen descriptions for SPC $<$ LPC.
* See Tables 5.8, 5.9, and 5.10 for the symbol descriptions of other specimens.

5.2 TWO POORLY-GRADED SOILS

5.2.1 A Poorly-Graded Sand: SP

Washed mortar sand, WMS, is a poorly-graded sand that has been used as a standard testing material at the University of Texas at Austin in the dynamic torsional resonant column (RC) testing (Ni 1987, Kim 1991, Laird 1994, Menq 2003, and Keene 2017). The WMS is obtained from the flood plain of the Colorado River in Austin, Texas. The small-size granular material of binary mixtures tested in this research was created by sieving the WMS. As a result, a poorly-graded sand (SP) was manufactured from the WMS with average diameter of 0.33 mm (Figure 5.1).

In Table 5.2, a summary of the physical properties of the SP material are presented. As shown in the table, this soil is classified as a poorly-graded sand (SP) by the Unified Soil Classification System (USCS). The minimum and maximum void ratio (i.e., e_{min} and e_{max}) values of 0.57 and 0.89, respectively, were measured. Because of difficulties associated with calibrating and adjusting the shaking table used to measure e_{min}, the ASTM D 4253 [1] standard method was not used to determine e_{min} in this research. Instead, the maximum dry density ($\gamma_{d,max}$) was determined by the modified Proctor compaction method (ASTM D1557-12 [4]). The value of $\gamma_{d,max}$ was then used

Figure 5.1: Photograph of the Poorly-Graded Sand (SP) Used in this Study (Note: The units of the ruler in the photograph are in inches.)

to estimate the e_{min}. The value of e_{max} of the SP material was determined by scooping soil into the sample mold as described in ASTM 4254 [2]. Lastly, the gradation characteristics, i.e., median grain size (D_{50}) and uniformity of coefficient (C_u), of this poorly-graded sand were determined to be 0.33 mm and 1.33, respectively, as shown in the Table 5.2.

Table 5.2: Physical Properties of the Poorly-Graded Sand (SP) Tested in the RC Device

Unified Soil Classification System	SP
Grain Character	Sub-angular
	to sub-rounded
Soil Composition (Laird, 1994)	40% Quartz
	30% Feldspar
	20% Other Minerals
	10% Shell Fragments
Maximum Dry Density	105.5 pcf ($5.05 kN/m^2$)
Minimum Dry Density	87.6 pcf ($4.19 kN/m^2$)
Maximum Void Ratio	0.89
Minimum Void Ratio	0.57
Particle Size Distribution:	
Median Grain Size, D_{50}	0.33 mm
Effective Grain Size, D_{10}	0.27 mm
C_u, (D_{60}/D_{10})	1.33
C_c, $(D_{30}^2$ / $(D_{60} \times D_{10}))$	1.00

5.2.2 A Poorly-Graded Gravel: GP

A river gravel (RG), which is also obtained from the flood plain of the Colorado River in Austin, Texas, was used to create a poorly-graded gravel (GP). This GP material was used as the large particles in the binary mixtures in this research. The uniform size of the gravel was manufactured by sieving with a half-inch (12.7 mm) sieve and a 3/8 in. (9.5 mm) sieve. After passing through the two sieves, the gravel that remained on the sieve of a 3/8 in. (9.5 mm) was collected, leaving gravel with estimated D_{50} and C_u values of 0.44 in. (11.10 mm) and 1.16, respectively. (See Table 5.3.)

Table 5.3: Physical Properties of the Poorly-Graded Gravel (GP) Tested in the RC Device

Unified Soil Classification System	GP
Grain Character	Angular to sub-rounded
Maximum Void Ratio	0.90
Minimum Void Ratio	0.56
Particle Size Distribution:	
Median Grain Size, D_{50}	11.10 mm
Effective Grain Size, D_{10}	9.82 mm
C_u, (D_{60}/D_{10})	1.16
C_c, $(D_{30}^2$ / $(D_{60} \times D_{10}))$	1.00

The D_{50} value of the GP (0.44 in.) is slightly smaller than the maximum particle size of 0.46 in., which is determined on the basis of the ASTM D4015-87

[3]. The standard of ASTM D4015-87 recommends to set the ratio of specimen diameter (2.8 inches in this study) to the maximum particle size to a value less than six. This large-particle size relative to the small-particle size of the SP material mitigates concerns about whether the principle assumption for a binary mixture will be met. This assumption is that the large-particle size should be approximately more than twenty times greater than the smaller particle size (Chang and Phantachang, 2016 [8]), and a factor of 34 was used in this study.

The "manufactured" poorly-graded gravel (the GP material) is shown in Figure 5.2. The physical and mechanical properties of the GP material are summarized in Table 5.3. As shown in the table, the grain character of the GP material is in the range of "angular" to "sub-rounded". This grain character falls in a similar range to that of the SP material, which is in the range of "sub-angular" to "sub-rounded", as seen in Table 5.2. Also, the minimum and maximum void ratios ($e_{min} = 0.56$ and $e_{max} = 0.90$, respectively, for the GP material) are very close to the values of the SP material ($e_{min} = 0.57$ and $e_{max} = 0.89$, respectively, for the SP material). These similarities between the GP and the SP materials indicate that adopting these materials as the parent materials for binary mixtures is appropriate in this study.

Figure 5.2: Photograph of the Poorly Graded Gravel (GP) Used in this Study (Note: The units of the ruler in the photograph are in inches.)

5.2.3 Physical Properties of the Poorly-Graded Granular Soil Specimens

A total of six poorly-graded specimens were reconstituted in this study: three specimens of the SP material; and three specimens of the GP material. Gradation curves for the SP and GP materials are shown in Figure 5.3. The physical properties of the two poorly-graded materials are compared in Table 5.4. In the figure and table, each gradation is characterized as either made up of only small particles or only large particles. The name of the small-particle

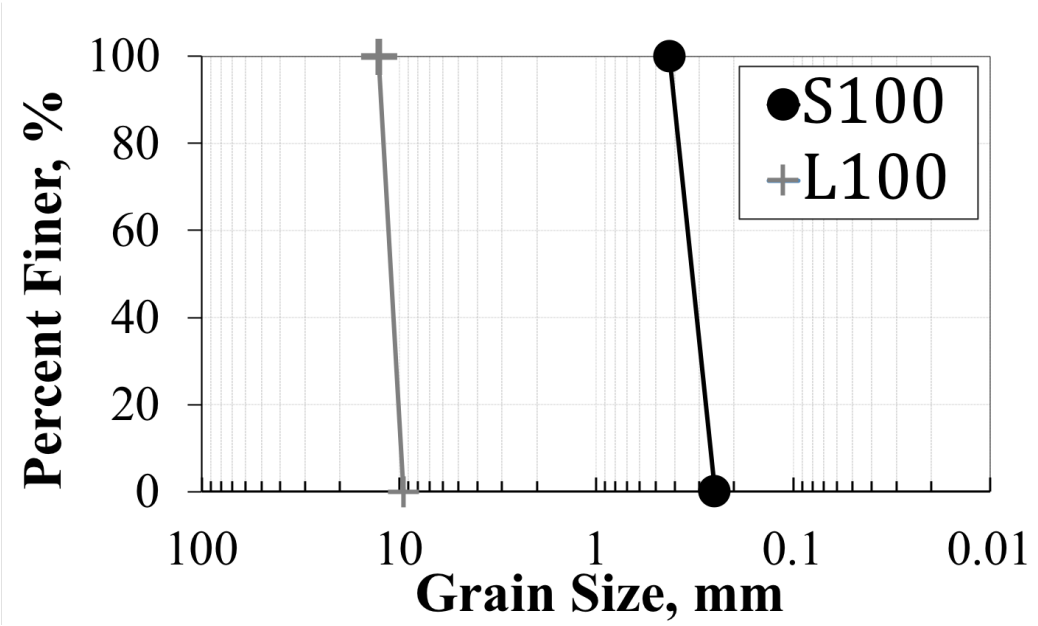

Figure 5.3: Gradation Curves of the Two Poorly-Graded Materials (the SP and GP Materials) Which Have a Ratio of 34 for $D_{50,GP}/D_{50,SP}$

gradation is represented by the letter "S", along with the percentage of small-particle content (SPC) in the specimen. For example, "Gradation S100" or "S100" stand for specimens composed of 100 percent small particles. In terms of the small-particle content (SPC), the SPC values for the S100 specimens are 100 percent. (See SPC column in Table 5.4.) Similarly, the letter "L" stands for large particles in the name of the large-particle gradation, and the number following "L" indicates the percentage of large particles. Regarding the SPC, the values for the GP specimens are zero percent as can be seen in the Table 5.4.

As shown in the Table 5.4, the gradations of S100 and L100 were reconstituted with three different densities. The void ratio values associated with the three different densities for each gradation are also presented in the table. It is worth noting that the smallest void ratios of each gradation (the SP and GP materials) are very close to each other.

Table 5.4: Physical Properties of the Six Poorly Graded Specimens

No.	**Material ID.**[1]	**SPC**[2] **%**	**LPC**[3] **%**	e	γ_d **(pcf)**	**w (%)**	D_{50} **(mm)**	C_u
1	S100	100	0	0.57	105.0	7.5	0.34	1.33
2	S100	100	0	0.67	98.8	7.5	0.34	1.33
3	S100	100	0	0.76	93.8	7.5	0.34	1.33
4	L100	0	100	0.56	106.2	0	11.10	1.16
5	L100	0	100	0.61	102.7	0	11.10	1.16
6	L100	0	100	0.71	96.5	0	11.10	1.16

[1] "S" stands for "small particles" that are sand size and "L" stands for "large particles" that are gravel size in the Material ID.
[2] "SPC" stands for small-particle content.
[3] "LPC" stands for large-particle content.

5.3 BINARY MIXTURES

5.3.1 Physical Properties of Binary Mixtures

The author manufactured twelve binary gradations by mixing the poorly-graded sand (the SP material) and poorly-graded gravel (the GP material) to investigate the dynamic properties of the binary mixtures. The results of gradation distribution analysis of the twelve binary mixtures manufactured are shown in Figure 5.4. This figure also includes with the two poorly-graded gradation curves, the S100 (SP) and L100 (GP) materials.

As shown in the figure, each of the 12 binary gradations was named according to the same rules used for the poorly-graded materials discussed Section 5.2.3. For example, the name (also called "ID" in this study) of Gradation

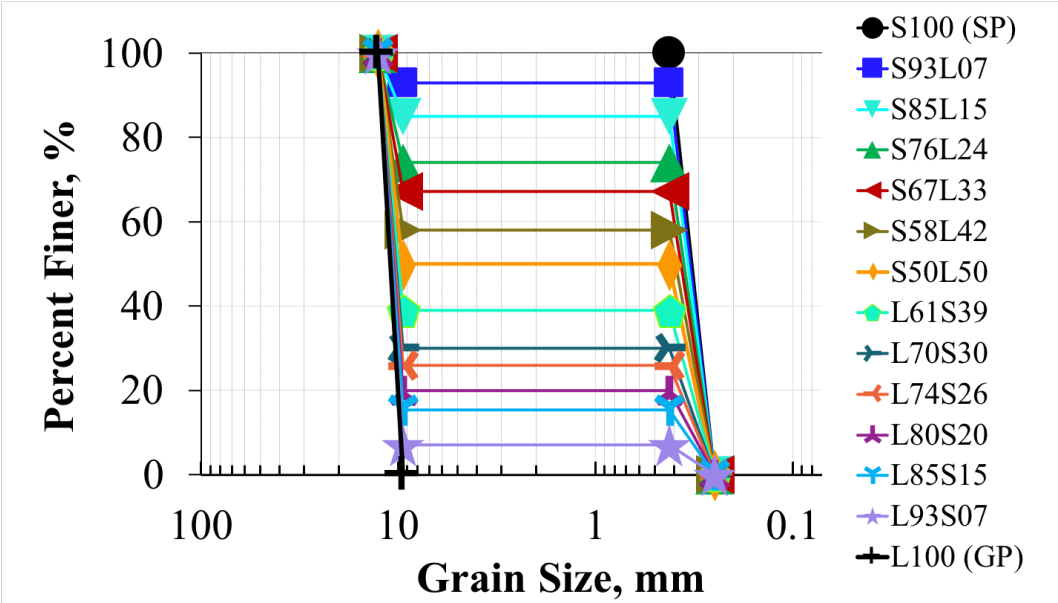

Figure 5.4: Gradation Distribution Curves of Fourteen Materials: Two Poorly-Graded Materials (with USCS designations of SP and GP) and Twelve Binary Mixtures

S50L50 (or S50L50) explicitly indicates that the specimens of this gradation were manufactured by 50 percent of small particles (the SP material) and 50 percent of large particles (the GP material).

In contrast to the poorly-graded materials, the names of the binary gradations are composed of two parts: (1) the percentage of small-particle content (SPC), and (2) the percentage of large-particle content (LPC). When the percentage of small particles in the material is more than half (SPC $\geq$ 50 percent), the combination of the letter of "S" and the associated percentage precedes the combination for the large particles (e.g., S85L15).

Table 5.5 summarizes the gradation characteristics of the 12 binary

Figure 5.5: Photograph of Gradation S50L50 (Note: The units of the ruler in the photograph are in inches)

Table 5.5: Physical Properties of the Specimens from the 14 Gradation Curves Shown in Figure 5.4

No.	**Gradation ID.**	**SPC (%)**	**LPC (%)**	D_{50} **(mm)**	C_u	**USCS**
1	S100	100	0	0.34	1.33	SP
2	S93L07	93	7	0.34	1.35	SP
3	S85L15	85	15	0.35	1.38	SP w/ gravel
4	S76L24	76	24	0.37	1.43	SP w/ gravel
5	S67L33	67	33	0.38	1.47	SP w/ gravel
6	S58L42	58	42	0.40	34.5	SP w/ gravel
7	S50L50	50	50	4.97	35.6	SP-GP
8	L61S39	39	61	10.09	36.0	GP w/ sand
9	L70S30	30	70	10.42	35.3	GP w/ sand
10	L74S26	26	74	10.54	34.6	GP w/ sand
11	L80S20	20	80	10.71	32.9	GP w/ sand
12	L85S15	15	85	10.81	30.8	GP w/ sand
13	L93S07	7	93	10.98	1.18	GP
14	L100	0	100	11.10	1.16	GP

mixtures and the two poorly-graded materials. In the table, the gradation identifications (IDs), the associated content percentages (SPC and LPC), and the USCS designations of the 14 materials are also provided. Added to the USCS designations are descriptions of the lesser percentages (i.e., either "with sand" or "with gravel") (Holtz and Kovacs, 2010). For Gradation S50L50, a double designation of "SP-GP" was used.

Interestingly, significant variations were found in terms of D_{50} and C_u for the binary mixtures. All the values of D_{50} for SPC $\geq$ 58% are less than 0.5 mm, however, the D_{50} values significantly increased between Gradations S58L42 and L61S39 (from 0.40 mm to 10.09 mm). As a result, the D_{50} value of Gradation S50L50 was estimated to be the median variation of 4.97 mm (0.20 in.). As for the C_u values, it was observed that there are two significant variations: (1) between the Gradations S67L33 and S58L42, and (2) between the Gradations L85S15 and L93S07. In other words, when the SPC $\geq$ 67%, the values of C_u ranged from 1.35 to 1.47, which are almost constant; however, the C_u value increased significantly from 1.47 to 34.5 for the Gradation S58L42. The high C_u values for 15% $\leq$ SPC $\leq$ 58%, which typically represents significantly well-graded soils, ranged from 30.8 to 34.5; however, the value decreased significantly again to the range of 1.16 to 1.18 for 0% $\leq$ SPC $\leq$ 7%. These dramatic changes in the values of D_{50} and C_u for the binary mixtures are well illustrated in Figures 5.6a and 5.6b.

A possible explanation of these significant changes in the values of D_{50} and C_u for the binary mixtures is that these gradation characteristics (D_{50} and

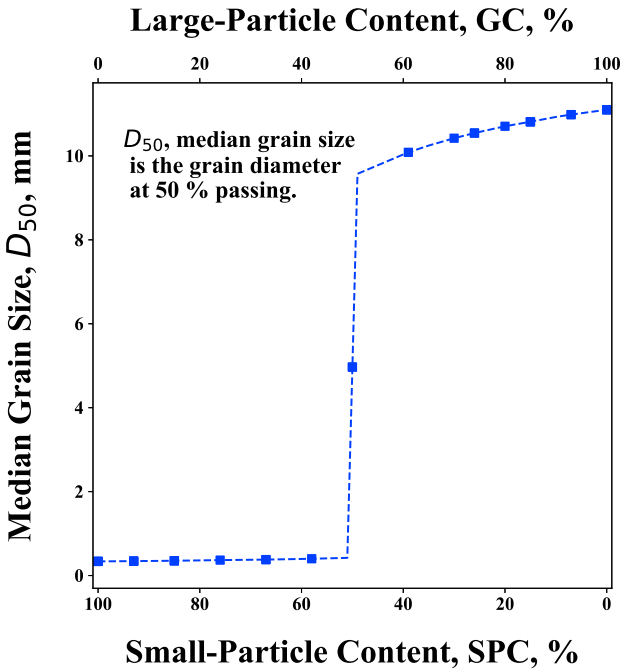

(a) Variation in Median Grain Size, D_{50}, with Small-Particle Content (SPC), %

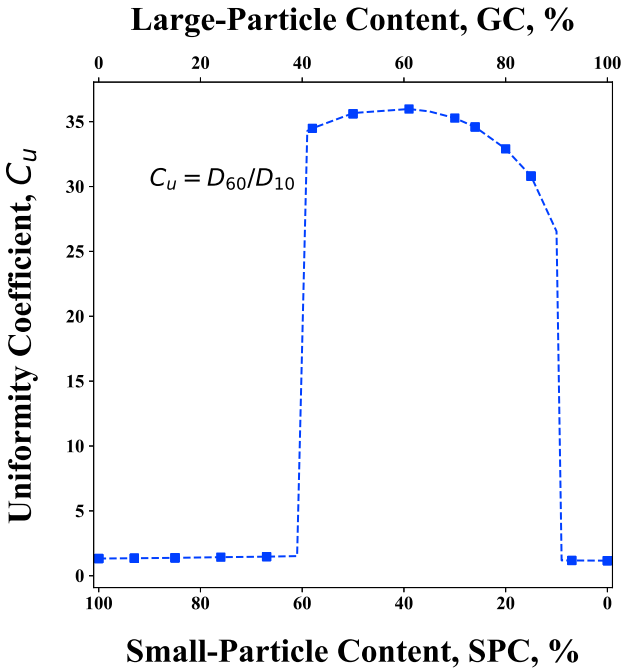

(b) Variation in Uniformity Coefficient, C_u, with Small-Particle Content (SPC), %

Figure 5.6: Variation in Median Grain Size, D_{50}, and Uniformity Coefficient, C_u of the SP, GP, and Binary Mixtures

C_u) are determined by the USCS definitions: (1) D_{50} is the grain diameter at 50 percent passing, and (2) $C_u = D_{60}/D_{10}$, where D_{60} is the grain diameter at 60 percent passing, and D_{10} is the grain diameter at 10 percent passing. The significant variations were seen when these percentage values were close to the values of the passing percentages associated with the discrete particle sizes in the USCS definitions such as D_{10}, D_{30}, D_{50}, and D_{60}. Therefore, cautions should be used to estimate the dynamic properties using the the D_{50} and C_u values determined by the USCS definitions for binary mixtures. Despite the uncertainties surrounding D_{50} and C_u values, it is still worthwhile to quantitatively evaluate their effectiveness in estimating the dynamic properties of the binary mixtures. In the following chapters, the use of D_{50} and C_u values to estimate these dynamic properties is discussed.

5.4 VOID RATIO FOR BINARY MIXTURES

As discussed in Chapter 4, the void ratio, e, is one of the key variables affecting the dynamic properties of granular soils. In addition, estimating the critical packing void ratios or their range of a binary mixture, which is the void ratios associated with the critical packing condition, is important for not only differentiating the binary specimens and but also understanding their dynamic behaviors. This section investigates the critical packing condition of the binary mixtures discussed in the previous section. It also evaluates the critical packing condition (theoretically determined), using both the empirical estimation and the measured data.

5.4.1 Background and Classification

The ideal binary packing model discussed in the Chapter 4 requires three major assumptions: (1) only two distinct particle sizes are considered; (2) the ratio of large particles to small particles is large enough (The particle size ratio is typically more than a factor of 20 and a factor of 34 was used in this study.); and (3) the packing of large particles is not affected by small particles, and vice versa (Chang and Phantachang, 2016 [8]). In this binary packing framework, a unique packing condition theoretically exists where all void spaces between large particles are filled in with each group of small particles (Zhang, 2011) [36]. (See Figure 4.13.) In the literature, the small-particle content (SPC, %) in this critical packing condition is often called the critical small-particle content, SPC*. Estimating this SPC* and the associated void

ratio (i.e., the critical packing void ratio) are starting points to understand binary mixtures.

As mentioned in the Chapter 4, the critical small-particle content (SPC*) can be calculated using the following equation:

$$SPC^* = \frac{e_l}{1 + e_s + e_l} \tag{5.1}$$

where,

e_l = the void ratio of large particles, and

e_s = the void ratio of small particles.

Because a void ratio for each particle size is in a range between the minimum and maximum values, the SPC* value of binary mixtures, which is calculated by the void ratios of small and large particles (Equation 5.1), span along the minimum and maximum values calculated by the e_{min} and e_{max} values for each particles. The four possible theoretical SPC* values calculated by the Equation 5.1 using the e_{min} and e_{max} values of the SP and GP materials are summarized in Table 5.6. Among the four values in the table, the minimum value of SPC* is 23%, which is the combination of the e_{min} of the GP and the e_{max} of the SP, and the maximum value is 36%, which is the combination of the e_{max} of the GP and the e_{min} of the SP. In other words, the critical packing condition can only theoretically occur when the large-particle content (LPC)

is between 64 percent and 77 percent with the small-particle content (SPC) between 23 percent and 36 percent.

Table 5.6: Calculations of the SPC* Values of Binary Materials Composed of the Poorly-Graded Sand (SP) and the Poorly-Graded Gravel (GP)

		SPC*	
		Large Particles (GP[1])	
		e_{min}**=0.56**	e_{max}**=0.90**
Small Particles (SP[2])	e_{min}**=0.56**	26%	36%
	e_{max}**=0.89**	23%	32%

[1] Poorly-Graded Gravel, GP
[2] Poorly-Graded Sand, SP

The twelve different gradations manufactured for binary mixtures were reconstituted with either two or three different densities in this study. The void ratio (e) values corresponding to the densities were calculated with an assumed specific gravity (G_s) of 2.65. The e values of the 14 gradations (i.e., 12 binary and 2 poorly-graded gradation curves) are plotted with the associated SPC values in Figure 5.7. Additionally, the e_{min} and e_{max} values measured for both SP and GP materials are also presented in the figure.

Evans (1995) [13] determined the minimum and maximum void ratios of a set of granular binary mixtures he tested. The binary mixtures were several combinations of a poorly-graded sand (D_{50} = 0.4 mm, C_u = 2.0, and a sub-angular material) poorly-graded gravel (D_{50} = 6.5 mm and C_u = 1.4) resulting in the particle size ratio of about a factor of 16. Based on the difference of the

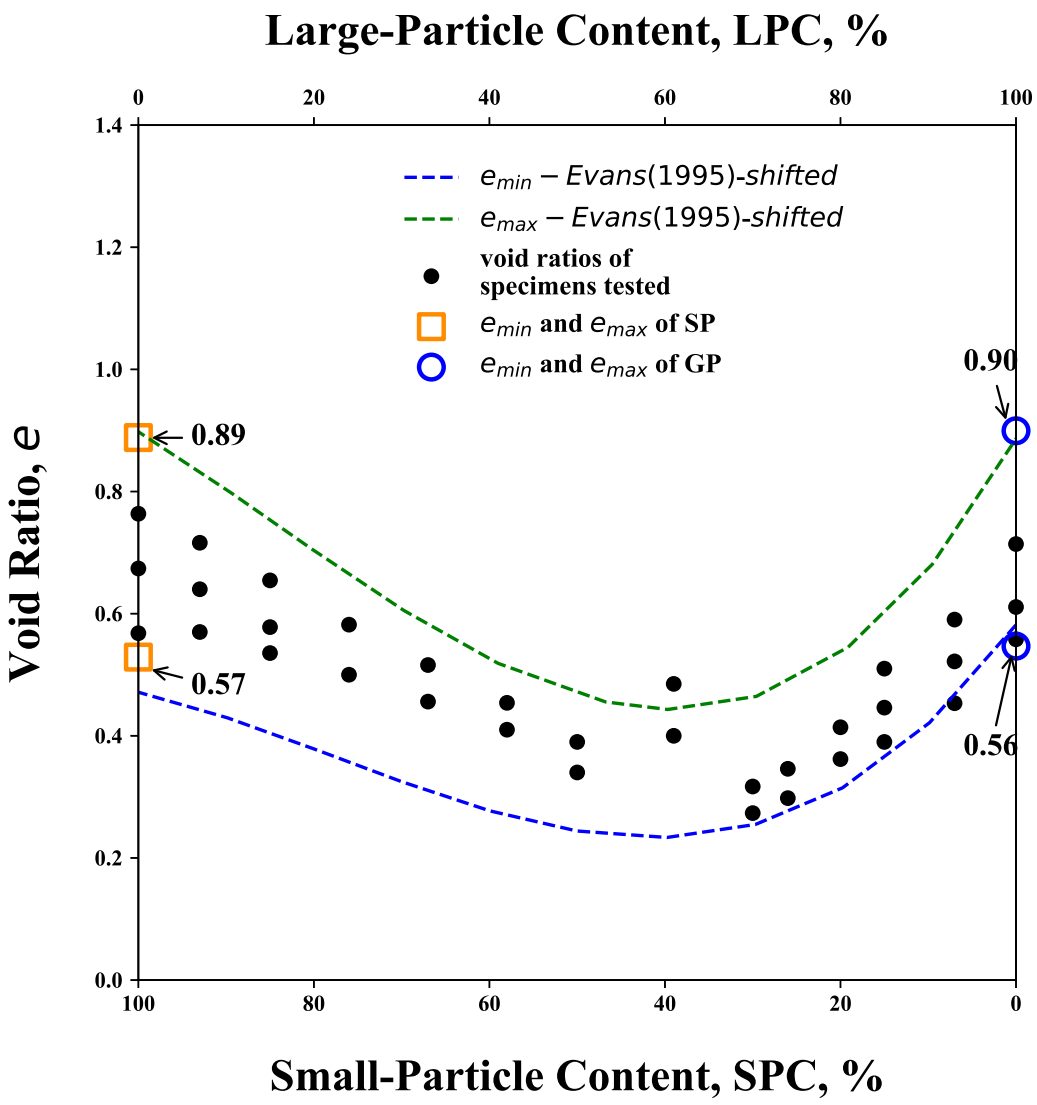

Figure 5.7: Variation in Void Ratio with Small-Particle Content and Large-Particle Content with Empirical e_{max} and e_{min} Trends by Evans (1995)

materials as well as the e_{min} and e_{max} values between the study of Evans (1995) and this dissertation study, the determined e_{min} and e_{max} values from Evans (1995) were slightly shifted down to fit the e_{min} and e_{max} values determined for the SP and GP materials in this study. The shifted trends of the e_{min} and e_{max} values for the binary mixtures tested by Evans (1995) were plotted with the associated SPC values in the Figure 5.7. It is noticed in the figure that the binary specimens tested in this study for $50\% \leq \text{SPC} \leq 100\%$ are medium to medium loose specimens and the binary specimen for $0\% \leq \text{SPC} \leq 30\%$ are medium to dense specimens based on the e_{min} and e_{max} trends by Evan (1995).

In Figure 5.8, the e values of the binary specimens presented in the Figure 5.7 and the critical small-particle content (SPC*) values calculated based on the e_{min} and e_{max} values for the SP and GP materials are plotted together. As can be seen, the range of the SPC* is from 23% to 36% in terms of the SPC. Surrounding the SPC* range, the existence of a transition zone, where the packing conditions are more complicated than the conditions of a single particle-size packing dominating (called "metastable" condition), is well attested in the literature (Thevanayagam and Martin, 2002 [33]).

Thevanayagam and Martin (2002) [33] emphasized that the SPC* for a specific composition is a range rather than a single value, with more wide range than the theory-based values, and this range is often called "transition zone" or TZ in the literature. Soils in the transition zone (TZ) are in a metastable condition where the engineering characteristics are quite different from those

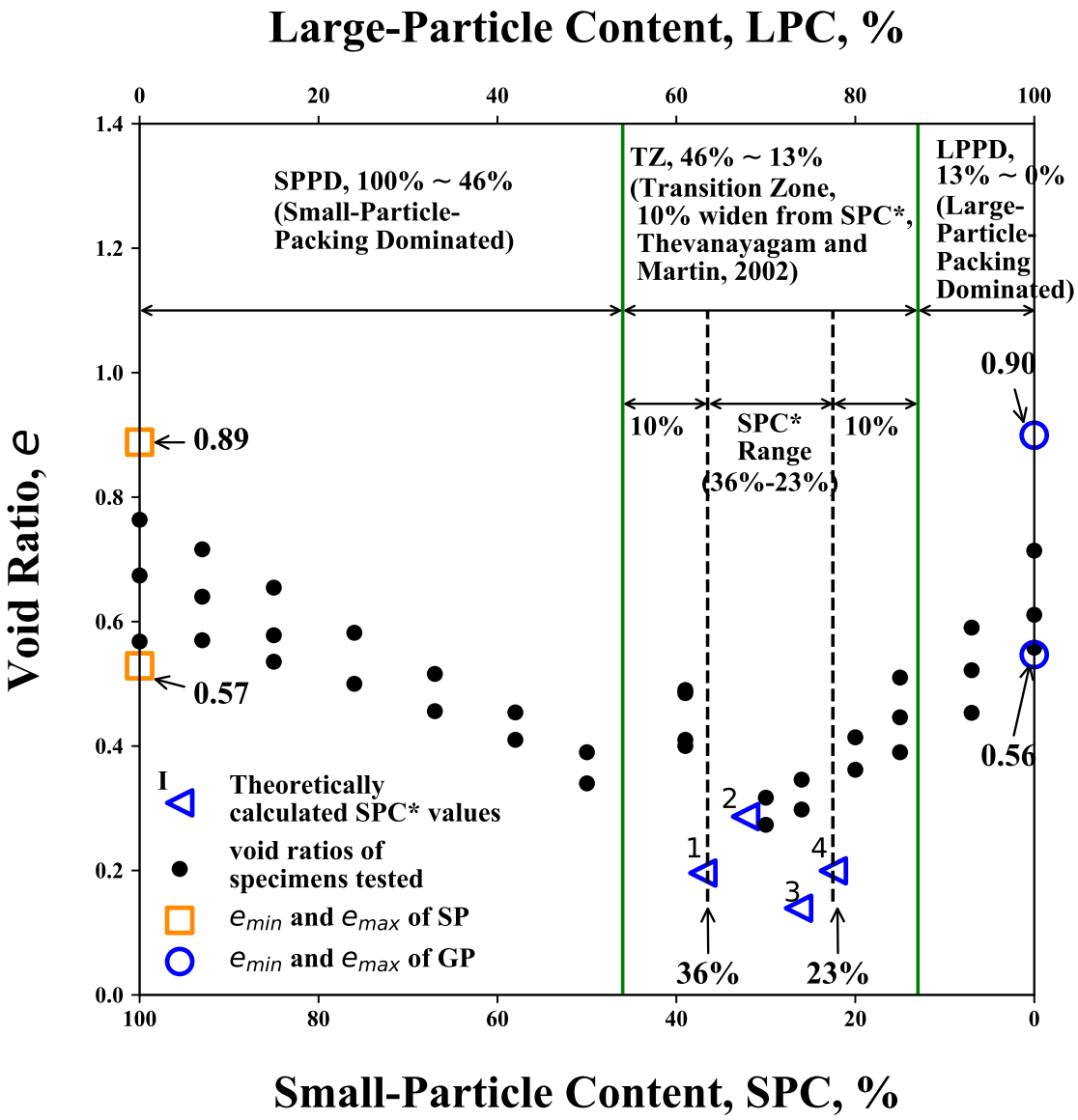

Figure 5.8: Variation in Void Ratio with Small-Particle Content and Large-Particle Content of the Binary Specimens Tested as well as Theoretically Calculated SPC* Values (Note: Four SPC* values are shown in the figure. The condition of ${}^{1}\triangleleft$ is calculated with the e_{max} of the GP and the e_{min} of the SP. The condition of ${}^{2}\triangleleft$ is calculated with the e_{max} of the GP and e_{max} of the SP. The condition of ${}^{3}\triangleleft$ is calculated with the e_{min} of the GP and the e_{min} of the SP. The condition of ${}^{4}\triangleleft$ is calculated with the e_{min} of the GP and the e_{max} of the SP.)

of either SPPD or LPPD. Base on the consideration of the calculation of the SPC* range (23% $\leq$ SPC $\leq$ 36%) in this study and the 10% widening of the SPC* range (Thevanayagam and Martin, 2002 [33]), the range of 13% $\leq$ SPC $\leq$ 46% is assumed to be the transition zone (TZ) in this study. Accordingly, the Gradations S100 through S50L50 (the specimens for 46% $\leq$ SPC $\leq$ 100%) are assumed to be the small-particle-packing dominated (SPPD) condition, and when the SPC is less than or equal to 13 percent, the large-particle-packing dominated (LPPD) condition is assumed. (See Figure 5.8.) Theses three classes and the associated percentages of each particle size (i.e., SPC and LPC) are summarized in Table 5.7

Table 5.7: Three Classes for the Binary Mixtures Tested in this Study

Class ID.	$SPPD$[1]	TZ[2]	$LPPD$[3]
SPC[4], %	100 $\sim$ 46	46 $\sim$ 13	13 $\sim$ 0
LPC[5], %	0 $\sim$ 54	54 $\sim$ 87	87 $\sim$ 100

[1] Small-particle packing dominated
[2] Transition zone
[3] Large-particle packing dominated
[4] Small-particle content
[5] Large-particle content

A total of 28 binary specimens tested in this study were classified into three classes: (1) SPPD, comprising specimens with small-particle-packing conditions dominating, (2) TZ, comprising materials within the transition zone, and (3) LPPD, comprising specimens with large-particle-packing conditions

dominating. Table 5.8 shows the physical properties of the 14 SPPD specimens and the 3 poorly-graded sand (SP) specimens. The physical properties shown in the table are: void ratio (e); dry unit weight (γ_d); moisture content (w); median grain size (D_{50}); and uniformity coefficient (C_u).

Table 5.8: Physical Properties of the 3 Poorly-Graded Sand (SP) Specimens and 14 Small-Particle-Packing Dominated (SPPD) Specimens

No.	**Material ID.**	**SPC %**	**Class ID.**	e	γ_d **(pcf)**	w **(%)**	D_{50} **(mm)**	C_u
1	S100	100	SP	0.57	105.0	7.5	0.34	1.33
2	S100	100	SP	0.67	98.8	7.5	0.34	1.33
3	S100	100	SP	0.76	93.8	7.5	0.34	1.33
4	S93S07	93	SPPD	0.57	107.5	7.0	0.34	1.35
5	S93L07	93	SPPD	0.64	104.8	7.0	0.34	1.35
6	S93L07	93	SPPD	0.72	96.4	7.0	0.34	1.35
7	S85L15	85	SPPD	0.54	107.7	7.5	0.35	1.38
8	S85L15	85	SPPD	0.58	104.8	6.4	0.35	1.38
9	S85L15	85	SPPD	0.65	99.9	6.4	0.35	1.38
10	S76L24	76	SPPD	0.50	107.5	5.7	0.37	1.43
11	S76L24	76	SPPD	0.58	104.6	5.5	0.37	1.43
12	S67L33	67	SPPD	0.46	113.6	5.2	0.38	1.47
13	S67L33	67	SPPD	0.52	109.0	5.0	0.38	1.47
14	S58L42	58	SPPD	0.41	120	4.4	0.40	34.5
15	S58L42	58	SPPD	0.45	113.7	4.4	0.40	34.5
16	S50L50	50	SPPD	0.34	124.8	3.8	4.97	35.6
17	S50L50	50	SPPD	0.39	117.5	3.8	4.97	35.6

The physical properties of the TZ specimens (e, γ_d, w ,D_{50}, and C_u) are shown in Table 5.9. As can be seen, the values of D_{50} and C_u are almost constant for these specimens. These relatively constant values of D_{50} and C_u allow for a study of the effect of e on the dynamic properties of the specimens.

Table 5.9: Physical Properties of the Transition Zone (TZ) Specimens

No.	**Material ID.**	**Group ID.**	e	γ_d **(pcf)**	w **(%)**	D_{50} **(mm)**	C_u
1	L61S39	TZ	0.40	105.0	7.5	10.09	36.0
2	L61S39	TZ	0.49	98.8	7.5	10.09	36.0
3	L70S30	TZ	0.32	93.8	7.5	10.42	35.3
4	L70S30	TZ	0.27	107.5	7.0	10.42	35.3
5	L74S26	TZ	0.30	104.8	7.0	10.54	34.6
6	L74S26	TZ	0.35	96.4	7.0	10.54	34.6
7	L80S20	TZ	0.36	107.7	7.5	10.91	32.9
8	L80S20	TZ	0.41	104.8	6.4	10.91	32.9
9	L85S15	TZ	0.39	99.9	6.4	10.81	30.8
10	L85S15	TZ	0.45	107.5	5.7	10.81	30.8
11	L85S15	TZ	0.51	104.6	5.5	10.81	30.8

As shown in Table 5.10, the specimens of Gradation L93S07 only fell into the large-particle-packing dominated (LPPD) class. The physical properties (e, γ_d, w ,D_{50}, and C_u) of the poorly-graded gravel (GP) and LPPD specimens are presented in the table. This classification of the binary specimens will be evaluated by their dynamic behaviors in Chapters 6 and 7.

Table 5.10: Physical Properties of the Poorly-Graded Gravel (GP) and Large-Particle-Packing Dominated (LPPD) Specimens

No.	**Material ID.**	**Group ID.**	e_g	γ_d **(pcf)**	w **(%)**	D_{50} **(mm)**	C_u
1	L100	GP	0.56	106.2	0	11.10	1.16
2	L100	GP	0.61	102.7	0	11.10	1.16
3	L100	GP	0.71	96.5	0	11.10	1.16
4	L93S07	LPPD	0.57	107.5	7.0	10.98	1.18
5	L93S07	LPPD	0.64	104.8	7.0	10.98	1.18
6	L93S07	LPPD	0.71	104.8	7.0	10.98	1.18

5.5 GAP-GRADED MATERIALS

5.5.1 A Well-Graded Sand

A well-graded sand was manufactured by seven different particle sizes. Materials of these seven different particles were obtained from the washed mortar sand (WMS) used for the SP material. The seven particle sizes were collected by the remaining materials on the seven size sieves of: No. 4 (4.75 mm); No. 10 (2 mm); No. 14 (1.41 mm); No. 20 (0.85 mm); No. 40 (0.425 mm); No. 60 (0.25 mm); and No. 200 (0.075 mm). This results in the uniformity coefficient (C_u) of 8.0 and median grain size (D_{50}) of 0.6 mm. By the USCS designation, this manufactured material was assigned as a well-graded sand (i.e., SW). A photograph of the well-graded sand (SW) used in this study is provided in Figure 5.9.

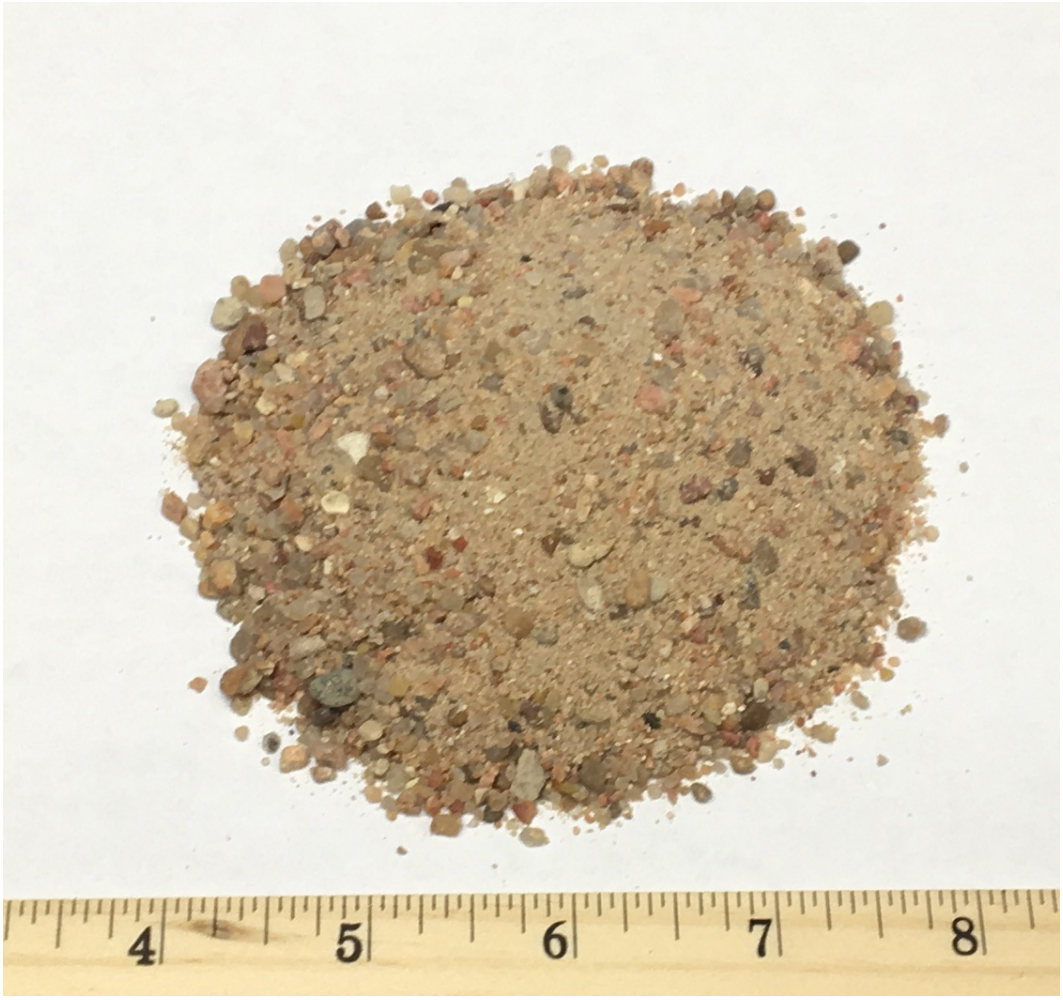

Figure 5.9: Photograph of a Well-Graded Sand (SW) Used in the Study (Note: The units of the ruler in the photograph are in inches.)

5.5.2 Physical Properties of Gap-Graded Mixtures

A single density of well-graded sand (SW) specimen was reconstituted with the void ratio of 0.65 in this study. And a total of seven gap-graded materials were manufactured using the SW material and the poorly-graded gravel (GP) which is used for the binary mixtures. Contrary to the binary mixtures in the previous section, each gap-graded mixture was reconstituted with a single density (i.e., one void ratio value).

The 9 gradation distribution curves: one manufactured SW, one poorly-graded gravel (the GP material), and 7 gap-graded materials are presented in Figure 5.10. The physical properties of these 9 materials are summarized in Table 5.11.

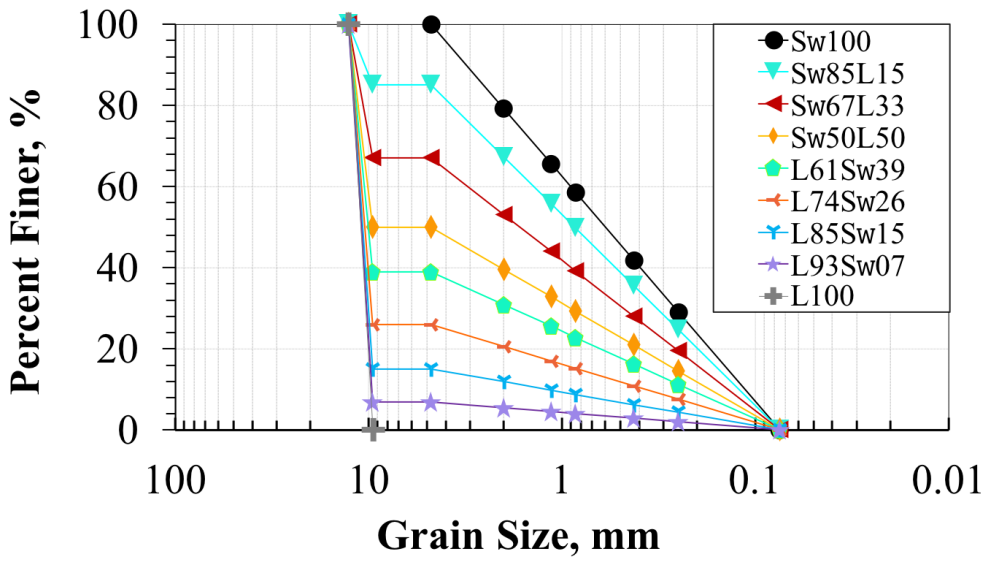

Figure 5.10: Gradation Curves of All Nine Materials: One SW, One GP and Seven Gap-Graded Materials

Table 5.11: Physical Properties of One SW Specimen, One GP Material, and Seven Gap-Graded Specimens

No.	**Material ID.**	**SPC**[1] **%**	**LPC**[2] **%**	e	γ_d **(pcf)**	w **(%)**	D_{50} **(mm)**	C_u	**USCS**
1	S_w100	100	0	0.65	100.0	7.5	0.60	8.0	SW
2	S_w85L15	85	15	0.55	106.7	7.5	0.86	11.5	SW
3	S_w67L33	67	33	0.43	115.7	7.5	1.66	22.1	SW
4	S_w50L50	50	50	0.32	125.1	0	9.51	58.6	SW-GP
5	$L61S_w39$	39	61	0.34	123.6	0	10.02	48.4	GW
6	$L74S_w26$	26	74	0.29	128.0	0	10.45	29.4	GW
7	$L85S_w15$	15	85	0.46	113.7	0	10.71	9.3	GW
8	$L93S_w07$	7	93	0.59	104.7	0	10.87	1.2	GP
9	$L100$	0	100	0.71	104.7	0	10.87	1.2	GP

[1] Small-particle content
[2] Large-particle content

5.6 SPECIMEN PREPARATION

The total of 42 specimens were reconstituted with the diameters of 2.8 inches (71.1 mm) and the heights of 5.6 inches (142.2 mm). Each specimen was compacted in 10 lifts, with the final lift having five percent in the undercompaction. As proved in the previous section (Section 5.3), the undercompaction method was very effective for reaching the minimum dry densities for most of the specimens except for in Gradation L61L39. For the undercompaction method, a 1.5-foot-long polyurethane rod (45 cm) with a diameter of 2.2 inches (5.6 cm) and a weight of 2.6 pounds (1.2 kg) was used as a hammer. This rod

(polyurethane) was selected to minimize soil particle crushing during strong compaction (Menq, 2003 [26]).

To make the specimens uniform, each lift was prepared with equally-apportioned partial materials. Then, each partial material was compacted to each target height calculated prior to the reconstitution. This method guaranteed that the specimens would reach the total target heights associated with the target densities.

5.7 TEST PROCEDURE

A dynamic torsional resonant column (RC) device was used for testing the poorly-graded, binary, and gap-graded specimens in this research. At first, confining pressure was increased in a series of steps from 4 to 64 psi (0.1 to 4.4 atm) to study the effect of confining pressure on the small-strain dynamic properties (small-strain shear modulus, G_{max}, and small-strain material damping ratio in shear, D_{min}). At each confining pressure level, the regulated air pressure was applied to the specimen for at least 60 minutes to allow the specimen to equilibrate. The discrete variations of G_{max} and D_{min} with time at a constant pressure were calculated on the basis of the measurements of related parameters. (See Chapter 3.) Changes in the values of G_{max} and D_{min} were generally within two percent over the test period of 60 minutes.

The specimens of transition zone (TZ) and large-particle-packing dominated (LPPD) frequently underwent membrane puncture as the pressure transitioned from 32 psi (2.2 atm) to 64 psi (4.4 atm). The most likely cause of

these membrane punctures was the relatively high pressure applied to the large void spaces between large particles on the surface of the specimen. In the case of each membrane puncture observed, the entire testing for the specimen was suspended.

After the series of low-amplitude dynamic torsional resonant column (LARC) tests at four or five different confining pressures was completed, the specimen was unloaded to the pressure level of 16 psi for a series of high-amplitude dynamic torsional resonant column (HARC) tests. Typically, 10 to 15 high-amplitude tests were performed in this series of HARC tests. The excitation torque used during the HARC test range approximately from 1.41×10^{-3} lb-in. (1.59×10^{-3} NT-m) to 14.1 lb-in. (1.59 NT-m) (Menq 2003 [26]). The effort to double the strain was made after each high-amplitude dynamic torsional resonant column test (HARC). During each test, shear modulus and material damping ratio in shear were measured. As a result of the series of HARC tests, the shear modulus reduction and material damping ratio curves were generated.

5.8 SUMMARY

A total of 42 reconstituted specimens were tested in this study. Among these, one is a well-graded sand, six were composed of two poorly-graded materials (three poorly-graded sand and three poorly-graded gravel specimens), 7 gap-graded specimens were manufactured by the well-graded sand and the poorly-graded gravel, and the 28 were made up of binary mixtures.

The poorly-graded sand (the SP material) manufactured using washed mortar sand was used as the small-particle material in the binary mixtures, and the poorly-graded gravel (the GP material) from a river gravel served as the large-particle material. The well-grade sand was manufactured with 7 different particle size collected from the washed mortar sand. The physical and mechanical properties of the poorly-graded, binary, and gap-graded material specimens are presented in this chapter. Additionally, the gradation characteristics, such as D_{50} and C_u, are also determined for the specimens.

The 28 binary specimens are classified into three classes based on their percentages of small-particle content (SPC): (1) small-particle-packing dominated (SPPD) specimens for $50\% < \text{SPC} < 100\%$, (2) transition zone (TZ) specimens for $15\% \leq \text{SPC} \leq 39\%$, and (3) large-particle-packing dominated (LPPD) specimens for $0\% < \text{SPC} < 7\%$. The next two chapters (Chapters 6 and 7) will discuss the dynamic behaviors of these specimens observed in the small-strain range and nonlinear range, respectively. Additionally, the test results of the well-graded sand and gap-graded specimens are compared with the results of the binary specimens.

Chapter 6

Small-Strain Dynamic Properties of Binary and Gap-Graded Mixtures

6.1 INTRODUCTION

The small-strain range is typically defined as the strain range in which the dynamic properties (i.e., shear modulus, G, and material damping ratio in shear, D,) are constant, indicating that the dynamic properties are independent of shear strain amplitude. The shear modulus (G) in the small-strain range is typically denoted as the small-strain shear modulus, G_{max}, and the material damping ratio in shear (D) in this strain range is denoted as the small-strain material damping ratio in shear, D_{min}. As discussed in Chapter 5, six poorly-graded specimens (three SP specimens and three GP specimens) and one well-graded sand (SW) specimen were reconstituted as reference specimens for the binary and gap-graded specimens, respectively. A total of 28 binary specimens were reconstituted with the mixtures of poorly-graded sand (SP) and poorly-graded gravel (GP). Additionally, 7 gap-graded specimens were also reconstituted with the mixtures of a well graded sand (SW) and the poorly-graded gravel (GP).

In this chapter, the small-strain stiffness and material damping ratio

characteristics of the binary and gap-graded specimens are discussed and compared based on the G_{max} and D_{min} values determined by dynamic torsional resonant column (RC) testing. The effects of void ratio and gradation characteristics are evaluated for the binary and gap-graded specimens. At the end of this chapter, the small-strain dynamic properties of the binary and gap-graded materials are compared.

6.2 SMALL-STRAIN SHEAR MODULUS, G_{max}, OF THE TWO POORLY-GRADED MATERIALS, SP AND GP

The two poorly-graded materials, SP and GP, used in creating the binary specimens were first tested individually. The gradation curves for the SP and GP materials are presented in Figure 6.1a. Variations in small-strain shear modulus (G_{max}) with confining pressure (σ_o) of the two poorly-graded materials, which are also referred to as Gradations S100 and L100, are presented in Figure 6.1b. In Figures 6.1a and 6.1b, the circular symbols (i.e., ◯) represent the specimens of Gradation S100, and the plus symbols (i.e., +) represent the specimens of Gradation L100. The S100 specimens are poorly-graded sand (SP) with a uniformity coefficient (C_u) of 1.3. The L100 specimens are poorly-graded gravel (GP) with a C_u value of 1.2. As discussed in Chapter 5, each gradation of these two poorly-graded materials was reconstituted at three different values of void ratio (e). In the case of the S100 specimens, the specimens had some added water with the water content of 7.5%, but no water was added

to the L100 specimens due to the high permeability.

In the Figure 6.1b, the log G_{max} - log σ_o relationships of these six poorly-graded specimens (three S100 and three L100 specimens) are compared.

The effect of confining pressure (σ_o) on G_{max} can be expressed by the following equation as a normalized confining pressure raised to the power n_G as:

$$G_{max} = A_G \left(\frac{\sigma_o}{P_a}\right)^{n_G} \tag{6.1}$$

where:

A_G is the value of G_{max} at a mean confining pressure of one atmosphere and the specimen void ratio, and

P_a is atmosphere pressure (1 atm).

Using Equation 6.1, the log G_{max} - log σ_o relationships of the six poorly-graded specimens were determined. Each relationship is represented by a straight line in this log-log plot in the Figure 6.1b. Also, for "relative" comparison purposes throughout this dissertation, a reference log G_{max} - log σ_o relationship, which is the lowest relationship with $e = 0.76$ among the poorly-graded specimens, is shown by the dashed black line in the figure. The relationships of log G_{max} - log σ_o for the S100 and L100 specimens are linear, indicating that the G_{max} increases with increasing σ_o (Richart et al., 1970)[28].

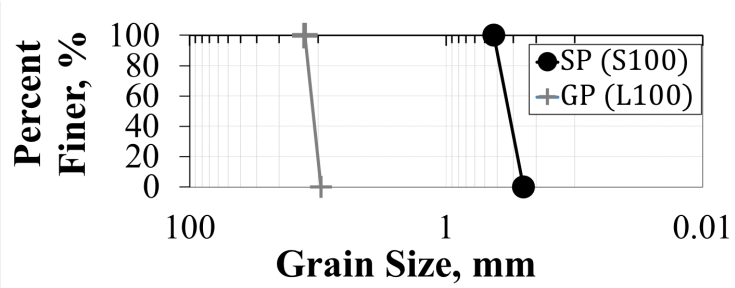

(a) Grain-Size Distribution Curves of the SP and GP Materials

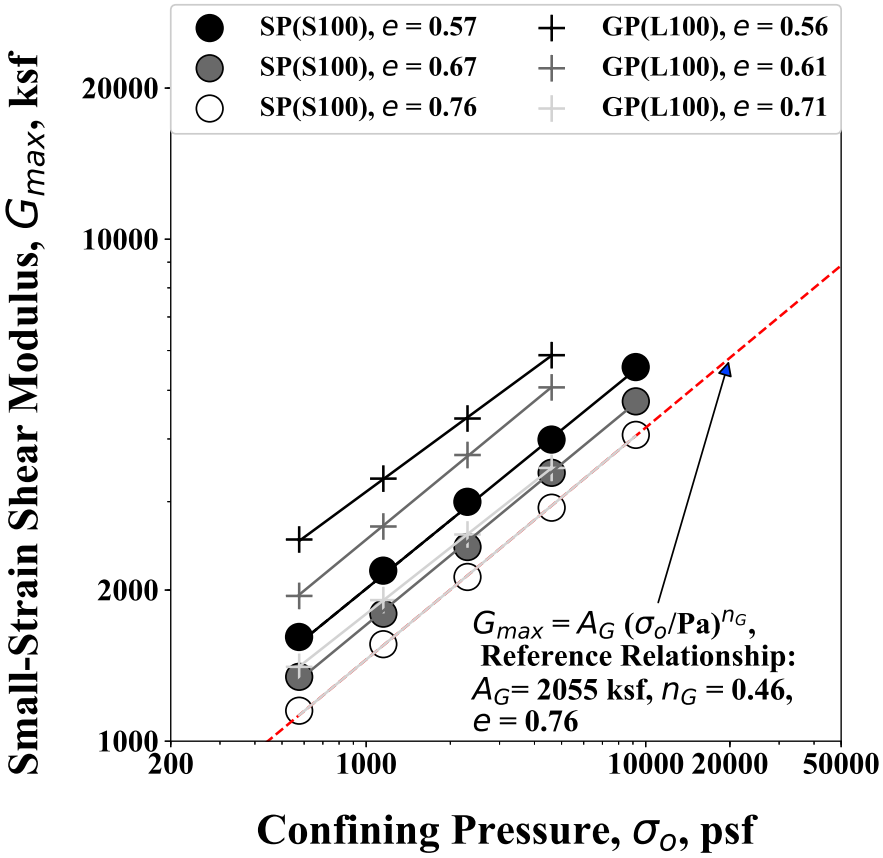

(b) Log G_{max} - Log σ_o of the SP and GP Materials

Figure 6.1: Gradation Curves and Variations in Small-Strain Shear Modulus with Confining Pressure of the SP and GP Materials (referred to as the S100 and L100 Specimens in this Dissertation)

In the Figure 6.1b, it is apparent that the relationship of log G_{max} - log σ_o is a function of e for each gradation. As e decreases (i.e., as the symbol becomes darker), the log G_{max} - log σ_o relationship translates vertically. For the slope of the relationships (n_G) no significant change is observed among the specimens for both poorly-graded materials. This result is consistent with the study by Menq (2003) [26] that the value of e does not significantly affect the slope of the log G_{max} - log σ_o relationships of granular soils.

It is interesting to compare the log G_{max} - log σ_o relationships between the two specimens: (1) the S100 with e=0.57 (i.e., solid circle), and (2) the L100 specimen with $e = 0.56$ (i.e., black plus). The L100 specimen with $e = 0.56$ is stiffer than the S100 specimen with $e = 0.57$ in spite of their similar void ratio values. This difference in stiffness can be explained by the difference between the D_{50} values of the two specimens. The D_{50} value of the L100 specimen is about 30 times larger than that of the S100 specimen. This effect of median grain size (D_{50}) for granular soils was well explained by Menq (2003) [26] that the small-strain shear modulus is mainly a function of D_{50} at constant e and C_u values. This difference occurs, in fact, due to the reduced number of particle contact in the cases of the much larger particle sizes.

6.3 SMALL-STRAIN SHEAR MODULUS, G_{max}, OF BINARY MIXTURES

6.3.1 Log G_{max} - Log σ_o relationships of the SPPD Specimens

As discussed in the Chapter 5, the small-particle-packing dominated (SPPD) specimens are the specimens in which the percentage of small-particle content (SPC) are greater than or equal to 46 percent (i.e., 46% $\leq$ SPC $\leq$ 100%) in this study. It is shown subsequently that, in these specimens, the small-particle packing (SPP) condition dominates the load transfer network (LTN) during shear.

There are 17 SPPD specimens in this study as shown in Table 5.8 in Chapter 5.. The dynamic torsional resonant column (RC) test was performed with the SPPD specimens in the small-strain range. The seventeen log G_{max} - log σ_o relationships of the SPPD specimens are shown in Figure 6.2. In the figure, the reference log G_{max} - log σ_o relationship (i.e., the relationship of the S100 specimen with $e = 0.76$) is also provided for the relative comparison purposes with the constant values of $A_G = 2055$ ksf and $n_G = 0.46$ as a dash line. Among the 17 SPPD relationships, the S50L50 specimen with $e = 0.34$ is the stiffest and has the lowest e value. The other relationships stand between the two relationships of the S50L50 with $e = 0.34$ (i.e., the stiffest SPPD specimen) that was tested and the reference relationship. Overall, the log G_{max} - log σ_o relationships vertically increased as the global void ratio (e) values decreased. During the increase of the G_{max} values, no significant change was observed in the slope of the relationship (n_G) as shown subsequently in

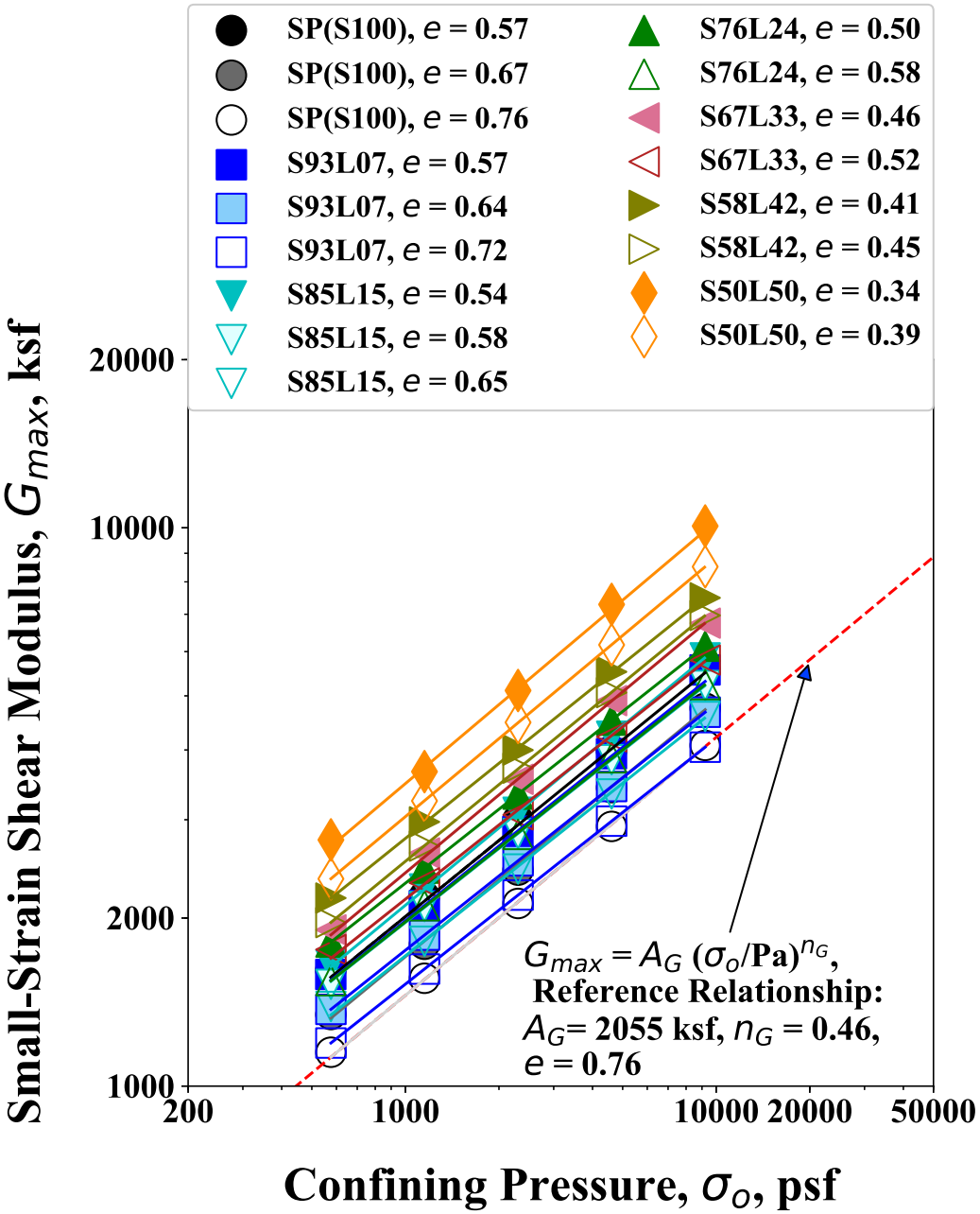

Figure 6.2: Variations in Small-Strain Shear Modulus with Confining Pressure of the Small-Particle-Packing Dominated (SPPD) Specimens (i.e., for 50% $\leq$ SPC $\leq$ 100%)

Section 6.2.

To illustrate better the effect of e on the SPPD specimens, the loosest SPPD specimens that were tested for each gradation are re-plotted in Figure 6.3. As can be seen, initially no significant difference is observed between the relationships for the S93L07 specimen with $e = 0.72$ and the S100 specimen with $e = 0.76$. In other words, the relatively small amount of large particles (i.e., about 7 percent) had no significant effect on the small-strain shear modulus of the parent material (i.e., the SP material). However, as the percentage of large particles increases beyond 7%, the value of global void ratio decreases and the value of A_G increases. This result further supports the previous research by Shin (2014) [30], which found that oversized particles with the amount of less than 10 percent did not affect significantly the dynamic stiffness of a granular soil.

In the Figure 6.3, it is also clear that the log G_{max} - log σ_o relationships of the SPPD specimens increases as e decreases. This effect of e on the G_{max} can be more quantitatively described with the two variables: (1) G_{max} at one atmosphere, A_G, and (2) the slope of the relationship, n_G. These factors are discussed in the following sections.

6.3.2 G_{max} at 1 atm (A_G) of the SPPD Specimens

Hardin and Richart (1963) [16] concluded that void ratio (e), which equals global void ratio, e_g, in this dissertation, was the main factor affecting the small-strain shear modulus of granular sandy soils. They also found that

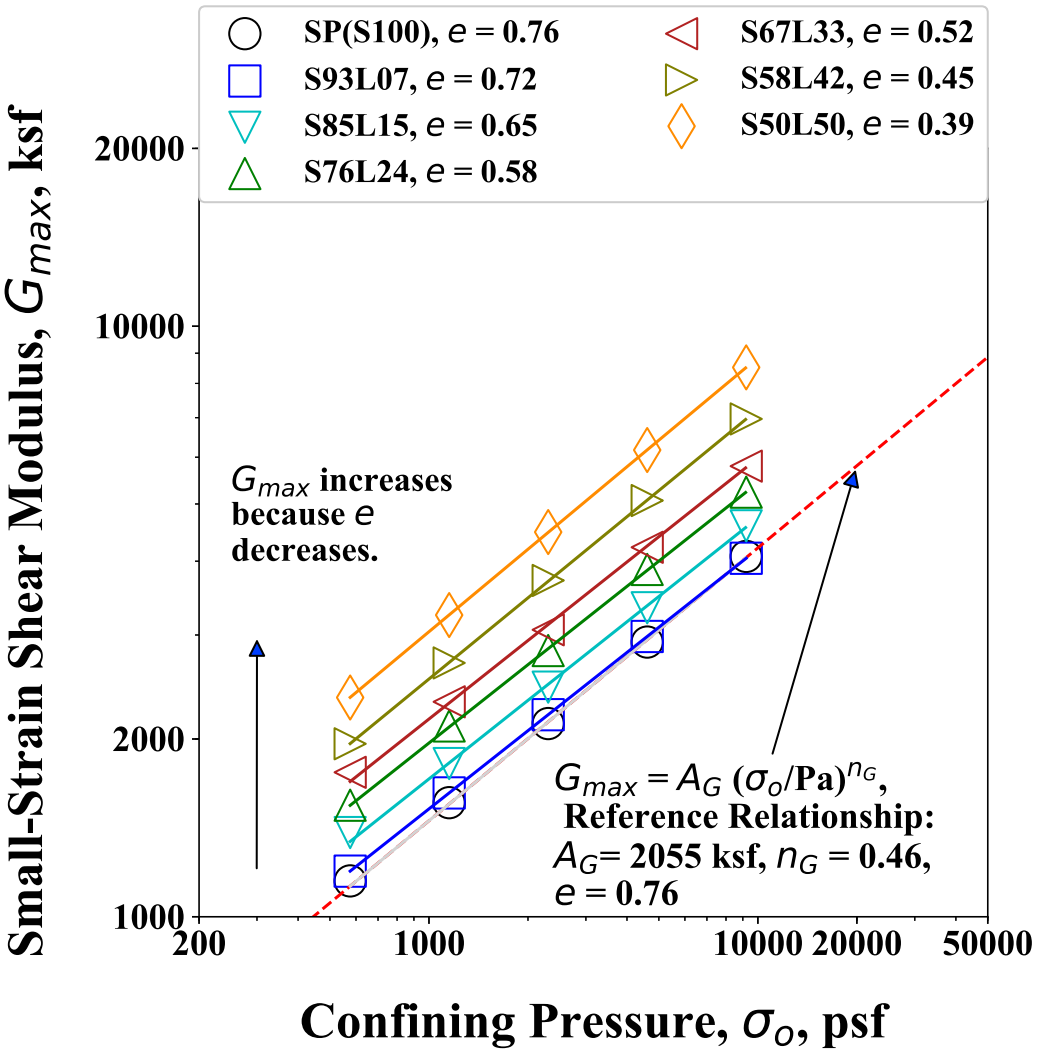

Figure 6.3: Variations in Small-Strain Shear Modulus with Confining Pressure of All the Loosest of Small-Particle-Packing Dominated (SPPD) Specimens That were Tested

the void ratio function was affected by gradation characteristics such as C_u, C_c, and D_{50}. In this section, the void ratio correction function proposed by Hardin (1978) [15] will be used for the values of G_{max} at 1 atm (A_G) for all SPPD specimens as shown below.

The A_G values of the SPPD specimens with the e values are shown in Figure 6.4. A A_G trend line calculated by the void ratio function proposed by Hardin (1978) [15] is presented in Figures 6.4a and 6.4b. In the Figure 6.4a, Hardin's trend line is compared to the A_G values when the percentage of small-particle content is greater than or equal to 67 percent (SPC $\geq$ 67%). As expected, the A_G values increase with decreasing the e values. It is interesting to see that the increase of A_G values very closely follows the increasing trend of Hardin (1978)'s void ratio function. In other words, the SPPD specimens for SPC $\geq$ 67% showed the small-strain dynamic stiffness behavior of the typical poorly-graded sand (i.e., the parent sand material in binary mixtures). This result may be explained by the hypothesis that the small-particle packing (SPP) condition dominates the load transfer network (LTN) during the shear in a particular range of SPC range (SPC $\geq$ 67%). Furthermore, it is also possible to say that estimating the void ratio function of the parent poorly-graded sand is especially very effective for estimating the A_G values of binary mixtures in that SPC range.

In the Figure 6.4b, the A_G values of Gradations S58L42 and S50L50 specimens are appended to the A_G values presented in the Figure 6.4a. Interestingly, these appended A_G values began to deviate from the Hardin's trend.

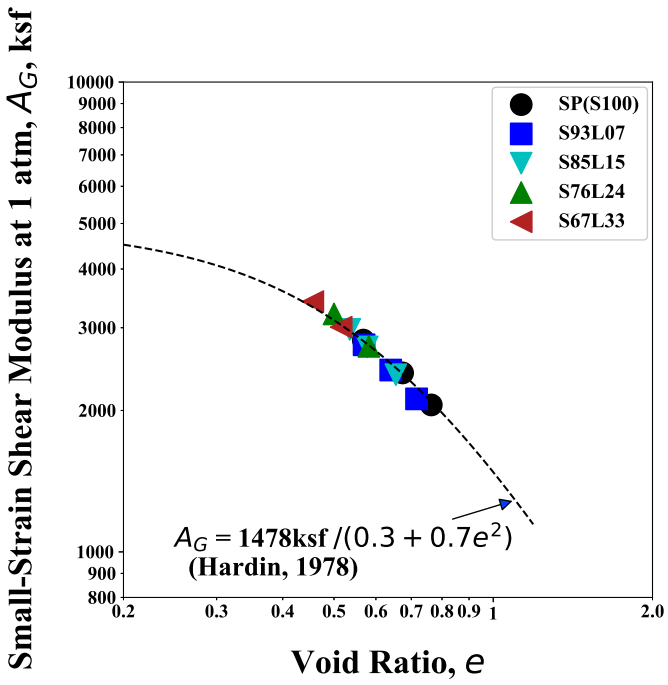

(a) Log A_G - Log e for 67% $\leq$ SPC $\leq$ 100%

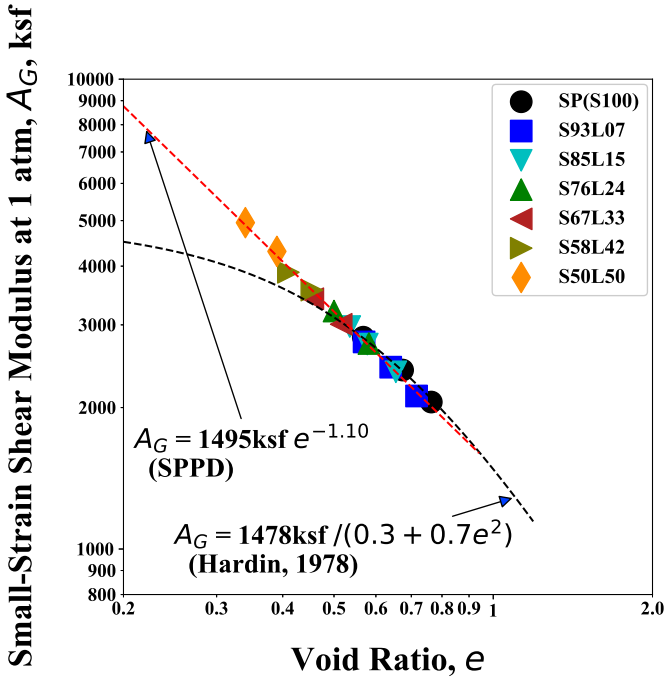

(b) Log A_G - Log e for 50% $\leq$ SPC $\leq$ 100%

Figure 6.4: Variation in Small-Strain Shear Modulus at 1 Atm, A_G, with Void Ratio of the Small-Particle-Packing Dominated (SPPD) Specimens

Moreover, all the A_G values in the Figure 6.4b followed a straight-line trend in the log A_G - log e relationship. This clear straight-line trend of the SPPD specimens for SPC $\geq$ 50% in the relationship of log A_G - log e can be equated using the method of "least square" to generate a void ratio correction function for the specimens. The "least square" curve fitting was performed with an exponential function for the void ratio correction function multiplied by (Jamiolkowski et al., 1995; Lo Presti et al., 1997; and Menq, 2003). As a result, the small-strain shear modulus at one atmosphere (A_G) values of the SPPD specimens for SPC $\geq$ 50% can be estimated with the following equation:

$$\begin{aligned} A_G &= A_{G,e=1.0} \times F(e) \\ &= 1495\ ksf \times e^{-1.10} \quad for\ SPC \geq 50\% \end{aligned} \tag{6.2}$$

where:

$A_{G,e=1.0} = A_G$ at 1 atm as well as e=1.0, and

$F(e)$ = a void ratio correction function.

In the void ratio correction function, the exponent component is about -1.0. This indicates the significant usefulness of the F(e), since the A_G values for the SPPD specimens (i.e., the binary specimens for SPC $\geq$ 50%) can be simply estimated with the value of $A_{G,e=1.0}$ divided by the void ratio of the specimen.

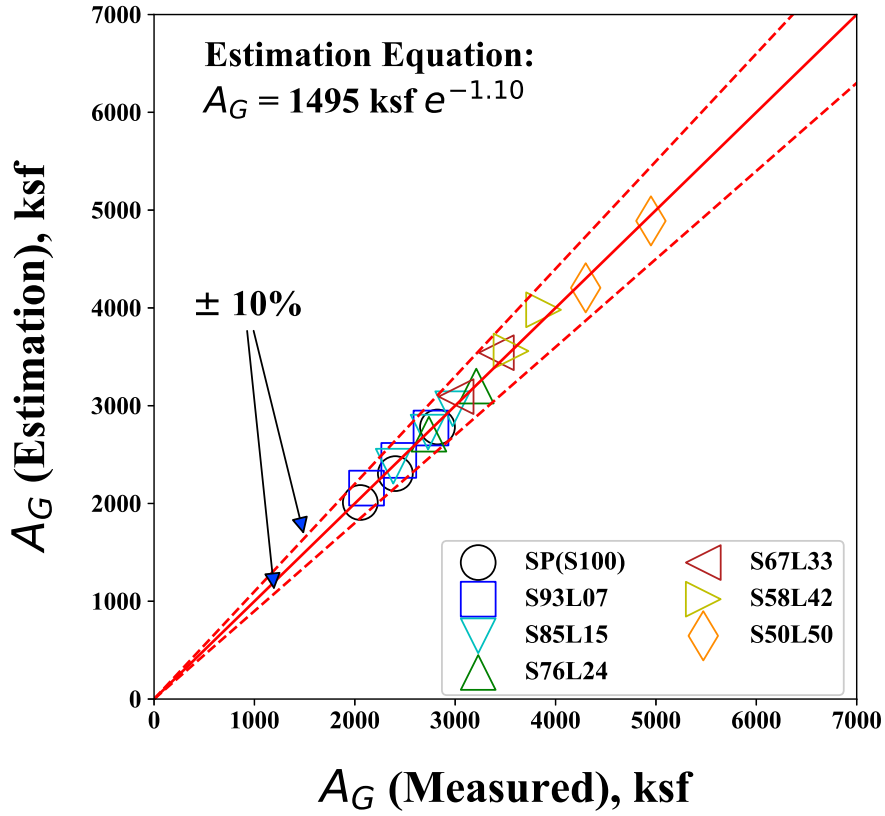

Figure 6.5: Comparison between Measured and Estimated Values of A_G for $50\% \leq \text{SPC} \leq 100\%$

The use of Equation 6.2 to calculate the A_G estimations of the SPPD specimens can be more quantitatively evaluated through a comparison of them to the A_G measurements. As shown in Figure 6.5, all estimations are significantly accurate within ± 10 percent, and generally within ± 5 percent.

The concept of the skeleton void ratio is often used to describe the packing condition of the dominant particle fraction in binary (or gap-graded) granular mixtures. In binary mixtures, two skeleton void ratios are defined and

are based on the dominant fraction: (1) the sand skeleton void ratio, $e_{sk,sand}$, and (2) the gravel skeleton void ratio, $e_{sk,gravel}$ as described in Figure 6.6. In Figure 6.6a, the term of global void ratio (e_g), which is the same as the term of void ratio (e) used in this dissertation, is defined as the volumetric ratio between voids and all solid particles (i.e., both the small particles and large particles in binary materials). In Figures 6.6b and 6.6c, the sand skeleton void ratio ($e_{sk,sand}$) and gravel skeleton void ratio ($e_{sk,gravel}$) are described with each phase relationship, respectively. The sand skeleton void ratio (Figure 6.6b) is defined as the volumetric ratio between voids and the solids of sand (small particles), and the gravel skeleton void ratio (Figure 6.6c) is defined as the volumetric ratio between apparent voids, which include voids and volumetric sand particles, and the solids of gravel (large particles).

The variation in A_G with sand skeleton void ratio ($e_{sk,sand}$) of the SPPD specimens is shown in Figure 6.7. Overall, the log A_G - log $e_{sk,sand}$ relationships of the SPPD specimens shift vertically with the increase of large-particle content (LPC). In other words, at a given $e_{sk,sand}$ value (e.g., $e_{sk,sand} = 0.79$) the value of A_G increases as more large particles replace the small particles in the binary specimens for $50\% \leq \text{SPC} \leq 100\%$. However, it should be careful to interpret the effect of LPC on A_G for the SPPD specimens because the increase of large particle in binary materials also impact the decrease of global void ratio (e_g) of the specimens.

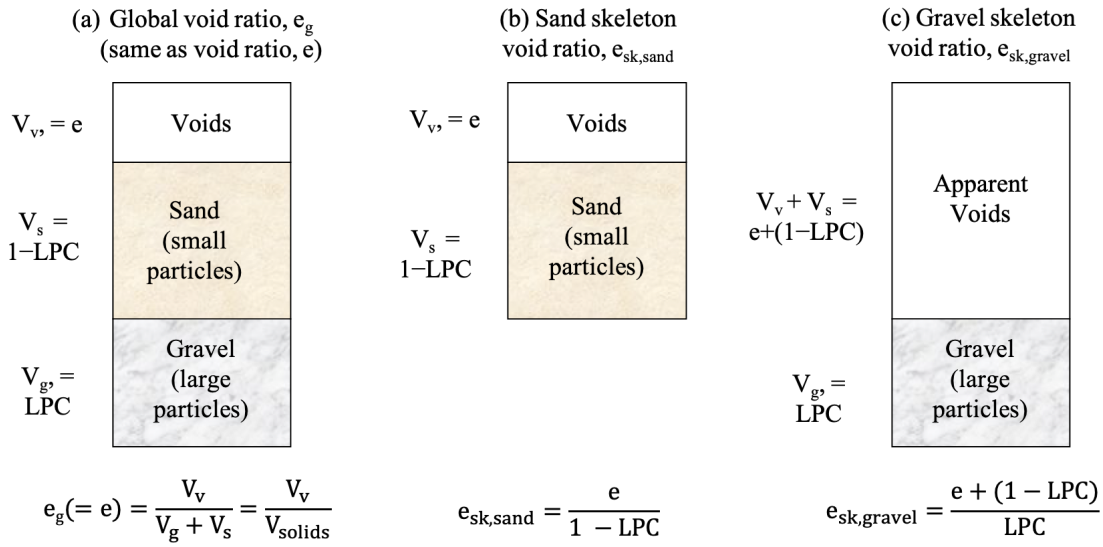

Figure 6.6: Illustration of Global Void Ratio, e_g (= Void Ratio, e) and Two Skeleton Void Ratios ($e_{sk,sand}$ and $e_{sk,gravel}$) Used in Describing of Binary Granular Soils

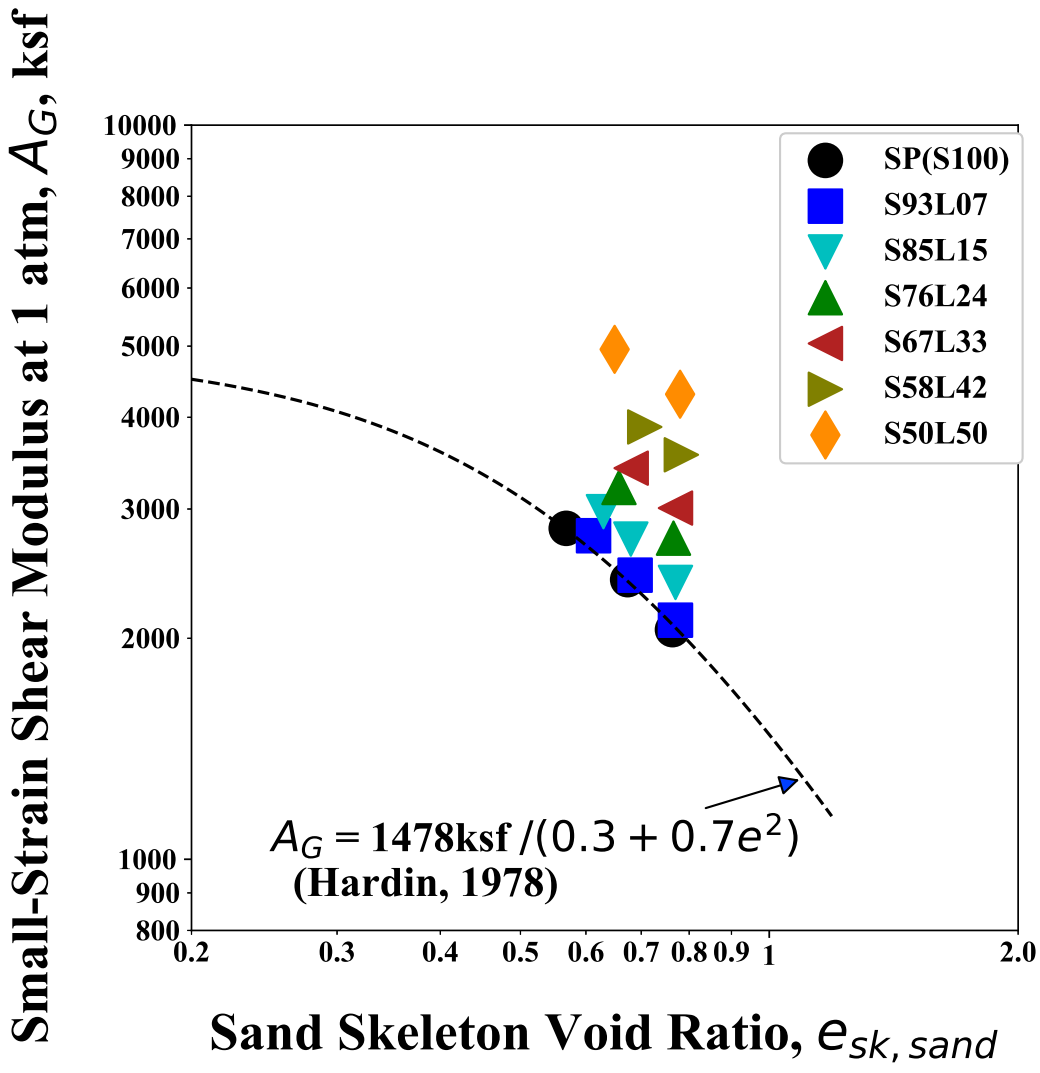

Figure 6.7: Variation in Small-Strain Shear Modulus at 1 Atm, A_G, with Sand Skeleton Void Ratio of the Small-Particle-Packing Dominated (SPPD) Specimens

6.3.3 Log G_{max} - Log σ_o relationships of the TZ and LPPD Specimens

As discussed in the Chapter 5, the transition zone (TZ) specimens are ones with between 54 percent and 87 percent of large particles (or between 13 percent and 46 percent of small particles) in this research. For these specimens, both packing conditions (i.e., small-particle packing (SPP) and large-particle packing (LPP) conditions) can exist in one specimen. Also, the critical packing condition can exist in more than one of the specimens. (See Figure 5.8.) The large-particle-packing dominated (LPPD) specimens are ones with between 87 percent and 100 percent of large-particle content (LPC) (or $0\% \leq \text{SPC} \leq 13\%$) in this research. As with the SPPD specimens, the load transfer network (LTN) during the shear in the LPPD specimens would be presumably be dominated by the large-particle packing (LPP) condition.

The log G_{max} - log σ_o relationships of the eleven TZ specimens are presented in Figure 6.8. To provide the relative comparisons, the reference relationship determined in the previous section with the constants of $A_G = 2055$ ksf, $n_G = 0.46$, and $e = 0.76$ is also presented as a dashed line in the figure. Between the eleven relationships, the specimen of Gradation L70S30 has the stiffest log G_{max} - log σ_o relationship with the lowest void ratio of $e = 0.27$. The rest of the relationships fall between the stiffest relationship (Gradation L70S30, $e = 0.27$) and the reference relationship. Interestingly, all TZ specimens have higher log G_{max} - log σ_o relationships with the steeper slopes relative to the reference relationship. This can indicate that the TZ speci-

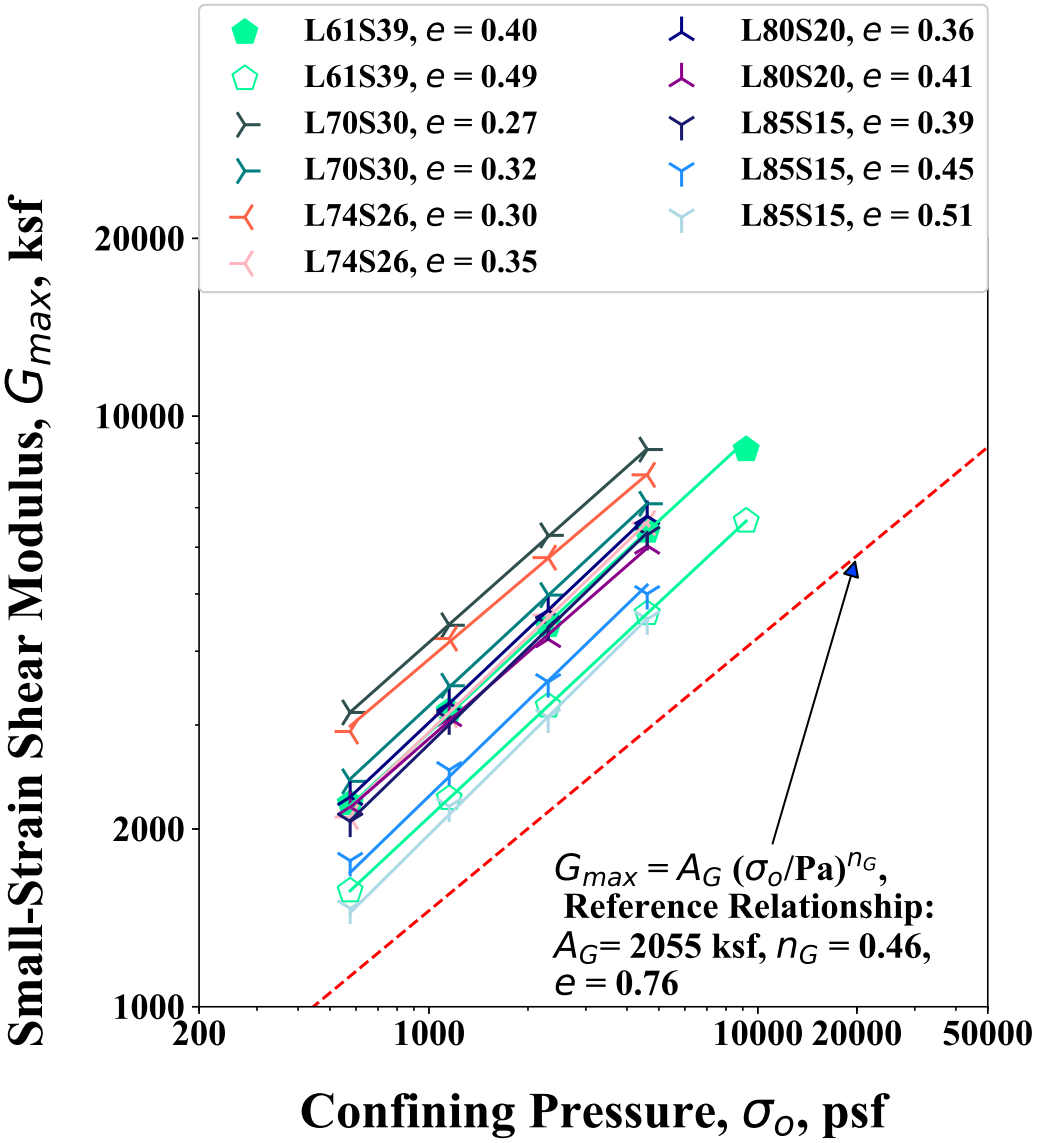

Figure 6.8: Variations in Small-Strain Shear Modulus with Confining Pressure for the Transition Zone (TZ) Specimens ($61\% \leq$ LPC $\leq 85\%$)

mens are relative stiffer and have higher confining pressure change sensitivity compared to the SPPD specimens.

The log G_{max} - log σ_o relationships of the LPPD specimens are presented in Figure 6.9. Overall, the LPPD specimens have higher G_{max} - log σ_o relationships relative to the reference relationship with no significant change in the slope except for the L100 specimen with $e = 0.56$ and the L93S07 specimen with $e = 0.45$. Additionally, the LPPD specimens don't seem to have a function of void ratio in the G_{max} - log σ_o relationship. For example, the log G_{max} - log σ_o relationships of the L100 specimen with $e = 0.61$ and the L93S07 specimen with $e = 0.52$ behave similarly, while they have different void ratios in the absolute value of 0.1.

6.3.4 G_{max} at 1 atm (A_G) for the TZ and LPPD Specimens

This section will compare the values of small-strain shear modulus at one atmosphere (A_G) of the TZ and LPPD specimens. The A_G values of the TZ and LPPD specimens with the e values is shown in Figure 6.10. The A_G estimation curve calculated by the Hardin (1978)'s void ratio function (assuming $A_G = 1478$ ksf at e=1.0) is also plotted in Figures 6.10a and 6.10b.

Interestingly, in the Figure 6.10a, the A_G values of the TZ specimens show a clear relationship with the void ratio. This relationship seems a straight line trend as similarly to the trend of log A_G - log e relationship for the SPPD specimens. (See Figure 6.5.) On the other hand, the LPPD specimens (the L100 and L93S07 specimens) show different trends from the TZ specimens in

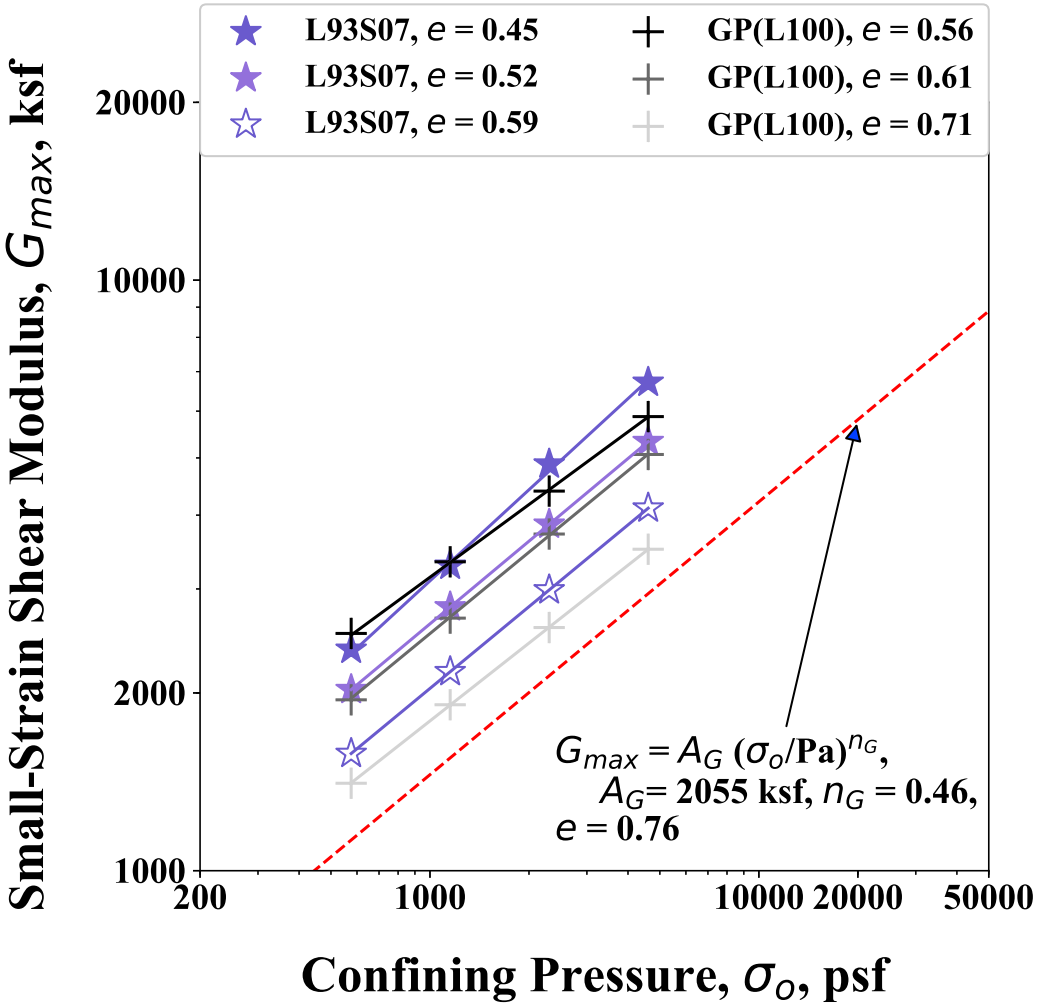

Figure 6.9: Variations in Small-Strain Shear Modulus with Confining Pressure for the Large-Particle-Packing Dominated (LPPD) Specimens (97% $\leq$ LPC $\leq$ 100%)

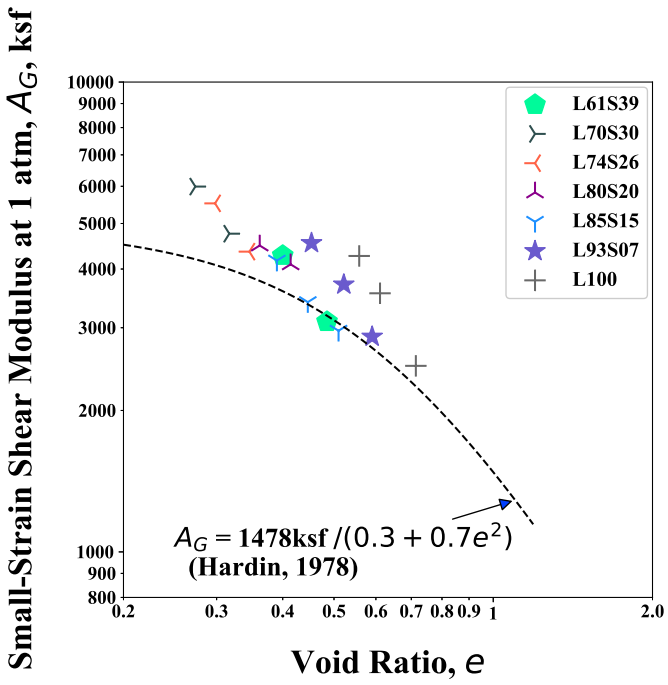

(a) Log A_G - Log e for 61% $\leq$ LPC $\leq$ 100%

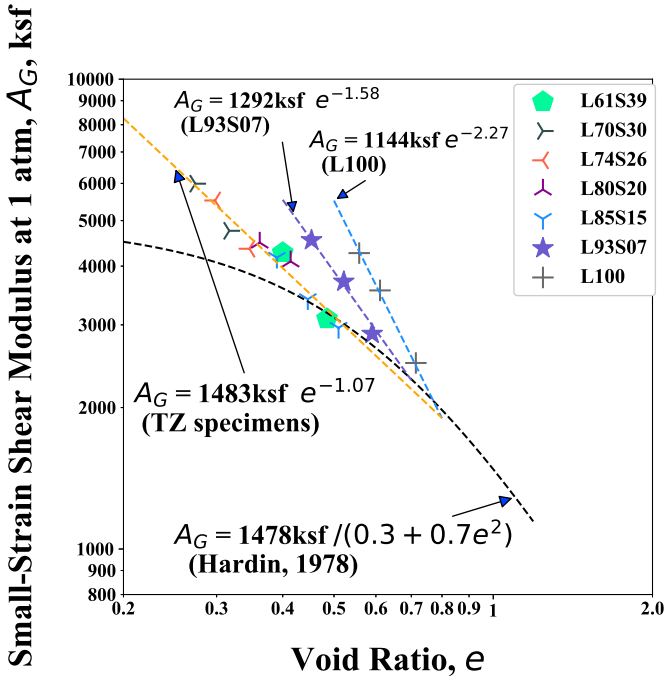

(b) Log A_G - Log e for 61% $\leq$ LPC $\leq$ 100% with Fitting Curves

Figure 6.10: Variation in Small-Strain Shear Modulus at 1 Atm, A_G, with Void Ratio for 61% $\leq$ LPC $\leq$ 100%

the log A_G - log e relationship. Moreover, the L100 specimens are stiffer than the L93S07 specimens at a give void ratio showing different log A_G - log e relationship.

These three different trends in the log A_G - log e relationship for the TZ and LPPD specimens can be quantified with the method of "least square". In Figure 6.10b, the results of regression analyses for the LPPD and the TZ specimens were plotted together. Also, the values of constants such as the small-strain shear modulus at 1 atm as well as $e = 1.0$ (i.e., $A_{G,e=1.0}$) and the exponential component in a void ratio correction function (α) for the three different trends in the Figure 6.10b are summarized with the median grain size (D_{50}) and uniformity coefficient (C_u) values in Table 6.1.

Table 6.1: Comparison of the values of $A_{G,e=1.0}$, the exponential component in a void ratio correction function (α), median grain size (D_{50}), and uniformity coefficient (C_u) for the TZ, L93S07, and L100 Specimens

ID.	$A_{G,e=1.0}$**, ksf**	α	$^2D_{50,avg}$**, mm**	$^2C_{u,avg}$
^{1}TZ	1483	-1.07	10.5	33.5
L93S07	1292	-1.58	11	1.16
L100	1144	-2.27	11	1.18

[1] Transition zone, TZ
[2] The average number of each group was calculated.

As can be seen in both Figure 6.10band Table 6.1, the L100 and L93S07 specimens behaved quite differently in terms of the variables of $A_{G,e=1.0}$ and α, even though the majority particles of both groups (L100 and L93S07) are

the gravel (LPC $\geq$ 93%) but only 7% of sand particles were replaced from the L100 specimens. A possible explanation for this discrepancy is that particle segregation occurred during the reconstitution of the L93S07 specimens for the sand particles to settle down toward the bottom of the specimens.

Interestingly, the clear straight-line trend of the TZ specimens in the log A_G - log e relationship is significantly similar to that of the SPPD specimens as shown in Table 6.2. The two variables of $A_{G,e=1.0}$ and α for the SPPD and TZ specimens are almost identical within 1 percentage difference, while the D_{50} and C_u values are significantly different.

Table 6.2: Comparison of the values of $A_{G,e=1.0}$, the exponential component in a void ratio correction function (α), median grain size (D_{50}), and uniformity coefficient (C_u) for the SPPD and TZ Specimens

Group ID.	$A_{G,e=1.0}$**, ksf**	α	[3]D_{50}**, mm**	[3]C_u
[1]SPPD	1495	-1.10	0.35	1.38
[2]TZ	1483	-1.07	33.5	10.5

[1] Small-Particle-Packing Dominated, SPPD
[2] Transition zone, TZ
[3] The average number of each group was calculated.

This finding induces to combine those two groups (SPPD and TZ) specimens based on the consistencies in the $A_{G,e=1.0}$ and α variables for estimating the small-strain shear modulus at one atmosphere of the binary specimens in this particular SPC range (15% $\leq$ SPC $\leq$ 100%). Therefore, when the SPC is less than or equal to 100 percent and greater than or equal to 15 percent, a

simplified equation for estimating G_{max} at one atmosphere (A_G) of the binary specimens tested in this study can be derived as follow:

$$A_G = A_{G,e=1.0}\ e^{\alpha} \tag{6.3}$$

where $A_{G,e=1.0}$ = 1489 ksf and α = -1.08.

As discussed in Section 6.3.2, the gravel skeleton void ratios ($e_{sk,gravel}$) can be also calculated for the TZ and LPPD specimens. However, it should be careful to calculate the gravel skeleton void ratio for the TZ specimens because the concept of gravel skeleton void ratio assumes that only the gravel particles are dominating the load transfer network of the binary specimens. Accordingly, based on the unrealistic high $e_{sk,gravel}$ values of the L61S39 specimens, the same way of calculating the sand skeleton void ratios for the SPPD specimens was chosen for the L61S39 specimens that the e value is divided by the corresponding LPC value in decimal for each specimen. The variation in A_G with gravel skeleton void ratio ($e_{sk,gravel}$) of the TZ and LPPD specimens is presented in Figure 6.11. Overall, the A_G - $e_{sk,gravel}$ relationships of the TZ and LPPD specimens shift vertically with the increase of small-particle content (SPC) and drop down for the L61S39 specimens. Therefore, it seems to be possible to explain the increase in A_G with the increase of small-particle content (SPC) at a given gravel skeleton void ratio ($e_{sk,gravel}$) for the TZ and LPPD specimens for SPC $\leq$ 30%. However, as mentioned in the Section 6.3.2 in regards to the $e_{sk,sand}$ values for the SPPD specimens, the interpretation

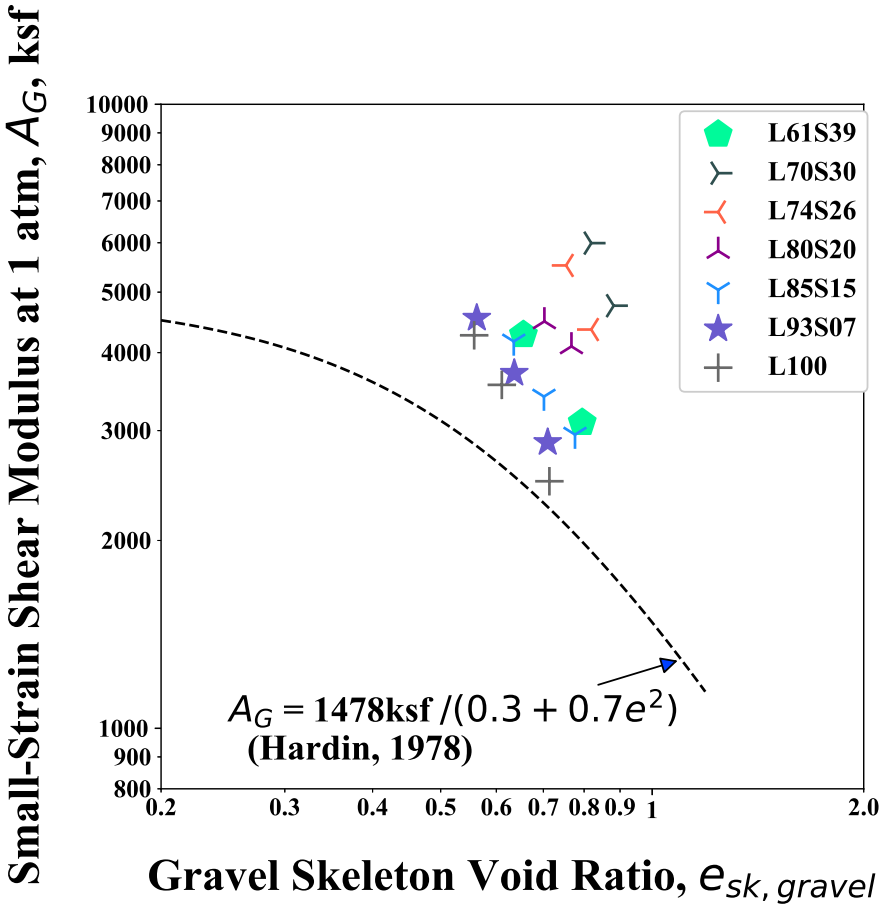

Figure 6.11: Variation in Small-Strain Shear Modulus at 1 Atm, A_G, with Gravel Skeleton Void Ratio of the Large-Particle Packing Dominated (LPPD) and Transition Zone (TZ) Specimens

with the skeleton void ratio should be careful due to the subjectiveness of the global void ratio.

6.3.5 Slopes of the Log G_{max} - Log σ_o Curve, n_G of Binary Mixtures

Variation in small-strain shear modulus (G_{max}) with confining pressure change can be illustrated with the the slope of the log G_{max} - log σ_o relationship, which is denoted as n_G. This n_G value typically expresses that how sensitive the G_{max} is to change in the confining pressure.

The n_G values of the SPPD specimens (the binary specimens for 50% $\leq$ SPC $\leq$ 100%) with their void ratio values are presented in Figure 6.12a. As can be seen in the figure, the n_G values are relatively constant ranging from 0.44 to 0.47. The mean value ($n_{G,\mu}$) and standard deviation ($n_{G,\sigma}$) of these specimens are 0.45 and 0.1, respectively. The relative constant n_G values of the SPPD specimens indicate that the effect of confining pressure change on the G_{max} values is relatively insignificant for the SPPD specimens. However, it is noteworthy that the n_G values of the S50L50 specimens seem to diverge from the constant trend.

To explore further implications, the n_G values of the L61S39 specimens were appended to the n_G values of the SPPD specimens in Figure 6.12b. Interestingly, the n_G values of L61S39 were about 10 percent greater than the average n_G value for the S50L50 specimens; which are approximately 15 percent higher than the mean n_G value for all SPPD specimens. In other words, the divergence from the constant trend of the SPPD specimens in terms of

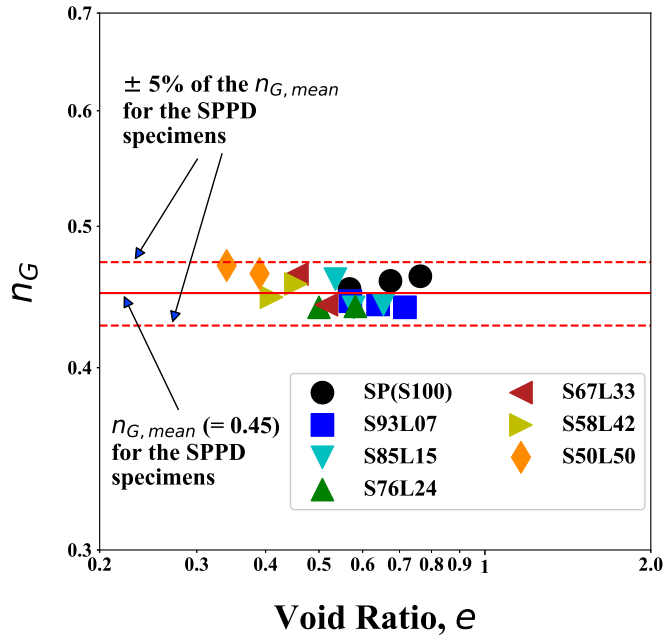

(a) Log n_G - Log e for 50% $\leq$ SPC $\leq$ 100%

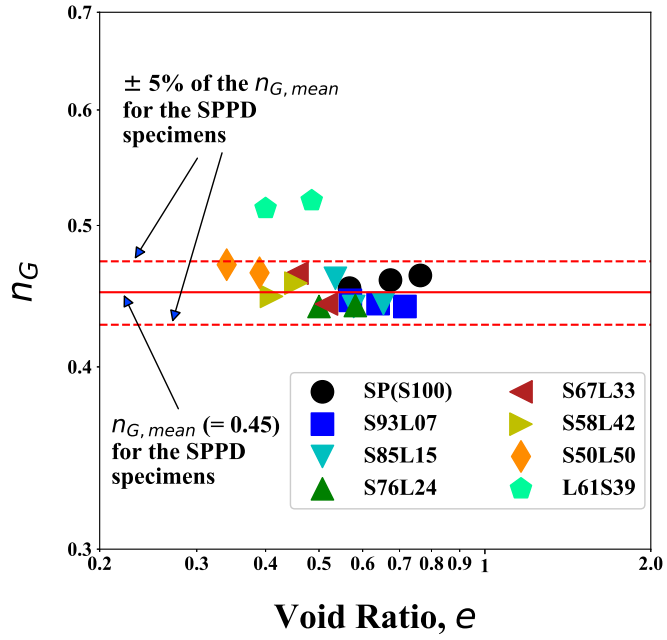

(b) Log n_G - Log e for 39% $\leq$ SPC $\leq$ 100%

Figure 6.12: Variation of the slope of Log G_{max} - Log σ_o , n_G, with Void Ratio for 39% $\leq$ SPC $\leq$ 100%

the n_G seems to start between the S58L42 and S50L50 specimens and continues toward the TZ specimens. Therefore, in a conservative engineering point of view the S50L50 specimens can be classified as the transition zone (TZ) specimens.

The variation in the n_G with e of the TZ specimens are presented in Figure 6.13. The range of the n_G values for the TZ specimens is from 0.48 to 0.54, with an average number of 0.51. No significant trend is found between the n_G and e for the TZ specimens.

In Figure 6.13b, the n_G values of the LPPD specimens ($0\% \leq \text{SPC} \leq 13\%$) are also appended to the n_G values of the TZ specimens presented in the Figure 6.13a. As can be seen in the Figure 6.13b, the n_G values of the LPPD specimens (L100 and L93S07 specimens) are highly scattered. This scatter pattern of the n_G values was also found on the test result by Menq (2003) [26] that the relationship between n_G and e are not as clearly defined as the relationship between A_G and e for granular soils. In the comparison of the n_G values between the TZ and LPPD specimens, the TZ specimens have generally higher n_G values with the smaller e values than those of the LPPD specimens with the larger e values .

Among the poorly-graded and binary specimens tested in this study, four specimens were selected for a comparison of shear wave velocity profile. The four binary specimens are : (1) a poorly-graded sand specimen (SP) of S100 with e=0.67, (2) a poorly-graded gravel specimen (GP) of L100 with e=0.61, (3) a binary specimen of S67L33 with e = 0.52, and (4) a binary

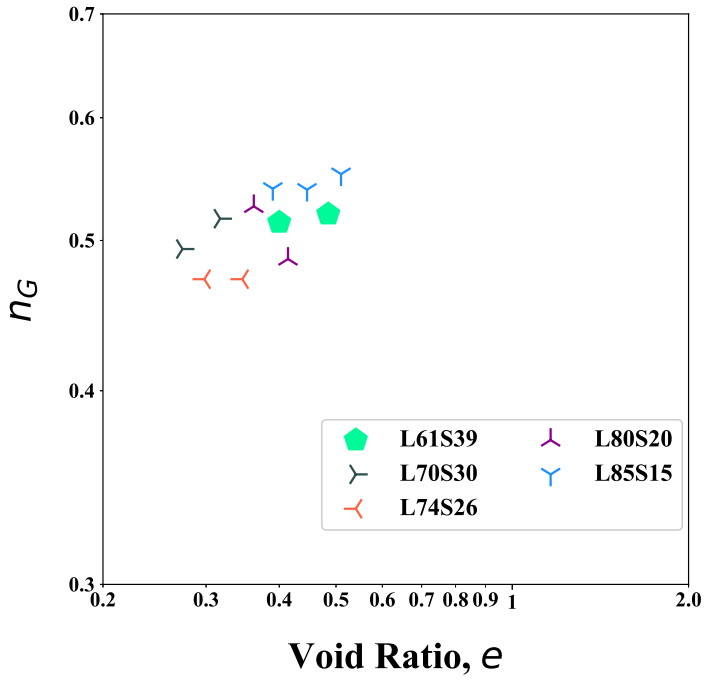

(a) Log n_G - Log e for 61% $\leq$ LPC $\leq$ 100%

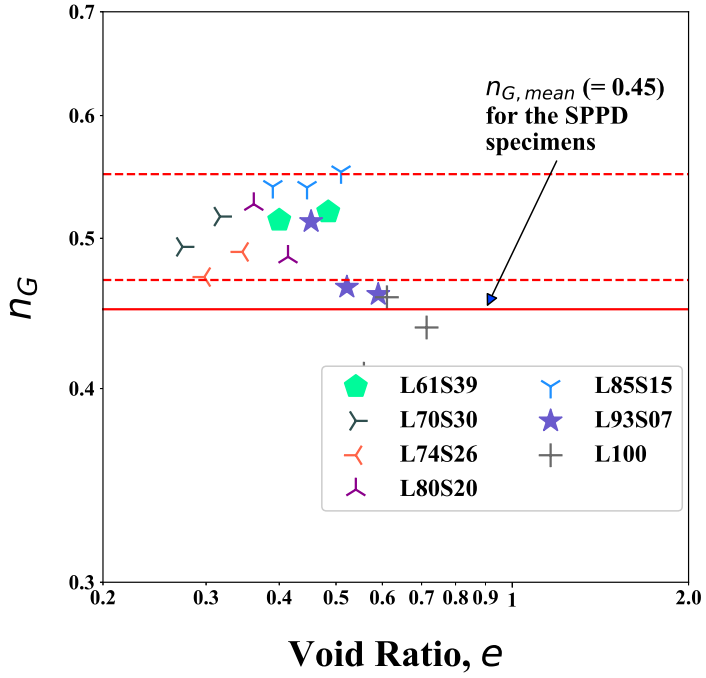

(b) Log n_G - Log e for 61% $\leq$ LPC $\leq$ 85%

Figure 6.13: Variation of the slope of the Log G_{max} - Log σ_o , n_G, with Void Ratio for 61% $\leq$ LPC $\leq$ 100%

specimen of L74S26 with e = 0.35. Using the measurements of shear wave velocity (V_S) at 1 atm (A_S) and the slope of the log V_S - log σ_o relationship (n_S) for the four specimens, the V_S profile with depth for each of the four specimens can be constructed. In Figure 6.14, the variation in V_S with depth for the four specimens are presented. As can be seen in the figure, the relative densities (D_r) of the four specimens are assumed to be about from 60% to 80% based on the e_{min} and e_{max} values of the specimens that can be determined by the e_{min} and e_{max} trends by Evans (1995) in Figure 5.7. Overall, the S100 (SP) is the softest material among the four materials and the GP material and L74S26 specimens are much stiffer than the SP and S67L33 materials. On the top 20 ft (6 m) of depth, the GP material (100% gravel material) is slightly stiffer than the L74S26 material, but as passing the top 20 ft the L74S26 specimen becomes stiffer than the GP material. The stiffening behavior of the gravel or gravelly soils relative to the sand or sandy soils match the effectiveness of Rammed Aggregate Piers^{TM} (RAP), which is one of shallow ground improvement methods in mitigating the liquefaction damaged area (Stokoe et al., 2014 [31]).

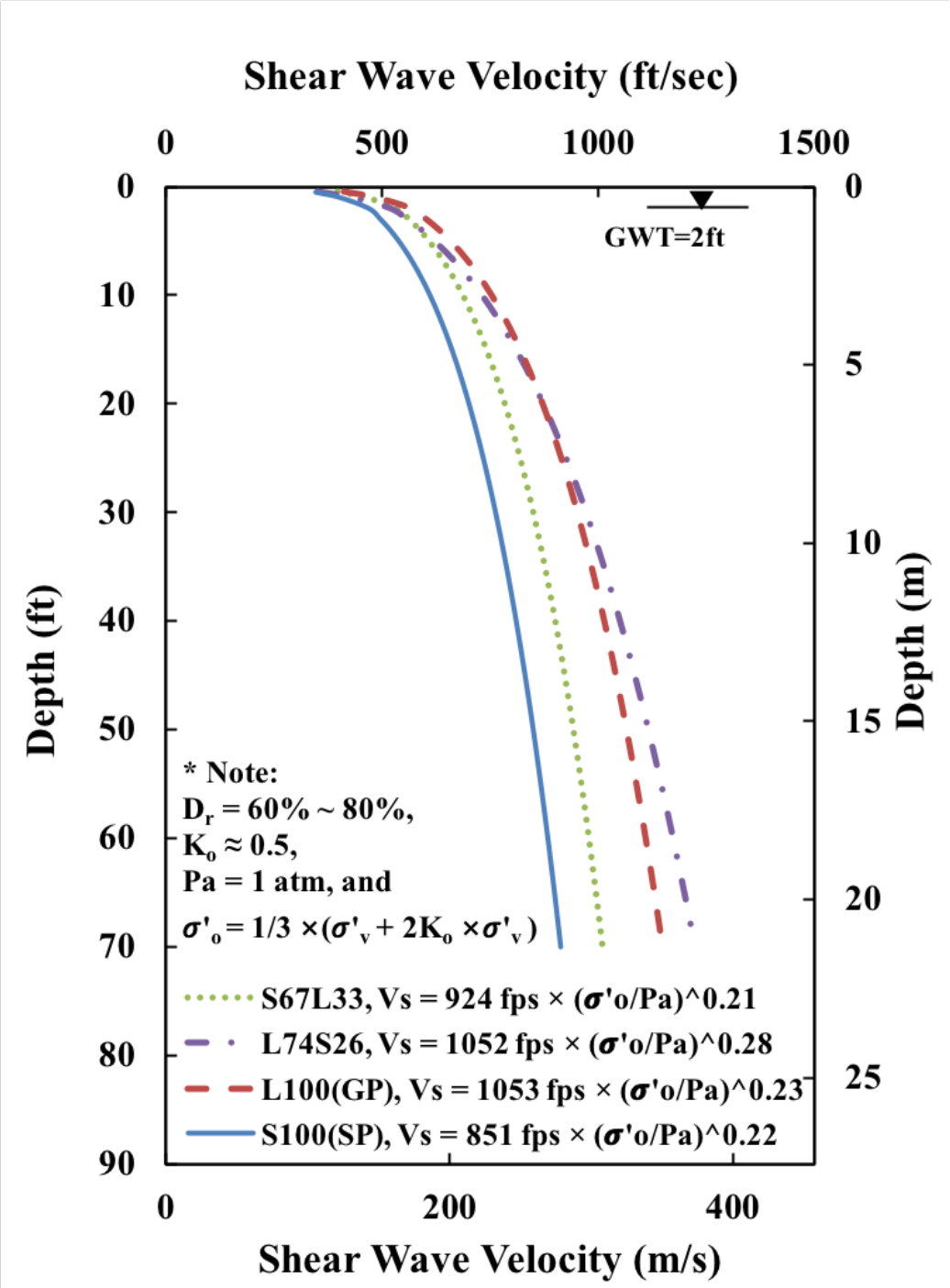

Figure 6.14: Variation in Shear Wave Velocity, V_s, of Some Medium Dense Specimens for Two Poorly Graded and Two Binary Materials

6.3.6 Effects of Gradation Characteristics on the G_{max} of Binary Mixtures

As discussed in Chapter 4, Menq (2003) [26] carried out an extensive study of the effects of the gradation characteristics, e.g., uniformity coefficient (C_u) and median grain size (D_{50}) on the small-strain shear modulus of granular materials. Based on the results, he quantified the effects of C_u and D_{50} with an estimation model of small-strain shear modulus, G_{max}:

$$G_{max} = C_{G3}\ {C_u}^{\ b1}\ e^x\ (\frac{\sigma_o}{Pa})^{\ n_G} \tag{6.4}$$

where:

C_{G3} is the G_{max} at 1 atm, $C_u = 1.0$, and e=1.0,

b1 = -0.20,

$x = -1 - (D_{50}/20)^{0.75}$, and

$n_G = 0.48 \times {C_u}^{\ 0.09}$.

When the confining pressure is equal to one atmosphere, this equation is simply as follow:

$$A_G = C_{G3}\ {C_u}^{\ b1}\ e^x \tag{6.5}$$

where:

A_G is the G_{max} at 1 atm.

Even though the equation of A_G by Menq (2003) (Equation 6.4) was intentionally formulated for typical sandy and gravelly soils, not for binary mixtures, it seems meaningful to use the Equation 6.4 and calculate the A_G estimations of the binary specimens tested in this study.

A comparison between the A_G values measured in this study and the A_G values estimated by Menq (2003) for the SPPD specimens is illustrated in Figure 6.15. Interestingly, the A_G estimations for SPC $\geq$ 67% are very close to the measurements within $\pm$ 5 percent difference. However, the A_G measurements for the S58L42 and S50L50 specimens were approximately 20 percent lower than the estimations. This finding lends further support to the observation discussed in Section 6.3 that the A_G values of the S58L42 and S50L50 specimens began to deviate from the Hardin (1978)'s trend. In other words, the significant increases in the C_u and D_{50} values of these specimens make relatively low correlation with their void ratio values.

In Figure 6.16, a comparison between the measured A_G values and the estimations by Menq (2003) for the TZ and LPPD specimens are presented. In the figure, the solid line represents a one-to-one relationship, the two dashed lines closer to the solid line mark the range for $\pm$ 10% difference and the others mark the range for $\pm$ 20% difference between the measured and estimated A_G values. As can be seen, the A_G values of the L100 specimens (the GP material) are very close to the solid line as a poorly-graded material. The A_G values of the L70S30 and L74S26 specimens are overestimated by about 10 percent, while the L61S39, L80S20, and L85S15 specimens are underestimated

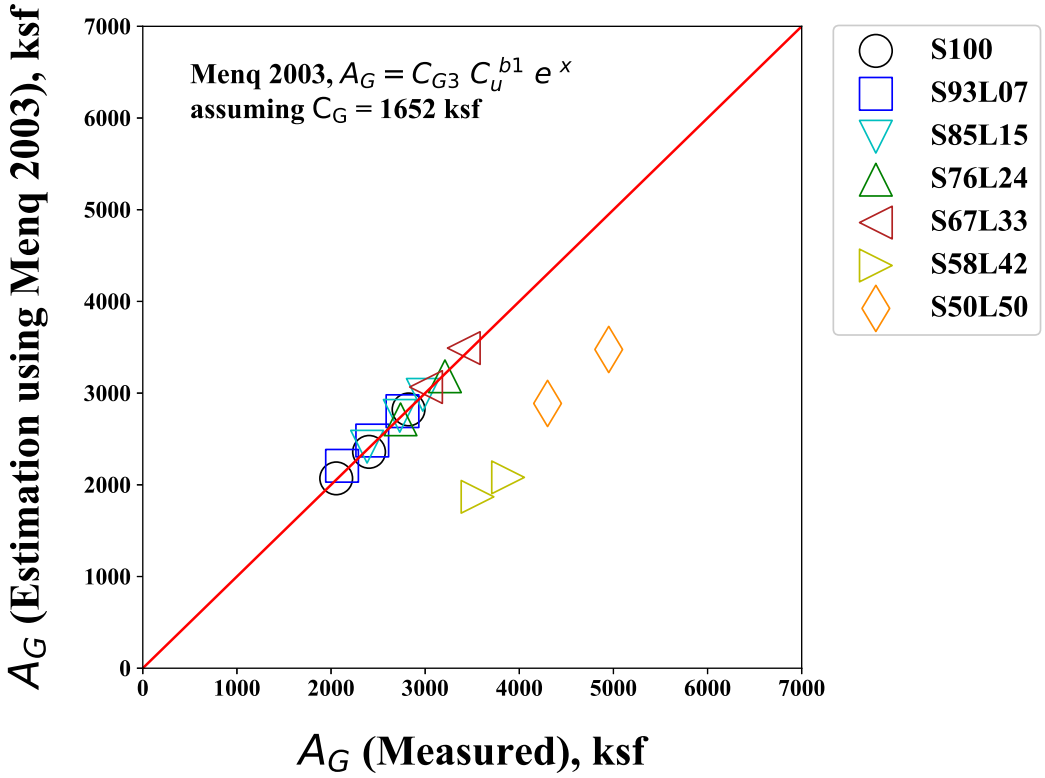

Figure 6.15: Comparison between the Measured and Estimated (Menq, 2003) Values of A_G for 50% $\leq$ SPC $\leq$ 100%

by less than 20 percent. One of the issues that emerges from the L93S07 specimens is that the A_G measurements of those specimens go beyond the 20 percent difference range. The significant outlier behavior of the L93S07 specimens seems consistent proving that the particle segregation would occur by settling down of the sand particle to the bottom of the specimens during reconstitution.

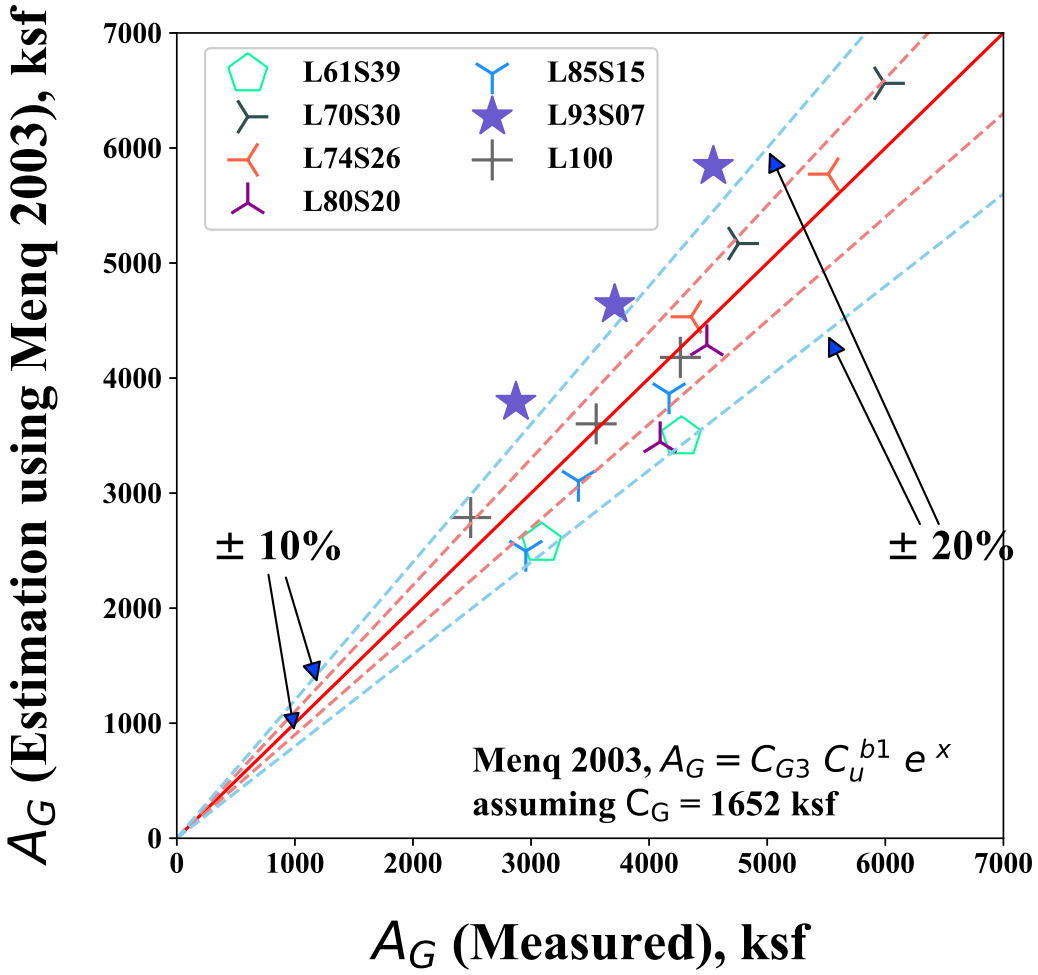

Figure 6.16: Comparison between the Measured and Estimated (Menq, 2003) Values of A_G for 61% $\leq$ LPC $\leq$ 100%

6.3.7 Effects of Gradation Characteristics on the n_G of Binary Mixtures

Menq (2003) [26] also equated the slope of the log G_{max} - log σ_o curve (n_G) with the uniformity coefficient (C_u) for granular materials. The equation is as follows:

$$n_G = 0.44\ C_u{}^{0.09} \tag{6.6}$$

The comparisons between the measured n_G values and the values estimated by Equation 6.6 for the SPPD, TZ, and LPPD specimens are shown in Figure 6.17. In Figure 6.17a, the n_G measurements and the estimations by Equation 6.6 for the SPPD specimens are compared. The resulting trend closely resembles the trend from the A_G values comparison for the SPPD specimens that for SPC $\geq$ 67% the estimations and measurements of the A_G values are close each other, however, the A_G values for the S58L42 and S50L50 specimens, which contain high C_u values, were overestimated by about 20 percent. In Figure 6.17b, the estimated and measured n_G values for the TZ and LPPD specimens are compared. As can be seen, overall, the n_G values for the TZ specimens (the specimens for 61% $\leq$ LPC $\leq$ 85%) are overestimated by about 20 percent; while the n_G values for the LPPD specimens (the specimens for 93% $\leq$ LPC $\leq$ 100%) are relatively scatter.

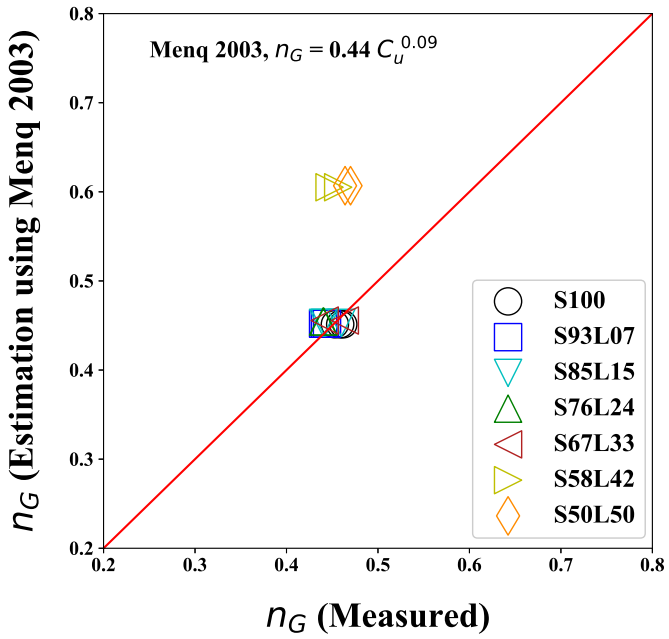

(a) Comparison between the Measured and Estimated (Menq, 2003) n_G values for $50\% \leq \text{SPC} \leq 100\%$

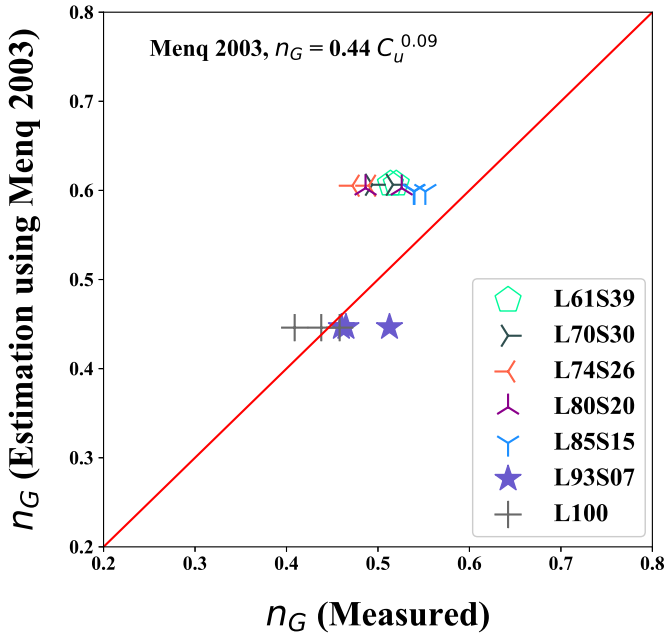

(b) Comparison between the Measured and Estimated (Menq, 2003) n_G values for $61\% \leq \text{LPC} \leq 100\%$

Figure 6.17: Comparison with the n_G Values Measured and Estimated (Menq, 2003) for the SPPD, TZ, and LPPD Specimens

6.4 SMALL-STRAIN MATERIAL DAMPING RATIO IN SHEAR, D_{min}, OF THE TWO POORLY-GRADED MATERIALS, SP AND GP

As with G_{max}, the effect of confining pressure (σ_o) on D_{min} can be expressed by a normalized confining pressure by one atmosphere raised to the power n_D as follows:

$$D_{min} = A_D(\frac{\sigma_o}{P_a})^{n_D} \tag{6.7}$$

where:

A_D = the value of D_{min} at a mean confining pressure of one atmosphere,

P_a = atmosphere pressure (1 atm), and

n_D = the exponent component in the log D_{min} - log σ_o relationship.

The gradation curves for the SP and GP materials are presented in Figure 6.18a. Variations in small-strain material damping ratio in shear (D_{min}) for the SP and GP materials (the S100 and L100 specimens) with isotropic confining pressure are presented in Figure 6.18b. In the Figures 6.18a and 6.18b, the circular symbols (i.e., ◯) represent the S100 specimens, and the plus symbols (i.e., +) represent the L100 specimens. As discussed in Chapter 5, each gradation of these two poorly-graded materials was reconstituted at three different values of void ratio (e). (It is noteworthy that, as mentioned

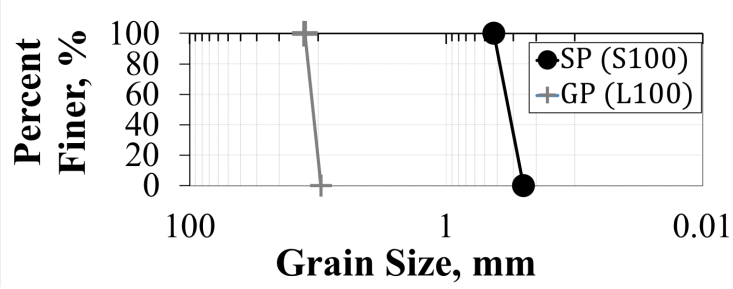

(a) Grain-Size Distribution Curves of the S100 and L100 Specimens

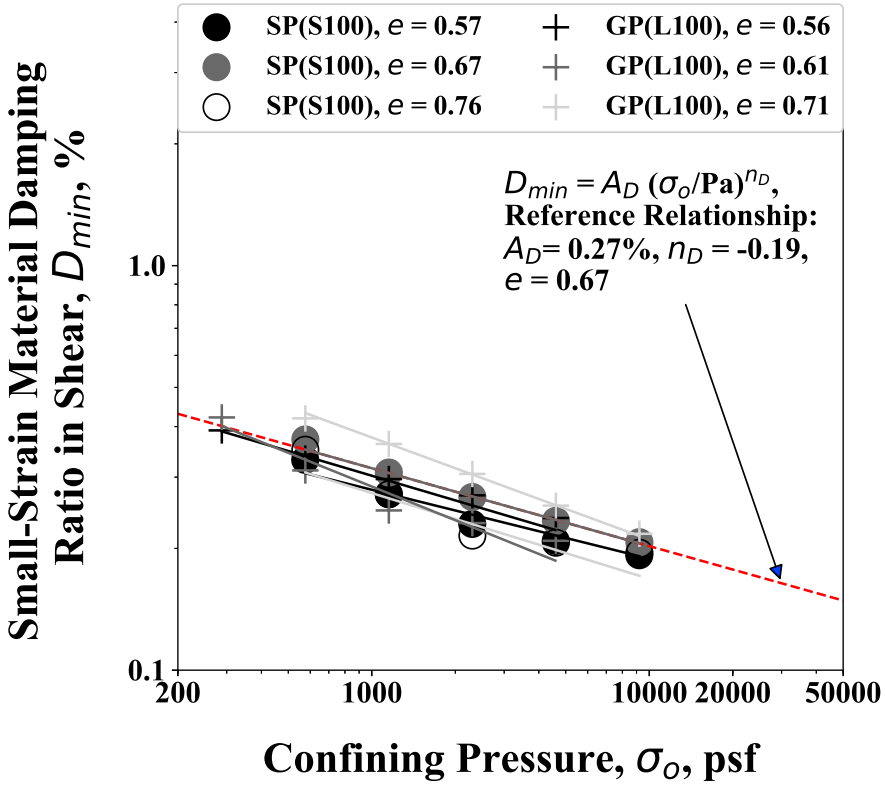

(b) Log D_{min} - Log σ_o of the S100 and L100 Specimens

Figure 6.18: Gradation Curves and Variations in Small-Strain Material Damping Ratio in Shear with Confining Pressure of the SP and GP Materials (Referred to as the S100 and L100 Specimens in this Dissertation)

in Section 6.3.2, the term of void ratio with the symbol of e represents the global packing condition as same as the term of global void ratio (e_g) for all specimens tested in this study.) The values of e range from 0.57 to 0.76 for the S100 specimens, and from 0.56 to 0.71 for the L100 specimens, respectively. To provide the relative comparisons, a reference log D_{min} - log σ_o relationship with the constants of $A_D = 0.27$ percent, n_G = -0.19, and $e = 0.67$ is presented in the Figure 6.18b.

Overall, the log D_{min} - log σ_o relationships of these poorly-graded specimens are not as clearly defined as the log G_{max} - log σ_o relationships for the SP and GP materials presented in Figure 6.1b. This increased variability in log D_{min} - log $sigma_o$ relationship stems, at least in part, from the greater difficulty involved in measuring material damping ratio in shear (Menq, 2003) [26]. However, it is noteworthy that all D_{min} values in the Figure 6.18b are less than 0.5 percent with a relatively weak trend that the D_{min} values are slightly decreasing with the increase of confining pressure (σ_o). Lastly, the effect of e on D_{min} for the SP and GP material seems unclear.

6.5 SMALL-STRAIN MATERIAL DAMPING RATIO IN SHEAR, D_{min}, OF BINARY MIXTURES

6.5.1 Small-Strain Material Damping Ratio in Shear, D_{min}, of the SPPD Specimens

The log D_{min} - log σ_o relationships of the seventeen SPPD specimens are shown in Figure 6.19. To provide the relative comparisons, the reference D_{min} - log σ_o relationship (the dashed line with $A_D = 0.27\%$, n_D = -0.19,

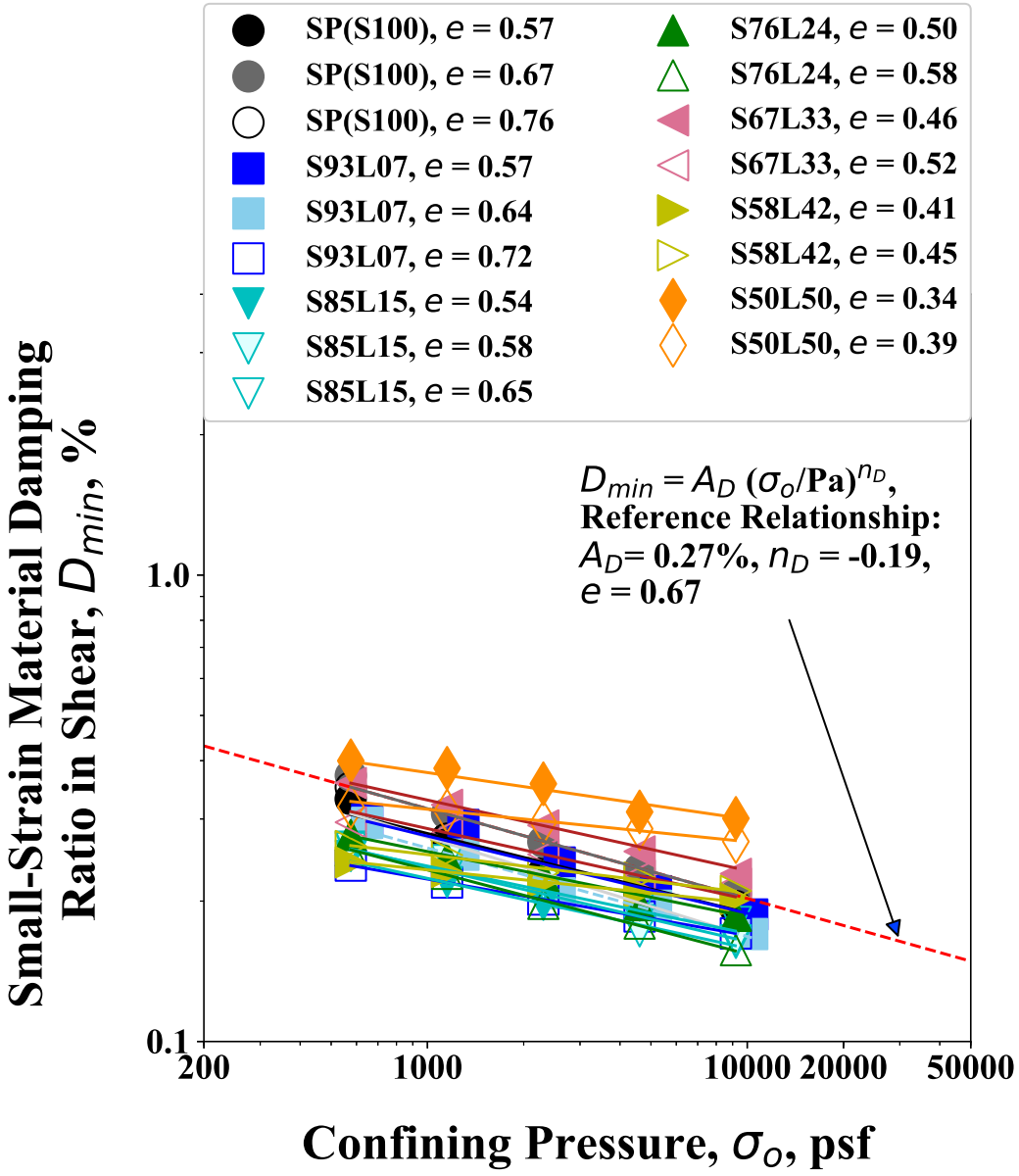

Figure 6.19: Variations in Small-Strain Material Damping Ratio in Shear with Confining Pressure for 50% $\leq$ SPC $\leq$ 100%

and $e = 0.67$) is also presented in the figure. All values of D_{min} are less than one percent. Among the seventeen log D_{min} - log σ_o relationships, the one with the highest relationship is observed in the densest specimen of Gradation S50L50 (i.e., the one with the lowest void ratio, e=0.34), however, for the lowest relationships the S93L07 specimen with $e = 0.72$ and the specimen S76L24 with $e = 0.58$ are overlapped each other. In other words, the highest small-strain material damping ratio in shear is the D_{min} value of the S50L50 with $e = 0.37$ specimen at the confining pressure of 4 psi, and the lowest D_{min} value is for the S85L15 with $e = 0.65$ specimen at the highest confining pressure of 64 psi. The other SPPD specimens fall between theses highest and lowest values of D_{min}. However, contrary to the log G_{max} - log σ_o relationships for the SPPD specimens, the reference relationship is in the middle between the highest and lowest log D_{min} - log σ_o relationships. This indicates that the effect of e is not clearly defined on the D_{min} - log σ_o relationship as on the G_{max} - log σ_o relationship for the SPPD specimens.

6.5.2 Small-Strain Material Damping Ratio, D_{min}, of the TZ and LPPD Specimens

The log D_{min} - log σ_o relationships of the seventeen TZ and LPPD specimens are plotted in Figure 6.20. In the figure, the reference relationship, (the dashed line with A_D=0.27%, n_D=-0.19, and e=0.67) is also presented. Overall, the TZ and LPPD specimens have the higher and wider range of the D_{min} values (0.2% $\sim$ 1.2%) relative to those of the SPPD specimens. Among the seventeen log D_{min} - log σ_o relationships, the highest relationship

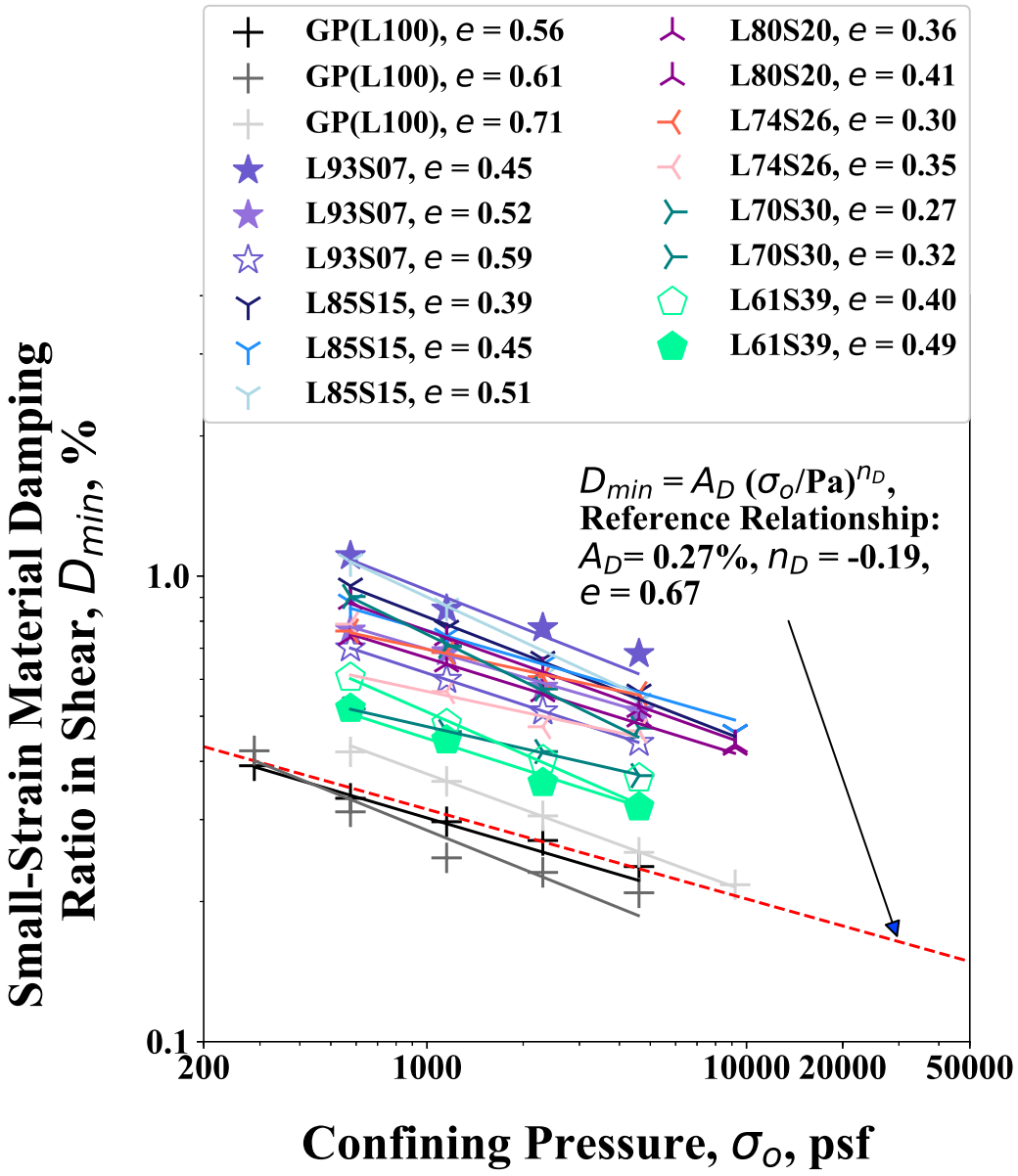

Figure 6.20: Variations in Small-Strain Material Damping Ratio in Shear with Confining Pressure for 61% $\leq$ LPC $\leq$ 100%

is observed for the specimen of L93S07 with the $e = 0.45$, however, the lowest one is observed for the L100 specimen with $e = 0.61$, which is slightly lower than the reference relationships (A_D=0.27%, n_D=-0.19, and e=0.67). In other words, the binary specimens for 7% $\leq$ SPC $\leq$ 39% have relatively higher D_{min} values than the poorly-graded specimens. In terms of the value of D_{min}, the highest value was about 1.2 percent for the L93S07 specimen with $e = 0.45$ at the confining pressure of four psi, and the lowest one is 0.21 percent for the L100 specimen with $e = 0.65$ at the confining pressure of 32 psi.

6.5.3 D_{min} at 1 atm (A_D) for SPPD, TZ, and LPPD specimens

The variation in A_D with void ratio (e) for the SPPD is presented in Figure 6.21a, and for the TZ, and LPPD specimens is shown in Figures 6.21b. In the Figure 6.21a, all A_D values range from 0.2 percent to 0.35 percent. The A_D values of the SPPD specimens for 58% $\leq$ SPC $\leq$ 93% are within about $\pm$ 10% variability range of the A_D measurements for the S100 specimens (the SP material). This finding indicates that the void ratio (e) has no significant effect on the small-strain material damping ratio in shear at one atmosphere for these particular binary materials. Another important finding from the figure (Figure6.21a) is that the A_D values of the S50L50 specimens are moderately higher than the other A_D values. Especially, the A_D value of the S50L50 with $e = 0.34$ specimen is significantly high than the value of the S50L50 with $e =$ 0.36 specimen. This finding further supports the discussion that the S50L50 specimens are supposed to be considered as the TZ specimens than the SPPD

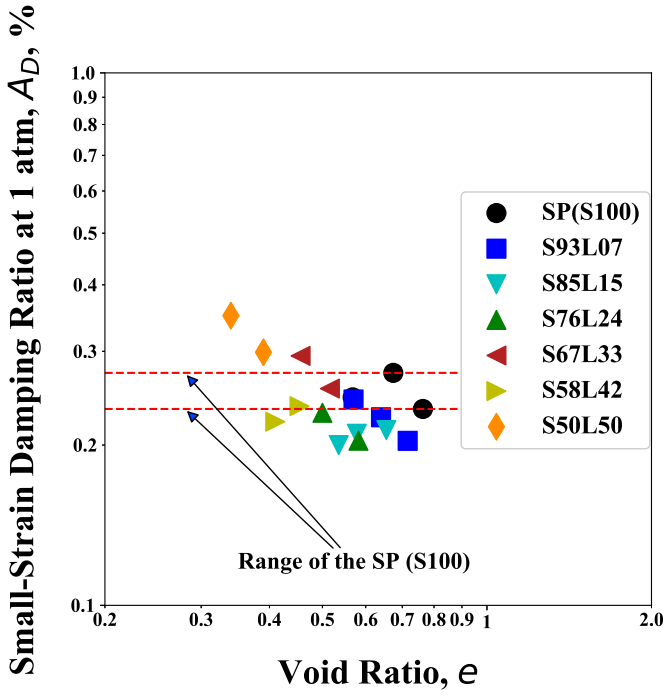

(a) Log A_D - Log e for 50% $\leq$ SPC $\leq$ 100%

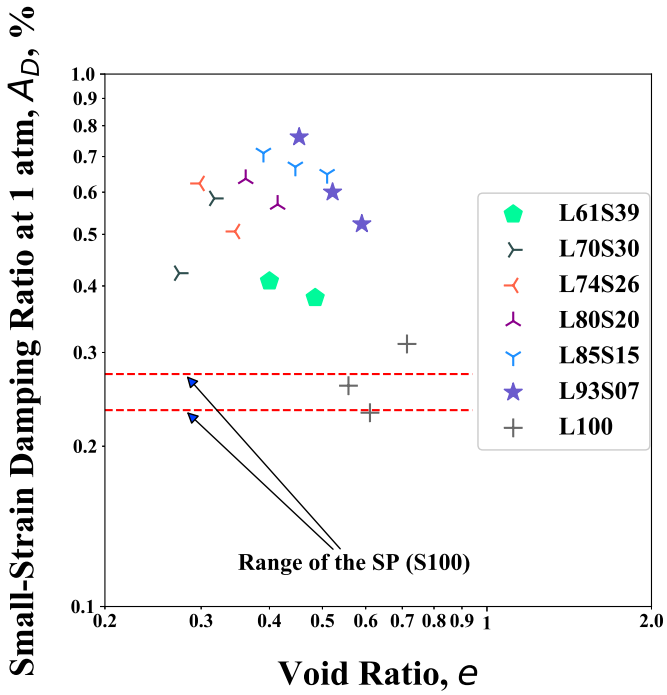

(b) Log A_D - Log e for 61% $\leq$ LPC $\leq$ 100%

Figure 6.21: Variation in Small-Strain Material Damping Ratio in Shear at 1 Atm, A_D, with Void Ratio, e, for the Binary Mixtures (SPPD, TZ , LPPD Specimens)

specimens.

The A_D values of the TZ and LPPD specimens are plotted with the void ratios in Figure 6.21b. The A_D values of the TZ specimens range from 0.38 to 0.7, and from 0.25 to 0.8 for the LPPD specimens. The range of A_D for the TZ specimens is much wider than the range for the SPPD specimens. This finding indicates that the binary specimens in the transition zone (TZ) have more variability in the the small-strain material damping characteristic than the SPPD specimens. The significant higher A_D values for the L93S07 specimens relative to the L100 specimens further supports that the L93S07 specimens might not be reconstituted uniformly due to the particle segregation of the sand particles.

6.5.4 Slopes of the Log D_{min} - Log σ_o Curve, n_D, of Binary Mixtures

The variation in n_D (the slopes of the log D_{min} - log σ_o relationship) with e for the SPPD specimens is presented in Figure 6.22a and the variation in n_D with e for the TZ and LPPD specimens is provided in Figure 6.22b. In the Figure 6.22a, the n_G values range from -0.07 to -0.21, with an average value of -0.14. The negative sign in the values of n_D indicate that D decreases with the increase of confining pressure. Therefore, the absolute value of the n_D represents how much the material damping ratio in shear is sensitive to the confining pressure change. In the comparison between the absolute values of n_D and n_G for the SPPD specimens (i.e., $|n_{D,avg}| = 0.14$ vs. $|n_{G,avg}| = 0.45$), it is apparent that the n_D values are much smaller than the n_G values. This indi-

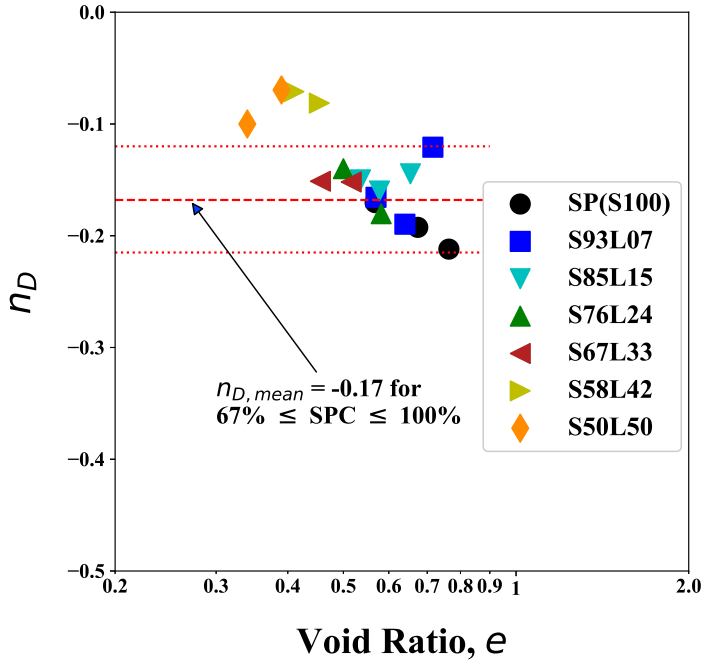

(a) Log n_D - Log e for 50% $\leq$ SPC $\leq$ 100%

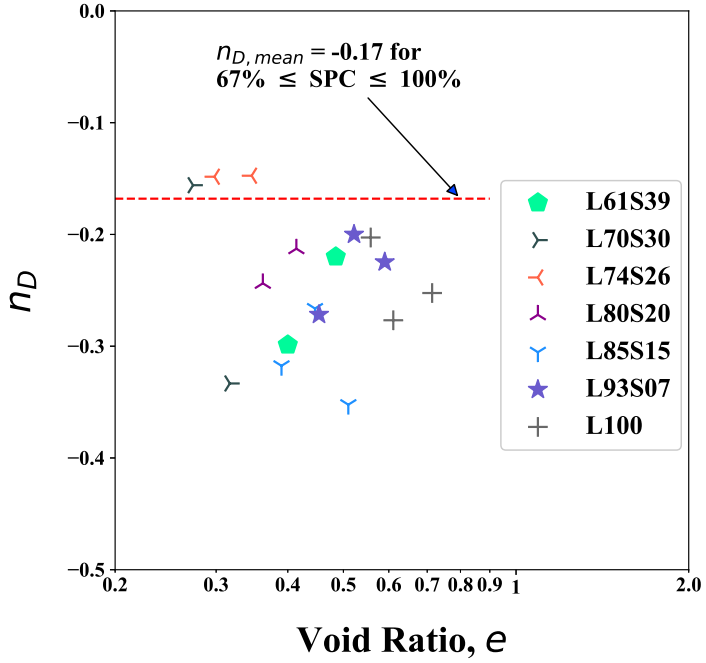

(b) Log n_D - Log e for 61% $\leq$ LPC $\leq$ 100%

Figure 6.22: Variation in Exponent Component, n_D, with Void Ratio, e, for Binary Mixtures (SPPD, TZ, and LPPD Specimens)

cates that G is affected much more significantly by confining pressure change than D for the SPPD specimens. Overall, even though it seems that there is a slightly increasing trend of n_G with the decrease of e, the n_G values of the SPPD specimens are unclear for a relationship. Based on the accordance with the finding by Menq (2003) [26] that the n_G value is not strongly correlated with e, the slightly increasing trend was not equated in this study.

In the Figure 6.22b, the absolute n_G values of the TZ and LPPD specimens range from 0.35 to 0.15 (with an average value of 0.25) and 0.20 to 0.28 (with an average value of 0.24), respectively. In the comparison of n_G between the TZ and LPPD specimens, the TZ specimens have a larger range of n_G than the LPPD specimens, although the average values are close each other. However, as mentioned, the relationship between the n_G values with the void ratios seem no significant for both TZ and LPPD specimens.

6.6 SMALL-STRAIN CHARACTERISTICS OF THE GAP-GRADED MIXTURES

6.6.1 Introduction

The gap-graded specimens tested in this study are the mixtures of a well-graded sand (SW) manufactured and the poorly-graded gravel (GP) used in the binary mixtures. The SW material was manufactured with the sieved materials from the washed mortar sand (WMS) resulting in the uniformity coefficient (C_u) of 8.0 and the median grain size (D_{50}) of 0.6 mm. The dynamic torsional resonant column (RC) test was performed with one SW specimen,

and a total of seven gap-graded specimens in the small-strain range.

6.6.2 Small-Strain Shear Modulus of Gap-Graded Materials

The log G_{max} - log σ_o relationships of one well-graded sand (SW) specimen (i.e., the S_w100 with $e = 0.65$ specimen), one poorly-graded gravel specimen (i.e., the L100 with $e = 0.61$ specimen), and the 7 gap-graded specimens are provided in Figure 6.23. In the figure, a reference relationship is plotted with a dashed line using the log G_{max} - log σ_o relationship of the S100 with $e = 0.76$ specimen (i.e., the highest e value among the SPPD specimens with the constants of $A_D = 2055$ ksf, $n_G = 0.46$, and $e = 0.76$. The SW specimen (i.e., S_w100 with $e = 0.65$) is very similar with the reference relationship in the log G_{max} - log σ_o relationship except for the slight change in the slope. This can be explained by the opposite effects between the high C_u values and low e values. The gap-graded specimen of S_w85L15 with $e = 0.55$ also behave very similarly with the reference relationship except for the slightly higher G_{max} values for the confining pressures in the range of 8 to 64 psi. Among the total of nine relationships, the L74S_w26 with $e = 0.29$ specimen (i.e., the lowest e value among the gap-graded specimens) has the stiffest log G_{max} - log σ_o relationship. The other relationships stand between the stiffest specimen (L74S_w26 with $e = 0.29$) and the well-graded specimen (S_w100 with $e = 0.65$).

The A_G values of one SW specimen, three L100 specimens (the GP specimens), and 7 gap-graded specimens are plotted with the void ratios in Figure 8.4. In the figure, the A_G estimation curve calculated using the void

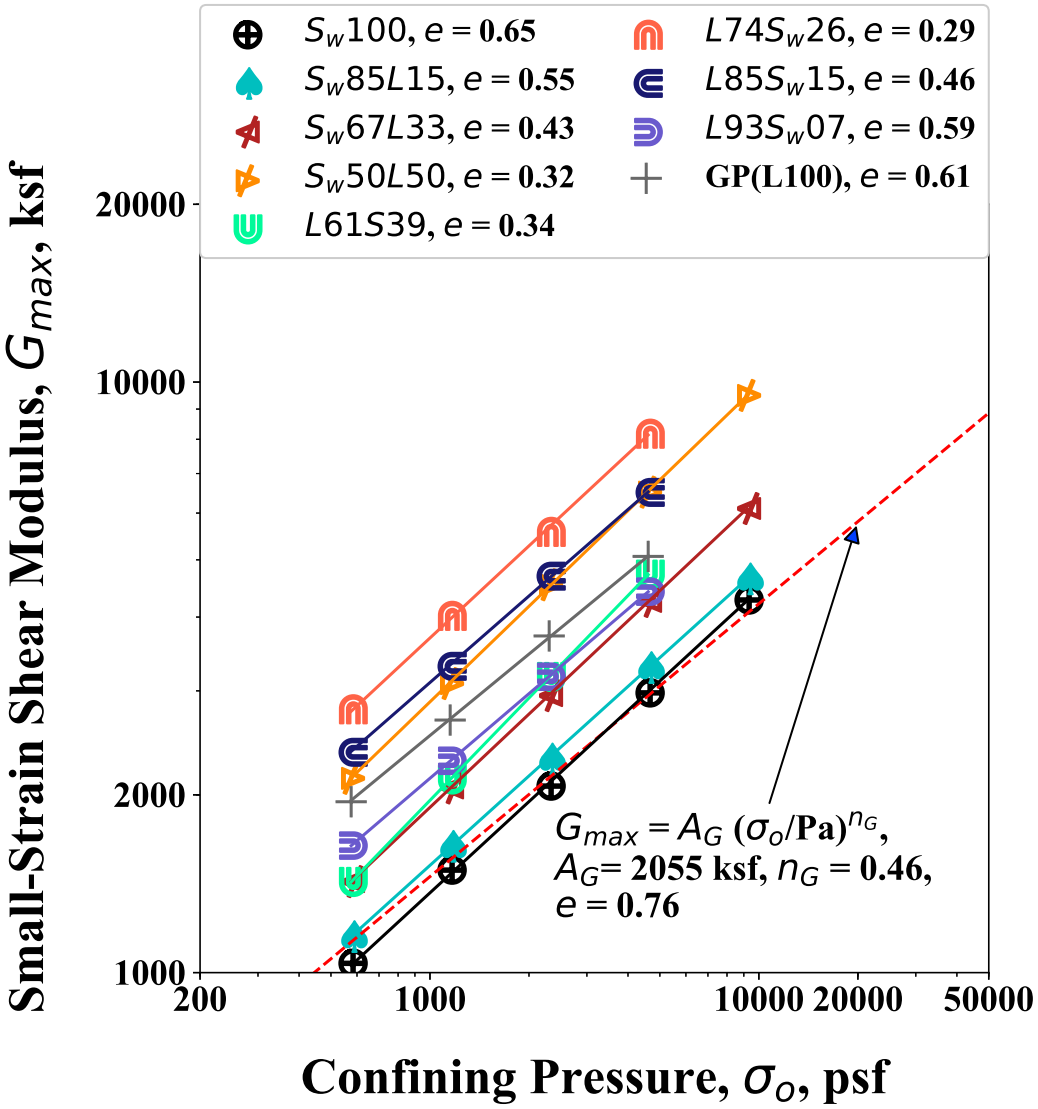

Figure 6.23: Variations in Small-Strain Shear Modulus with Confining Pressure of One SW Specimen, One GP Specimen, and Seven Gap-Graded Specimens

ratio correction function proposed by Hardin (1987) is also presented. In the A_G estimation curve, the value of $A_{G,e=1.0}$ is assumed to be 1183 ksf to fit the A_G value of the SW specimen. Additionally, the result of regression analysis in A_G for the SPPD specimens is also provided in the Figure 8.4.

Interestingly, the A_G values of the S_w85L15 and S_w67L33 specimens seem to very closely fall into the Hardin's trend line. In other words, the gap-graded specimens of S_w85L15 and S_w67L33 specimens that the amount of large particles are relatively small (LPC $\leq$ 33%) behave similarly with the parent material (i.e., the SW specimen) on the small-strain shear modulus at one atmosphere. The accordance in A_G with the Hardin's estimation curve was also observed for the SPPD specimens for SPC $\geq$ 67% in Figure 6.4a. In addition, the S_w50L50 specimen behave very similarly with the binary specimens for 50% $\leq$ SPC $<$ 67% in that the A_G values for both binary and gap-graded specimens (S50L50 and S_w50L50) began to deviate from the parent material trend (i.e., the SP and SW specimens, respectively). The maximum A_G value among the specimens presented in the Figure 8.4 is observed for the specimen of L74S_w26, which has with the lowest e value ($e = 0.29$). After the maximum A_G values, the A_G values of the gap-grade specimens seem to converge to the A_G trend of the GP specimens as the e values increase.

The slope of the log G_{max} - log σ_o relationship (n_G) of the SW, GP, and seven gap-graded specimens are provided in Figure 6.25. In the figure, the average n_G value for the SPPD specimens ($n_{G,mean}$) and the corresponding $\pm$5% variability of the average value are also presented. Overall, the gap-

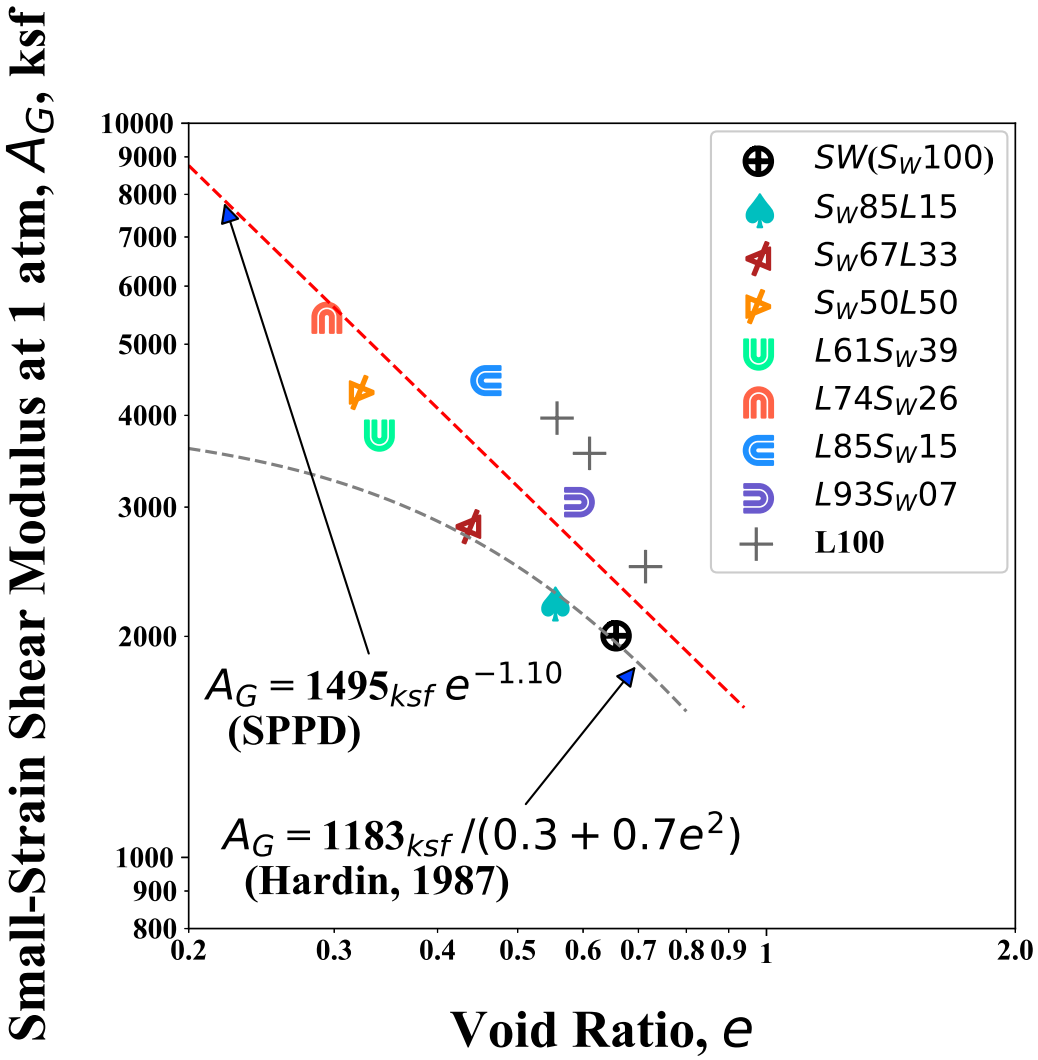

Figure 6.24: Variation in Small-Strain Shear Modulus at 1 Atm with Void Ratio of One SW Specimen, Three GP Specimens, and Seven Gap-Graded Specimens with Curve Fittings

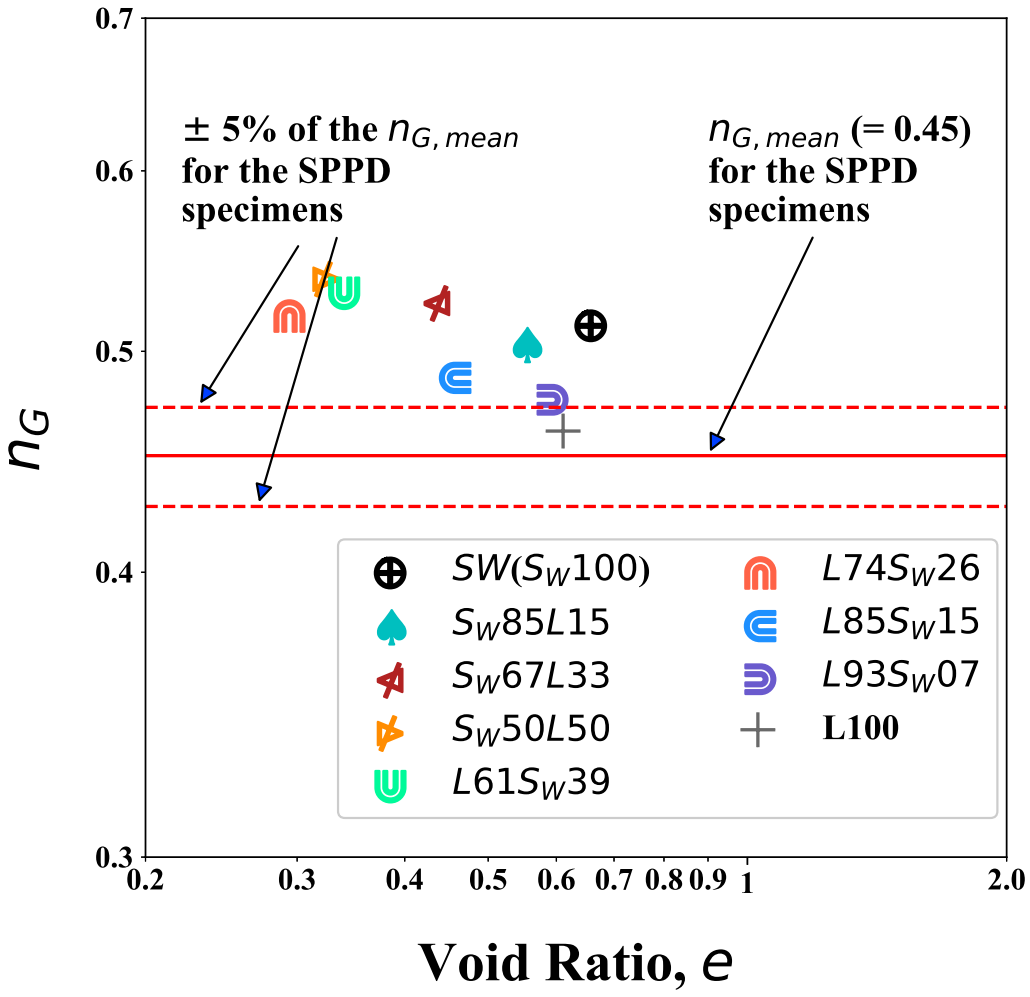

Figure 6.25: Variation of n_G with Void Ratio for One SW Specimen, Three GP Specimens, and Seven Gap-Graded Specimens

graded specimens including the SW specimen have higher n_G values than the SPPD specimens ranging from 0.48 to 0.54, which is similar to the range of the TZ specimens (from 0.48 to 0.55).

6.6.3 Small-Strain Material Damping Ratio of Gap-Graded Materials

The log D_{min} - log σ_o relationships for the SW specimen (with e = 0.65), the GP specimen (with $e = 0.61$), and seven gap-graded specimens are presented in Figure 6.26. To provide the relative comparisons, the reference relationship of the dashed line calculated with the constants of $A_D = 0.27\%$, n_D = -0.19, and $e = 0.67$ is also presented in the figure. All values of D_{min} are less than one percent. Among the total of the nine log D_{min} - log σ_o relationships, the specimens of L74S$_w$26 with $e = 0.29$ and L85S$_w$15 with $e = 0.46$ have the highest log D_{min} - log σ_o relationships indicating the most energy dissipation. The three gap-graded specimens of the S$_w$100 with $e = 0.65$, the S$_w$85L15 with $e = 0.55$, and the S$_w$67L33 with $e = 0.43$ behave very similarly in the log D_{min} - log σ_o relationship. Additionally, there is a significant change in both variables of the A_D and n_D for the S_w50L50 with $e = 0.43$ specimen.

The small-strain material damping ratio in shear at 1 atm (A_D) values and the slope of the D_{min} - log σ_o relationship (n_D) for the SW, GP, and gap-graded specimens are provided in Figures 6.27a and 6.27b, respectively. For both relationships, the gap-graded specimens do not show strong relationships with void ratio.

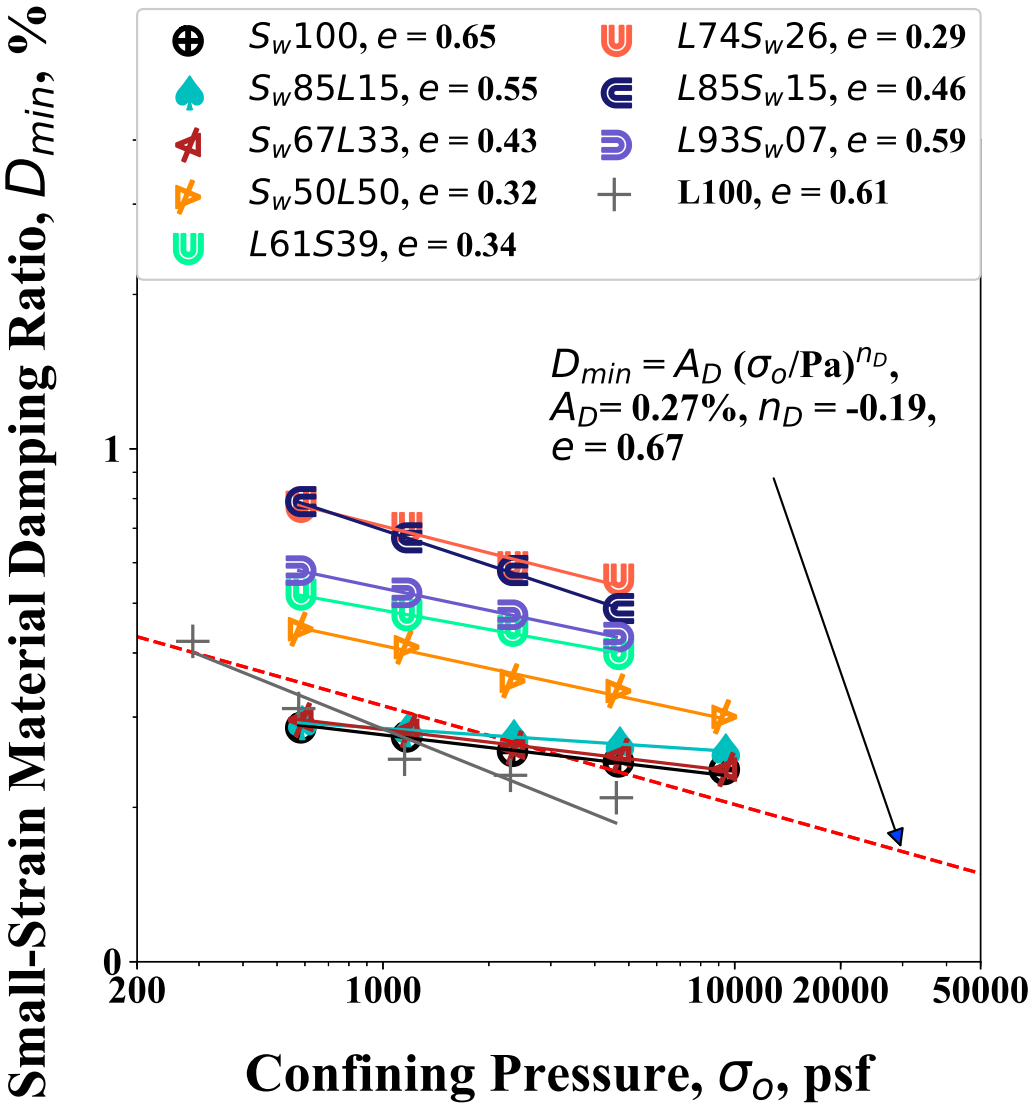

Figure 6.26: Variations in Small-Strain Material Damping Ratio in Shear with Confining Pressure of the Gap-Graded Specimens

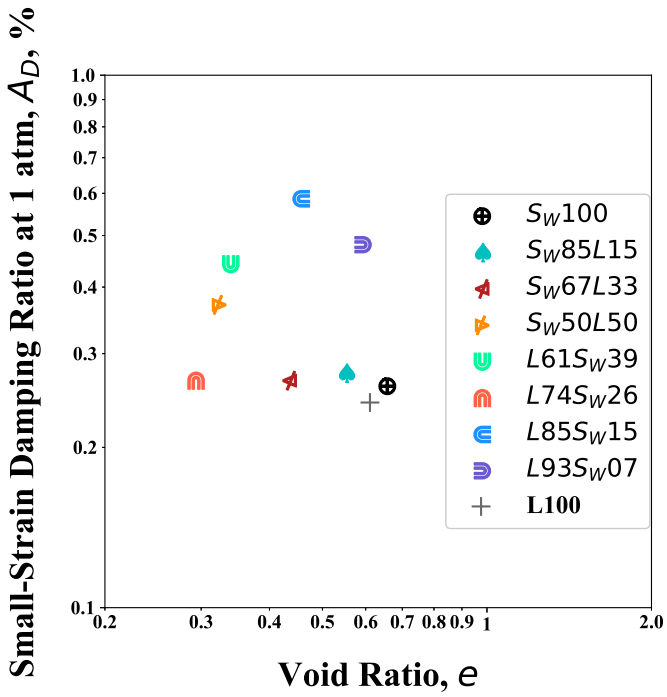

(a) Log A_D - Log e

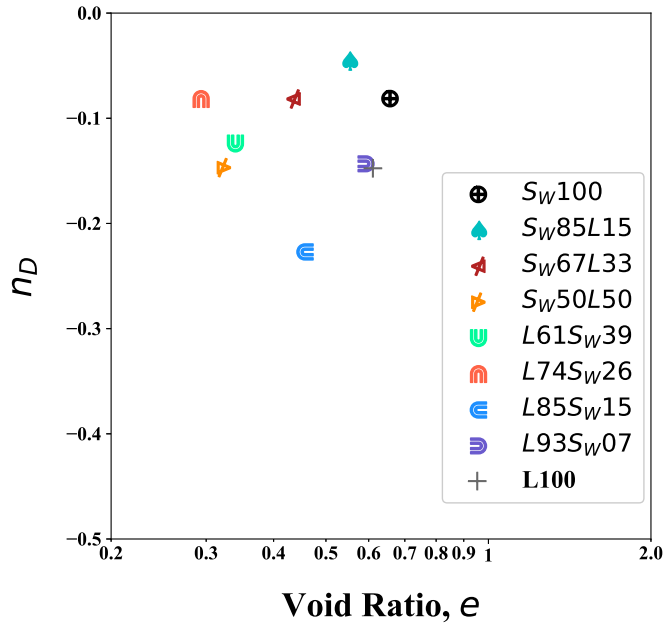

(b) Log n_D - Log e

Figure 6.27: Variation in Material Damping Ratio Parameters with Void Ratio of One SW Specimen, One GP Specimen,and Seven Gap-Graded Specimens

6.7 SUMMARY

The effects of isotropic confining pressure (σ_o), void ratio (e), and gradation characteristics (C_u) on the small-strain dynamic properties of reconstituted binary mixtures that were tested in this research are discussed in Section 6.3 through Section 6.5. In Section 6.6, the dynamic properties of gap-graded materials are discussed.

6.7.1 Binary Specimens

The binary specimens with small-particle contents (SPC) $\geq$ 67% behave very similarly to their parent, poorly-graded sand (the SP material) in terms of G_{max} at 1 atm (A_G). Overall, the small-particle-packing dominated (SPPD) specimens (i.e., the specimens for 50% $\leq$ SPC $\leq$ 100%) have a clear straight-line trend in the relationship of A_G and e. (See Figure 6.4b.) Interestingly, the A_G values of the transition zone (TZ) specimens also show a similar trend with the SPPD specimens. The large-particle-packing dominated (LPPD) specimens show a different A_G - e relationship compared to the SPPD and TZ specimens, which are more sensitive change in A_G to the change in void ratio.

In the analyses of the exponent of σ_o of the log G_{max} - log σ_o relationship (i.e., n_G), the SPPD specimens have the relatively constant values of n_G ranging from 0.44 to 0.47, while, the n_G values of the TZ and LPPD specimens are relatively scatter and higher than those of the SPPD specimens (See Figure 6.12a.).

Overall, the D_{min} of the binary specimens did not show strong relationships with void ratio (e) as much as the G_{max}. In the analysis of the A_D values of the SPPD binary materials, all A_D values ranged from 0.20% to 0.35%, which are about ± 10% variability from the SP material (the S100 specimens). No significant effect of e on D_{min} for the SPPD specimens was observed. Classifying the S50L50 specimens as the transition zone (TZ) specimens than the SPPD specimens seemed to be more reasonable due to the slightly higher n_G and A_D values than the other SPPD specimens (Figure 6.28). The A_D values of the TZ and LPPD specimens ranged from 0.38 to 0.70 and 0.25 to 0.80, respectively. Both TZ and LPPD specimens showed the wider range of the A_D values than those of the SPPD specimens indicating more variability in the small-strain material damping characteristics.

A significant outlier behavior was observed in the specimens of Gradation L93S07 through the dynamic parameters of A_G, n_G, and A_D. Accordingly, it is possible to say that significant particle segregation occurred for the L93S07 specimens during the reconstitution with settling down for the sand particles to the bottom of the specimens.

6.7.2 Gap-Graded Materials

Similar to the SPPD specimens, the gap-graded specimens began to deviate from the A_G estimation trend of the parent sand material in the log A_G - log e relationship when the percentage of the large particles became greater than or equal to 33 percent. In addition, the S_w50L50 specimen, which

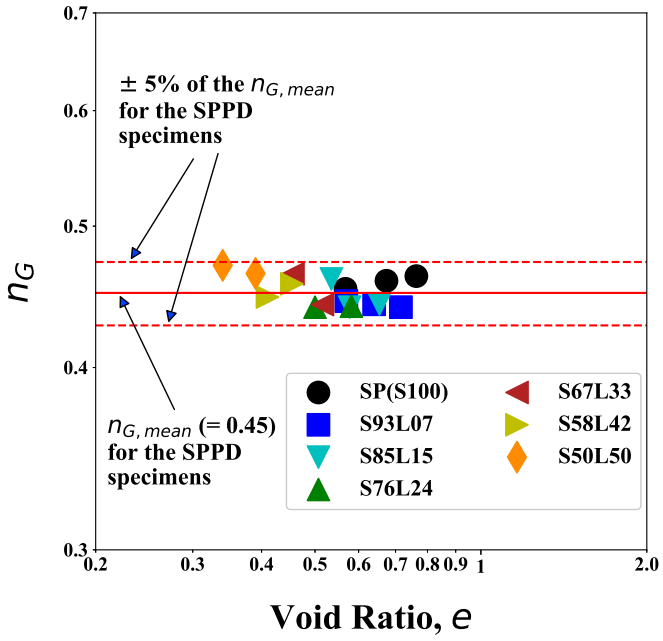

(a) Log n_G - Log e for 50% $\leq$ SPC $\leq$ 100%

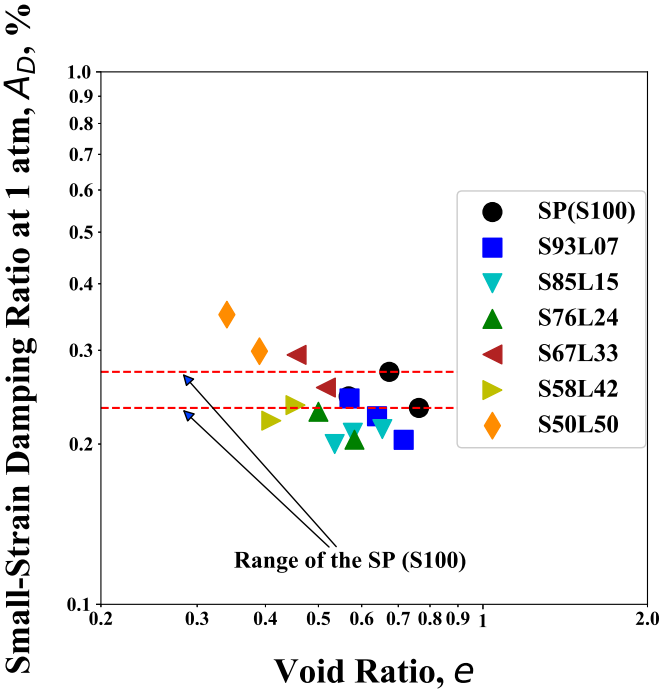

(b) Log A_D - Log e for 50% $\leq$ SPC $\leq$ 100%

Figure 6.28: Variation of the n_G and A_D with Void Ratio for 50% $\leq$ SPC $\leq$ 100%

is consisting of 50% of a well-graded sand as small particles and 50% of the poorly-grade gravel used for the binary mixtures as large particles, behaved very similarly with the binary specimens for S50L50 in that those specimens began to deviate from the parent material trend (i.e., the SP and SW specimens, respectively). This indicated that the hypothesis from testing results of the binary mixtures that the stiffness in the small-strain range of the binary mixtures is dominated by the parent sand material for $50\% \leq \text{SPC} \leq 100\%$ is also applicable to the gap-graded materials. (See Figure 6.24.)

Overall, the D_{min} and n_D values of the gap-graded specimens did not show strong trends with their e values as much as on the binary specimens.

Chapter 7

Nonlinear Characteristics of Binary and Gap-Graded Mixtures

Variations of shear modulus (G) and material damping ratio in shear (D) with the magnitude of shear strain (γ) of a total of 42 specimens tested in this study are discussed in this chapter. The 42 specimens are composed of: three SP specimens, three GP specimens, 28 binary specimens, one well-graded sand (SW) specimen, and seven gap-graded specimens. The measurements of shear moduli and material damping ratios in shear in the nonlinear strain range were only performed at a confining pressure of 16 psi (1.1 atm).

7.1 NONLINEAR SHEAR MODULUS OF TWO POORLY-GRADED MATERIALS, SP AND GP

The two poorly-graded materials (SP and GP materials) used in creating the binary specimens were first tested individually in the nonlinear range. The gradation curves for the SP and GP materials are presented in Figure 7.1a. As discussed in Chapter 5, these SP and GP materials were reconstituted at three different void ratio (e) values. Variations in shear modulus (G) with strain (γ) of the six poorly-graded specimens, three S100 and three L100 specimens, are presented in Figure 7.1b. In the Figures 7.1a and 7.1b, the cir-

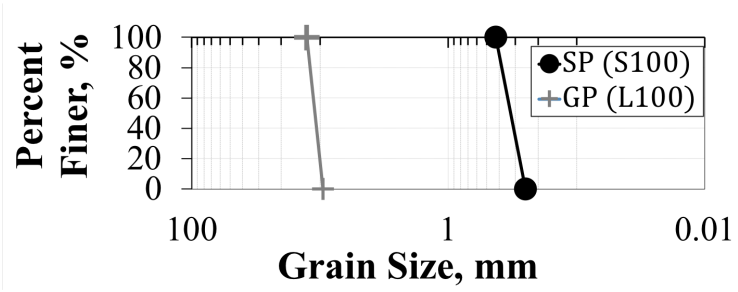

(a) Gradation Curves of the SP and GP Materials

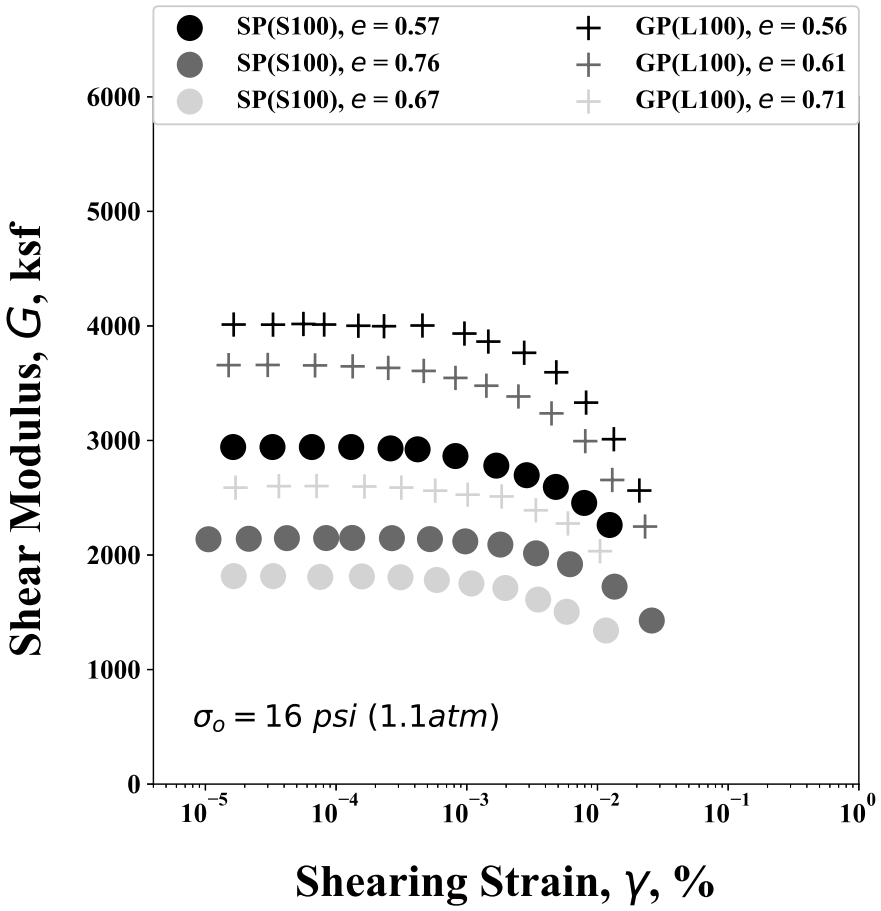

(b) G - Log γ of the SP and GP Materials

Figure 7.1: Variation in G - Log γ Relationship of the SP and GP Materials (Referred to as the S100 and L100 Specimens, respectively, in this Dissertation)

cular symbols (i.e., ◯) represent the S100 specimens, and the plus symbols (i.e., +) represent the L100 specimens. As can be seen in the Figure 7.1b, the G - log γ relationships for the six poorly-graded specimens are generally in a function of void ratio (e). As e values decrease (i.e., as each symbol of the poorly-graded materials becomes darker), the G - log γ relationships increase vertically. The obvious effect of e on the small-strain shear modulus of the poorly-graded specimens was also discussed on Section 6.2.

Similarly, the variations in normalized shear modulus (G/G_{max}) with strain (γ) of the SP and GP materials are presented in Figure 7.2b. As can be noticed in the figure, no significant effect of void ratio (e) is observed among the six poorly-graded specimens in terms of the G/G_{max} - log γ relationship. This minor effect of e on the G/G_{max} - log γ relationship for the poorly-graded materials is consistent with the finding by Menq (2003) [26] in which he emphasized that the nonlinearity in shear modulus of granular soils is mainly related with the parameter of uniformity coefficient (C_u) than the parameter of void ratio (e).

Based on the testing results of the six poorly-graded specimens, a reference range in the G/G_{max} - log γ relationship. As can be seen in the Figure 7.2b, the reference range was constructed with the two poorly-graded specimens: (1) the S100 with $e = 0.76$ specimen as the upper bound, and (2) the L100 with $e = 0.71$ specimen as the lower bound. The between is filled with the gray color to represent the variability of G/G_{max} - log γ relationship for the SP and GP materials. The C_u range of the reference range is 1.1 to 1.3. This

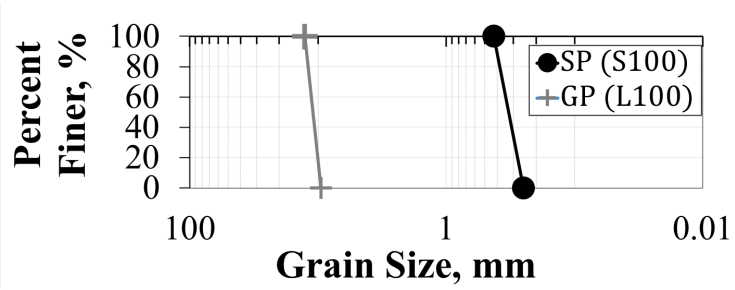

(a) Gradation Curves of the SP and GP Materials

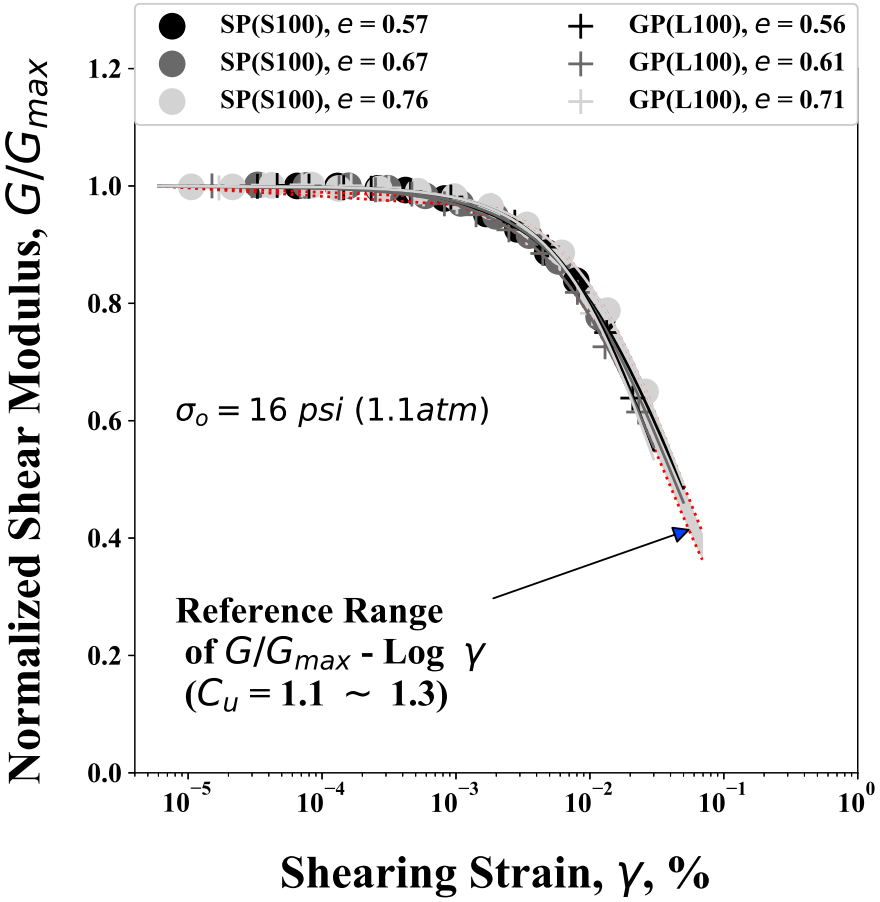

(b) G/G_{max} - Log γ of the SP and GP Materials

Figure 7.2: Variation in the G/G_{max} - Log γ Relationship of the SP and GP Materials (Referred to as the S100 and L100 Specimens, respectively, in this Dissertation)

reference range is used in the following sections for the relative comparisons.

To investigate the factors influencing on the G/G_{max} - log γ relationship, it is convenient to model the shear modulus measurements using the modified hyperbolic equation proposed by Darendeli (2001)[11]. As discussed in section 4.3.3, the modified hyperbolic equation can be expressed as:

$$\frac{G}{G_{max}} = \frac{1}{1 + (\frac{\gamma}{\gamma_r})^a} \tag{7.1}$$

where:

γ = any given shearing strain,

γ_r = the reference strain with respect to shear modulus, which is the sheare strain at $G/G_{max} = 0.5$, and

a = the curvature coefficient in the G/G_{max} - log γ relationship.

In this hyperbolic model, the two variables such as the reference strain (γ_r) and the curvature coefficient (a) can characterize the nonlinear behavior in shear modulus of granular soils. For example, γ_r decreases with more nonlinearity in shear modulus at a given value of a. On the other hands, at a given value of γ_r the higher a value represents more nonlinear behavior.

The value of γ_r for the SP and GP materials range from 0.034% to 0.048% and from 0.92 and 1.10 on the a values which indicates insignificant

change in the nonlinearity for the poorly-graded materials.

7.2 NONLINEAR SHEAR MODULUS OF BINARY MIXTURES

7.2.1 G - Log γ and G/G_{max} - Log γ Relationships of the SPPD Specimens

In Figure 7.3, the G - log γ relationships of the loosest small-particle-packing dominated (SPPD) specimens for each gradation are shown. In the figure, no significant difference in the G - log γ relationship is observed between the specimens of the S93L07 with $e = 0.72$ and the S100 with $e = 0.76$. This similar dynamic behavior between these two specimens was also found in the log G_{max} - log σ_o relationships for those specimens. (See Figure 6.3.) Overall, the G - log γ relationships of the loosest SPPD specimens increase vertically with the decrease of e. However, it is noticed that the S50L50 with $e = 0.39$ specimen behave more nonlinearly than the other SPPD specimens.

Among the SPPD specimens, the G/G_{max} - log γ relationships of the SPPD specimens for $58\% \leq \text{SPC} \leq 100\%$ are presented first in Figure 7.4. The reason that the S50L50 specimens were excluded in this Figure 7.4 is that the dynamic characteristics such as n_G and G - log γ relationship for the S50L50 specimens consistently differed from the other SPPD specimens. For the relative comparisons, the reference range constructed with the G/G_{max} - log γ curves of the poorly-graded specimens (the SP and GP materials) is also present in the figure. As can be seen, the specimens of Gradations S93L07, S85L15, and S76L24 are significantly close to the upper bound of the reference

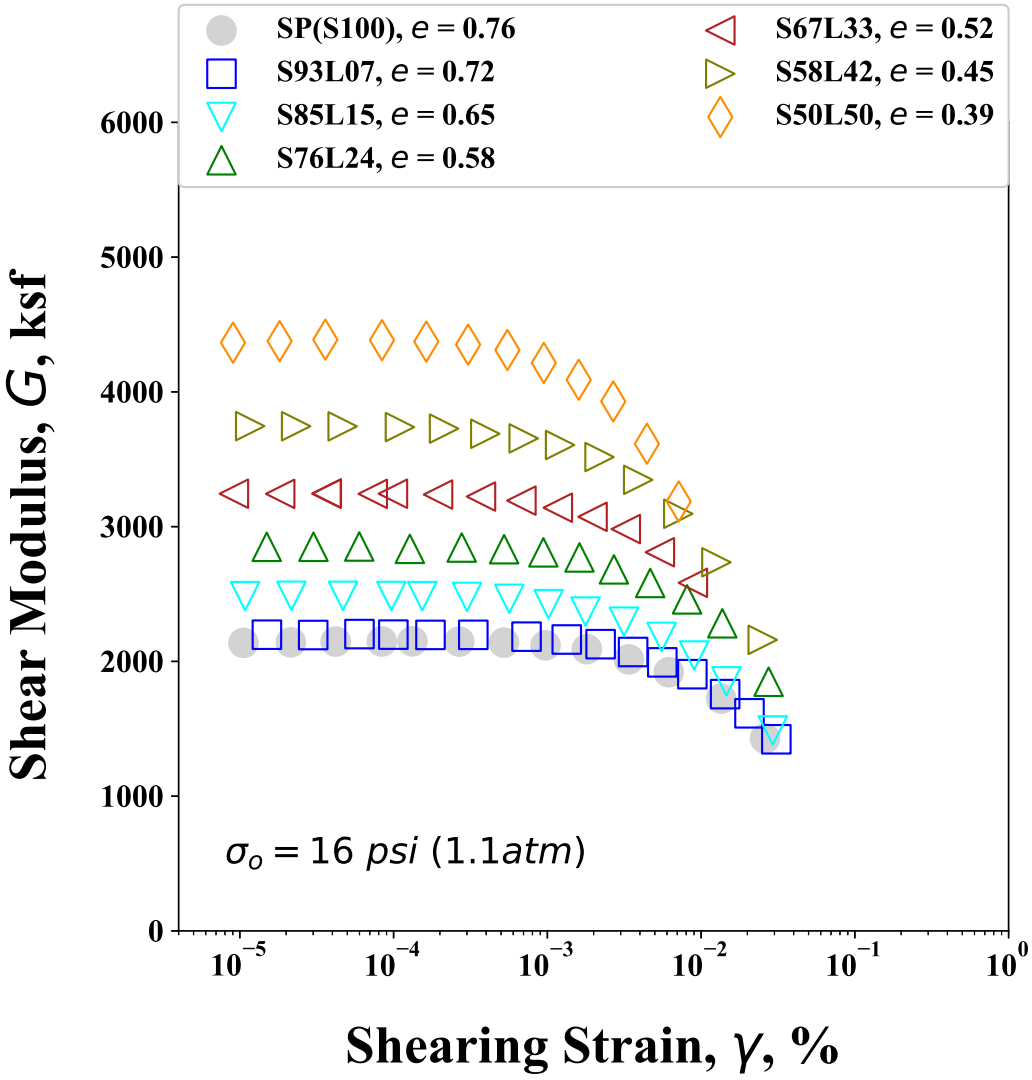

Figure 7.3: Variation in G - Log γ Relationship for the Loosest Small-Particle-Packing Dominated (SPPD) Specimens ($50\% \leq$ SPC $\leq 100\%$)

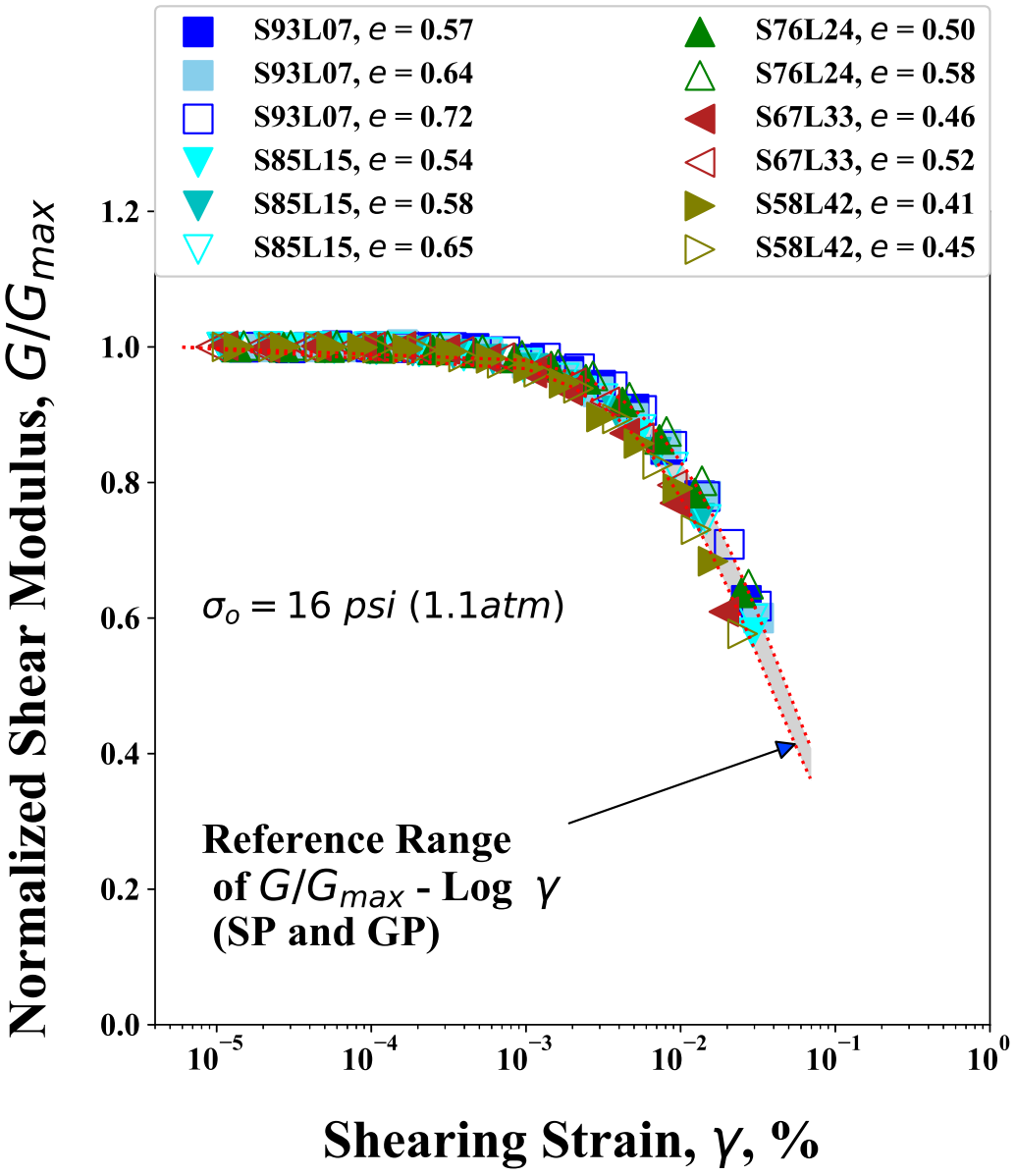

Figure 7.4: Variation in the G/G_{max} - Log γ Relationship for 58% $\leq$ SPC $\leq$ 100%

range. On the other hand, the specimens of Gradations S67L33 and S58L42 show similar nonlinear behavior one another in the G/G_{max} - log γ relationship, which are also very close to the lower bound of the reference range. Overall, as indicated previously, the SPPD specimens for 58% $\leq$ SPC $\leq$ 100% behave very similarly in terms of the G/G_{max} - log γ relationship. This indicates that the relative small amount of large particles (i.e., LPC $\leq$ 24%) do not significantly affect the G/G_{max} - log γ relationships of the SP material (i.e. the nonlinearity of the parent sand material). This insignificant effect of the small amount of large particles also accords with the finding that the A_G (small-strain shear modulus at 1 atm) values of the SPPD specimens for SPC $\geq$ 67% followed accurately the A_G - e trend of the SP material estimated by using Hardin (1978)'s void ratio function.

In Figure 7.5, the G/G_{max} - log γ relationships of the S50L50 specimens are appended to the G/G_{max} - log γ relationships of the SPPD specimens for 58% $\leq$ SPC $\leq$ 100% presented in the Figure 7.4. As expected, the moderately higher nonlinearites are observed on the S50L50 specimens compared to the other SPPD specimens. The more quantitative difference in nonlinearity for the SPPD specimens will be discussed in the following sections with the reference strain (γ) and curvature coefficient (a) values.

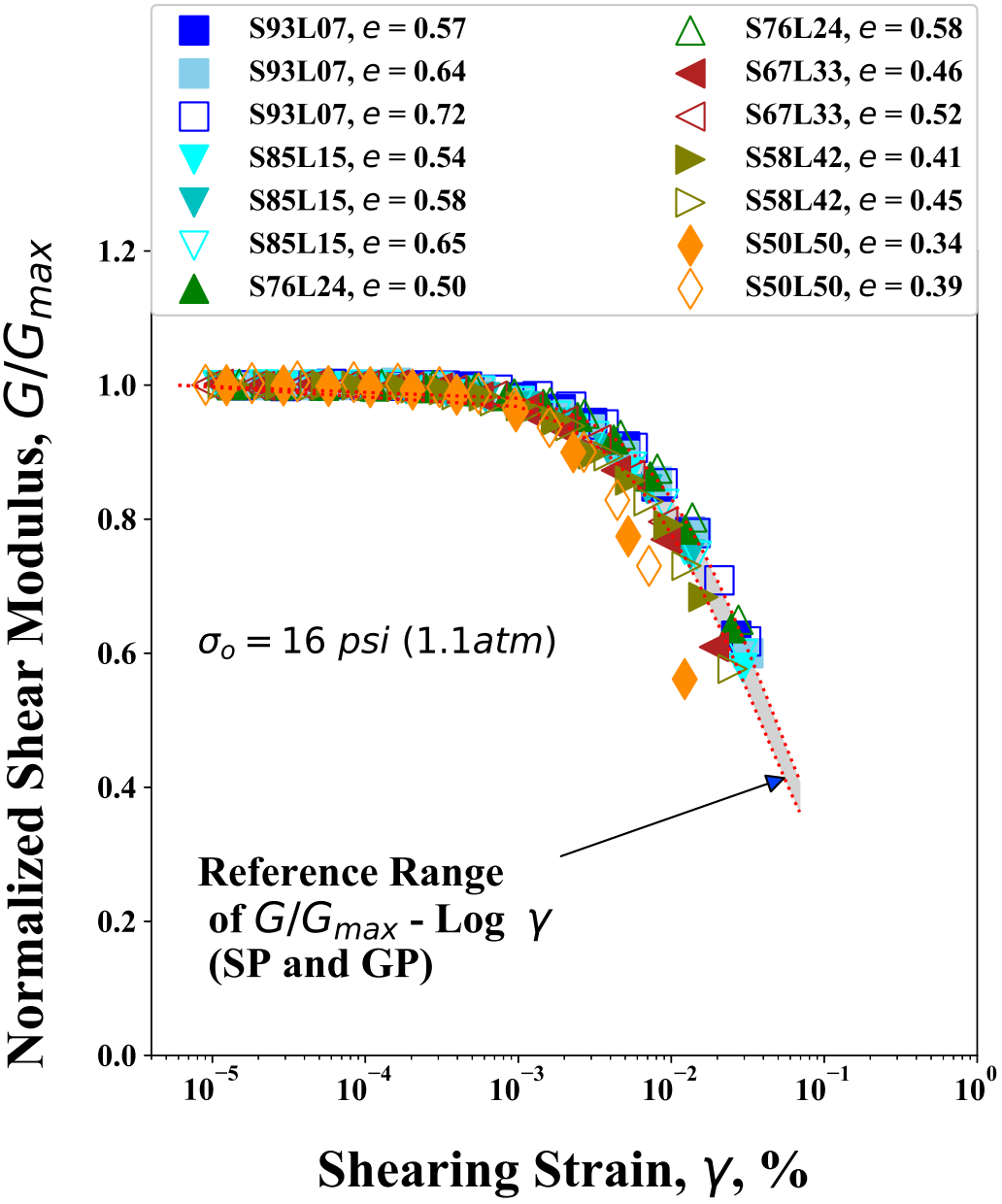

Figure 7.5: Variation in the G/G_{max} - Log γ Relationship for All Small-Particle-Packing Dominated (SPPD) Specimens (50% $\leq$ SPC $\leq$ 100%)

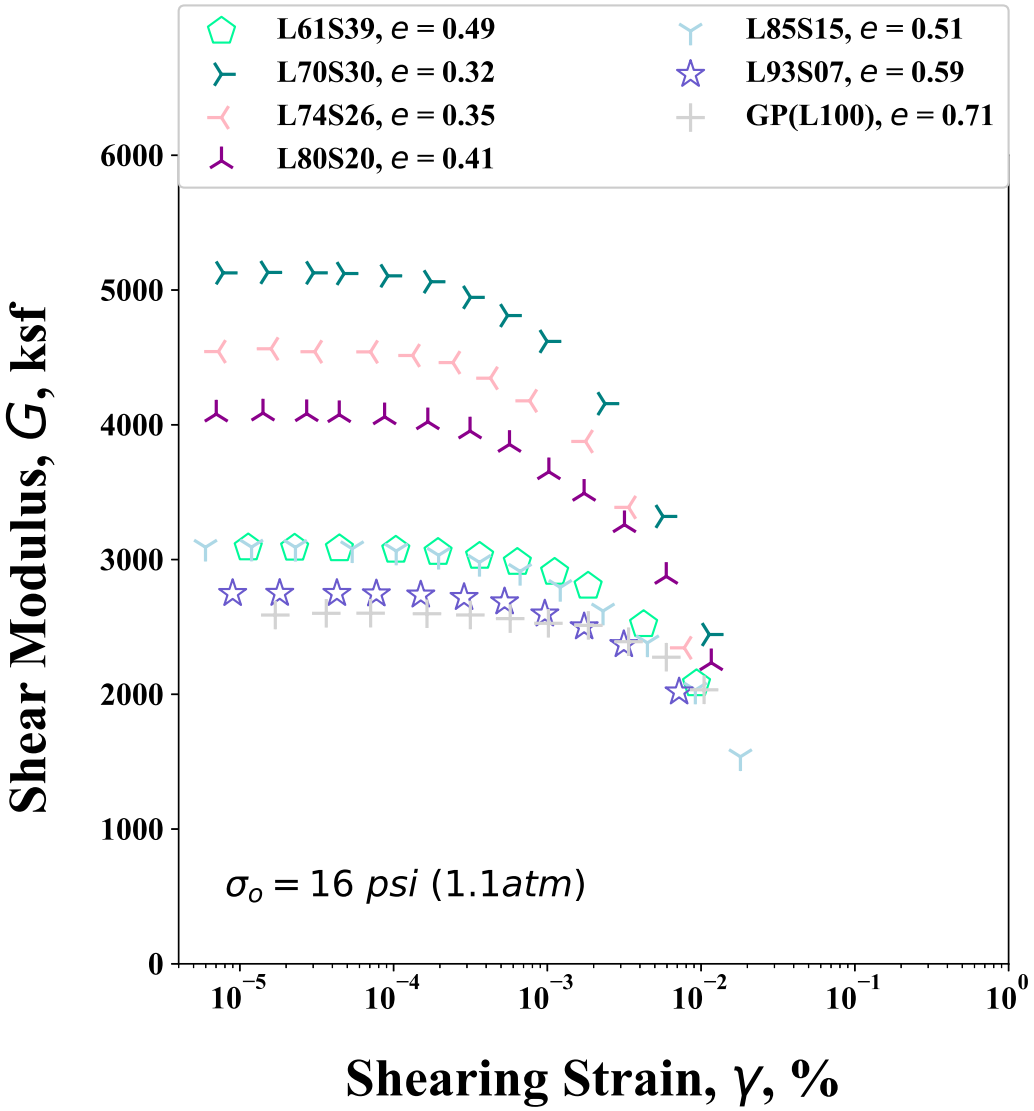

Figure 7.6: Variation in the G - Log γ Relationship for the Loosest Transition Zone (TZ) and Large-Particle-Packing Dominated (LPPD) Specimens (61% $\leq$ LPC $\leq$ 100%)

7.2.2 G - Log γ and G/G_{max} - Log γ Relationships of the TZ and LPPD Specimens

In Figure 7.6, the G - log γ relationships of the loosest transition zone (TZ) and large-particle-packing dominated (LPPD) specimens are provided. The TZ specimens generally have the higher G_{max} values than the LPPD specimens with the lower void ratios except for the L61S39 and L85S15 specimens. These two specimens have the higher void ratios relative to the other TZ specimens resulting in the G - log γ relationships close to the S100 and L100 specimens. Overall, the TZ specimens seem to behave more nonlinear than the LPPD specimens.

The G/G_{max} - log γ relationships of all transition zone (TZ) and large-particle-packing dominated (LPPD) specimens are shown in Figure 7.7. In the figure, the reference range constructed with the G/G_{max} - log γ relationships of the SP and GP materials is also provided as a gray zone. Overall, the TZ and LPPD specimens show more nonlinear behavior in the G/G_{max} - log γ relationship relative to the poorly-graded materials (the SP and GP materials, the gray zone in the figure). It is noteworthy that the G/G_{max} - log γ relationships of the L93S07 specimens are significantly different from the poorly-graded parent material (i.e., the L100 specimens) in spite of the small amount of small-particle content (SPC $\sim$ 7%) substitution. To more quantitative analysis, the reference strain (γ_r) and curvature coefficient (a) comparisons for these specimens will be performed in the following sections.

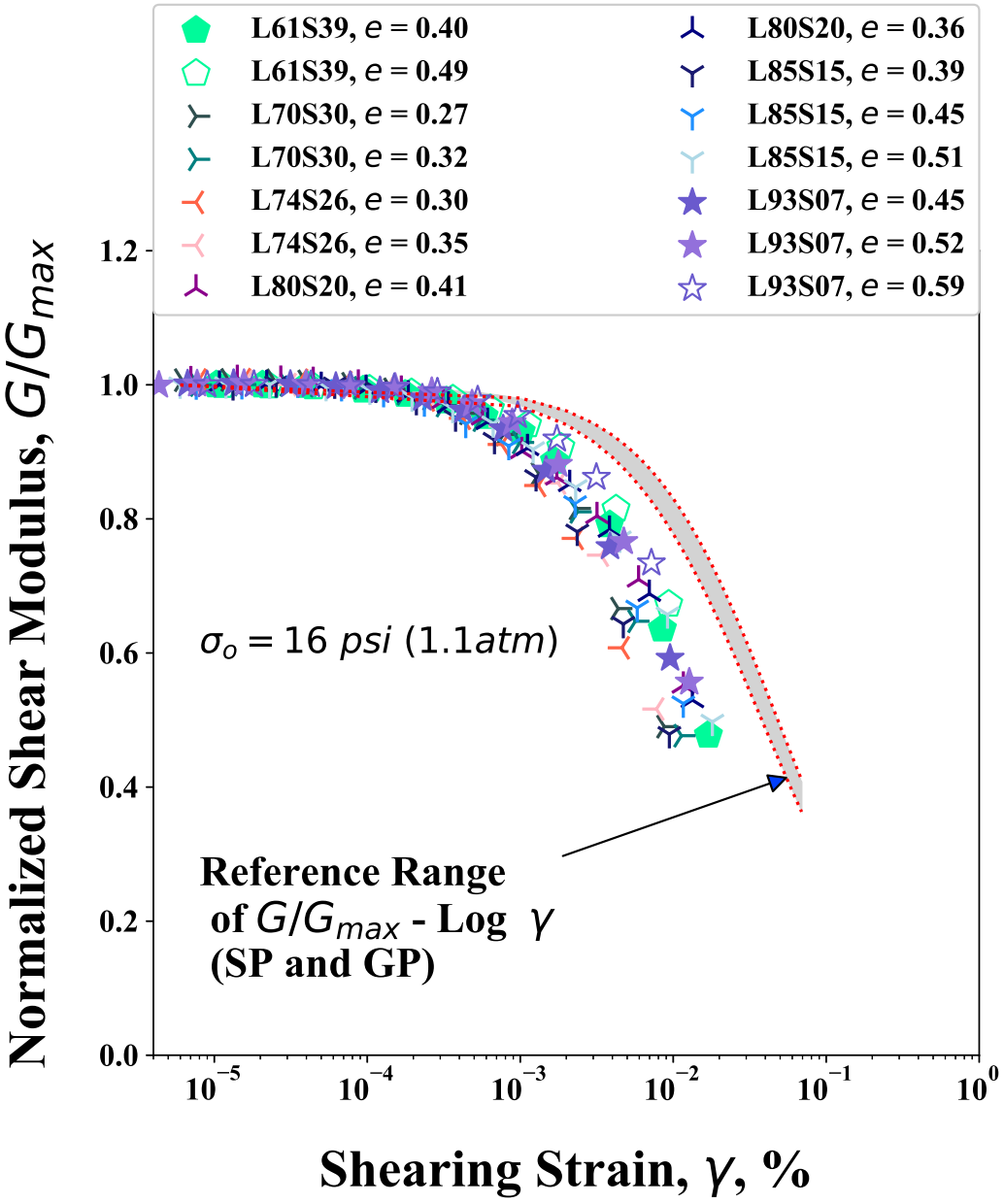

Figure 7.7: Variation in the G/G_{max} - Log γ Relationship for All Transition Zone (TZ) and Large-Particle-Packing Dominated (LPPD) Specimens (61% $\leq$ LPC $\leq$ 100%)

7.2.3 Reference Strain, γ_r, of Binary Mixtures

The variations of reference strain (γ_r) at 16 psi with void ratio (e) as well as uniformity coefficient (C_u) of the SPPD specimens are plotted in Figures 7.8a and 7.8b, respectively. No significant variation of reference strain (γ_r) is observed for the specimens of Gradations S100 through S76L24. In other words, the SPPD specimens for SPC $\geq$ 76% behave similarly with the poorly-graded materials in the G/G_{max} - log γ relationship at 16 psi (1.1 atm). Accordingly, the shear modulus of the binary specimens for SPC $\geq$ 76% in both strain ranges, i.e., the small-strain range as well as the nonlinear range, can be effectively estimated by investigating the parent poorly-graded sand. For the S67L33 and S58L42 specimens, the γ_r values are slightly lower than those of the specimens for 76% $\leq$ SPC $\leq$ 100%. However, the slightly lower γ_r values seem to be insignificant with the average γ_r value of 0.02%. As expected, a significant decrease in γ_r occurred for the S50L50 specimens. This indicates that classifying the S50L50 specimens as the transition zone (TZ) specimens is more reasonable based on the different nonlinear behavior from the other SPPD specimens.

Menq (2003) [26] suggested the estimation of γ_r for granular soils using the parameters of uniformity coefficient (C_u) and effective confining pressure (σ'_o). The γ_r estimation equation (Menq, 2003) is as follows:

$$\gamma_r = C_{\gamma_r} \times C_u^{-0.6} \times \left(\frac{\sigma'_o}{P_a}\right)^{0.5 \times C_u^{-0.15}} \tag{7.2}$$

where:

C_{γ_r} = reference strain (γ_r) at $C_u = 1.0$ as well as one atmosphere, and

P_a = atmosphere pressure.

In the Figure 7.8b, the reference strains (γ_r values) of the SPPD specimens are plotted with the C_u values of the corresponding SPPD specimens. Also, a γ_r estimation curve calculated by Equation 7.2 (a dashed line) for the SPPD specimens is provided in the figure. For the γ_r estimation curve, the constant of C_{γ_r}, which is the reference strain (γ_r) at $C_u = 1.0$ as well as at one atmosphere, was determined as 0.005% to match the γ_r values of the poorly-graded materials. Also, the gray zone in the figure represents a standard deviation of $\pm$ 0.014% for the estimation. As can be seen, the gray zone decreases with the increase of C_u indicating the typical granular soil behavior for which the more nonlinearity occurs with the increase of C_u. The specimens of Gradations S100 through S76L24 (i.e., SPC $\geq$ 76%) fall closely into the estimation curve due to the almost constant C_u values. Interestingly, the γ_r values of the S50L50 specimens also fall accurately into the estimation curve. Surprisingly, the S58L42 specimens have much higher γ_r values than those of the S50L50 specimens, even though the C_u values of these two gradations are very close one another. Base on this γ_r comparison between the S58L42 and S50L50 specimens, it is implied that the high C_u values of the S58L42 specimens may mislead to estimate the γ_r for those specimens.

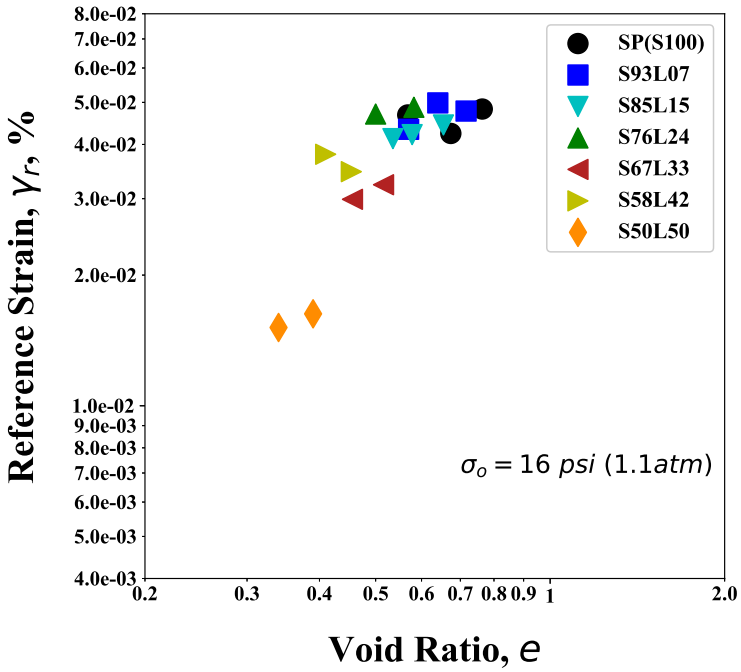

(a) Log γ_r - Log e for 50% $\leq$ SPC $\leq$ 100%

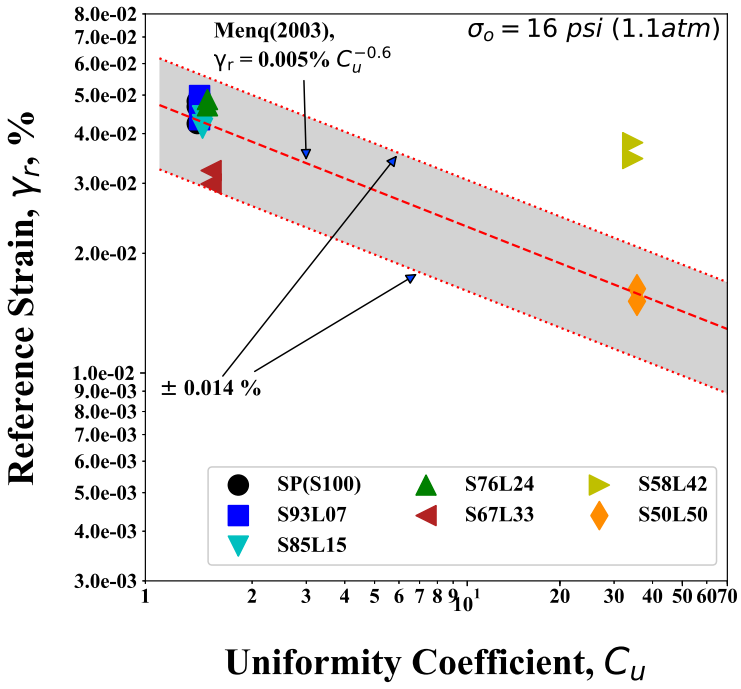

(b) Log γ_r - Log C_u for 50% $\leq$ SPC $\leq$ 100%

Figure 7.8: Variation in the Reference Strain, γ_r, at 16 psi with Void Ratio (e) and Uniformity Coefficient (C_u) for the SPPD Specimens

The variation in γ_r at 16 psi with e and C_u for the TZ and LPPD specimens are shown in Figures 7.9a and 7.9b, respectively. In the Figure 7.9a, the γ_r at 16 psi values of the TZ and LPP specimens ($61\% \leq$ LPC $\leq 100\%$) contain a decreasing trend with the decrease of e. This trend can be quantified by an equation following as:

$$\gamma_r = 0.068\% \times \ e^{1.77} \quad for\ 61\% \leq LPC \leq 100\% \tag{7.3}$$

The γ_r variation of the TZ and LPPD specimens with C_u is shown in the Figure 7.9b. In the figure, the γ_r estimation curve calculated by Equation 7.2 and the standard deviation range are also presented as the gray zone. The TZ specimens have relatively high C_u values compared to those of the SPPD specimens with the average C_u value of 38. Interestingly, the γ_r values of the five densest TZ specimens fall out of the gray zone down to the highly nonlinear range. These five specimens also show the smallest reference strain (γ_r) values indicating that the highly nonlinear behavior occurred among the TZ specimens. The significant variation in reference strain (γ_r) among the TZ specimens in the relatively constant C_u values indicates that the C_u is not a good parameter to estimate the nonlinearity for the TZ specimens. Lastly, the LPPD specimens of Gradation L93S07 have significantly lower γ_r values in accordance with the outlier behavior of the specimens in terms of n_G and A_D.

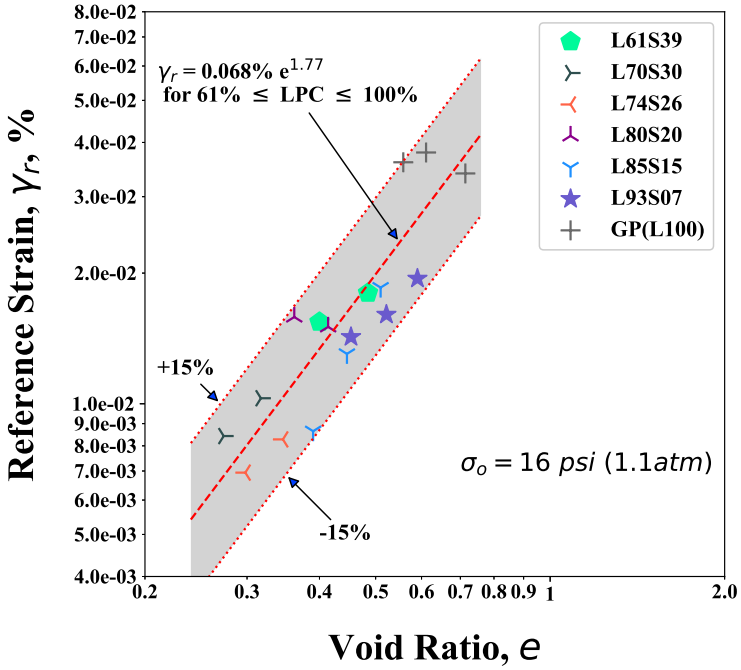

(a) Log γ_r - Log e for 61% ≤ LPC ≤ 100%

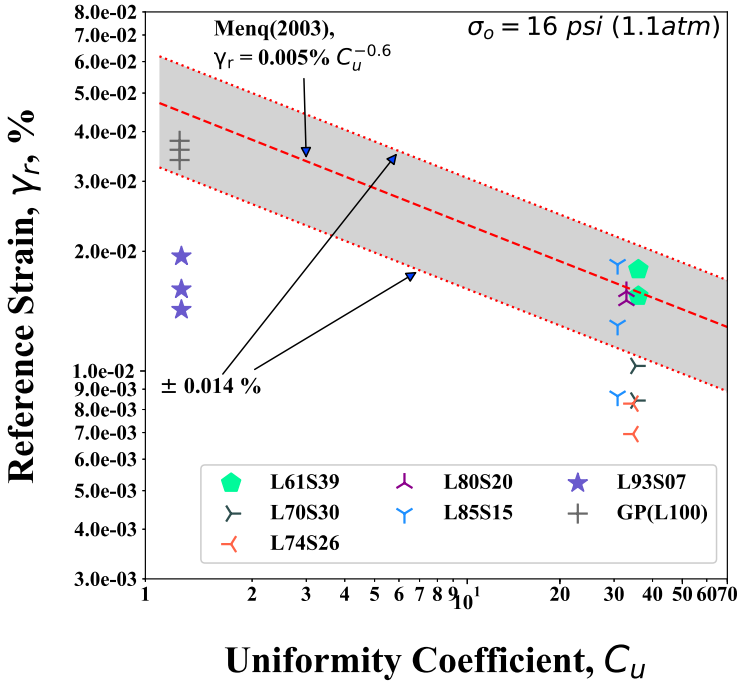

(b) Log γ_r - Log C_u for 61% ≤ LPC ≤ 100%

Figure 7.9: Variations in the Reference Strain, γ_r, at 16 psi with Void Ratio (e) and Uniformity Coefficient (C_u) for the TZ and LPPD Specimens

7.2.4 Curvature Coefficient of Binary Mixtures

The variations of the curvature coefficient in the shear modulus reduction curve (a), with the void ratio (e) and uniformity coefficient (C_u) values of the SPPD, TZ, and LPPD specimens are presented in Figures 7.10a and 7.10b, respectively. In the Figure 7.10a, the gray zone represents the range of a for the SP and GP materials ($a = 0.92 \sim 1.1$). No significant variations and patterns in a with e are observed for the SPPD, TZ and LPPD specimens. In the Figure 7.10b, the a - log C_u relationships of the SPPD, TZ, and LPPD specimens are presented. Similarly, in the figure, the gray zone represents the range of a for the SP and GP materials ($a = 0.92 \sim 1.1$). As expected, no significant variations and patterns in a with C_u are observed for the SPPD, TZ, and LPPD specimens.

7.3 NONLINEAR MATERIAL DAMPING RATIO IN SHEAR OF BINARY MIXTURES

7.3.1 D - Log γ Relationships of Two Poorly-Graded Materials, SP and GP

The variations in D - log γ relationship for the two poorly-graded parent materials (i.e., the SP and GP materials) are presented in Figure 7.11. In the figure, a reference D - log γ relationship is constructed using the two poorly-graded specimens: (1) L100 with $e = 0.61$, and (2) S100 with $e = 0.57$. This reference range represents the variability of the D - log γ relationship of the poorly-graded specimens with the uniformity coefficients range from 1.1 to 1.3.

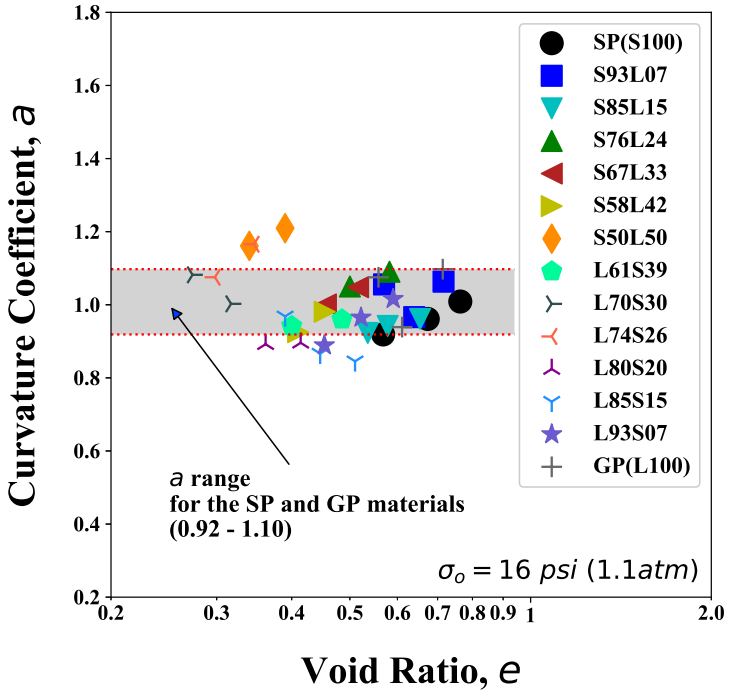

(a) Log a - Log e for 0% $\leq$ SPC $\leq$ 100%

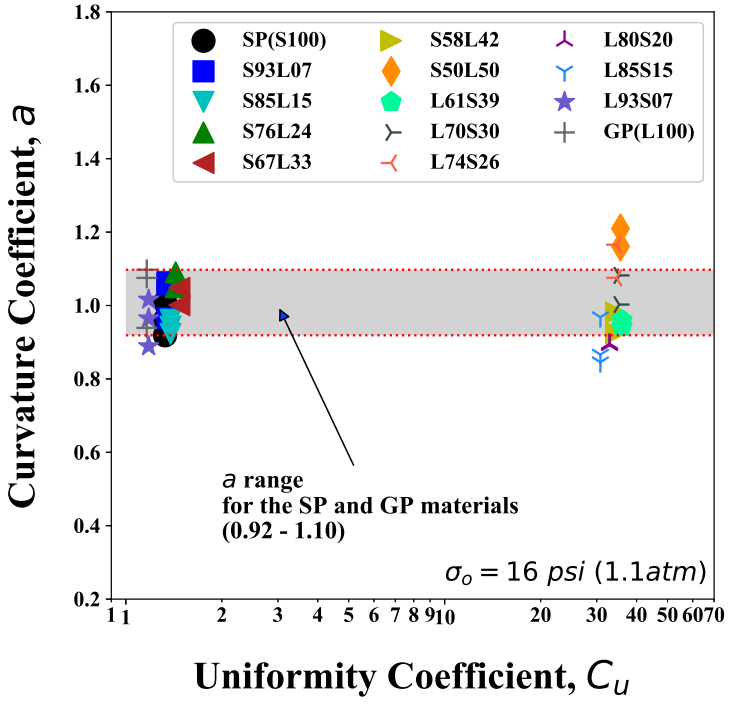

(b) Log a - Log C_u for % $\leq$ SPC $\leq$ 100%

Figure 7.10: Variations in the Curvature Coefficient, a, at 16 psi with Void Ratio (e) and Uniformity Coefficient (C_u) for the SPPD, TZ, and LPPD Specimens

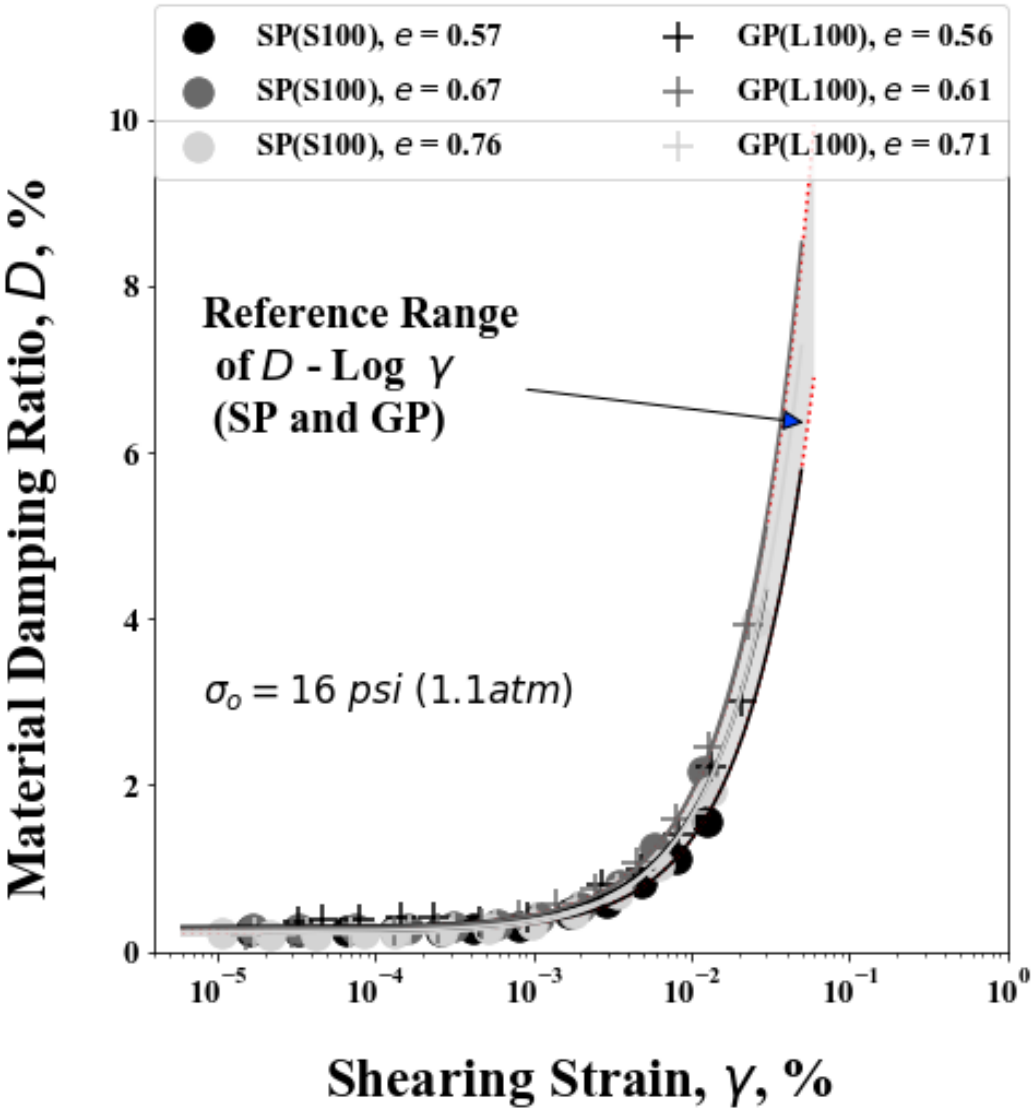

Figure 7.11: Variations in the D - Log γ Relationship of the Two Poorly-Graded Materials (the SP and GP Materials)

7.3.2 D - Log γ Relationships of the SPPD, TZ, and LPPD Specimens

The variations in the D - log γ relationships of the small-particle-packing dominated (SPPD) specimens are shown in Figure 7.12. In the figure, the reference D - log γ relationship range constructed in the previous section is also provided with a gray zone. The D - log γ relationships of the SPPD specimens for SPC $\geq$ 58% seem to be within the reference range (i.e., the variability of the SP and GP materials) except for one specimen of the S93L07 with $e = 0.57$. It is not clearly explained why the S93L07 specimen with $e = 0.57$ has less nonlinearity in terms of the D - log γ relationship compared to the other SPPD specimens. However, it is noteworthy that the S50L50 specimens show the most nonlinear behavior among the SPPD specimens in the D - log γ relationships as the specimens showed the most nonlinear behavior in the G/G_{max} - log γ relationships.

The variations in the D - log γ relationships of the transition zone (TZ) and large-particle-packing dominated (LPPD) specimens are presented in Figure 7.13. The reference range constructed with the two poorly-graded materials (i.e. the SP and GP materials) is also provided as the gray zone in the figure. Overall, the TZ and LPPD specimens show highly nonlinear behavior in terms of the D - log γ relationship relative to the SP and GP materials.

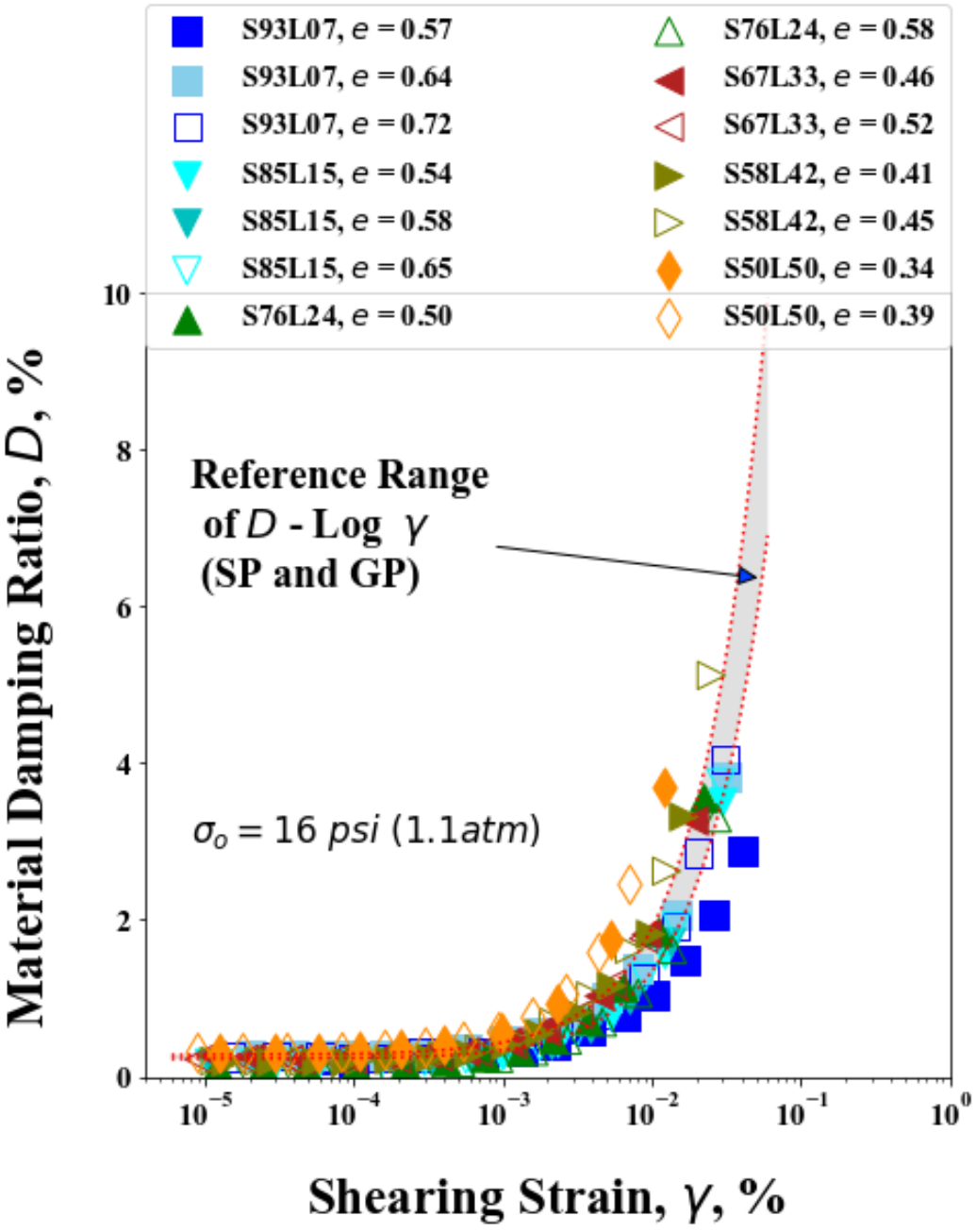

Figure 7.12: Variation in the D - Log γ Relationship of the SPPD Specimens ($50\% \leq \text{SPC} \leq 100\%$)

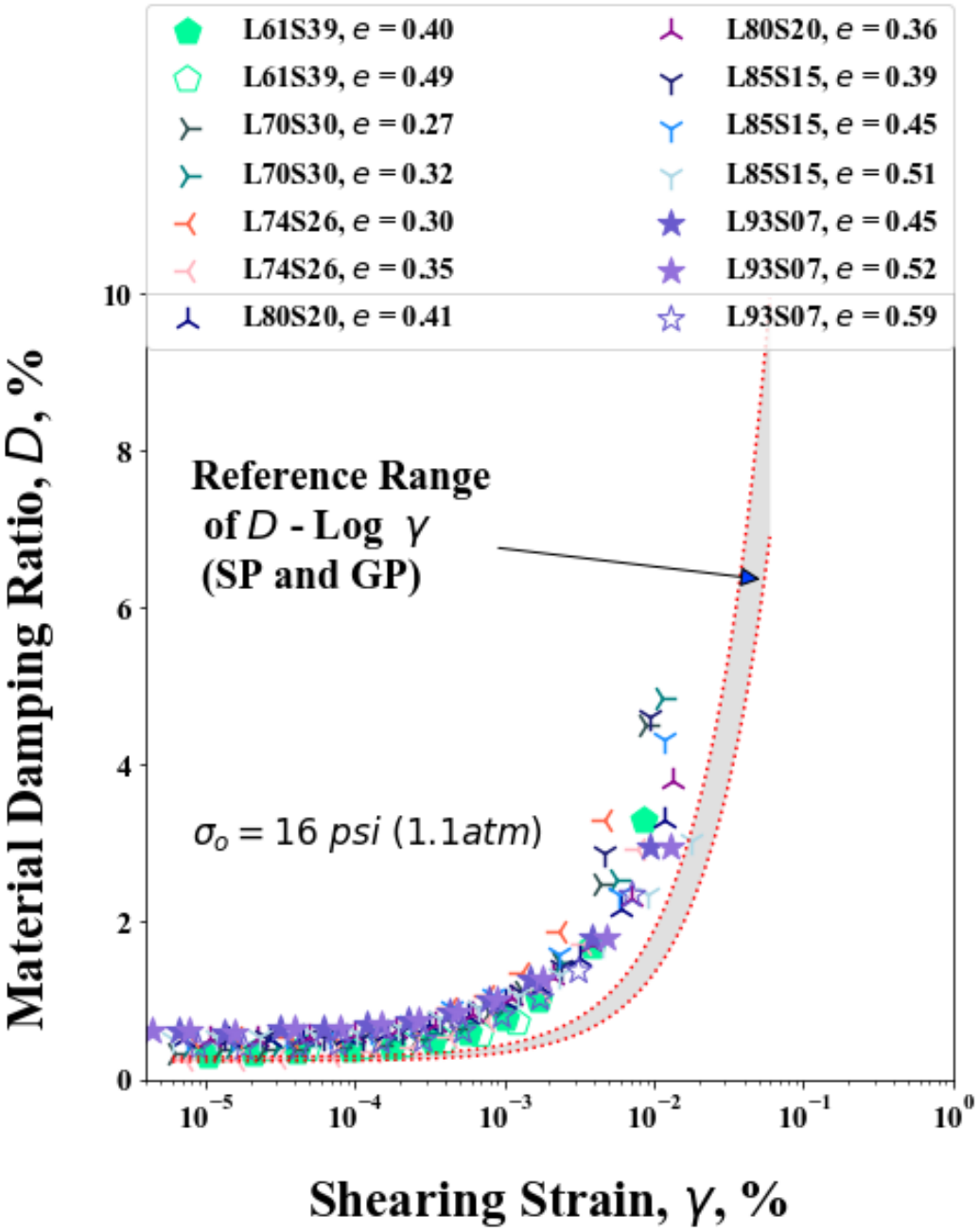

Figure 7.13: Variation in the D - Log γ Relationship of the TZ and LPPD Specimens ($61\% \leq$ LPC $\leq 100\%$)

7.4 NONLINEAR CHARACTERISTICS OF GAP-GRADED MIXTURES

In Section 6.6, the small-strain characteristics of the seven gap-graded specimens are discussed in terms of the small-strain shear modulus at 1 atm (A_G) and the exponent component in the log G_{max} - log σ_o relationship (n_G) comparing the parameters of the poorly- and well-graded materials. This section will investigate the nonlinear shear modulus characteristics of the gap-graded specimens.

The reference strain (γ_r) at 16 psi of one SW specimen and seven gap-graded specimens as well as the SP and GP materials (i.e., the S100 and L100 specimens) are shown in Figure 7.14a. The γ_r at 16 psi value of the SW specimen (i.e., the S_w100 specimen) is about 0.024%, which is about 50% lower than the average γ_r value of the SP and GP materials. This significant lower γ_r value for the SW specimen can be well explained by the higher C_u value of the SW specimen ($C_{u,SW} = 8.0$). Interestingly, the γ_r value of the SW and gap-graded specimens have a decreasing trend with the decrease of e. This trend can be represented by an equation as follows:

$$\gamma_r = 0.028\% \times \ e^{0.48} \qquad for\ the\ gap-graded\ specimens \tag{7.4}$$

In Figure 7.14b, the γ_r values of the SW, SP, GP, and gap-graded specimens are plotted with the C_u values. In the figure, the γ_r estimation curve calculated by Equation 7.4 (Menq, 2003) including ± 0.014% standard deviation range are also presented with the gray zone. Surprisingly, the gap-grade

specimens generally fall into the standard deviation range (i.e., the gray zone) excerpt for the L93S$_w$07 specimen. It is noteworthy that the small-particle content (SPC) of the L93S$_w$07 specimen is 7 percent, which is the same as the SPC value of the L93S07 specimens (i.e., the binary specimens with the similar SPC value). The similarity indicates that the relatively small amount of small particles would induce the high possibility of particle segregation during sample reconstitution resulting in the outlier behavior.

The variations of curvature coefficient (a) in the G/G_{max} - log γ relationship (a) with the e and C_u values of the SW and gap-graded specimens are presented in the Figures 7.15a and 7.15b, respectively. In both figures, the reference range constructed with the a values of the poorly-graded parent materials ($0.92 \sim 1.1$) are also provided. Aa can be seen, no significant variations in the a values are observed within the a values of the SP and GP materials (i.e., the S100 and L100 binary specimens) for the gap-graded specimens.

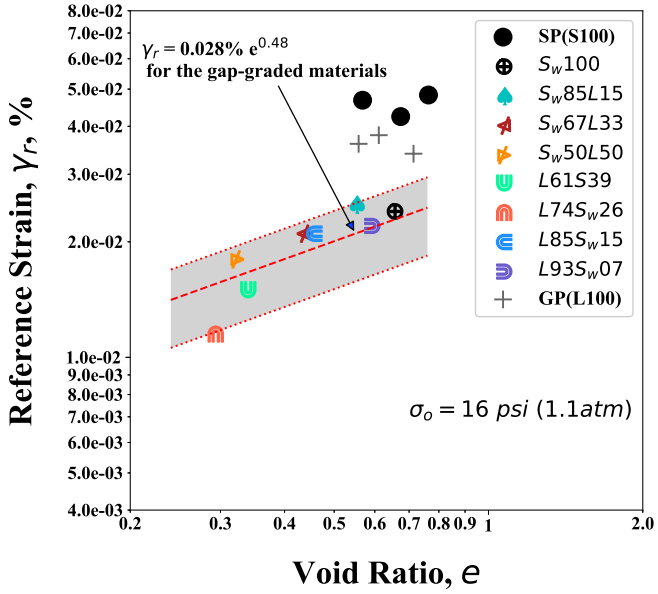

(a) Log γ_r - Log e for 0% $\leq$ SPC $\leq$ 100%

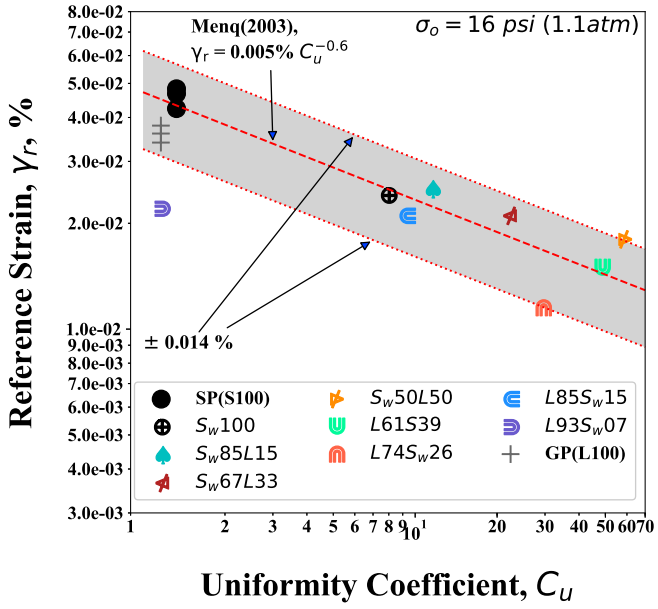

(b) Log γ_r - Log C_u for 0% $\leq$ SPC $\leq$ 100%

Figure 7.14: Variation in Reference Strain, γ_r, at 16 psi with Void Ratio (e) and Uniformity Coefficient (C_u) of One Well-Graded and Seven Gap-Graded Specimens

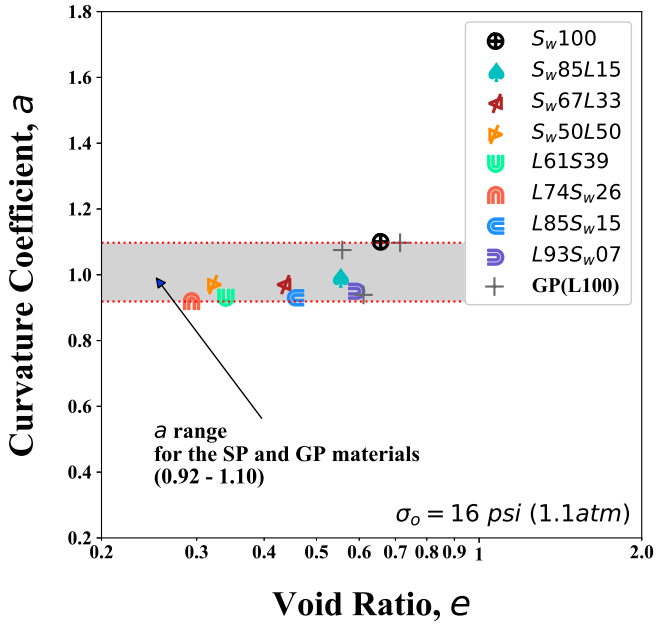

(a) Log $a_{n,16psi}$ - Log e for 0% $\leq$ SPC $\leq$ 100%

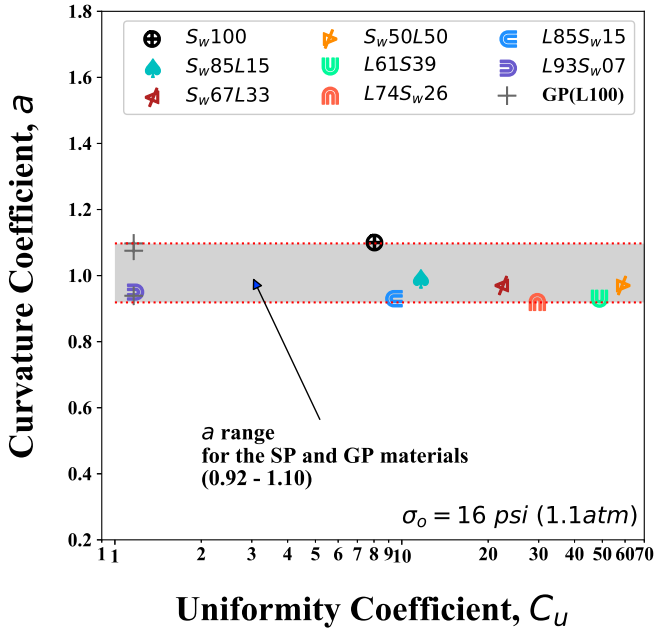

(b) Log a - Log C_u for 0% $\leq$ SPC $\leq$ 100%

Figure 7.15: Variation in Curvature Coefficient, a, at 16 psi with Void Ratio (e) and Uniformity Coefficient (C_u) of One Well-Graded and Seven Gap-Graded Specimens

7.5 SUMMARY

In this chapter, the nonlinear behavior of the binary and gap-graded specimens is discussed. The nonlinear behavior in the normalized shear modulus reduction curves (G/G_{max} - log γ curves) is generally characterized by two parameters: (1) reference strain γ_r, and (2) curvature coefficient, a.

The relative small amount of large-particle sizes (LPC $\leq$ 24%) does not significantly affect the G/G_{max} - log γ curves of the small-particle-packing dominated (SPPD) binary specimens (i.e., binary specimens for 50% $\leq$ SPC $\leq$ 100%). In other words, the G/G_{max} - log γ curves of the SPPD specimens for SPC $\geq$ 76% follows quite closely the G/G_{max} - log γ curve trend of the SP and GP materials. This insignificant effect of the small amount of large particles on the binary specimens is also found in terms of the A_G parameter (small-strain shear modulus at 1 atm) - e relationship. Accordingly, it is possible to say that, when the LPC is relatively small (i.e., for LPC $\leq$ 24%), the stiffnesses of the binary mixtures not only in the small-strain range but also in the nonlinear range can be estimated by investigating the parent SP material.

The S50L50 specimens (i.e., the specimens composed of 50% of the SP material and 50% of the GP material) show significantly higher values of reference strain (γ_r) compared to the other SPPD specimens. Therefore, as discussed in Chapter 6, classifying the S50L50 specimens as falling in the transition Zone (TZ) specimens instead of the SPPD specimens is reasonable based on the comparisons of the n_G, A_D, and γ_r values between the SPPD and TZ specimens.

The variations of γ_r for the TZ specimens show a weakly decreasing trend with decreasing void ratios. On the other hands a significant variation of γ_r is observed for the TZ specimens in which the uniformity coefficient (C_u) values are almost constant. Therefore, it seems that the void ratio (e) is a better parameter than the uniformity coefficient (C_u) to estimate the nonlinear behavior of the TZ specimens.

The nonlinear shear modulus characteristics of the gap-graded specimens were also investigated and the results are presented in this chapter. The gap-grade specimens show a decreasing trend of γ_r with a decrease in e. The gap-graded specimens also show a relatively strong relationship in the log γ_r - log C_u compared to the binary mixtures.

Chapter 8

Conclusions

8.1 BACKGROUND

In the framework of binary granular soils, estimating the critical packing condition in binary mixtures is very important in predicting their behavior. Conceptually, the critical packing condition is that all void spaces between the large particles in binary mixtures are filled with small particles.(See Figure 8.1b.) The associated critical small-particle content (SPC*), which is the small-particle content (SPC) under the critical packing condition, can be calculated using the void ratios of the small- and large-particle materials. Based on the critical small-particle content (SPC*), the state when the SPC is greater than SPC* (i.e., SPC > SPC*) is denoted as the small-particle-packing dominated, SPPD, condition (Figure 8.1a). On the other hand, the state when SPC is less than SPC* (i.e., SPC < SPC*) is denoted as the large-particle-packing dominated, LPPD, condition (Figure 8.1c).

In this dissertation research, a total of 28 binary specimens were reconstituted with the mixtures of two poorly-graded materials, also called the "parent" materials in this research. These parent materials are: (1) an SP material: the washed mortar sand (WMS) was processed to create a poorly-

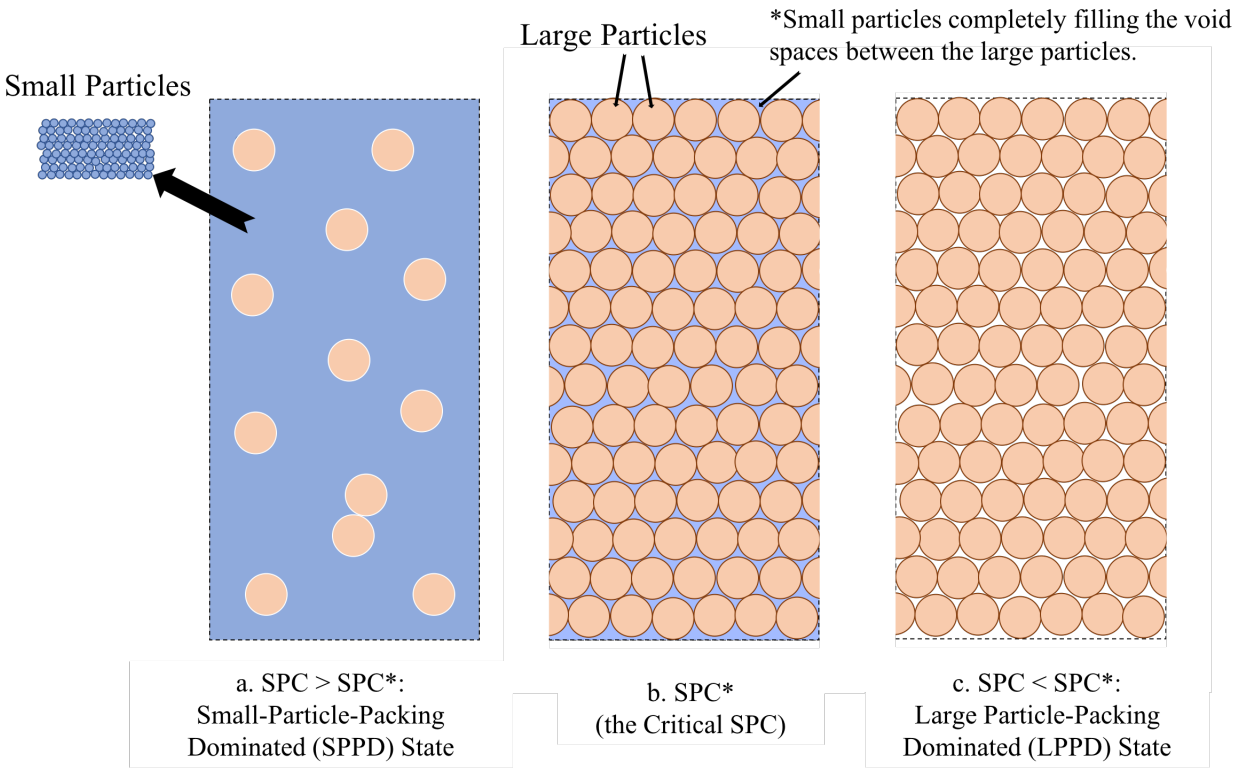

Figure 8.1: Schematic of Three Possible Binary Packing Conditions

graded sand (SP) which formed the small particles; and (2) a GP material: a river gravel was processed to create a poorly-graded gravel (GP) which formed the large particles. Additionally, seven gap-graded specimens were also reconstituted with the mixtures of a well-graded sand (SW) and the GP material.

Using the minimum and maximum void ratio values (e_{min} and e_{max}, respectively) of the parent materials (the SP and GP materials) for the binary mixtures, a range of the critical small-particle content (SPC*) was calculated and is shown in Table 8.1. As seen in the table, the minimum and maximum percentages of SPC* values are 23% and 36%, respectively, indicating the critical packing condition that can theoretically occur when the large-particle content (LPC) is between 64% and 77% and the small-particle content (SPC) is between 23% and 36%. Considering the theoretically calculated SPC* range and the literature suggestion (Thevanayagam and Martin, 2002 [33]), three classifications and associated quantities based on the packing conditions of the binary specimens are determined and summarized in Table 8.2.

The three classifications for the binary specimens with respect to void ratio (e) and small-particle content (SPC) are presented in Figure 8.2. In this figure, the values of e_{min} and e_{max} of the SP and GP materials as well as the calculated SPC* range presented in the Table 8.1 are shown.

Table 8.1: Calculations of the SPC* Values of Binary Materials Composed of Poorly-Graded Sand (SP) and Poorly-Graded Gravel (GP

		SPC*	
		Large Particles (GP[1])	
		e_{min}**=0.56**	e_{max}**=0.90**
Small Particles (SP[2])	e_{min}**=0.56**	26%	36%
	e_{max}**=0.89**	23%	32%

[1] Poorly-Graded Gravel, GP
[2] Poorly-Graded Sand, SP

Table 8.2: Three Classes for the Binary Mixtures Tested in this Study

Class ID.	$SPPD$[1]	TZ[2]	$LPPD$[3]
SPC[4], %	$100 \sim 46$	$46 \sim 13$	$13 \sim 0$
LPC[5], %	$0 \sim 54$	$54 \sim 87$	$87 \sim 100$

[1] Small-particle packing dominated
[2] Transition zone
[3] Large-particle packing dominated
[4] Small-particle content
[5] Large-particle content

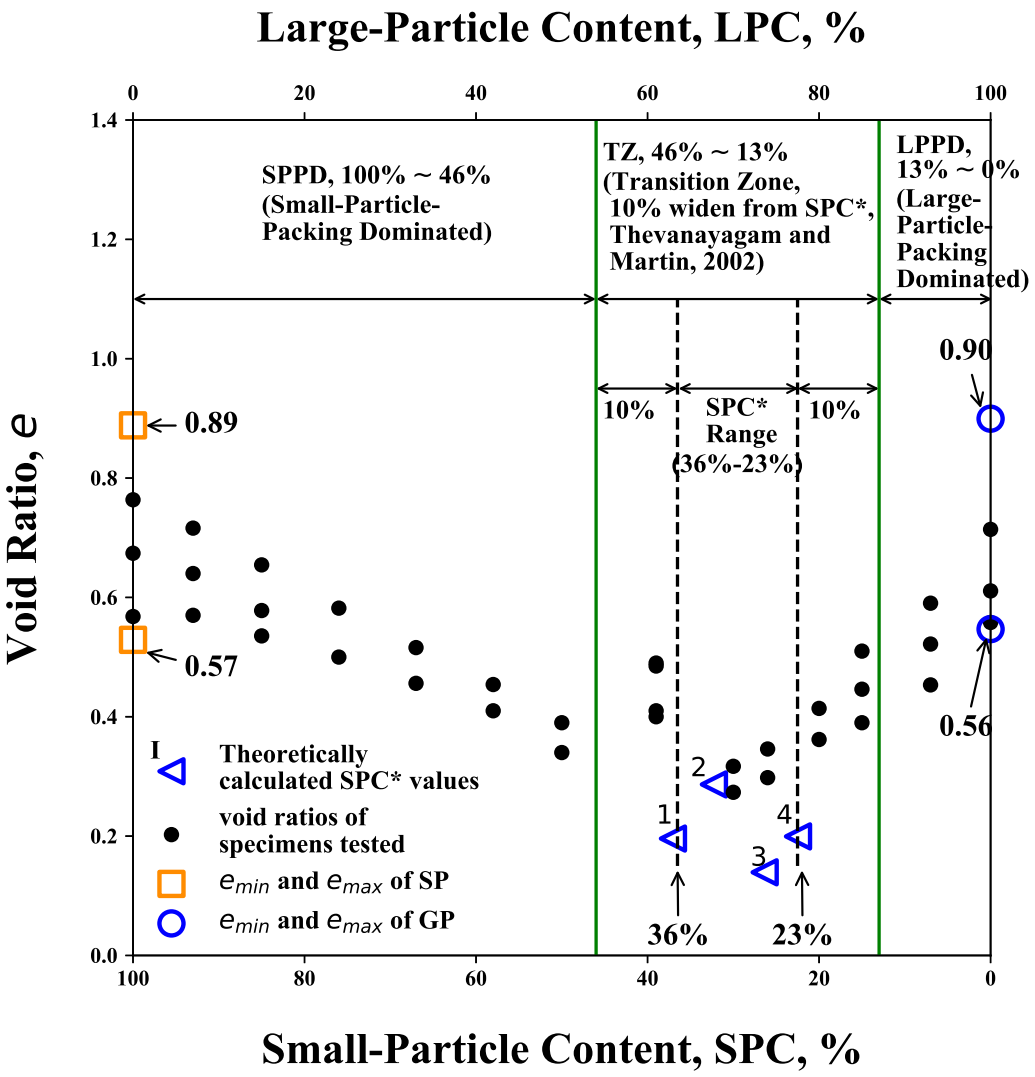

Figure 8.2: Variation in Values of e_{min} and e_{max} with the Small-Particle Content, SPC, % and the Three Classification Zones (SPPD, TZ and LPPD)

8.2 SMALL-STRAIN DYNAMIC PROPERTIES OF BINARY AND GAP-GRADED MIXTURES

8.2.1 Binary Mixtures

The effects of void ratio, e, isotropic confining pressure, σ_o, and uniformity coefficient, C_u, on small-strain shear modulus, G_{max}, and small-strain material damping ratio in shear, D_{min}, of the binary mixtures were investigated. For the confining pressure, the parameter of total confining pressure (σ_o) has been used through the entire this study rather the parameter of effective confining pressure (σ'_o) due to the insignificant difference between the two parameters of the specimens tested in this study. The effects of the same parameters (e, σ_o, and C_u) on G_{max} and D_{min} of the gap-graded mixtures were also investigated.

As shown in Figure 8.3a, the binary specimens for the small-particle content (SPC) $\geq$ 67% behave similarly to poorly-graded sand (i.e., the SP material which is the parent sand in the binary mixtures) in terms of the G_{max} at 1 atm (A_G) and e. However, the A_G values of the S58L42 specimens began deviating from the A_G estimation curve calculated by Hardin's (1978) void ratio function. Interestingly, the A_G values of the SPPD specimens (50% $\leq$ SPC $\leq$ 100%) are well approximated by a straight-line trend in log A_G - log e relationship as seem in Figure 8.3a, resulting in a simple equation as follows:

$$A_G = 1495\ ksf \times e^{-1.10} \quad for\ 50\% \leq SPC \leq 100\% \tag{8.1}$$

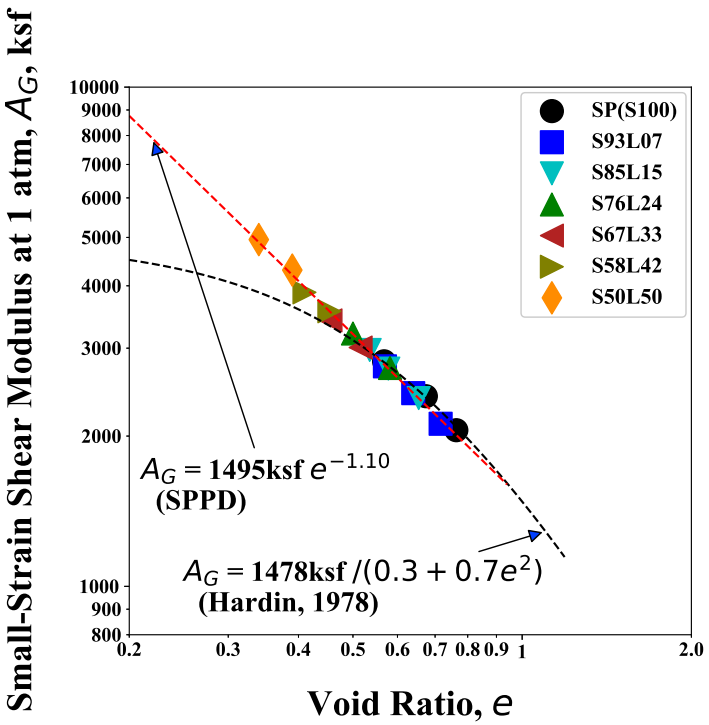

(a) Log A_G - Log e for 50% $\leq$ SPC $\leq$ 100%

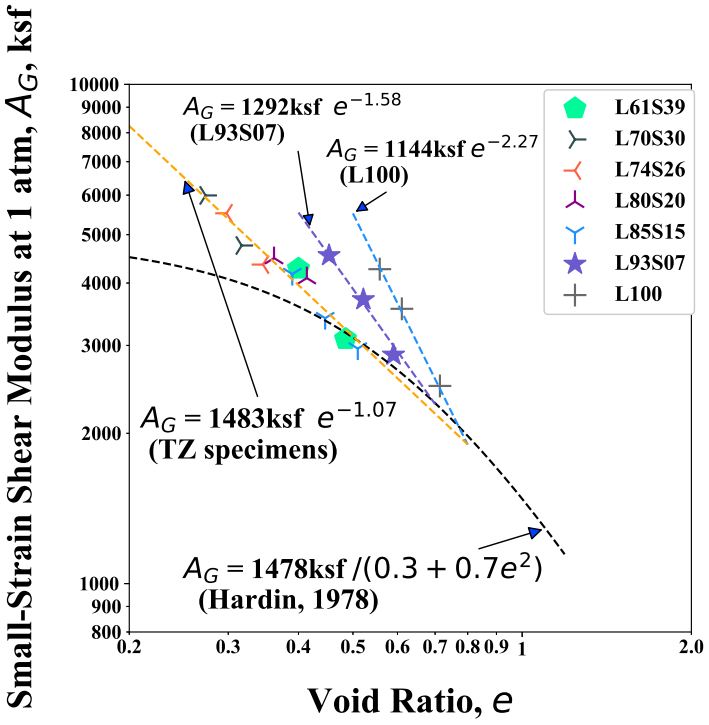

(b) Log A_G - Log e for 61% $\leq$ LPC $\leq$ 100%

Figure 8.3: Variation in Small-Strain Shear Modulus at 1 Atm, A_G, with Void Ratio of Binary Mixtures

In Figure 8.3b, the A_G values of the TZ specimens also showed a straight-line trend with the e values. Interestingly, the trends in the log A_G - log e relationship for both the SPPD and TZ specimens are significantly similar to each other as shown in Table 8.3. This finding indicates that the variation in A_G with e for a wide SPC range ($15\% \leq \text{SPC} \leq 100\%$) of the binary mixtures is independent of the packing condition, and a clear relationship between the A_G and e is shown.

On the other hand, the L100 and L93S30 specimens show different behaviors in the log A_G - log e relationship than the relationship for the SPPD and TZ specimens. The trend-line constants in the log A_G - log e relationships of the SPPD, TZ, and LPPD specimens are summarized in Table 8.3.

Table 8.3: Comparison of the values of $A_{G,e=1.0}$ and the exponential component in the void-ratio correction function, α, of the Binary Specimens Tested in this Study

Group ID.	$A_{G,e=1.0}$**, ksf**	α	D_{50}[3]**, mm**	C_u[3]
SPPD[1]	1495	-1.10	0.35	1.38
TZ[2]	1483	-1.07	33.5	10.5
Avg. of SPPD &TZ	1487	-1.08	-	-
L93S07	1292	-1.58	11	1.16
L100	1144	-2.27	11	1.18

[1] Small-Particle Packing Dominated, SPPD
[2] Transition zone, TZ
[3] The average number of each group was calculated.

In the analyses of the exponent of σ_o of the log G_{max} - log σ_o relation-

ship (i.e., n_G) of the SPPD, TZ, and LPPD specimens, it was found that the exponents (n_G) of the SPPD specimens are relatively constant ranging from 0.44 to 0.47, while, the n_G values of the TZ and LPPD specimens were scattered, i.e., the range of the n_G values for the TZ specimens is from 0.48 to 0.54, and somewhat larger than those of the SPPD specimens with an average number of 0.51.

Overall, the D_{min} values of the binary specimens do not show as a strong relationships with the e values as the relationships of G_{max} and e. In the analyses of the A_D values of the SPPD binary specimens, all A_D values of the SPPD specimens ranged from 0.20% to 0.35%, which are within about $\pm$ 10% variability of the SP material. It is suggested to classify the S50L50 specimens as part of the transition zone (TZ) specimens instead of the SPPD specimens due to the moderately higher A_D values compare to the other SPPD specimens.

The A_D values of the TZ and LPPD specimens ranged from 0.38 to 0.70 and 0.25 to 0.80, respectively. The TZ and LPPD specimens show a wider range in A_D than those of the SPPD specimens, indicating more variability in the small-strain material damping characteristics. Significantly higher values in A_D were observed for the L93S07 specimens. Based on the consistent outlier-behavior of the Gradation L93S07 specimens, it seems reasonable to assume that theses specimens have quite heterogeneous densities due to particle segregation of the sand particle settling down to the bottom of the specimens.

8.2.2 Gap-Graded Mixtures

Similar to the SPPD specimens, the gap-graded specimens began to deviate from the parent material trend in the log A_G - log e relationship when the percentage of large particles became greater than about 33 percent. In addition, the S_w50L50 specimen, which is consisting of 50% of a well-graded sand as small particles and 50% of the poorly-grade gravel used for the binary mixtures as large particles, behaved very similarly with the binary specimens for S50L50 in that those specimens began to deviate from the parent material trend (i.e., the SP and SW specimens, respectively). This indicated that the hypothesis from testing results of the binary mixtures that the stiffness in the small-strain range of the binary mixtures is dominated by the parent sand material for $50\% \leq \text{SPC} \leq 100\%$ is also applicable to the gap-graded materials. (See Figure 8.4.)

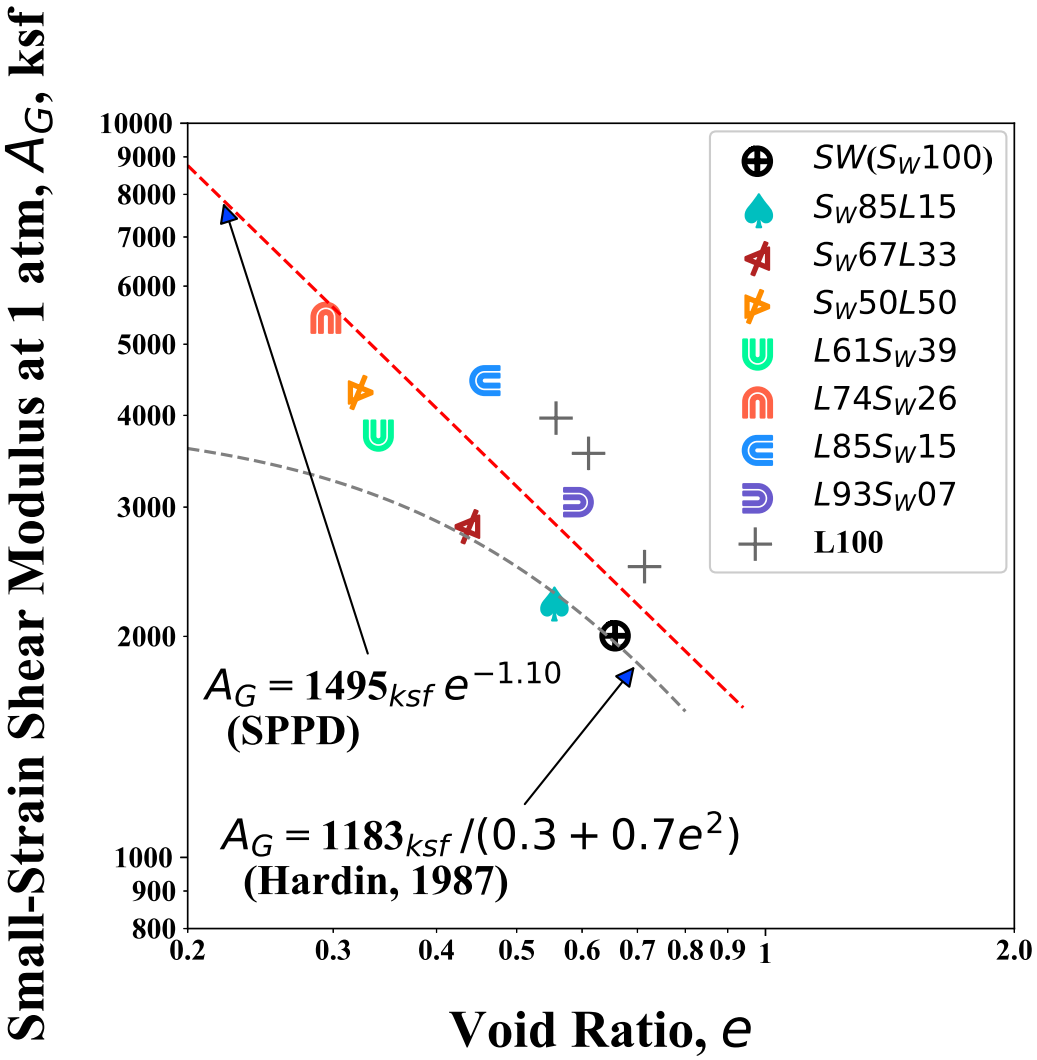

Figure 8.4: Variation in Small-Strain Shear Modulus at 1 Atm with Void Ratio of One SW Specimen, Three GP Specimens, and Seven Gap-Graded Specimens with Curve Fittings

8.3 NONLINEAR DYNAMIC PROPERTIES OF BINARY AND GAP-GRADED MIXTURES

8.3.1 Binary Mixtures

The relative small amount of large particles (i.e., 0% $\leq$ LPC $\leq$ 24% or 76% $\leq$ SPC $\leq$ 100%) do not significantly affect the nonlinear shear modulus behavior of the binary mixtures relative to the nonlinear behavior of the parent material (i.e., the SP material). This insignificant effect on the dynamic properties of the parent material also agrees with the small-strain shear modulus behavior of the binary mixtures. Accordingly, when the LPC is relatively small (i.e., for LPC $\leq$ 24%), the stiffnesses of the binary mixtures not only in the small-strain range but also in the nonlinear range can be estimated by investigating the parent SP material.

The S50L50 specimens also show the significantly higher reference strain (γ_r) values (i.e. the most nonlinear behavior) compared to the other SPPD specimens. Based on the consistent outlier-behavior of the S50L50 in terms of the n_G, A_D, and γ_r, it seems reasonable to classify the S50L50 specimens as the TZ specimens.

The variation of γ_r for the TZ specimens show a decreasing trend with the decrease of void ratio. The relatively weak relationship between γ_r and C_u for the TZ specimens implicates that the void ratio (e) is a better parameter than the C_u to estimate the nonlinear behavior of the TZ binary specimens.

In terms of the curvature coefficient in the G/G_{max} - log γ relationship (a), no significant pattern or relationship is observed for the binary and gap-

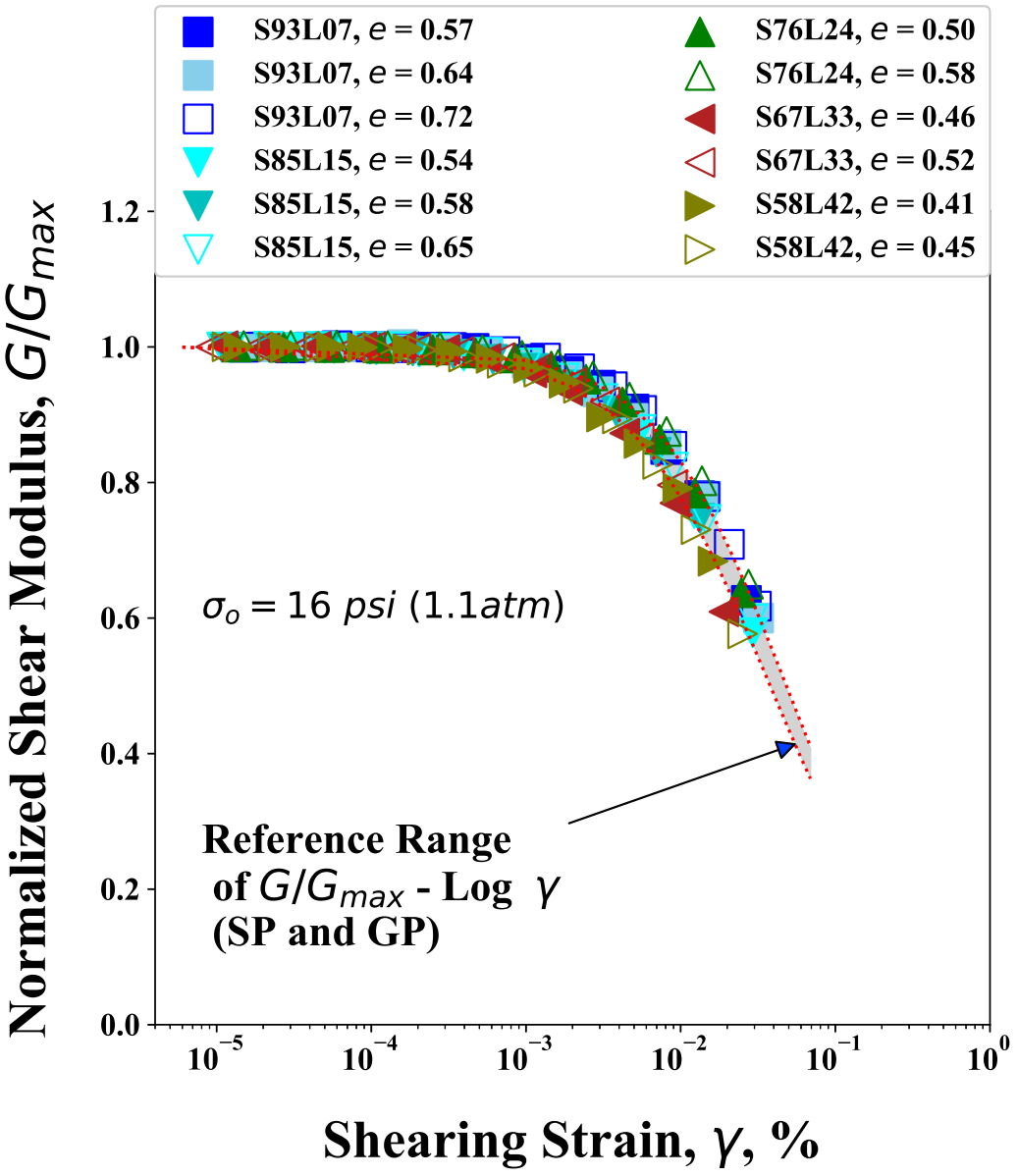

Figure 8.5: Variation in the G/G_{max} - Log γ Relationship for 58% $\leq$ SPC $\leq$ 100%

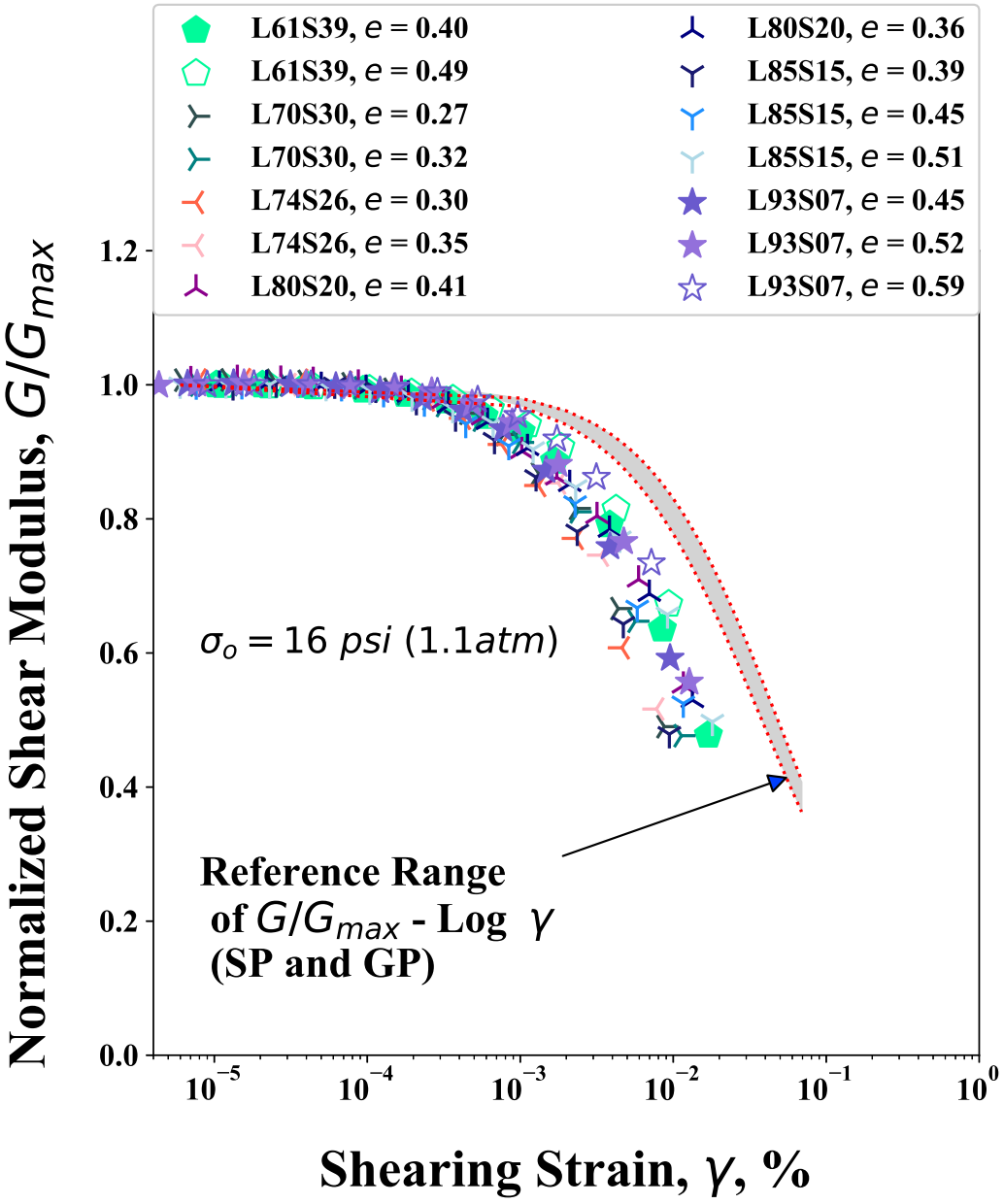

Figure 8.6: Variation in the G/G_{max} - Log γ Relationship for All Transition Zone (TZ) and Large-Particle-Packing Dominated (LPPD) Specimens (61% $\leq$ LPC $\leq$ 100%)

graded specimens with the variations of e and C_u.

8.3.2 Gap-Graded Materials

The nonlinear shear modulus characteristics of the gap-graded specimens were also investigated in this research. The gap-grade specimens show a decreasing relationship of γ_r with the decrease of e. The gap-graded specimens also show the relatively strong relationship of the log γ_r - log C_u compared to the binary mixtures.

8.4 RECOMMENDATIONS

1. The investigation on the dynamic behavior of binary mixtures in this study was successful. However, the test results and findings are limited to this specific binary size ratio of large particles to small particles (i.e., a factor of 34 in this study) as well as to the void ratio ranges used for each gradation in this research. Expanding the study with different binary size ratios and wider void ratio ranges can provide better understanding of the characteristics in binary materials.

2. Results of this study are primarily for binary and gap-graded specimens reconstituted with the parent sand materials for which the water contents in sands are held constant with the optimum water content of about 7.5%. Even though the total water contents in the binary and gap-graded specimens were reduced due to the dry status of the poorly-graded gravel material, however, moderate concerns about the effect of capillary reaction from the residual

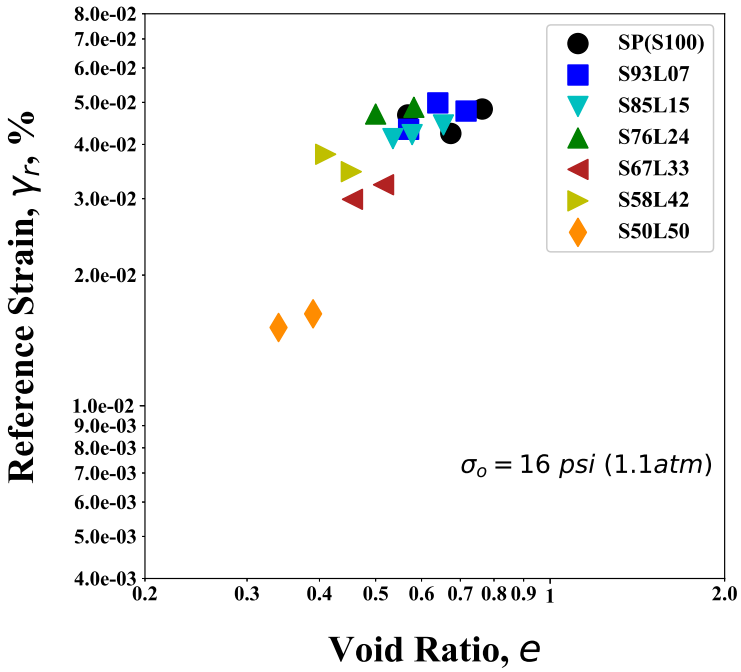

(a) Log γ_r - Log e for 50% $\leq$ SPC $\leq$ 100%

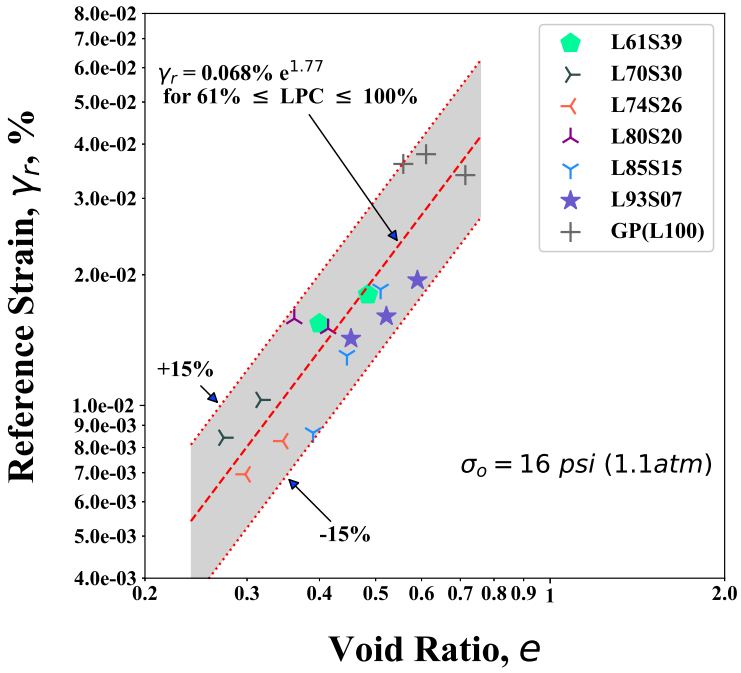

(b) Log γ_r - Log e for 61% $\leq$ LPC $\leq$ 100%

Figure 8.7: Variation in the Reference Strain, γ_r, at 16 psi with Void Ratio (e) and Uniformity Coefficient (C_u) for the SPPD Specimens

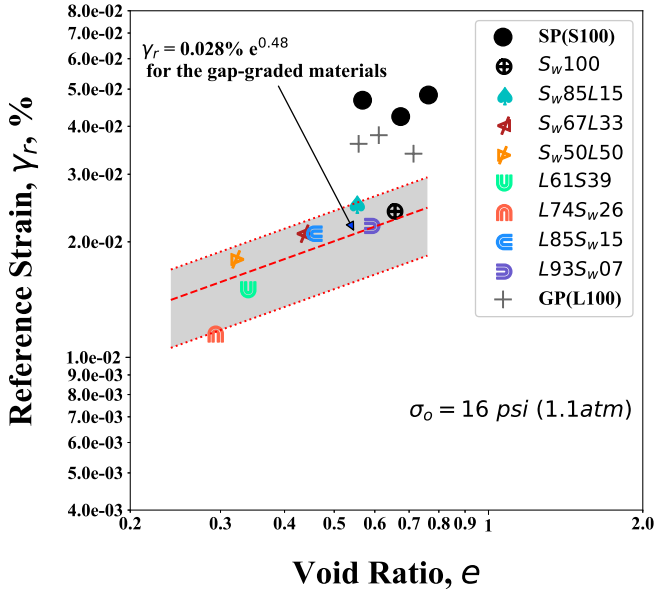

(a) Log γ_r - Log e for 0% $\leq$ SPC $\leq$ 100%

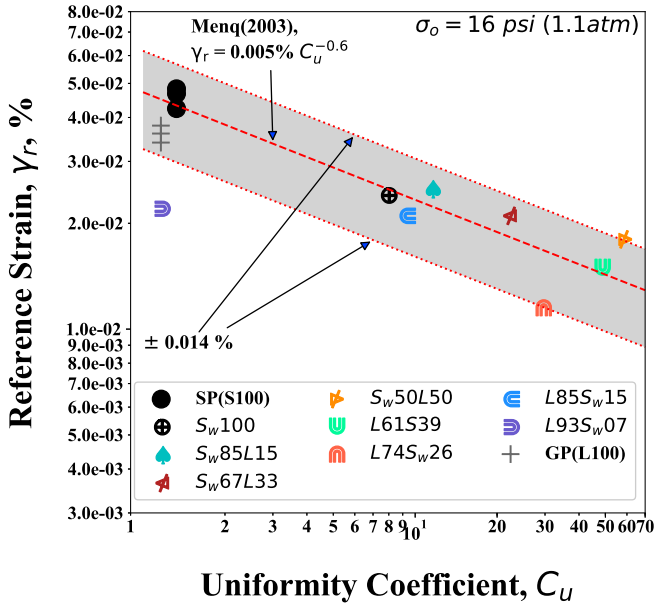

(b) Log γ_r - Log C_u for 0% $\leq$ SPC $\leq$ 100%

Figure 8.8: Variation in Reference Strain, γ_r, at 16 psi with Void Ratio (e) and Uniformity Coefficient (C_u) of One Well-Graded and Seven Gap-Graded Specimens

moisture in the specimens are still present. Further investigations of the effects of water content and capillary reaction on the linear and nonlinear dynamic properties of binary and gap-graded soils are needed.

3. The uniformity coefficient (C_u) of 8 for the well-graded sand used to manufacture the gap-graded specimens was appropriate to extend the investigation of binary materials to the gap-graded materials. However, the test results and findings are not guarantied to the other gap-graded granular mixtures with different uniformity coefficients and size ratios. It is highly recommended to further investigate the effects of different type of gap-graded materials and the various uniformity in the parent materials.

Bibliography

[1] Standard test methods for maximum index density and unit weight of soils using a vibratory table. *ASTM International, West Conshohocken, PA*.

[2] Standard test methods for minimum index density and unit weight of soils. *ASTM International, West Conshohocken, PA*.

[3] Standard test methods for modulus and damping of soils by fixed-base resonant column devices. *ASTM International, West Conshohocken, PA*.

[4] Standard test methods for laboratory compaction characteristics of soil using modified effort. *ASTM International, West Conshohocken, PA*, 2009.

[5] M. T. Bui, C. R. I. Clayton, and J. A. Priest. The universal void ratio function for small strain shear modulus. In *International Conferences on Recent Advances in Geotechnical Earthquake Engineering and Soil Dynamics*, volume 29, 2010.

[6] Misra A. Sundaram S.S. Chang, C.S. Properties of granular packing under low amplitude cyclic loading. *Soil Dynamics and Earthquake Engineering*, 4:201–211, 1991.

[7] W. J. Chang, C. W. Chang, and Jh. K. Zeng. Liquefaction characteristics of gap-graded gravelly soils in k0 condition. *Soil Dynamics and Earthquake Engineering*, 56:74–85, 2014.

[8] W. J. Chang and T. Phantachang. Effects of gravel content on shear resistance of gravelly soils. *Engineering Geology*, 207:78–90, 2016.

[9] A. T. F. Chen and II Stokoe, K. H. Interpretation of strain dependent modulus and damping from torsional soil tests. *Report No. USGS-GD-79-002 NTIS No. PB-298479*, page 46, 1979.

[10] R. H. Clarke. Reservoir properties of conglomerates and conglomeratic sandstones. *AAPG Bulletin*, 63(5):799, 1979.

[11] B. M. Darendeli. Develope of a new family of normalize modulus reduction and material damping curves. *Ph.D. Dissertation. University of Texas at Austin.*

[12] P.J. Digby. The effective elastic moduli of porous granular rocks. *Journal of Applied Mechanics*, 48:803–808, 03 1981.

[13] M. D. Evans and Sh. Zhou. Liquefaction behavior of sand-gravel composites. *Journal of Geotechnical Engineering*, 121, 03 1995.

[14] J. M. Gere and S. P. Timonshenko. Mechanics of materials (3 rd . ed.). *PWS-KENT Publishing Company, Boston*, 1990.

[15] B. O. Hardin. *The nature of stress-strain behavior of soils.* Proceedings, Geotech. Eng. Div. Specialty Conf. on Earthquake Eng. and Soil Dynamics, Vol. 1 ASCE, Pasadena, pp. 3-90, 1978.

[16] B. O. Hardin and Jr. Richart, F. E. Elastic wave velocities in granular soils. *Journal of the Soil Mechanics and Foundation Division*, 89(SM1):33–65, 1963.

[17] K. Ishihara. *Soil Behaviour in Earthquake Geotechnics.* Oxford engineering science series. Clarendon Press, 1996.

[18] Patrick J. Kamann, Robert W. Ritzi, David F. Dominic, and Caleb M. Conrad. Porosity and permeability in sediment mixtures. *Ground Water*, 45(4):429–438, 2007.

[19] A. K. Keene. Next-generation equipment and procedures for combined resonant column and torsional shear testing. *Ph. D. Dissertation, Univ. of Texas at Austin.*, 2017.

[20] D.S. Kim and II Stokoe, K.H. Torsional motion monitoring system for small-strain (10^{-5} to 10^{-3}%) soil testing. *ASTM Geotech. Testing J.*, 17:17–26, 1994.

[21] T. Kokusho and Y. Tnanaka. Dynamic properties of gravel layers investigated by in-situ freezing sampling. *Ground Failure under Seismic Conditions, Geotech. Spec. Pub*, 44:121–140, 1994.

[22] Christine E. Koltermann and Steven M. Gorelick. Fractional packing model for hydraulic conductivity derived from sediment mixtures. *Water Resources Research*, 31(12):3283–3297, 1995.

[23] Liggio C. Lade, P. and J. Yamamuro. Effects of non-plastic fines on minimum and maximum void ratios of sand. *Geotechnical Testing Journal,*, 21(4):336–347, 1998.

[24] J. P. Laird. Linear and nonlinear dynamic properties of soil at high confining pressures. *Ph. D. Dissertation, Univ. of Texas at Austin.*, 1994.

[25] Johnson L.D. Makse A.H., Gland N. and Schwartz L. Granular packings: Nonlinear elasticity, sound propagation, and collective relaxation dynamics. *Physical Review E*, 70:19, 2004.

[26] Fen-You Menq. Dynamic properties of sandy and gravelly soils. *Ph.D. Dissertation. University of Texas at Austin.*, 2003.

[27] S.-H. Ni. Dynamic properties of sand under true triaxial stress states from resonant column/torsional shear tests. *Ph. D. Dissertation, Univ. of Texas at Austin.*, 1987.

[28] Jr. Hall J. R. Jr. Richart, J. E. and Woods R. O. Vibrations of soils and foundations. *Prentice-Hall Inc. Englewood Cliff, New Jersey*, 1970.

[29] R. T. Idriss I. M. Seed, H. B. Wong and K. Tokimatsu. Moduli and damping factors for dynamic analyses of cohesionless soil. *Journal of Geotechnical Engineering, ASCE*, 112, 1986.

[30] Boonam Shin. Effects of oversized particles on the dynamic properties of sand specimens evaluated by resonant column testing. *The University of Texas at Austin, Thesis*, 2014.

[31] J. N.; Hwang S.; Cox B.; Menq F. Y.; Stokoe, K. H.; Roberts and S. Van Ballegooy. Effectiveness of inhibiting liquefaction triggering by shallow ground improvement methods: Initial field shaking trials with t-rex at one site in christchurch, new zealand. *Selected Papers from the New Zealand: Japan Workshop on Soil Liquefaction during Recent Large-Scale Earthquakes*, pages 193–202, 2014.

[32] Kudo K. Yoshida Y. Tanaka, Y. and M. Ikemi. A study on the mechanical properties of sandy gravel-dynamic properties of reconstituted sample. *Research report No.U87019, Central Research Institude of Electric Power Industry, abiko, Japan (in Japanese)*, 1987.

[33] S. Thevanayagam and G Martin. Liquefaction in silty soils: screening and remediation issues. *Soil Dynamics and Earthquake Engineering*, 22(9-12):1035–1042, 2002.

[34] K. Walton. The effective elastic moduli of a random packing of spheres. *Journal of the Mechanics and Physics of Solids*, 35(2):213–226, 1987.

[35] A. B. Yu and N. Standish. Estimation of the porosity of particle mixtures by a linear-mixture packing model. *Industrial & Engineering Chemistry Research*, 30(6):1372–1385, 1991.

[36] Z. Fred Zhang, Andy L. Ward, and Janson m. Keller. Determining the porosity and saturated hydraulic conductivity of binary mixturesall rights reserved. *Vadose Zone Journal*, 10(1):313, 2011.

Vita

Boonam Shin entered SungKyunKwan University in 2003. He enlisted in the Republic of Korea Airforce in 2005 and had served as a civil engineer for two years. After the military service, he returned to the SungKyunKwan University and graduated in 2011 with Bachelor of Science degree in Civil Engineering. After the graduation, he started graduate study in the Department of Civil, Architectural and Environmental Engineering of The University of Texas at Austin in August 2011.

Permanent address: bnshin83@gmail.com

This dissertation was typeset with LaTeX[†] by the author.

[†]LaTeX is a document preparation system developed by Leslie Lamport as a special version of Donald Knuth's TeX Program.